SELF-ASSEMBLY OF 3d AND 4f METAL IONS USING CHIRAL/FLEXIBLE LIGANDS

A Thesis

Submitted for the degree of

DOCTOR OF PHILOSOPHY

by

Suman Mondal

(16CHPH29)

School of Chemistry

University of Hyderabad

Hyderabad 500046

Telangana

India

December, 2022

Dedicated

to

My Baba, Maa, and my brother (Sourav)

“Science may set limits to knowledge,

but should not set limits to imagination”

Bertrand Russell

DECLARATION

I hereby declare that the matter embodied in the thesis entitled "*Self-assembly of 3d and 4f metal ions using chiral/flexible ligands*" is the result of investigations carried out by me in the School of Chemistry, University of Hyderabad, India under the supervision of **Prof. Viswanathan Baskar**.

In keeping with the general practice of reporting scientific investigations, acknowledgments have been made wherever the work described is based on the findings of other investigators. Any omission or error that might have crept in, is regretted. This work is also free from plagiarism. I hereby agree that my thesis can be submitted in Shodhganga/ INFLIBNET.

Prof. Viswanathan Baskar
(Supervisor)

V. BASKAR
Professor
School of Chemistry
University of Hyderabad
Hyderabad - 500 046.

Suman Mondal
(16CHPH29)

University of Hyderabad

December, 2022

CERTIFICATE

This is to certify that the thesis entitled "***Self-assembly of 3d and 4f metal ions using chiral/flexible ligands***" submitted by **Mr. Suman Mondal** bearing registration number **16CHPH29** in partial fulfillment of the requirements for the award of Doctor of Philosophy in the School of Chemistry is a bonafide work carried out by him under my supervision and guidance.

This thesis is free from plagiarism and has not been submitted previously in part or in full to this or any other University or Institution for an award of any degree or diploma.

Parts of this thesis have been:

A. Published in the following publications:

1. S. Mondal, S. P. Behera, M. Alamgir, V. Baskar, *ACS Omega* 2022, **7**, 1090-1099.
2. S. Mondal, C. Samuel, V. Baskar, Journal of Molecular Structure 2023, **1273**, 134274

B. Presented in the following Conferences:

1. Chemfest-2020, 2. Chemfest-2021, 3. MTIC-XIX (2022)

Further, the student has passed the following courses towards the fulfillment of course work required for a Ph.D.:

	Course No.	Title of the Course	No. of Credits	Grade
1.	CY801	Research Proposal	3	Pass
2.	CY802	Chemistry Pedagogy	3	Pass
3.	CY805	Instrumental Methods-A	3	Pass
4.	CY806	Instrumental Methods-B	3	Pass

Prof. Viswanathan Baskar
(Thesis Supervisor)

V. BASKAR
Professor
School of Chemistry
University of Hyderabad
Hyderabad - 500 046.

26/12/2022

Dean (I/c)
School of Chemistry
University of Hyderabad

Dean
School of Chemistry
University of Hyderabad
Hyderabad-500 046

हैदराबाद विश्वविद्यालय
UNIVERSITY OF HYDERABAD
School of Chemistry
P. O. Central University, Hyderabad-500 046

PH.D. COURSE WORK RESULTS

Name of the Scholar: Mr. Suman Mondal

Name of the Supervisor: Prof. V. Baskar

Regn. No.: 16CHPH29

Sl. No.	Course No.	Title of the Course	No. of Credits	Grade
1.	CY801	Research Proposal	3	Pass
2.	CY802	Chemistry Pedagogy	3.	Pass
3.	CY805	Instrumental Methods-A	3	Pass
4.	CY806	Instrumental Methods-B	3	Pass

Final Result: Passed

Coordinator
Date: 07/07/2022

Dean
Date: 07/07/2022

Dean
SCHOOL OF CHEMISTRY
University of Hyderabad
Hyderabad-500 046

ACKNOWLEDGEMENT

This work presented here in the thesis is my past few years' constant efforts. I enjoyed a hard time during my work. I am grateful to the almighty to give me the opportunity to work for science. So many people were present directly or indirectly to fulfill my thesis work either mentally or physically. Here I have a chance to express my gratitude to all of them.

I would like to express my genuine gratitude to my supervisor Prof. Viswanathan Baskar. His guidance, support, and science talk encouraged me always in my Ph.D. time. During the struggling time of my Ph.D. period, his inspirational talks always inspired me to overcome my failure, and always I was motivated by his every word. I am very glad that I joined his research group and worked with such freedom.

I would like to thank my doctoral committee members, Prof. S. K. Das and Prof. K. Muralidharan for their timely support.

I would like to thank the former and present Dean of the School of Chemistry Prof. M. Durga Prasad, Prof. T. P. Radhakrishnan, Prof. K. C. Kumarswamy, Prof. A. Samanta, and Prof. A. Nangia for providing the best research facilities and working atmosphere a loveable School.

I wish to thank all the technical staff, especially SCXRD(Single Crystal X-ray Diffractometer) operators Ramana Kumar Sir and Mahesh for their help whenever the time is required to collect the data.

My hearty thanks to my seniors Dr. Sanathana Raj Prabhu, Dr. Rasamsetty Amaleswari, Dr. Upparao Ugandhr, Dr. Junaid Ali, batchmate Gujju Narasimhulu and juniors Tokala Navaneeta, Smruti Pragya Behera, and Calvin Samuel for their valuable scientific discussions, moral support all the time. A healthy and friendly atmosphere I always gained in the lab to work. During Lab parties great fun we had always.

I would like to thank all my School of Chemistry, University of Hyderabad Ph.D. friends, and batchmates of 2016: Shubham, Soutrick, Alamgir, Sumanta, Pabitra, Somnath, Nilanjan, Pritam, Sarada, Anupam, Alim, Gorachand, Akram, Laxman, Irfan, Jada Ravi, Mamina, Santi, Jaykrishna, Shubham, Prachi,

I would like to thank my M.Sc. friends Rajib, Nithun, Apurba, Ankan, Sourav, Saptarshi, Mrinmoy, Sayantan, Joyento, Joy, Soumik, Sunny, Surojit, Anindya, Narendranath, Suvojit.

I would like to thank my B.Sc. friends Rathin, Samrat, Snehashish, Keya, Amrita, and Paromita and School friends Chiranjit(Choto), Pradipto, Tamal, Debashish, Deep, Ratan, Pritilata, Sujoy, Samrat, Shyamal, Manish, Chandni, Sapna, Anindita, Amit, Goutam, Chiranjit, Riya, Arpita, Rahul, Mallika, Sanam, Bijoy, Goutam.

I would like to thank my respected teachers without them I cannot reach this position. My M.Sc. teachers Bipul Sir, A.S. Sir, T.G. Sir, S.B. Sir, R.S. Sir, R.P. Sir, my B. Sc. teachers S.G. Madam, S.B. Sir, Bikash Sir, Sanhita Madam, my School teachers Pranab Sir, Jogen Sir, Jayanta Sir, Sakhi Madam, Chinmoy Sir, Bipasa Madam, Sajal Sir, Banalata madam.

My special thank to my lady love Samapti for her caring and mental support.

Finally to my Maa, Baba, Vai, and family members Choto mama-mami, Boro mama(late), boro-mami, Dida, Thamma(late), Soumen dada, boudi, and nephew(Debajyoti), Palas Da.

I gratefully acknowledge to University of Hyderabad for providing me financial support and School of Chemistry, University of Hyderabad for providing instrumental facilities and peaceful environment to accomplish my Ph. D. degree.

University of Hyderabad ***Suman Mondal***

December, 2022

CONTENTS

Abbreviations

MW	Microwave
3,5-DMPZ	3,5-dimethyl pyrazole
DCM	Dichloromethane
py	pyridine
phen	phenanthroline
dppi	diphenyl phosphinic acid
BIB	1,4-bis(1H-imidazol-1-yl)butane
bipy	bipyridine
CP	coordination polymer
dtbp-H	di-tert-butyl phosphate
fc	1,1'-ferrocenediyl
SMM	single molecular magnet
SIM	single ion magnet
ZFS	zero field splitting
QTM	quantum tunneling of magnetization
Pc	phthalocyanine
TM	transition metal
Cp	cyclopentadienyl
CSD	Cambridge Crystallographic Database
DFT	density functional theory
DBM	dibenzoyl methane
DCM	dichloromethane
TGA	thermogravimetric analysis
DMSO	dimethylsulfoxide
ILCT	intra-ligand charge transfer
MEA	monoethanolamine
HOMO	highest occupied molecular orbital
LUMO	lowest occupied molecular orbital

MOF	metal organic framework
EADX	energy dispersive X-ray analysis
SCXRD	Single Crystal X-ray Diffraction
PXRD	powder X-ray diffraction
SEM	scanning electron microscopy
IR	Infra-red spectroscopy
UV	Ultra-violet spectroscopy
NMR	Nuclear Magnetic Resonance Spectroscopy

Name of the Student	**Suman Mondal**
Roll Number	**16CHPH29**
School	**School of Chemistry**
Name of Thesis Supervisor	**Prof. V. Baskar**
Thesis Title	***Self-assembly of 3d and 4f metal ions using chiral/flexible ligands***

SYNOPSIS

This thesis entitled "***Self-assembly of 3d and 4f metal ions using chiral/flexible ligands***". It is divided into five chapters and details of each chapter are given below

Chapter 1

Introduction

This introduction chapter deals with a general introduction and the historical background of multinuclear clusters. Selected examples of zinc clusters of phosphinic acid, phosphonic acid, phosphates, and Schiff-base clusters of zinc and cadmium are discussed. In the later section, a detailed description of single molecular magnetism (SMM) and the working principle, the relaxation mechanism involved in the SMM, and different plots related to magnetism are included. Finally, the discussion of the first known example of transition metal and lanthanide metal SMM and a few of the literature reported breakthrough examples in terms of energy barrier / blocking temperature of lanthanide SMM.

Chapter 2

In-situ assembled polynuclear zinc-oxo clusters using modified Schiff-bases as ligands

In this chapter, a series of different core and nuclearity zinc metal clusters have been synthesized **2.1**-**2.5** using $Zn(ClO_4)_2.6H_2O$, Schiff-base primary ligand, and DBM or monoethanolamine(MEA) as co-ligand at room temperature reaction. The structure of the complexes is characterized by single-crystal X-ray diffraction. Among this (**2.1**) [Zn(L1)(DBM)] is mononuclear, (**2.2**) $[Zn(L2)_2(DBM)_4]$, (**2.3**) $[Zn_4(L2)_4(H_2O)_2(ClO_4)_2].2CH_2Cl_2$. (**2.4**) $[Zn_4(L3)_2(DBM)_4]$ has a cubane core. (**2.5**) $[Zn_4(L4)_4(MEA)_2(ClO_4)_2]$ is a ladder-like core structure. Compounds **2.1**-**2.5** has been also characterized by UV-Vis absorption and emission spectroscopy. For an in-depth understanding of the absorption spectrum of **2.1** and **2.3** DFT (Density Functional Theory) calculations have

been performed which suggests that the transitions correspond to the $\pi \rightarrow \pi^*$ intra-ligand charge transfer (ILCT).

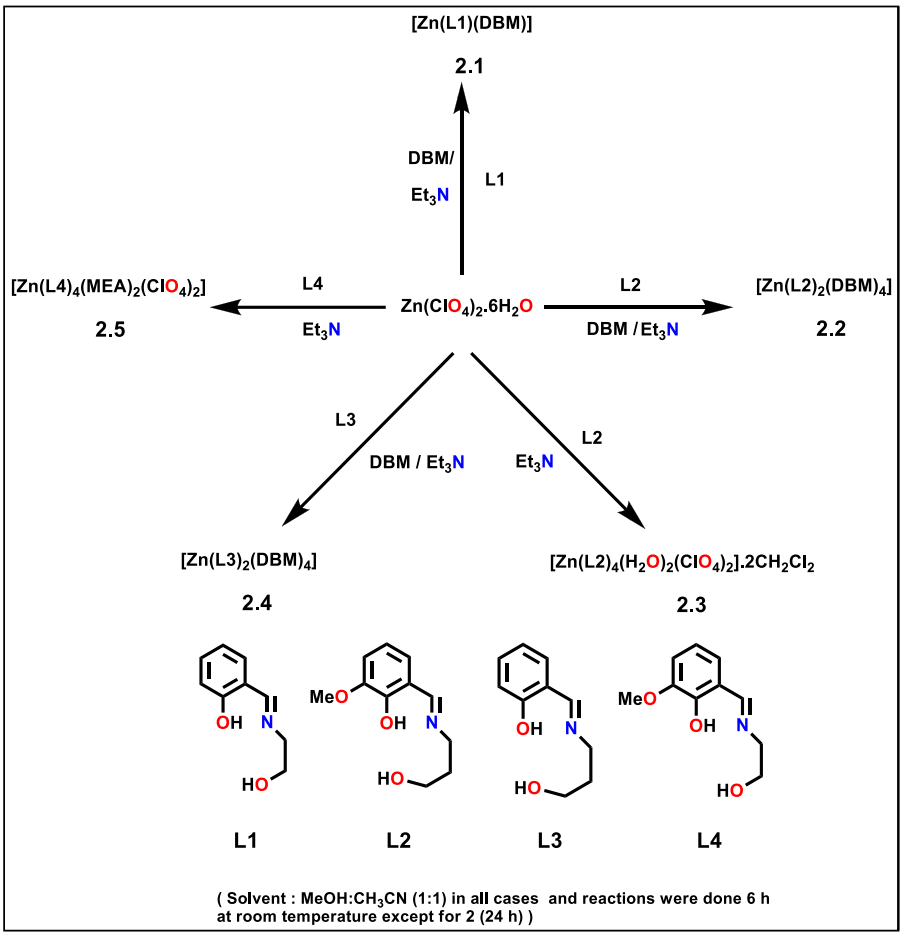

Figure 1. Synthetic scheme and solid-state structures of Zinc Schiff-base compounds

Chapter 3

Aza-donor ligands- A key to synthesizing mononuclear to coordination polymers of cadmium phosphinates

In this chapter four cadmium phosphinate complexes were synthesized based on Bis-[α-hydroxy(*p*-methylphenyl)methyl]phosphinic acid (L) ligand. These complexes $[Cd(L)_2(H_2O)_2]$ **(3.1),** $[Cd(L)_2(py)_3].py$ **(3.2),** $[Cd(L)_2(4,4'\text{-bpy})_4]_n$ **(3.3),** $[Cd(L)_4(4,4'\text{-azo-bpy})(H_2O)]_n$ **(3.4),** were well characterized by single-crystal X-ray diffraction, IR spectroscopy, powder X-ray diffraction, elemental analysis, and TGA. **3.1** and **3.2** are zero-dimensional (0D) structures while **3.3** and **3.4** are two-dimensional net-like (2D), one-dimensional chain-like (1D)

structures, respectively. N-donor co-ligands (py, 4,4'-bpy, 4,4'-azo-bpy) contribute to the formation of these architectures.

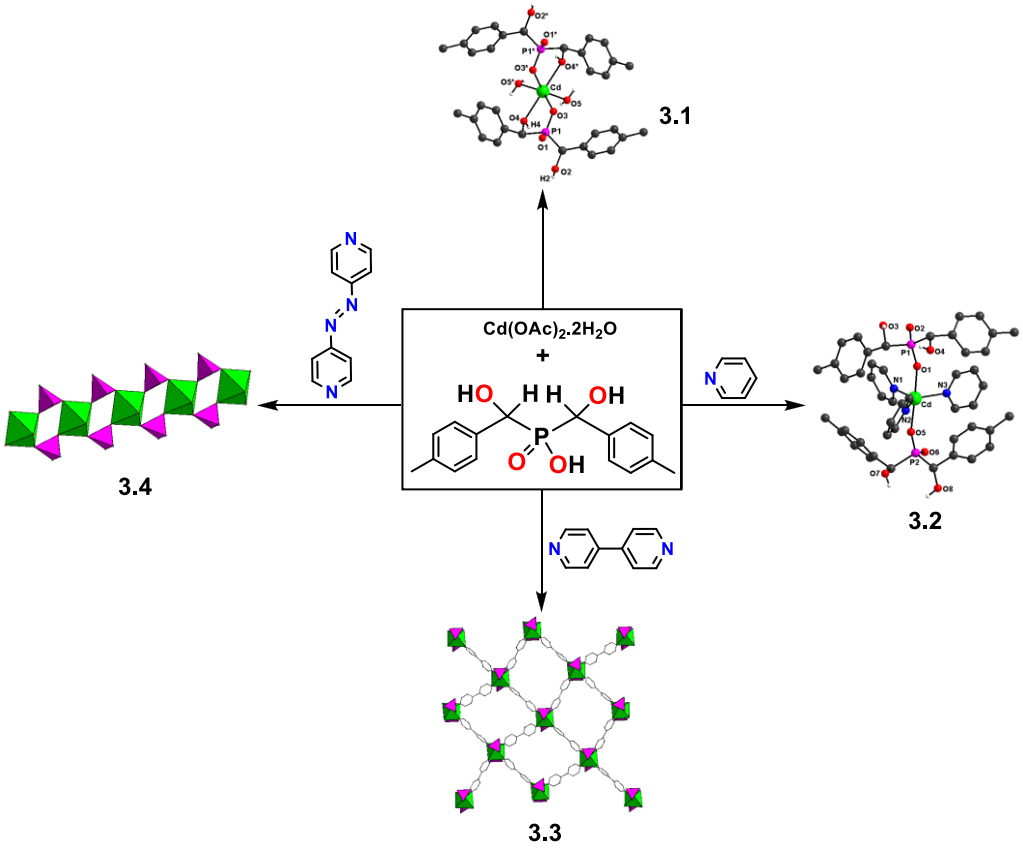

Figure 2. Synthetic scheme and solid-state structures of Cadmium-phosphinate compounds

Chapter 4

Synthesis and characterization of paddlewheel dinuclear and trinuclear lanthanide phosphinate clusters

In this chapter, a series of isostructural dinuclear and trinuclear paddlewheel Ln(III) clusters have been synthesized in reaction with chiral phosphinic acid ligand [(Bis-[α-hydroxy(p-methylphenyl)methyl]phosphinic acid] and [Bis-[α-hydroxy(p-bromophenyl)methyl]phosphinic acid] {($R^1_2/R^2_2PO_2H$)[R^1= CH(OH)PhMe], [R^2= CH(OH)PhBr]}. The complexes represented as $(Et_3NH)_3[Ln_2(\mu_2\text{-}\eta^1\text{:}\eta^1\ PO_2\ R^1_2)_3(NO_3)_6]$ where Ln= Dy (**4.1**), Ho (**4.2**), Nd (**4.3**), Y (**4.4**) and $(Et_3NH)_3[Ln_3(\mu_2\text{-}\eta^1\text{:}\eta^1\ PO_2\ R^2_2)_6(NO_3)_6]$ where Ln= Nd (**4.5**), Pr (**4.6**), Dy (**4.7**), $NdLa_2$ (**4.8**), characterized by SCXRD, IR. Among these

trinuclear linear paddlewheel clusters, **4.8** is a magnetically diluted structure where terminal atoms are diamagnetic lanthanide (La) and central lanthanide is paramagnetic Nd. Synthesis and structural interpretation are discussed in detail in this chapter.

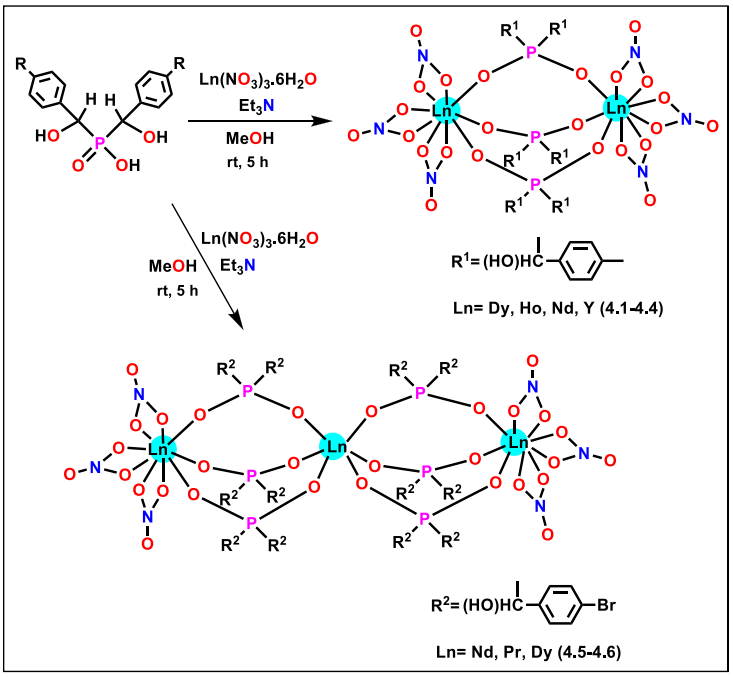

Figure 3. Synthetic scheme of lanthanide-phosphinates

Chapter 5

A new type of square grid [2 × 2] lanthanide Ln(III)$_4$ complexes self-assembled with chiral racemic (R, R / S, S) bis-[α-hydroxy(p-bromophenyl)methyl]phosphinic acid ligand

The chapter deals with a series of isostructural tetranuclear [2 × 2] square-grid-like Ln(III) clusters, which have been synthesized in reaction with chiral phosphinic acid ligand [Bis-[α-hydroxy(p-bromophenyl)methyl]phosphinic acid] {(R_2PO_2H)[R= CH(OH)PhBr]} represented as [$Ln_4(\mu_2\text{-}\eta^1\text{:}\eta^1\text{-}PO_2R_2)_8(\eta^2\text{-}CO_2Bu^t)_4$] where Ln= Er (**5.1**), Dy (**5.2**), Tb (**5.3**) and characterized by SCXRD, IR. Synthesis and structural interpretation are discussed in detail in this chapter.

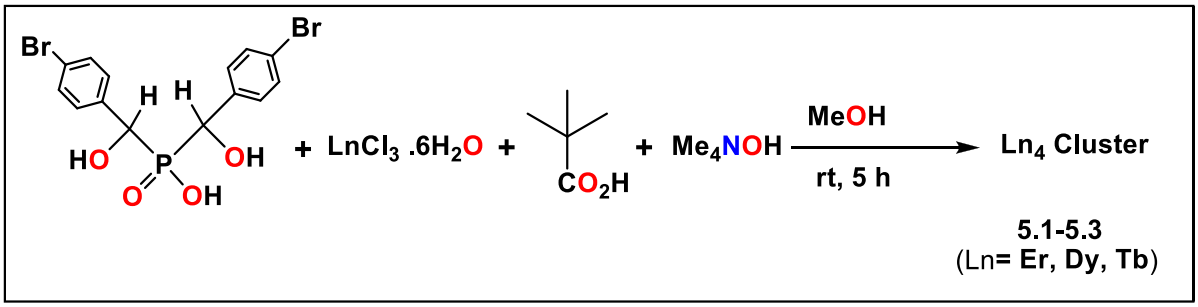

Figure 4. Synthetic scheme of compounds **5.1-5.3**

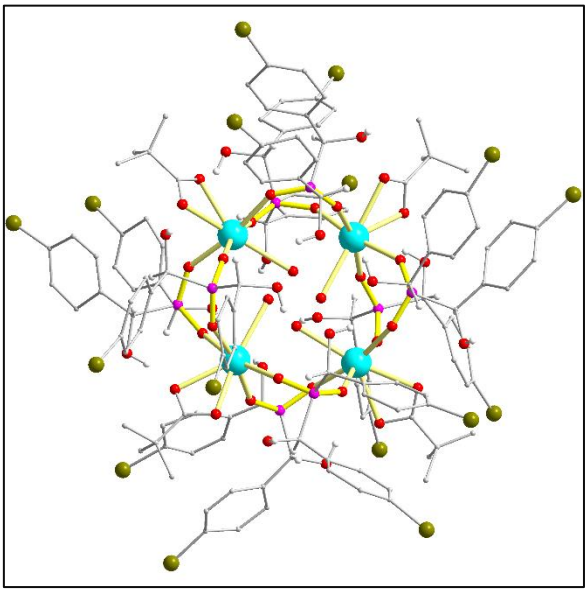

Figure 5. The solid-state structure of **5.2**

CHAPTER 1

Introduction

1.1 General Introduction:

Transition metal and lanthanide metal polynuclear complexes are extremely important in coordination chemistry. This is due not only to the structure's aesthetic beauty and complexity but also to its fascinating chemical and physical properties. These clusters/complexes have numerous applications in chemistry, including catalysis, water splitting, gas storage, luminescence, single molecular magnetism (SMM), and biological activity. We studied Zn, Cd, and lanthanide clusters/complexes of Schiff base and phosphinic acid in this thesis. In this regard, we will go over a few examples of Zn, Cd, and lanthanide clusters in the introduction section.

Polynuclear clusters/complexes were synthesized using two different approaches: (1) Targeted Self-assembly and (2) Serendipitous approach. In the thesis, we synthesized molecular clusters primarily using a serendipitous approach.

The self-assembly method has been used with less flexible ligands such as rigid bipyridine (bpy). Taking advantage of this type of directional ligands the formed complex structures can be preassumed. These complexes self-assemble in a controlled manner. The targeted self-assembly method is commonly used to synthesize transition metal complexes. Schiff-base Salen-type ligands contain pockets into which targeted metal atoms can be incorporated to form polynuclear self-assembled clusters.

Another synthetic approach is the serendipitous assembly approach where the formation of complexes/ clusters has not been done intentionally, it is an accidental formation. This approach is the most interesting because of its uncertain assembly and property of the clusters. A flexible multi-doner atom containing ligands is generally used to synthesize multinuclear clusters/complexes in this approach, viz., carboxylates(RCO_2^-), phosphinic acid($R_2PO_2^-$), phosphonic acid(RPO_3^{2-}), phosphates($(RO)_2PO_2^-$), alkoxide(RO^-), N, O-doner containing Schiff-base, etc. Different synthetic methods have been used to prepare serendipitous assembly:

(1) Mixing of metal and ligand together.

(2) Mixing of metal and ligand with various co-ligands which helps to aggregate(acts as bridging or terminal ligands) and limits the aggregation to form molecular cluster/complex.

(3) Preformed metal complex as a metal precursor source followed by mixing of flexible ligand.

(4) Hydrothermal/Solvothermal synthesis is another synthetic method to prepare polynuclear metal clusters. All the reactants have to be taken together in a closed vessel and under harsh conditions with autogenous pressure, molecular crystals can be formed serendipitously.

Above all, polynuclear cluster formation depends upon several factors like- metal to ligand ratio, metal salts, reaction temperature, solvent type, the volume of solvent, cooling rate, crystallization method, pH, etc. Compared to the transition metal, lanthanide metals form more serendipitous self-assembled polynuclear complexes. Lanthanides are very much prone to hydrolysis and form multinuclear clusters with flexible ligands in an unplanned random self-organized way.

1.2 Synthesis of phosphinic acid and Schiff-base:

(a) Phosphinic acid synthesis:

Phosphinic acid is analogous to carboxylic acid, the two similar or different substituents on phosphorous atom present in the molecular structure of phosphinic acid show a unique steric property, which opened a path to progress in the properties of phosphinic acid at the molecular level and solid-state chemistry. The pKa value of phosphinic acid is in between phosphonic acid and carboxylic acid. This intermediate acidity of the phosphinic acid and the two substituent tunability on the phosphorous atom makes these molecules a greater interest in the field of material chemistry. Phosphinic acids are used the various field as flotation agents, flame retardants, and ionic liquids (as a lubricating agent and separation of cations), in medical applications. Here we have given a few synthetic procedures of phosphinic acid.

Hydrolysis of reactive PCl_2 or alcoholysis followed by hydrolysis phosphinic acid can be prepared.[1] (Scheme 1)

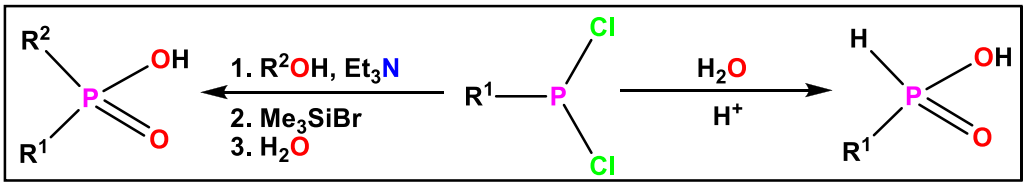

Scheme 1. Synthesis of phosphinic acid

Using radical initiator hypophosphorous acid or its salt such as sodium hypophosphite(NaH_2PO_2) with suitable alkene group mono alkyl intermediate is prepared. Then another same/different alkene is used to prepare symmetric/nonsymmetric dialkyl phosphinic acid.[2,3] (Scheme 2)

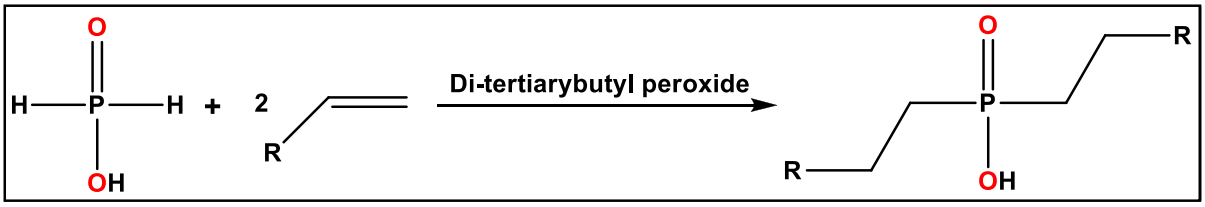

Scheme 2. Synthesis of dialkyl phosphinic acid

Condensation of 1°, 2° amines, aldehyde/ ketone, and >P(O)H species (H-phosphites and dialkyl phosphites) in a three-component reaction yields α-amino phosphonic acid/ phosphonates is called 'Kabachnik-fields reaction'. The benefit of this reaction is maximum reactions can be done in solvent-free microwave conditions and no sophisticated catalysts were used in the reaction condition.[4] (Scheme 3)

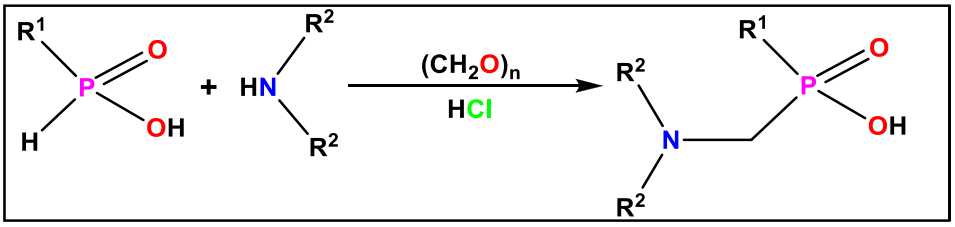

Scheme 3. Synthesis of α-amino phosphonic acid

Palladium coupling reaction following de-esterification is another way to synthesize phosphinic acid. Diaryl substituted phosphinic acid can be prepared by substituting the P-H bond of P-H containing precursor using Pd-catalyst following de-esterification and hydrolysis reaction.[1] (Scheme 4)

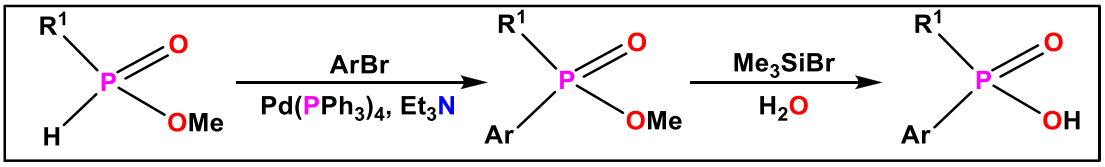

Scheme 4. Synthesis of diaryl phosphinic acid

From alkyne and alkene molecular precursors using hypophosphorous acid derivatives and Pd-catalyst, alkyl-substituted phosphinic acid can be synthesized.[5] (Scheme 5)

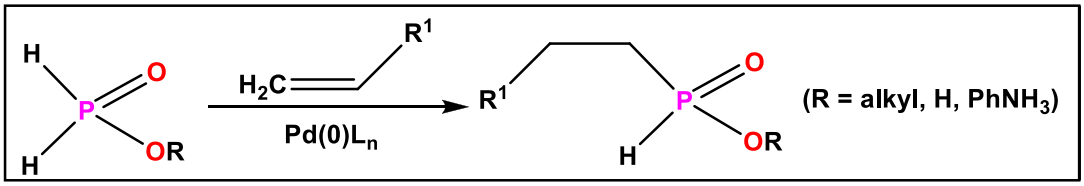

Scheme 5. Synthesis of monoalkyl phosphinic acid

Bis-phosphinic acid connected with an alkyl group can be synthesized by lithiated phenyl phosphinic acid followed by a reaction with an alkyl halide.[6] (Scheme 6)

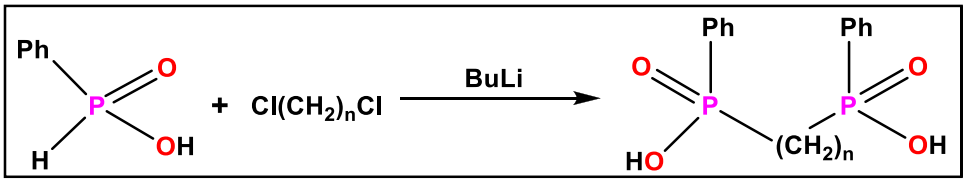

Scheme 6. Synthesis of bis-phosphinic acid

The reaction with P-H bond containing silylated molecular precursor $PH(OSiMe_3)_2$ and carboxylic acid substituted acid chloride has given silylated bisphosphinate which turns into Bis-phosphinic acid.[7] (Scheme 7)

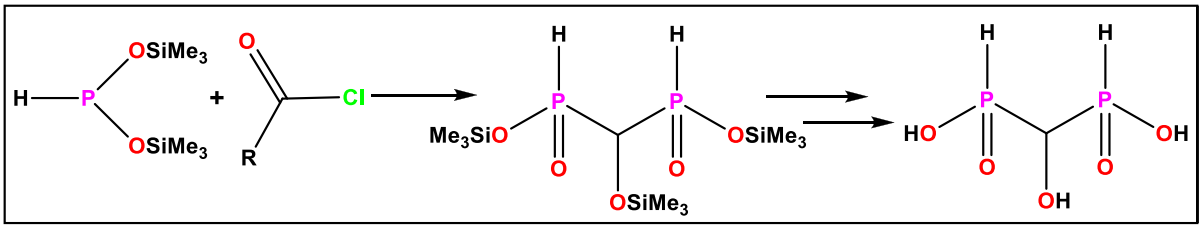

Scheme 7. Synthesis of bis-phosphinic acid

In this thesis Bis-(α-hydroxyalkyl)phosphinic acid was used which can be synthesized from aldehyde and hypophosphorous acid(H_3PO_2) using two processes 1) by solvent-free microwave(MW) synthesis or 2) by heating. The synthetic procedure is given below [8–10]. (Scheme 8)

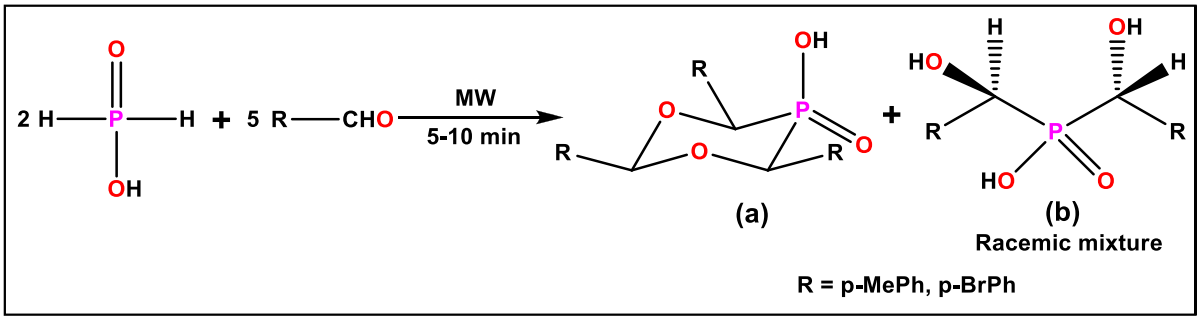

Scheme 8. Synthesis of bis-(α-hydroxyalkyl)phosphinic acid

A hypophosphorous acid (50% aq.) (20 mmol) has been added to aldehyde (50 mmol) and the reaction mixture was irradiated stepwise with a microwave reactor (a kitchen-type 180 W microwave for 5-10 min). After the reaction, ethyl acetate (10 ml) was added and the mixture was stirred vigorously for 5 min. A white powder precipitate was obtained when 30 ml of n-hexane was added to it. The precipitate was filtered and purified with column chromatography (silica-gel with an eluent chloroform-methanol (99:1)) (**a**). Methanol (300 ml) was eluted to acquire the pure product. The evaporation of the methanolic solution obtains a racemic mixture of Bis-(α-hydroxyalkyl)phosphinic acid as a white solid with a good yield.

For the heating reaction also same separation procedure was followed after 3 h at 90 ^{0}C reaction.

(b) Schiff-base synthesis:

Schiff-base ligands are formed by condensation of primary amine and aldehyde/ketone by the formation of imine or azomethine group. It was first prepared by Hugo Schiff in 1864.[11] Its simple synthetic procedure and complex forming ability with p, d, and f-block metals made it useful in a variety of applications in biology (antibacterial, antifungal, anticancer, antioxidant, anti-inflammatory, antimalarial, antiviral) and catalysis (polymerization reaction, catecholase activity, $SOCl_2$ reduction, epoxidation of alkene, ketones reduction, organic compounds oxidation, Henry-reaction, ketones hydrosilylation, D-A reaction (Diels-Alder).

Schiff-base synthesis depends on a three-step method. At the first nucleophilic attack of the amine group to the carbonyl group of aldehyde/ketone and formation of a charge-separated intermediate. Next step this intermediate forms carbinolamine by intramolecular proton transfer. The last step is the water elimination and imine/azo-methine group formation. All three steps are involved in a reversible process. The C=N bond is prone to hydrolysis according to the reverse equilibrium reaction. The formation of the Schiff-base is thermodynamically controlled. The strong and labile nature of the imine bond made it an efficient one-pot synthesis process with a good percentage of yield.

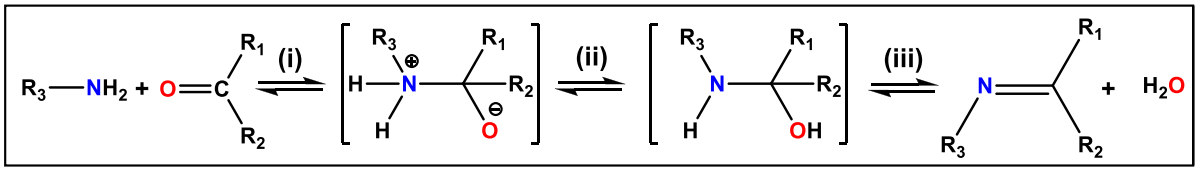

Scheme 9. General synthesis of Schiff-base

In this thesis, we have dealt with the following Schiff bases. All of these are synthesized in-situ reaction medium by a condensation reaction of specific primary amine and aldehyde as starting materials.

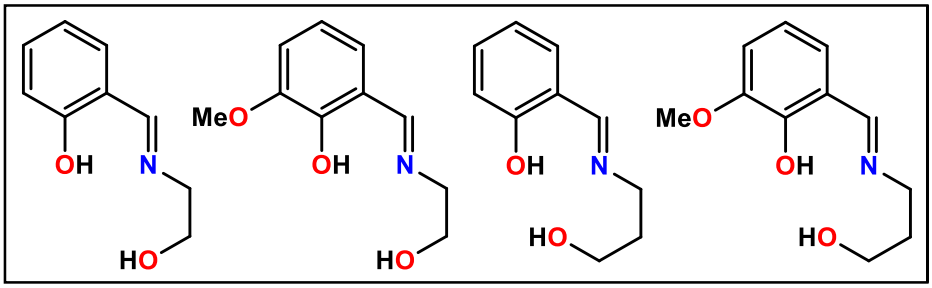

Chart 1 : Schiff base ligands used in thesis

1.3 (a) Zn- related clusters:

(i) Phosphinic acid clusters

Phosphinates are generated from the deprotonation of phosphinic acid, which is analogous to carboxylic acid. The general formula of phosphinic acid is [$\mathbf{R_2P(O)(OH)}$]. In 2005 V. Chandrasekhar et. al. reported [12] mononuclear zinc phosphinate complex $M(Ph_2PO_2)_2(DMPZ)_2$ reacting diphenyl phosphinic acid with zinc chloride and co-ligand 3,5-dimethyl pyrazole (DMPZ) in presence of triethylamine DCM as a solvent. Where Zn atom is tetrahedrally coordinated by surrounded ligands. [**Figure 1**] They showed the intramolecular H-bonding between each phosphinate P=O moiety and N-H protons of pyrazole and also interaction between the P=O unit and aryl hydrogen of diphenyl phosphinate moiety (C-H---O intermolecular interaction). The presence of C-H---O interaction between aryl-H and a coordinated P-O oxygen atom and π-π interaction between pyrazolyl ring and an Ar-moiety on the phosphinic acid ligand leads to the formation of two-dimensional (2D) sheet structure.

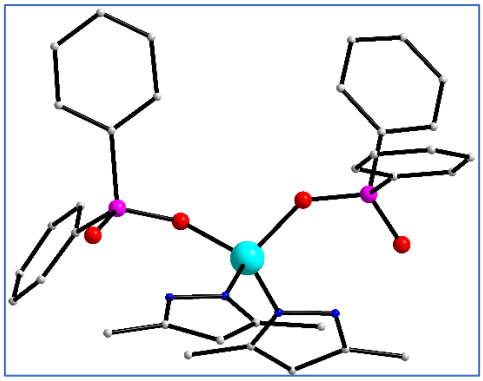

Figure 1: Structure of $Zn(Ph_2PO_2)_2(DMPZ)_2$

In 2008 Murugavel et. al. reported[13] two mononuclear octahedrally coordinated Zn phosphinates $[Zn(phen)_2(dppi)_2].2H_2O$; [**Figure 2a**] $[Zn(phen)_2(ppi)_2].H_2O$ using diphenyl phosphinic acid(dppi) and phenyl phosphinic acid(ppi) respectively in absence of any base. In this paper, one more dinuclear zinc phosphinates $[Zn(bpy)_2(ppi)_2]_2(ClO_4)_2$ [**Figure 2b**] is characterized by SCXRD. In this case $[Zn(bpy)_2(OAc)(ClO_4)(H_2O)$ is used as a molecular precursor of zinc.

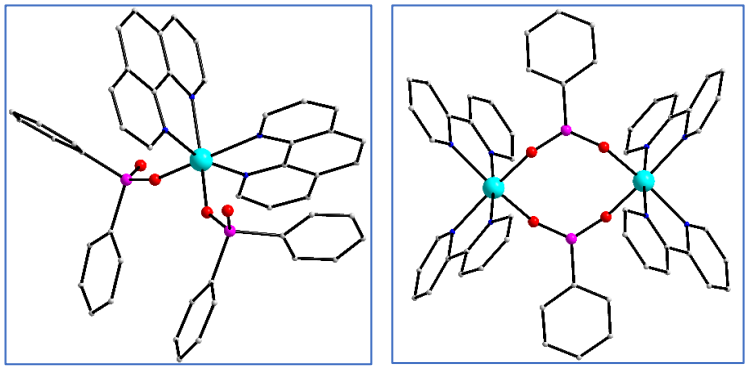

(a) **(b)**

Figure 2: (a) Structure of $[Zn(phen)_2(dppi)_2].2H_2O$, **(b)** Structure of $[Zn(bpy)_2(ppi)_2]_2(ClO_4)_2$

Ming-Jie Zhou et. al. reported[14] two distinguishable polymorphs of $[Zn(BIB)_{0.5}L]_n$ (BIB=1,4-bis(1H-imidazol-1-yl)butane; L^{2-}=2-carboxyethyl(phenyl)phosphinate) among which one is 2D ladder-like [**Figure 3a, 3b**] and another 3D framework [**Figure 3c, 3d**], a cause of different structures is the intramolecular arrangements.

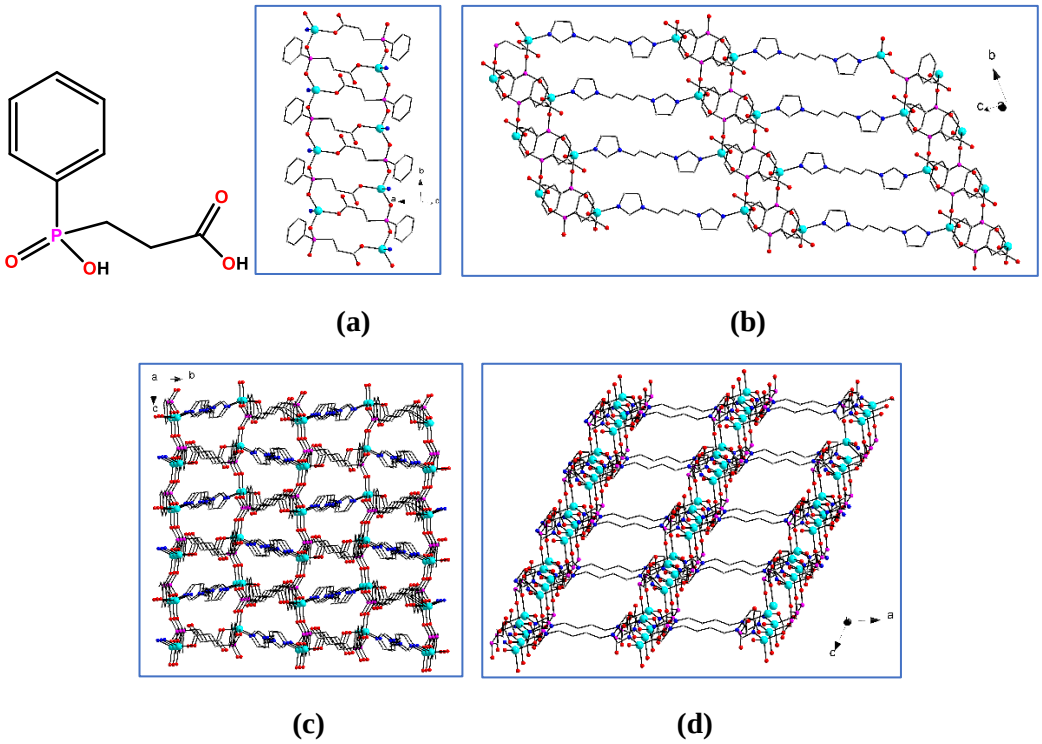

Figure 3: (a) & (b) Structure of 2D ladder-like polymorph $[Zn(BIB)_{0.5}L]_n$ view along ab-plane and bc-plane, **(c) & (d)** Structure of 3D framework polymorph $[Zn(BIB)_{0.5}L]_n$ view along bc and ac-plane

In 2016 Zhao-Xi Wang et. al.[15] reported three Zn-based phosphinates using 2,2'-phosphinico-dibenzoate. They showed different structural diversity. $\{[Zn_3L_2(H_2O)_4].2H_2O\}_n$ is a 1D chain CP [**Figure 4**] with a 3D supramolecular framework, $[Zn_3L_2(4,4'\text{-bipy})_2]_n$ is a three dimensional (3D) porous metal-organic framework (MOF) with two dissimilar 4,4'-bipyridine linkers [**Figure 5**], $[Zn(HL)(2,2'\text{-bipy})(H_2O)]_n$ show 1D zigzag chain structure [**Figure 6**].

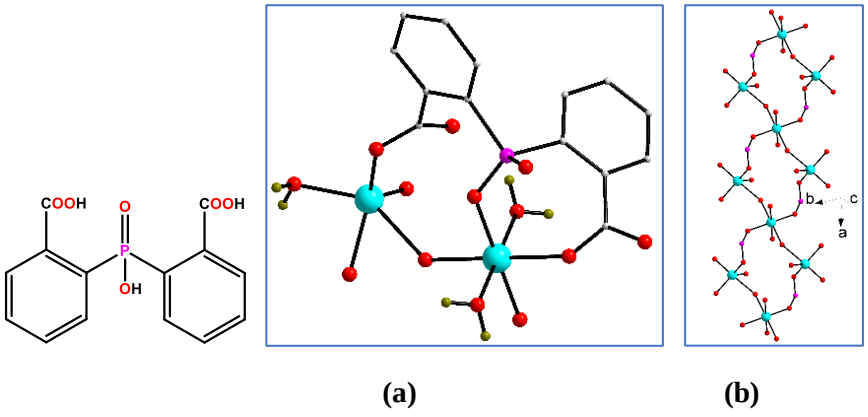

Figure 4: (a) Asymmetric unit of $\{[Zn_3L_2(H_2O)_4].2H_2O\}_n$ **(b)** 1D infinite chain structure of $\{[Zn_3L_2(H_2O)_4].2H_2O\}_n$ along the a-axis

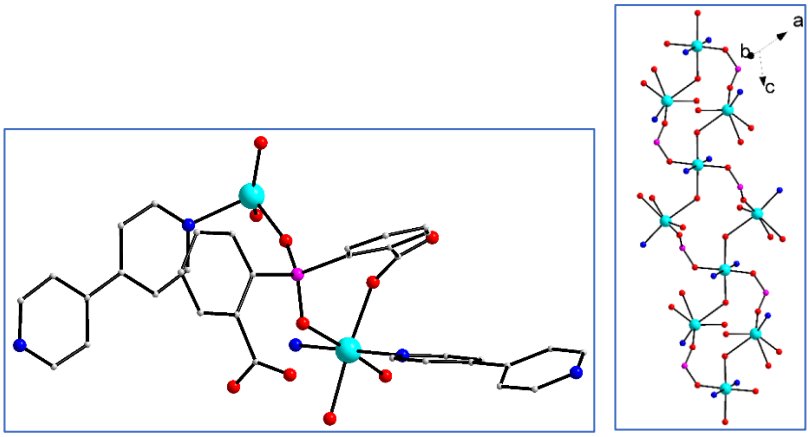

(a) **(b)**

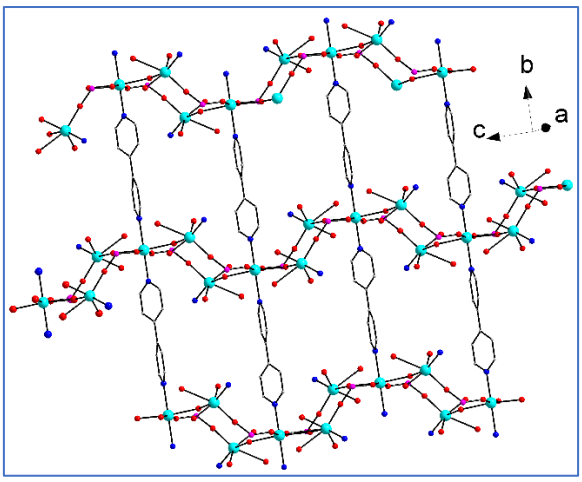

(c)

Figure 5: (a) Asymmetric-unit of $[Zn_3L_2(4,4'\text{-bipy})_2]_n$ **(b)** 1D infinite chain structure of $[Zn_3L_2(4,4'\text{-bipy})_2]_n$ **(c)** 3D MOF structure of $[Zn_3L_2(4,4'\text{-bipy})_2]_n$

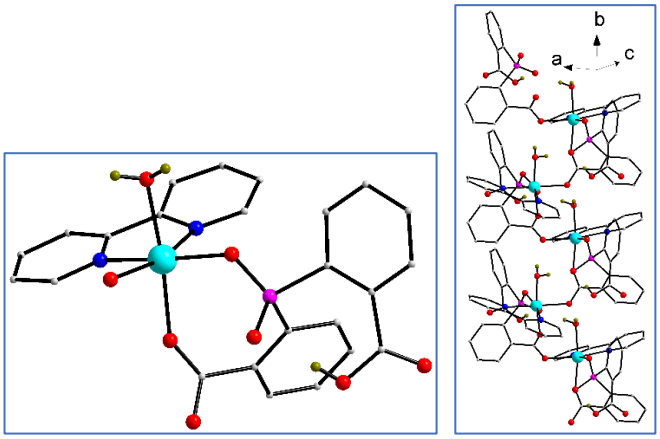

(a) **(b)**

Figure 6: (a) Asymmetric unit of $[Zn(HL)(2,2'\text{-bipy})(H_2O)]_n$ **(b)** 1-D zigzag chain. of $[Zn(HL)(2,2'\text{-bipy})(H_2O)]_n$

Recently 2016 Sebastian D. Pike et. al. reported[16] multinuclear(Zn_4, Zn_6, Zn_{11}) Zn clusters [**Figure 7**] using simple phosphinate ligands. They used a bottom-up synthetic approach and used organometallic zinc ($ZnEt_2$) as a molecular precursor of the Zn atom and studied the mechanistic pathway of the formation of zinc clusters; by investigation with the ^{31}P NMR in the reaction. They showed the role of specific molecular starting material in the preparation of small nanoparticles (2-4 nm).

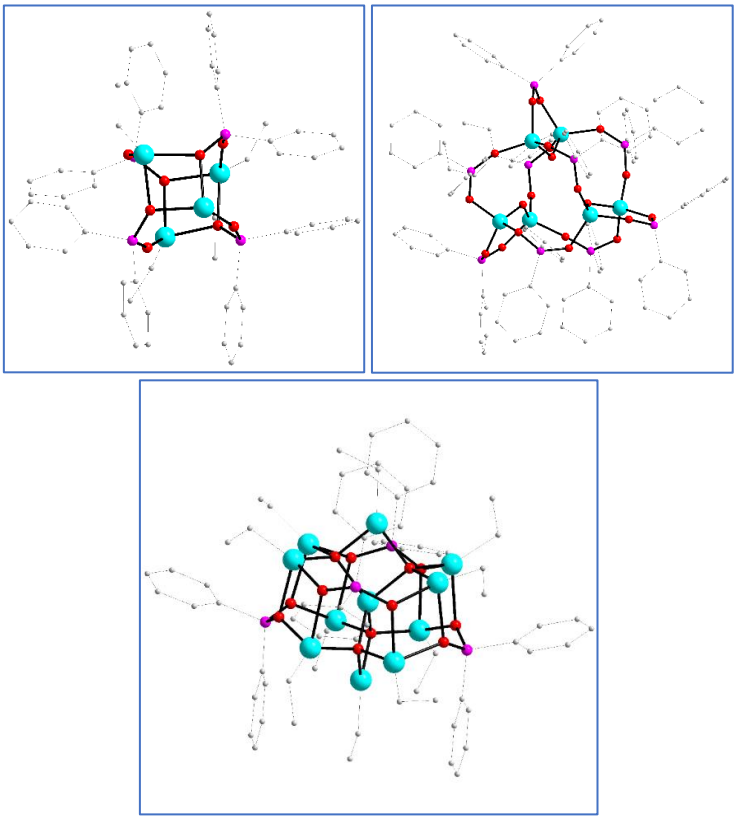

Figure 7: Structure of Zn_4, Zn_6, and Zn_{11} molecular clusters zinc phosphinates

In 2018 Elena Oleshkevich et. al. synthesized a one-dimensional coordination polymer(1D-CP) of zinc using *m*-carboxy phosphinate ligand and characterized. They have concluded the same structure of zinc as cadmium reported[17] with analytical and spectroscopic techniques.

(ii) Phosphonic acid clusters:

Phosphonates are the ligand prepared from the deprotonation of phosphonic acid having the general formula (**RPO_3H_2**). From the literature reports it has seen that homometallic Zinc(II) phosphonate clusters nuclearity varies between 1 to 12. An example of mononuclear zinc phosphonate is *trans-O,O*-[$Zn(H_2L)$] as shown in (**Figure 8**) It was prepared in a sealed vial at heating condition(hydrothermal) utilizing $Zn(OAc)_2.2H_2O$ and 1,4,8,11-tetraazacyclotetradecane-1,8-bis(methylphosphonicacid) (H_4L). The Zn(II) atom is octahedrally surrounded with a most stable trans configuration of the pedant moiety.[18]

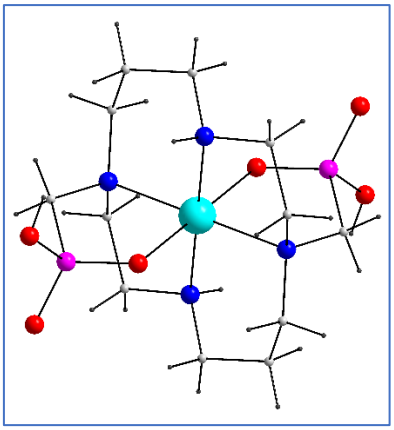

Figure 8: Structure of *trans-O,O*-[Zn(H_2L)] complex

There are several dinuclear zinc phosphonates clusters known. A prototype of that $(HNEt_3)_2\{Zn_2(\eta^1\text{-}3,5\text{-}Me_2PzH)_2Cl_2(Cl_3CPO_3)_2\}$ is described (**Figure 9**). It has been synthesized using $ZnCl_2$, 3,5-Me_2PzH, and $Cl_3CPO_3H_2$ in presence of a base; triethylamine. The crystal structure reveals that each zinc atom is tetrahedrally coordinated, the two zinc metal atoms bridges with two oxygen atoms of the $Cl_3CPO_3^{2-}$ moiety and forming an eight-membered puckered ring. Each zinc metal atom is co-ordinately saturated with one chloride ion and one pyrazole molecule.[19]

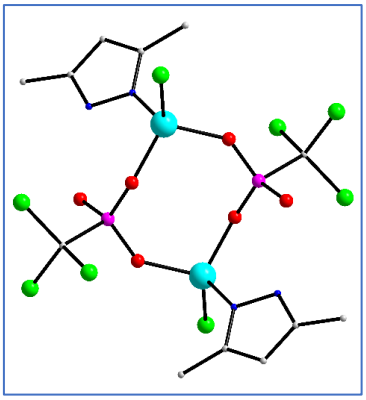

Figure 9: Structure of $(HNEt_3)_2\{Zn_2(\eta^1\text{-}3,5\text{-}Me_2PzH)_2Cl_2(Cl_3CPO_3)_2\}$ complex

Trinuclear zinc phosphonates are rare. $[Zn_3Cl_2(3,5\text{-}Me_2Pz)_4(t\text{-}BuPO_3)_2$ (**Figure 10**) is a trinuclear zinc cluster was synthesized using $ZnCl_2$, 3,5-dimethyl pyrazole (3,5-Me_2PzH) and t-butyl phosphonic acid (t-$BuPO_3H_2$) in presence of triethylamine base. Here three Zn-atoms are present in the same plane and each of two phosphonic acid tridentate ligands holds zinc atoms together in a bi-capping mode.[20]

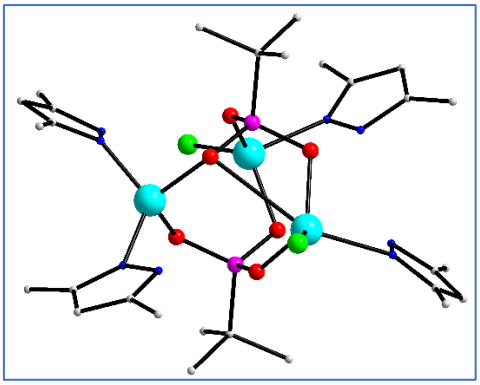

Figure 10: Structure of [$Zn_3Cl_2(3,5\text{-}Me_2Pz)_4(t\text{-}BuPO_3)_2$complex

Several types of tetranuclear zinc phosphonates are known in literature e.g.-planar, D4R, open-book tricyclic, etc.

An Organozinc compound dimethylzinc($ZnMe_2$) reacting with tertiary-butyl phosphonic acid gave a tetranuclear planar zincphosphonate[21] [$\{(ZnMe)_4(THF)_2\}\{t\text{-}BuPO_3\}_2$] (**Figure 11**). In this compound, all the zinc atoms are present in the same plane and two phosphonate ligands are present top and bottom of that plane in a 4.211 binding mode [Harris notation]. In the crystal structure among the two THF molecules, one THF molecule connects each pair of zinc atoms in a bridging mode.

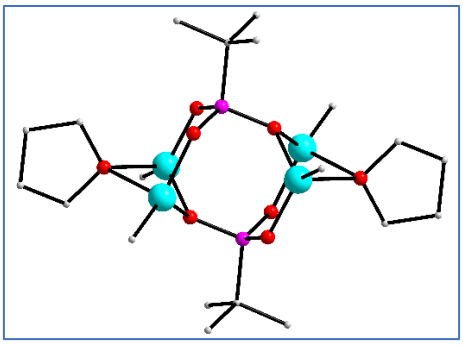

Figure 11: Structure of [$\{(ZnMe)_4(THF)_2\}\{t\text{-}BuPO_3\}_2$] complex

Zeolite-like D4R core containing zinc phosphonate cluster was synthesized from the reaction of $Zn(OAc)_2.2H_2O$, $t\text{-}BuPO_3H_2$, and 2-aminopyridine.[22] In the crystal structure a distorted cube is formed with the presence of Zn and Phosphorous atoms in the alternate corner of a cube. (**Figure 12**) Phosphonate ligands are situated edge of the cube.

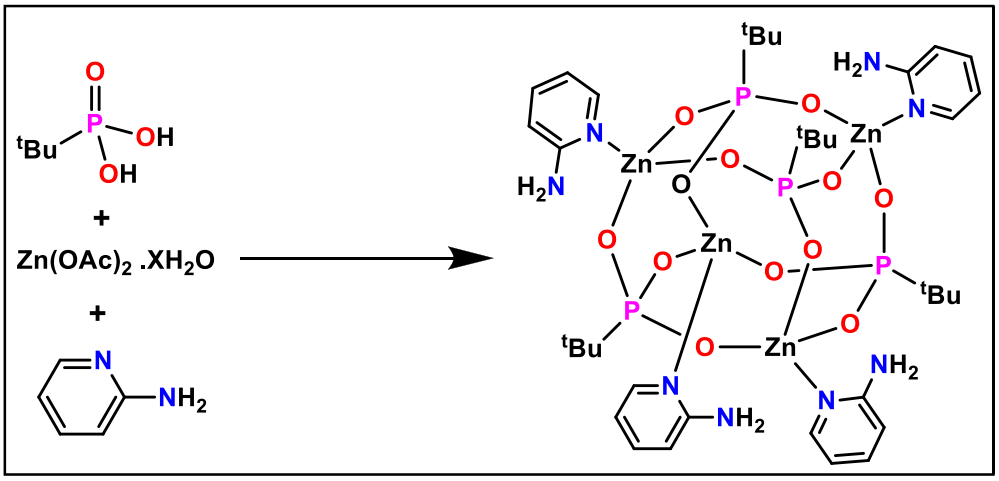

Figure 12: Structure of D4R Zn phosphonate cluster

An open book structure[23] formulated as $[Zn_4(ArPO_3)_2\text{-}\{(ArP(O)_2(OH)\}_2(3,5\text{-}Me_2PzH)_4(3,5\text{-}Me_2Pz)_2]\cdot 5MeOH$ (**Figure 13**) was obtained from a sterically hindered aryl phosphonic acid 2,4,6-i-$Pr_3{-}C_6H_2{-}PO_3H_2$ ($ArPO_3H_2$), using zinc salt $Zn(CH_3CO_2)_2\cdot 2H_2O$ and pyrazole derivative 3,5-Me_2PzH. All the zinc atoms are tetrahedrally coordinated, two phosphonate ligands are holding the center position, and two are present terminally. The central zinc and terminal zinc atoms hold one and two pyrazole ligands respectively.

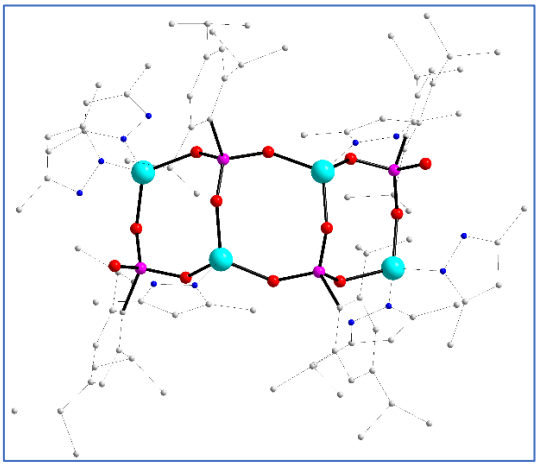

Figure 13: Structure of $Zn_4(ArPO_3)_2\{(ArP(O)_2(OH)\}_2(3,5\text{-}Me_2PzH)_4(3,5\text{-}Me_2Pz)_2]\cdot 5MeOH$ cluster

Zinc phosphonates having pentanuclear structures are not known in the literature.

Hexanuclear zinc phosphate cluster $[\{(ZnEt)_3\text{-}(Zn(THF))_3\}\{t\text{-}BuPO_3\}_4\{3\text{-}OEt\}]$ was synthesized from dimethylzinc and tertiary-butyl phosphonic acid. The crystal structure of the cluster (**Figure 14**) comprises three fully dealkylated zinc and the other three contain ethyl groups each.

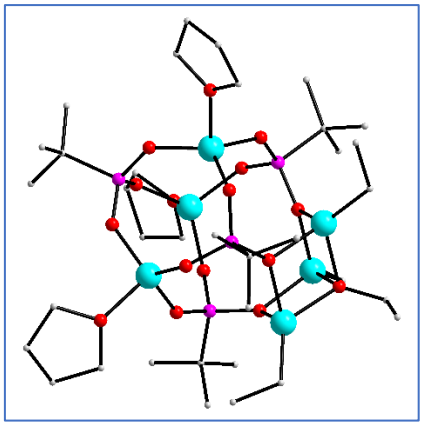

Figure 14: Structure of [{$(ZnEt)_3$-$(Zn(THF))_3$}{t-$BuPO_3$}$_4${3-OEt}] cluster

Under hydrothermal conditions $ZnSO_4.7H_2O$, 2-$C_5H_4NCH(OH)PO_3H_2$[hydroxy(2-Pyridyl) methyl phosphonic acid] and NaOH reacts to form heptanuclear[24] [Zn_7{(2-C_5H_4N)$CH(OH)PO_3$}$_6(H_2O)_6$]$SO_4 \cdot 4H_2O$ (**Figure 15**); a cylindrical drum-shaped zinc phosphonate cluster. The central Zn(II)-ion is surrounded by two Zn_3 subunits. Bridging phosphonate ligands interconnecting with each other by coordination with zinc to form Zn_3 subunits.

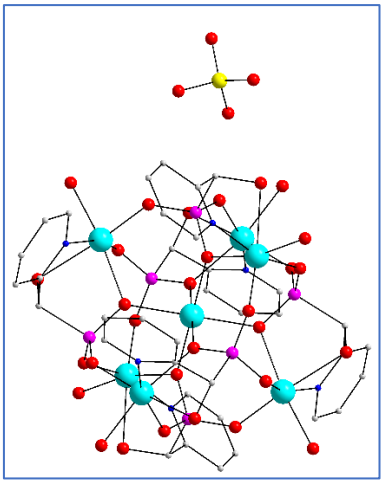

Figure 15: Structure of heptanuclear zinc cluster

An octa-nuclear Zn-phosphonate cage[25], [$Zn_8(Cl)_6${2,3,5,6-$(Me)_4C_6HCH_2PO_3$}$_6(Et_3N)_2(Et_3NH)_2$]·2n-hexane·$3H_2O$ (**Figure 16**) was synthesized using anhydrous $ZnCl_2$, $(Me)_4C_6HCH_2PO_3H_2$, and NEt_3. In the structure, eight Zn(II) ions are enclosed with six [2,3,5,6-$(Me)_4$-$C_6HCH_2PO_3$]$^{2-}$ ligands. The core structure of this compound $Zn_8P_6O_{18}$ has an ellipsoid-shaped, which contains six symmetry-related eight-membered $Zn_2P_2O_4$ rings. Six of the Zn(II) ions have a terminal chloride ligand, while the other two Zn(II) ions are bound to neutral triethylamine ligands.

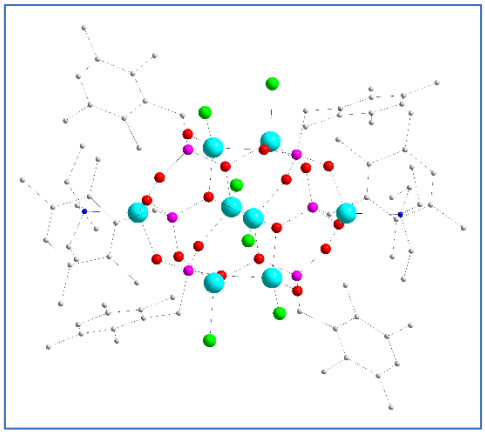

Figure 16: Structure of an octa-nuclear zinc cluster

Hydrothermally $Zn(OAc)_2$ and phosphonic acid ligand 1-$C_{10}H_7$–$CH_2N(CH_2CO_2H)(CH_2PO_3H_2)$ (H_3L), reacts to form a nonanuclear cluster[26] $[Zn_9(L)_6(H_2N(CH_2)_2NH(CH_2)_2NH(CH_2)_2NH_2)_2]\cdot 18H_2O$. Among these nine Zn atoms, two Zn atoms Penta-coordinated through carboxylate coordination. Phosphonates play an important role to make a heptanuclear motif.

The highest homonuclear zinc phosphonate cluster is dodecanuclear[27].

(iii) Phosphate clusters:

Phosphates are ligands prepared from phosphoric acid (H_3PO_3). Phosphoric acid has three acidic protons when the hydroxyl group of the phosphoric acid is replaced with one or two alkyl/aryl groups it forms mono and diester of phosphoric acid respectively, ((**OR**)**P**(**O**)(**OH**)$_2$) and ((**OR**)$_2$**P**(**O**)(**OH**)). The phosphoric acid diester ((**OR**)$_2$**P**(**O**)(**OH**)) is at some point very similar to carboxylic acid (**R$_2$COOH**) (but diverse in another way also). Like carboxylic acid, it forms mononuclear and di-nuclear complexes more readily than larger molecular clusters. For carboxylic acid chelating mode is common but in the case of the diester of phosphoric acid, it is absent. Bridging coordination mode is more common for diester phosphates. Several cases are there where the presence of phosphate diesters is monodentate through **P-O$^-$** group and remaining uncoordinated **P=O** dangling to form secondary interaction (through H-bonding). On the other hand, phosphate monoesters due to the presence of more coordinating sites tend to form larger molecular clusters. Similarly, phosphonic acid monoester phosphates can also use to model as building units of zeolitic structures. Phosphoric acid and phosphinic acids are comparable in framework to the phosphate monoester and diester respectively, with only extra oxygen present in between the alkyl/aryl and phosphorous atom. (**Figure 17**)

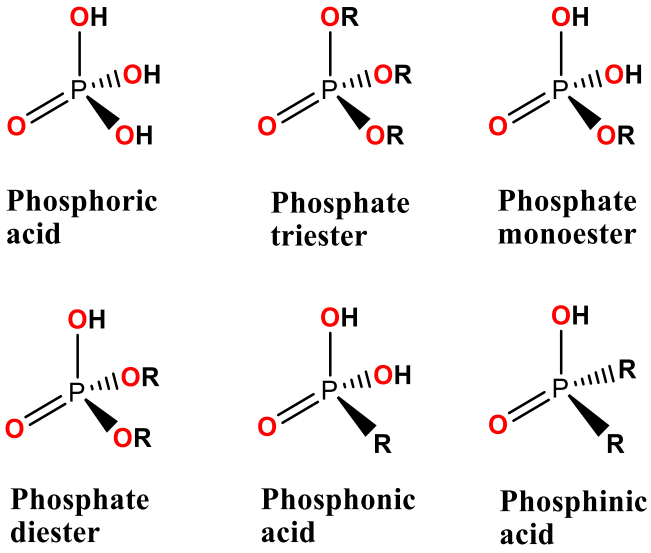

Figure 17: General structure of phosphonic acid, phosphinic acid, and phosphate esters

In 1998 Vahrenkamp et. al. prepared[28] monophosphate of zinc by hydrolytic cleavage of phosphate esters using sterically crowded tripod ligand tris(pyrazolyl)borate-zinc hydroxide with phosphate esters, where zinc atom is surrounded by tetrahedrally with tripodal tris(pyrazolyl)borate and phosphate ester. (**Figure 18**)

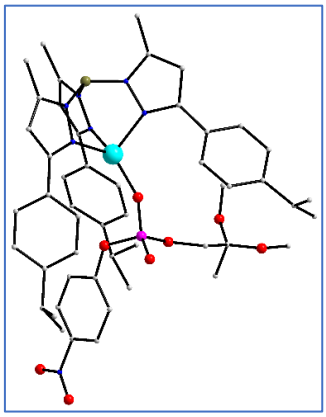

Figure 18: Structure of a mononuclear zinc phosphonate ester complex

An example of a binuclear zinc complex was synthesized by Meyer and co-workers in 2004.[29] They used pyrazole templated di-nucleating ligand, zinc perchlorate hexahydrate, and phosphoric acid dimethyl ester as a molecular precursor. Two zinc atoms are Penta-coordinated, and phosphate diester is bridged between the two zinc atoms. (**Figure 19**)

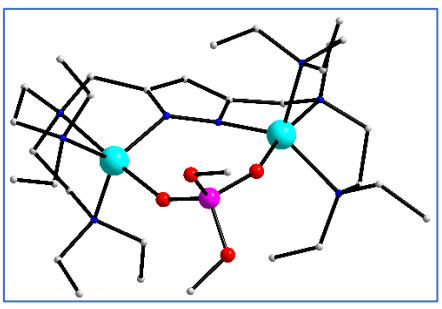

Figure 19: Structure of a dinuclear zinc phosphate cluster

$[Zn_2\{(L_3S)_2Zn\}\{dpp\}_4]$ (**Figure 20a**) ((L_3SH)= bis(3,5-dimethylpyrazolyl)(1-methyl-1-sulfanylethyl)methane)), a trinuclear zinc phosphate, reaction with $[Zn(L_3S)(CH_3)]$ and diphenyl phosphate by Carrano et al.[30] The crystal structure of the compound contains one hexacoordinated and two tetracoordinate zinc ions. In the structure, two tetracoordinate zinc atoms are bridged by two diphenyl phosphate anions. This dimeric Zn_2 -unit is connected to the six coordinated zinc through two thiolate anions. Kimura et al.[31] reported an interesting example of trinuclear complex $[Zn(cyclen)_3(\mu_3\text{-npp})](ClO_4)_4$ (**Figure 20b**) where each zinc atom is surrounded by a distorted tetragonal-pyramidal geometry with one O-atom of *p*-nitrophenyl phosphate and four cyclens N-atoms.

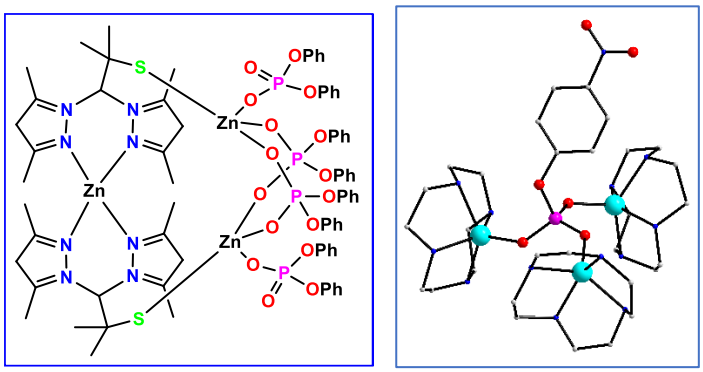

Figure 20: (a) Structure of $[Zn_2\{(L3S)_2Zn\}\{dpp\}_4]$ complex **(b)** Structure of $[Zn(cyclen)_3(\mu_3\text{-npp})](ClO_4)_4$ complex

Tetranuclear zinc phosphate cluster; $[Zn_4(\mu_4\text{-O})(dtbp)_6]$ (**Figure 21**) was prepared by Murugavel et. al.[32] Here $Zn(OAc)_2$ and di-*tert*-butyl phosphate (dtbp-H) reacts together toward getting the tetranuclear zinc phosphate cluster. The same product was synthesized by Tilley et. al. They used organo-zinc starting material ($ZnEt_2$) with dtbp-H which yields an insoluble polymeric compound $[Zn(dtbp)_2]_n$. In presence of a slight amount of water, they obtained the same tetranuclear zinc cluster.[33]

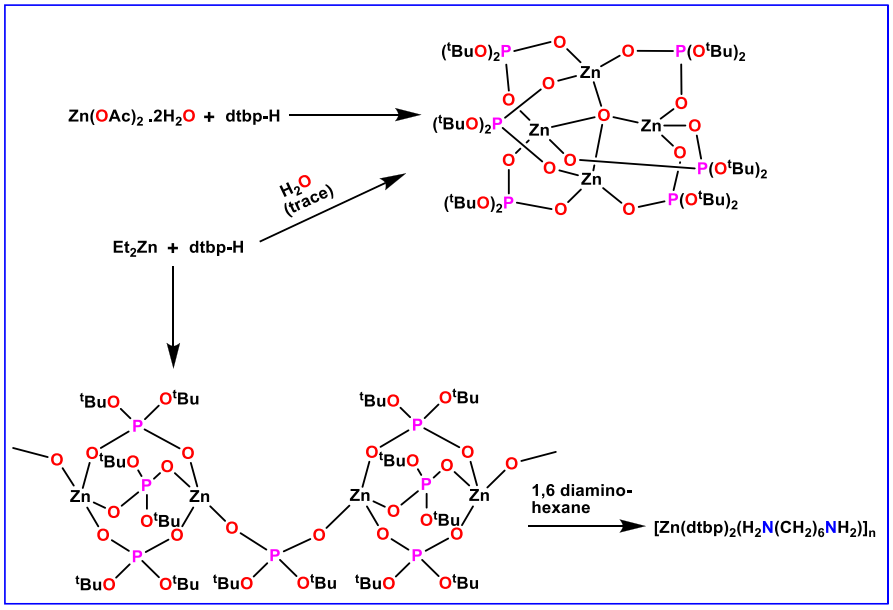

Figure 21: Synthesis of tetranuclear zinc phosphate cluster

Murugavel et. al. also synthesized zinc phosphate as cubic core clusters, $[Zn_4(ROPO_3)_4L_4]$ (R = 2,6-diisopropylphenyl, (L = methanol / 2,4,6-trimethylpyridine/ 2-aminopyridine/ -hydroxy pyridine/ 4-(hydroxymethyl)pyridine).(**Figure 22**) The crystal structure of these looks like the D4R (double four ring) SBU (secondary building unit) of zeolites. With the use of appropriate ligands, it can form 1D, 2D, and 3D supramolecular networks through the non-covalent interaction of the $-NH_2$, -NH, or -OH groups present on the surface of the molecular structure.[34]

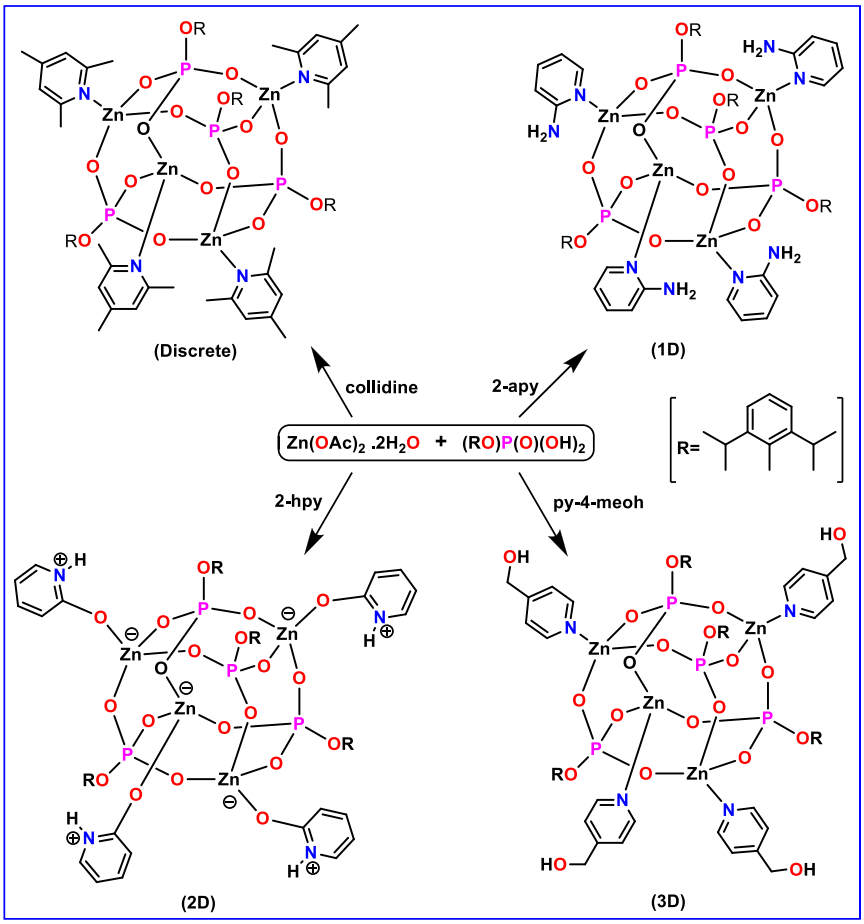

Figure 22: Synthesis of D4R zinc phosphate cubic clusters

(iv) Schiff-base clusters:

Transition metal Schiff base complexes have great potential applications in many fields, for instance, fluorescence, catalytic activity, adsorption, magnetic materials, biological mimicking, and sensors. Schiff bases are a good candidate to construct multinuclear complexes due to their flexible coordination capacity. It is a widely used ligand due to its simple synthesis, and excellent physical, chemical, and biological properties. There is a large number of molecular clusters of zinc reported in the literature, few of these examples are described here.

Zinc Schiff base mononuclear complexes are very much useful as a model of zinc metalloenzymes in bioinorganic chemistry. The various coordination number containing hydroxy-rich zinc complexes was synthesized by Mishtu Dey et al. in 2002.[35] They synthesized four, five, and six coordinated Zn (II) compounds of a hydroxy group-containing Schiff base complex. (**Figure 23**) Among these complexes, five coordinated water-bound complex shows enhanced hydrolysis rate of para-nitrophenyl acetate (pNPA) similar activity to zinc hydrolytic enzymes.

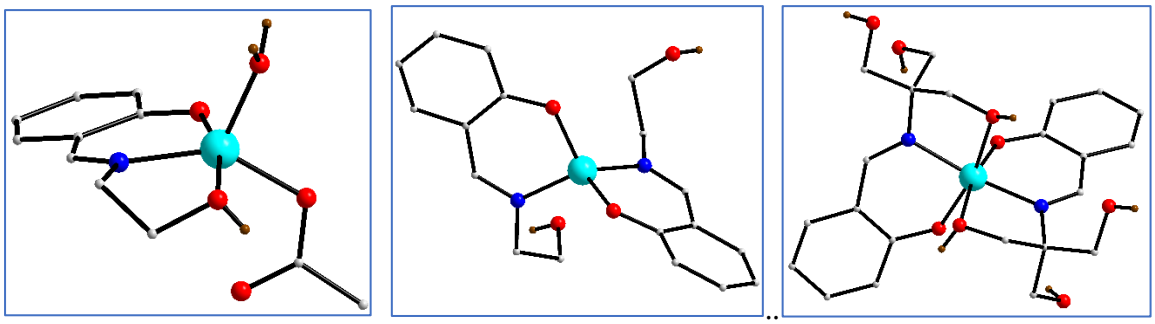

(a) **(b)** **(c)**

Figure 23: Structures of mononuclear zinc Schiff-base clusters

Yan Zao et al. in 2018 a dinuclear Zn complex was synthesized using Schiff-base derived from salicylaldehyde and 2-amino-2-ethyl-1,3-propanediol.[36] They have reacted zinc acetate methanolic solution(10ml) to a methanol/acetonitrile (10:3ml) solution of the ligand at room temperature for 4h. then filtered the solution and from the filtrate needle-like yellow-colored crystal was characterized by single-crystal X-ray analysis. In the crystal structure, both the Zn(II) ions are distorted square pyramidal. (**Figure 24**) From the acetate anions, Zn-O bond length indicates one Zn-O bond is weaker than the other. The unprotonated alkoxy group of the Schiff-base and the uncoordinated carboxyl oxygen atom has O-H---O hydrogen bonding interaction which leads to supramolecular network interaction.

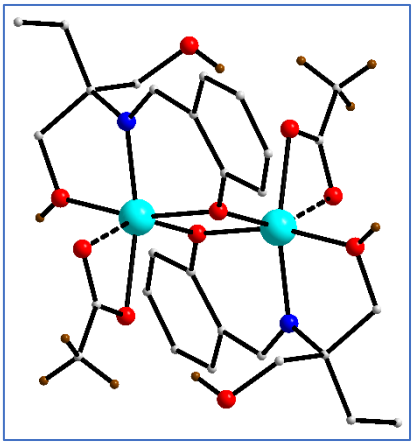

Figure 24: Structure of dinuclear zinc Schiff-base cluster

One more example of a di-nuclear Zn_2-complex was reported by O. Tsave et al.[37] They synthesized three sets of di-nuclear complexes using a different number of hydroxy-rich Schiff-base ligands. For all the cases two types of coordinating Zn(II) environments are present, distorted octahedral and distorted trigonal bipyramidal. (**Figure 25**)

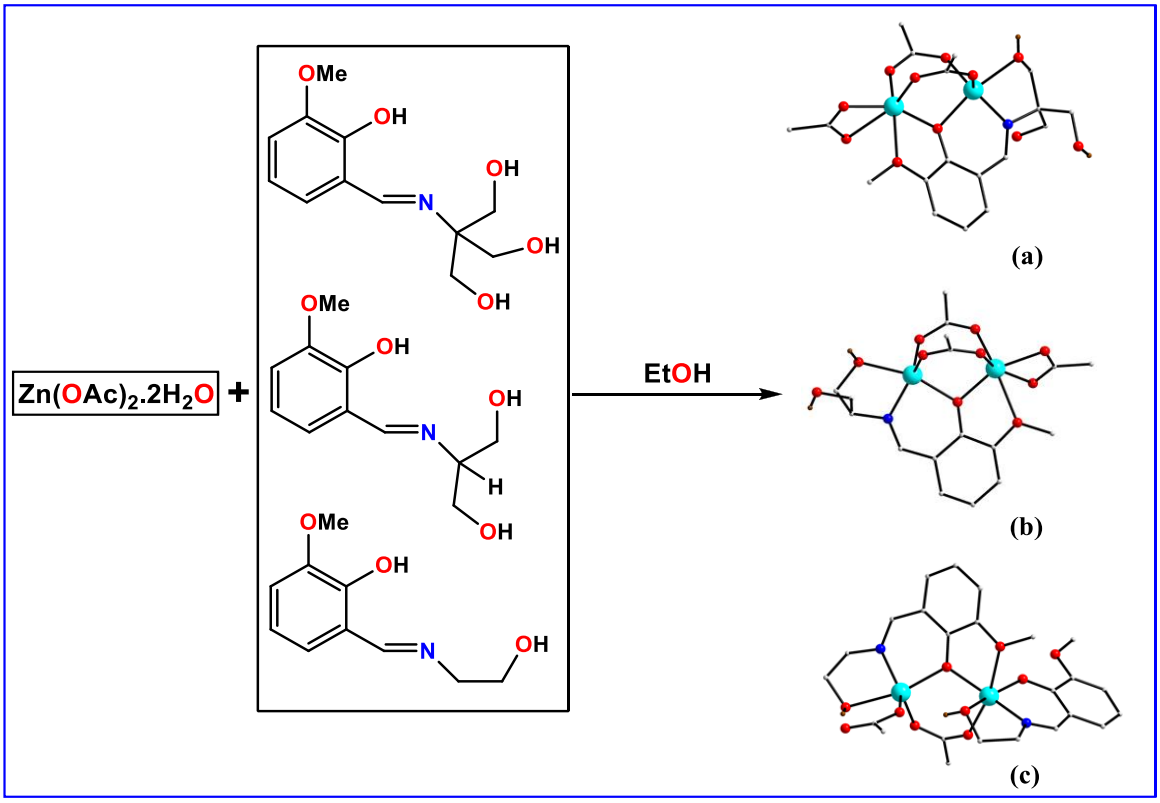

Figure 25: Structures of dinuclear zinc and polyhydroxy Schiff base complexes

Meiqi Liu et al. reported[38] a Zn-Schiff base compound from a Schiff-base of glycine and o-vanillin. $Zn(OAc)_2.2H_2O$, Schiff-base, and phenanthroline were used in a stoichiometric ratio of 1:2:1. The molecular structure has two Zn(II)-ions in five-coordinated distorted trigonal bipyramidal and hexacoordinated distorted octahedral geometry respectively. (**Figure 26**)

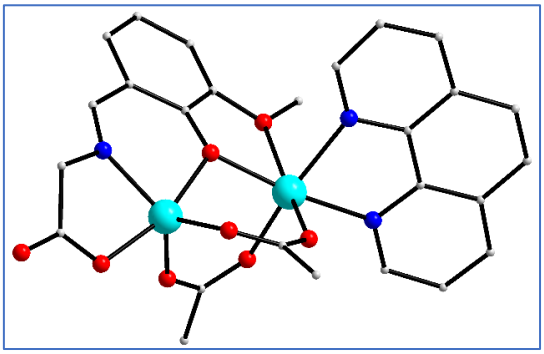

Figure 26: Structure of dinuclear zinc Schiff-base complex

A Zn(II)-Schiff base trinuclear cluster was reported by Bhaskar et al. in 2014.[39] They have synthesized zinc trinuclear complex with $Zn(OAc)_2 .2H_2O$ and pre-synthesized Schiff-base using ortho-vanillin and o-aminophenol condensation. The geometry of the trinuclear complex is an almost linear arrangement (angle Zn1-Zn2-Zn1* =150.3°). Terminal and central, both zinc atoms are formed in a distorted octahedral geometry. (**Figure 27a**)

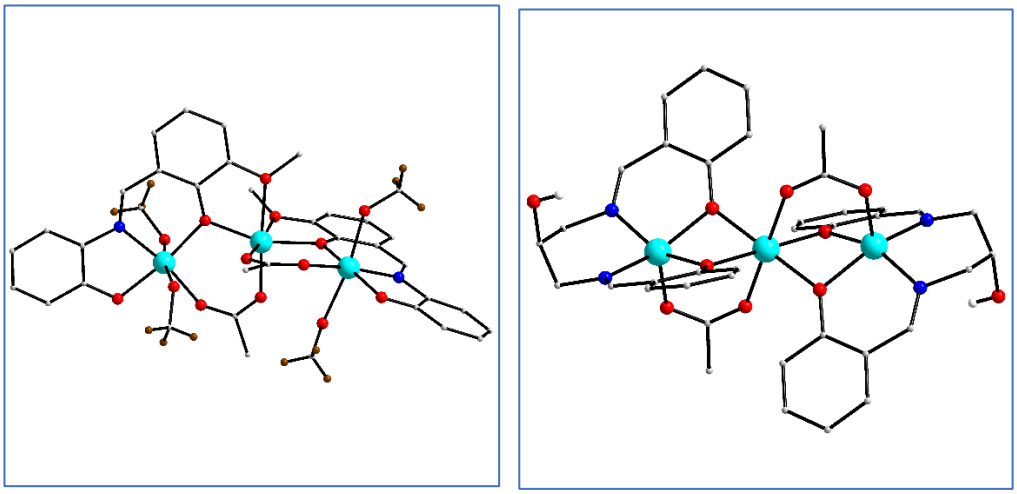

(a) **(b)**

Figure 27: Structure of trinuclear zinc Schiff base clusters

In the same year from the same group, trinuclear Zn(II)-Schiff base complex (perfectly linear) was synthesized.[40] They used salen-type Schiff-base ligand, N,N'-bis(salicyaldehydene)-1,3-diaminopropan-2-ol. $Zn(OAc)_2 .2H_2O$, Schiff-base in molar ratio 2:3 used to prepare the trinuclear complex in methanol-DMF mix-solvent. **(Figure 27b**) Single crystal X-ray analysis reveals that it crystallizes with the P-1 space group, the center of inversion lying on the middle Zn-atom of the trinuclear complex. Two terminal Zn(II)-ions are SP(square pyramid) geometry and the central zinc atom is described as distorted O_h (octahedral) geometry.

Yan Zhao et al.[36] reported two isostructural linear trinuclear Schiff-base complexes terminal two zinc atoms are in between trigonal-bipyramidal(TBP) and square pyramidal(SP) geometry and the central Zn(II)-ion is octahedrally coordinated. (**Figure 28**) In both, the cases Schiff-base ligand connecting two adjacent Zn centers μ_2: η^1: η^1: η^1 coordination mode and reinforcing them to stay connected in a stable linear trinuclear arrangement.

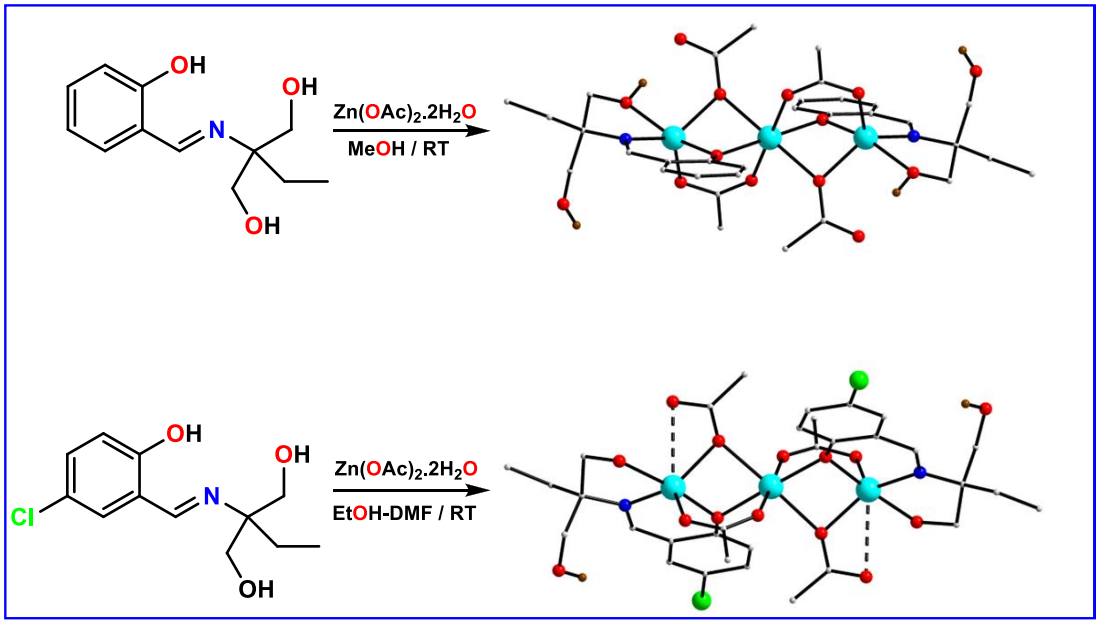

Figure 28: Synthesis of linear trinuclear zinc Schiff base clusters

A novel linear tetranuclear zinc Schiff base cluster was synthesized by M. Mikuriya et al. in 2001.[41] They synthesized the compound by using Schiff base 1,3-Bis(salicylideneamino)-2-propanol (H_3salpro), zinc perchlorate and co-ligand pyrazole(Hpz) in molar ratio 0.5:1:1.5 in methanol solvent. An interesting feature of this molecule is the geometrical arrangement of the zinc atoms as square-pyramidal-tetrahedral and tetrahedral. (**Figure 29**) Pyrazole acts as a bridging ligand for the central Zn(II) and coordination saturation of the terminal square-pyramidal Zn(II)-ions.

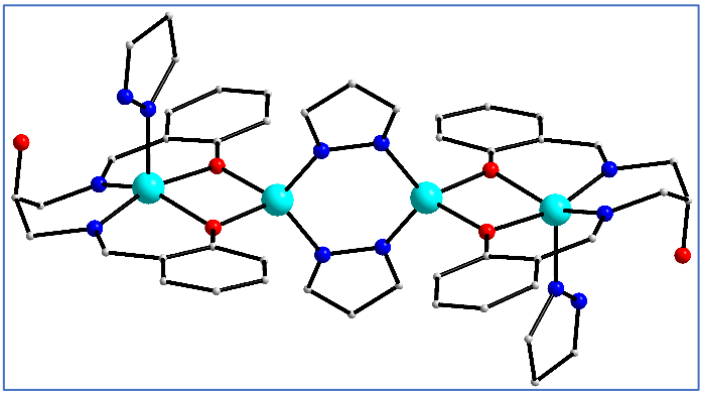

Figure 29: Synthesis of tetranuclear linear zinc Schiff base cluster

W. Sun et al. reported in 2014[42] two tetranuclear zinc Schiff-base different topological structures using different substituents containing Schiff-base ligand (**Figure 30**). Single crystal X-ray analysis reveals the formation of a linear tetranuclear cluster and another, a square-planar tetranuclear cluster. In the linear structure Zn(II)-ion adopts highly distorted tetragonal-pyramid geometry and for the square planar case distorted trigonal-dipyramidal coordination geometry.

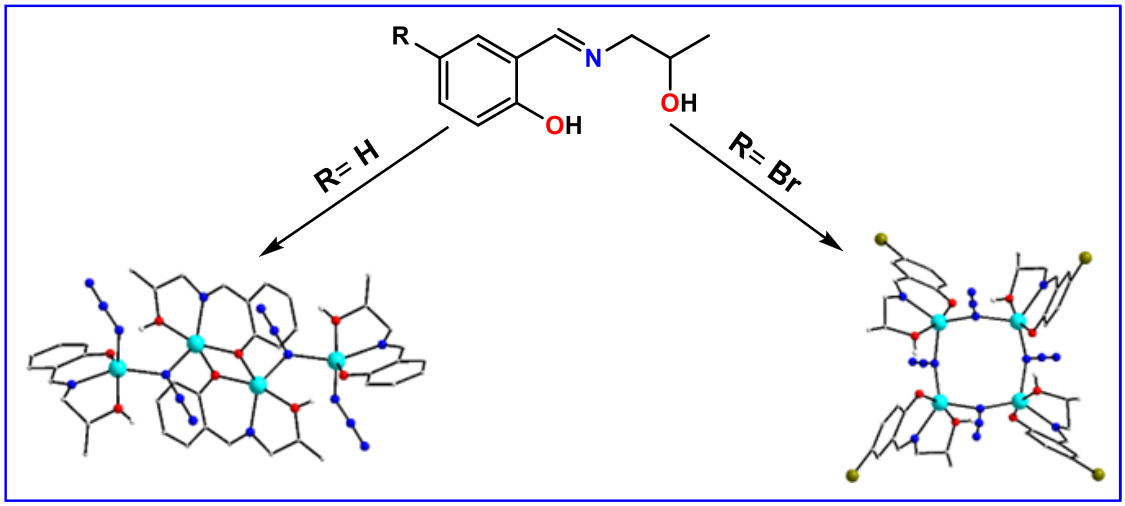

Figure 30: Synthesis of tetranuclear zinc Schiff base clusters

Another linear tetranuclear zinc Schiff-base cluster was reported by Q. Shi et al.[43] where two salen-zinc, $[Zn_2(L)(OAc)]$ (L=N,N′-bis(salicylidene)cyclohexane-1,2- diamine)) subunit are bridged by hydroxo-ion and acetate anion in a μ_2 manner. All the zinc atoms are existing in distorted square planar (SP) geometry. (**Figure 31a**) L. Jiang et al. synthesized[44] an M_4O_4 core containing a common face shared defective di-cubane structure with two missing vertices (**Figure 31b**) Poly Schiff-base ligand N,N′-bis(3-methoxysalicylidene)-1,3-diamino-2-propanol was used to prepare the tetranuclear zinc Schiff-base cluster.

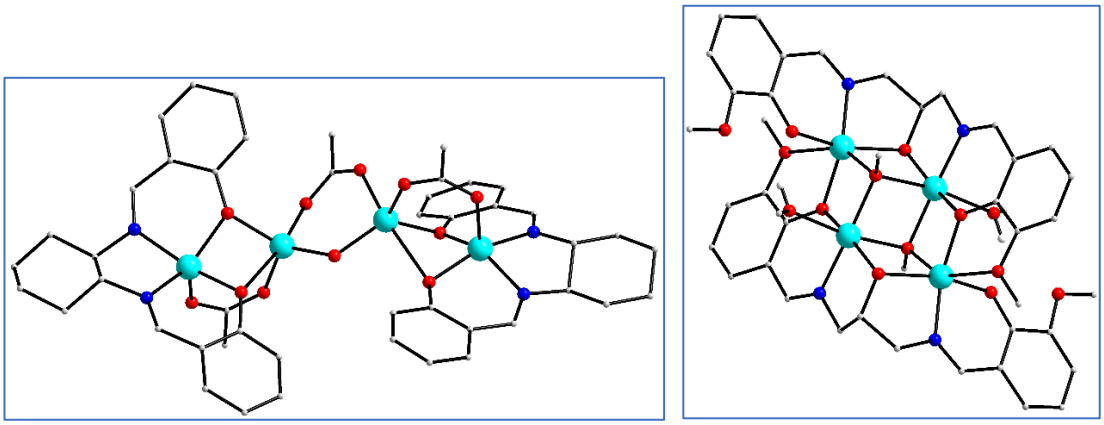

(a) **(b)**

Figure 31: Synthesis of tetranuclear zinc Schiff base clusters

Similar Zn(II)-tetranuclear arrangement structure was synthesized by M. Garai et al.[45] **(Figure 32a)** SCXRD reveals that all the Zn-atoms are octahedrally coordinated

S. Ghosh et al. reported[46] a tetranuclear cubane-like core structure $[Zn_4O_4]$. Diethylzinc ($ZnEt_2$) and Schiff-base ligand has taken as a molecular precursor in a 1:1 ratio for the reaction and toluene as a solvent for 12 h at 23 °C. From single-crystal X-ray analysis, it is clear that among all the crystal structures only dibromo-substituted ligand containing tetranuclear complex forms one open ring

tetranuclear cubane-core. (**Figure 32b**) Zinc atoms adopt square-pyramidal coordination geometry for all cases.

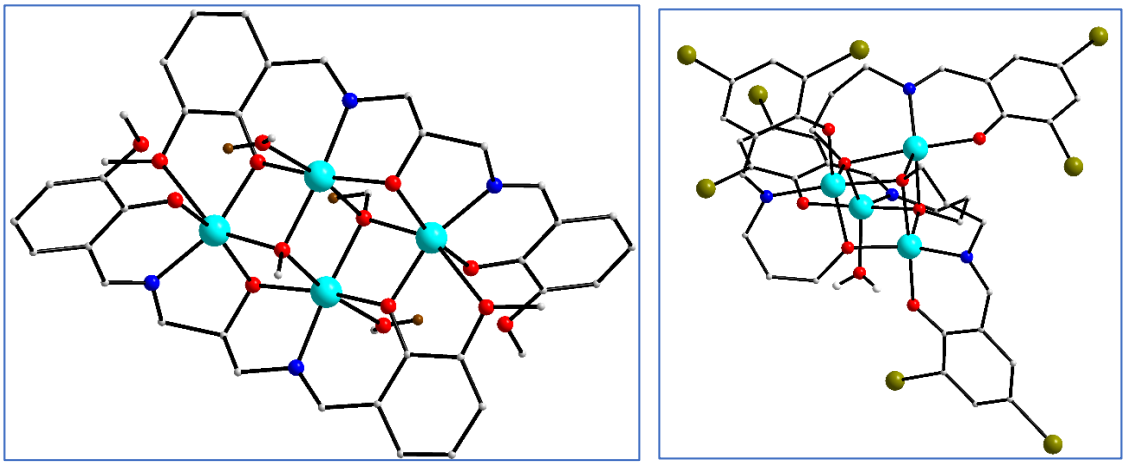

(a) **(b)**

Figure 32: (a) Synthesis of defective di-cubane and **(b)** cubane zinc Schiff base cluster

Interestingly two chiral enantiomeric novel clusters of tetranuclear zinc, formulated as, R-$[Zn_4(HL)_2(L)_2(CH_3OH)_2](NO_3)_2$ **(Figure 33(b))**and S-$[Zn_4(HL)_2(L)_2(CH_3OH)_2](NO_3)_2$ was reported by H. Yu et al.[47] They have used a chiral ligand R/S-H_2L (H_2L=2-[(1-benzyl-2- hydroxy-ethylimino)-methyl]-6-methoxy-phenol) (**Figure 33(a)**) to synthesized this clusters. SCXRD data indicate that zinc atoms present in the cluster have adopted two types of coordination modes; distorted square-pyramidal, and distorted octahedral geometry. The structural core of the cluster forms a Zn_4O_4 boat-shaped skeleton. (**Figure 33(c)**)

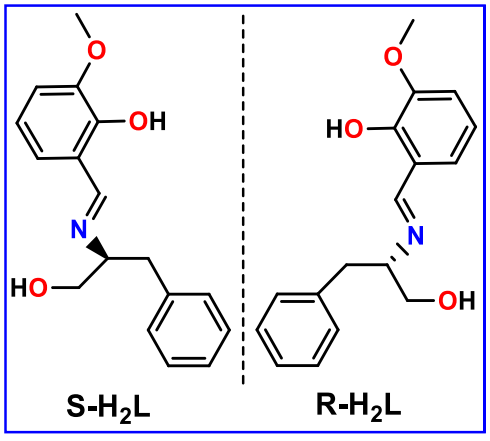

(a)

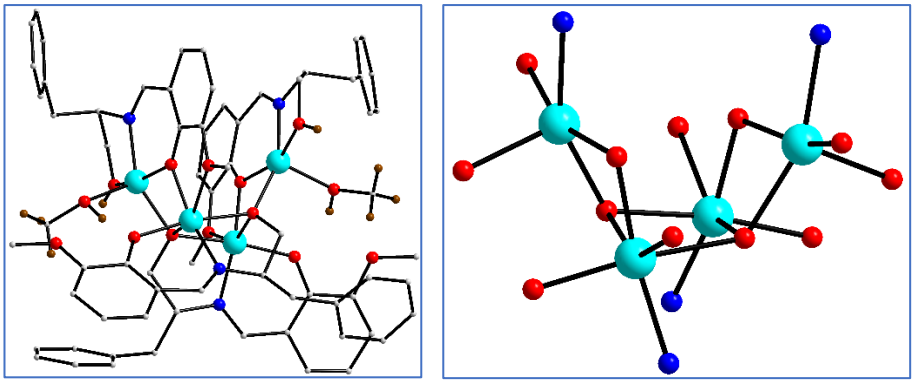

(b) **(c)**

Figure 33: (a) Chiral Schiff base 2-[(1-benzyl-2- hydroxy-ethylimino)-methyl]-6-methoxy-phenol **(b)** Structure of (R)-$[Zn_4(HL)_2(L)_2(CH_3OH)_2](NO_3)_2$ **(c)** Core structure of (R)-$[Zn_4(HL)_2(L)_2(CH_3OH)_2](NO_3)_2$

P. Ghorai et al. reported[48] another different type of tetranuclear Zn(II)-Schiff base cluster with corner defective cubane structure using Schiff-base (E)-2-methoxy-6-((quinolin-8-ylimi-no)methyl)phenol. (**Figure 34a**) Single-crystal X-ray analysis shows that a core structure of cluster three zinc atoms is hexacoordinated O_h geometry and one zinc atom is highly distorted trigonal bipyramidal geometry. **(Figure 34b)**

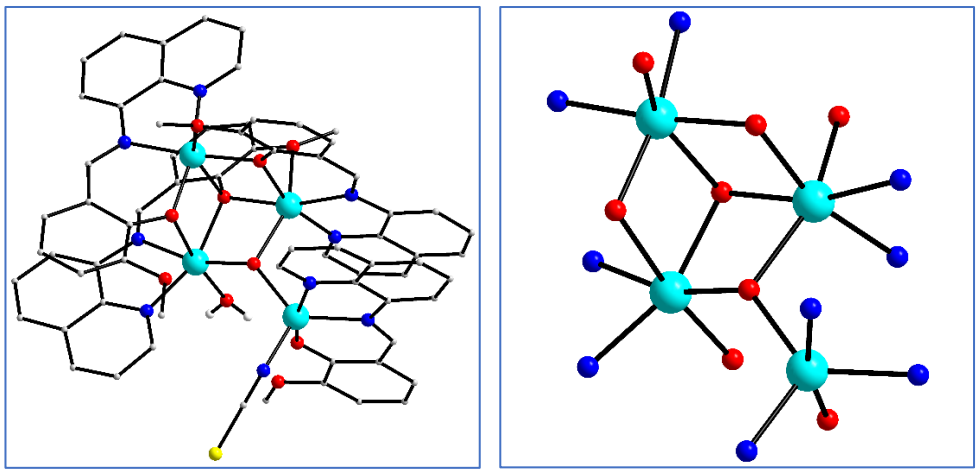

(a) **(b)**

Figure 34: (a) Structure of corner defective tetranuclear zinc Schiff base cluster **(b)** Core structure of the defective tetranuclear cluster

E.C. Constable et al. reported[49] a pentanuclear Zn(II)-Schiff-base cluster $2\{[Zn_5(L)_5(MeOH)(OH_2)]\}.6MeOH.H_2O$ (**Figure 35**) (**L=** 2-Ethoxy-6-(((2-hydroxyphenyl)imino)methyl)phenol) as a minor product. It was obtained self-assembly of $ZnCl_2$ and ligand (L) in basic condition mix solvent DCM/MeOH. SCXRD shows that in the moiety three zinc atoms are six coordinated (O_h geometry) with O_5N coordination sphere and two Zn (II)-ions are penta coordinated with O_4N coordination sphere. Among the two penta-coordinated Zn(II)-metal ions one

adopts square pyramidal geometry and the other is in-between SP and TBP geometry. $\{Zn_5(\mu\text{-}O)_3(\mu_3\text{-}O)_3\}$-motif is the first reported in discrete molecule cluster at that time.

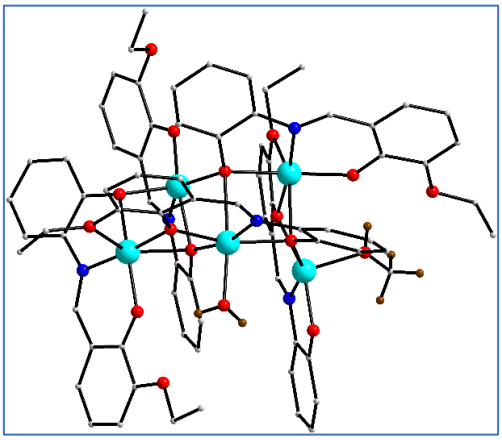

Figure 35: Structure of $\{[Zn_5(L)_5(MeOH)(OH_2)]\}$ cluster

Using an inflexible-conjugated bis-Schiff-base ligand N,N-bis(3-ethoxysalicylidene)hydrazine (H_2L) self-assembled pentanuclear zinc complex $[Zn_5(L)_2(OAc)_6(H_2O)_2]$ (**Figure 36a**)was synthesized E. Liu et al.[50] SCXRD discloses that central zinc atoms are perfectly octahedrally coordinated with ZnN_2O_4 core environment and besides the central metal atom two zinc atoms are distorted octahedral coordination with NO_5 core environment. The terminal two zinc atoms are tetra-coordinated with the ZnO_4 core.

N. Hari et al.[51], a new type of Zn_5-core containing Schiff-base complex $[Zn^{II}_5(HL)_2(\mu_3\text{-}OH)_2(NO_3)_4]$ (**Figure 36b**) was synthesized. X-ray structure analysis shows that two ligand molecule forms a tetranuclear Zn_4 fragment, to which one more Zn(II)-ion is dangling and connected the Zn_4 fragment with two alkoxide oxygen atom of the two Schiff-base ligands. Four zinc atoms are present as distorted square-pyramidal and one zinc atom is in a distorted tetrahedral geometry.

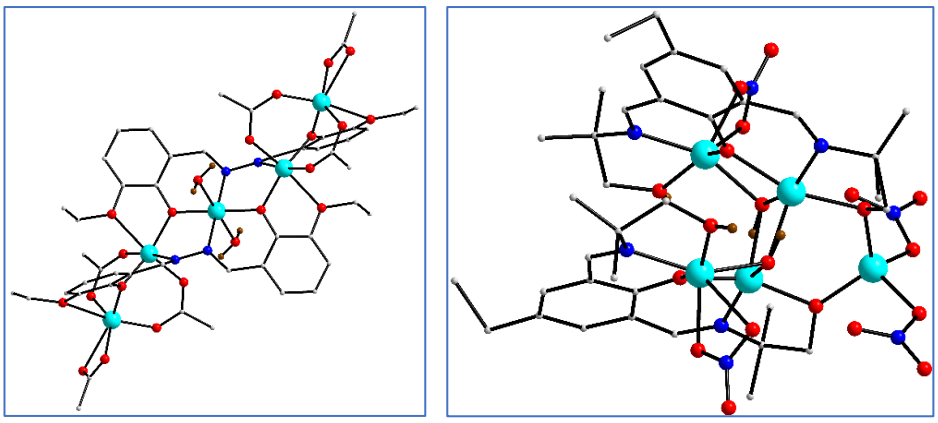

(a) **(b)**

Figure 36: (a) Structure of $[Zn_5(L)_2(OAc)_6(H_2O)_2]$ cluster and **(b)** Structure of $[Zn^{II}_5(HL)_2(\mu_3\text{-}OH)_2(NO_3)_4]$ cluster

E. C. Constable et al. reported[49] a hexa-nuclear Zn(II)-Schiff-base cluster $[Zn_6(L)_4Cl_2(OH)_2(OH_2)_2]$ (where H_2L=2-Ethoxy-6-(((2-hydroxyphenyl)imino)methyl)phenol). (**Figure 37a**) Two hexacoordinated octahedral ZnO_5N environments and four penta-coordinated by ZnO_5N and ZnO_4Cl are present in the crystal structure.

Another Hexa-nuclear Zn(II)-Schiff-base cluster reported by S.K. Kushvaha et al.[52] They have synthesized $[Zn(II)_6(L\text{-}Me)_6(MeOH)_2]\cdot 12MeOH$ (**Figure 37b**) at room temperature with two equivalent $ZnCl_2$ salt and one equivalent Schiff-base ligand in methanolic solution. SCXRD analysis reveals that four Zn(II)-ions are hexacoordinated and two are penta-coordinated.

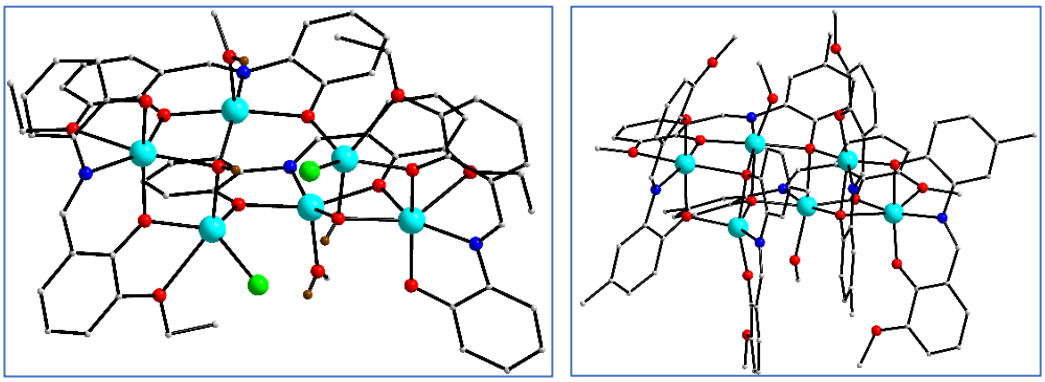

(a) **(b)**

Figure 37: (a) Structure of Hexa-nuclear zinc Schiff base cluster $[Zn_6(L)_4Cl_2(OH)_2(OH_2)_2]$ **(b)** Structure of Hexa-nuclear $[Zn(II)_6(L\text{-}Me)_6(MeOH)_2]\cdot 12MeOH$ clusters

Using three different Schiff-base ligands (**Figure 38**) similar disk-type core heptanuclear zinc Schiff-base cluster was synthesized.

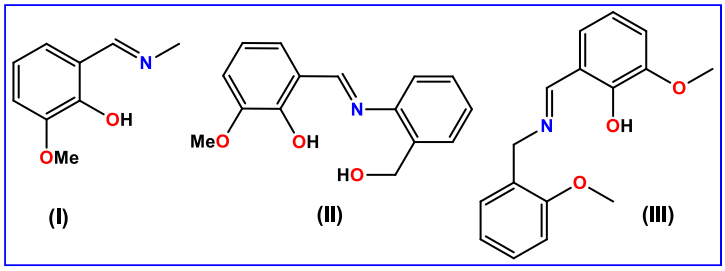

Figure 38: Schiff base ligands

S. H. Zhang et al. reported[53] a heptanuclear disc-shape cluster $[Zn_7(OH)_6(mimmp)_6](NO_3)_2$ (where mimmp= anion of 2-methoxy-6-methyliminomethyl-phenolic)(**Figure 39a**). It was synthesized using the solvothermal synthesis method in a microwave reactor. SCXRD shows that six zinc atoms are planar and inside this, a Zn-ion is situated forming a heptanuclear disc-like arrangement. The central Zn (II)-ion is positioned in a slightly distorted octahedral geometry and connected with the six Zn-metal ions with six μ_3-hydroxide bridges. All the six terminal Zn atoms are present in a distorted octahedral $ZnNO_5$ environment, and the core zinc atom has a ZnO_6 octahedral environment.

H. Zhang et al. synthesized[54] similar disk-shaped $\{Zn^{II}_7\}$ core polynuclear Zn(II)-Schiff-base cluster $[Zn_7L_6](NO_3)_2{\cdot}2CH_3OH$. (**Figure 39b**) 2-(2-hydroxy-3- methoxybenzylideneamino)phenol} (H_2L) was used to synthesize the molecular cluster under solvothermal conditions. Interestingly they have used $Gd(NO_3)_3.6H_2O$ as a source of counter ion nitrate even though no gadolinium ion is present in the product crystal structure. From different optimization, they concluded that the gadolinium ion helps the formation of the cluster. Single crystal X-ray analysis reveals a contradiction with the disk-like cluster reported by S.H.Zhang et al.[53], central zinc atoms and the six peripheral zinc atoms are linked by six μ_3-oxo bridges and six Zn(II)-ions present on the rim of the disk-like shape structure interlinked between them by μ_2-oxo bridges in a pairwise manner.

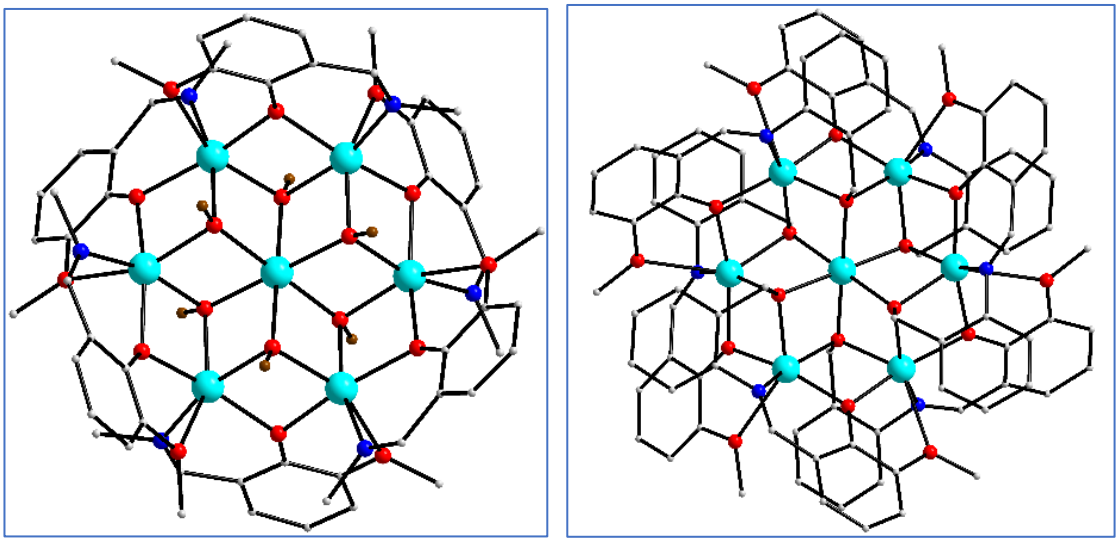

(a) **(b)**

Figure 39: (a) Structure of heptanuclear disc-like cluster $[Zn_7(OH)_6(mimmp)_6](NO_3)_2$ **(b)** Structure of heptanucler disk like $[Zn_7L_6](NO_3)_2{\cdot}2CH_3OH$ cluster

R. Gheorghe et al. reported[55] another similar disk-shaped heptanuclear Schiff-base cluster $[Zn_7L_6(\mu_3\text{-}OCH_3)_6](ClO_4)_2$ (**Figure 40**) using o-vanillin base Schiff-base, N-(2-hydroxy-3-methoxy-benzylidene)-2-methoxy-benzylamine (HL). Single crystal X-ray analysis shows that in comparison with the reported disk-like structure reported earlier the rim Zn(II)-ions and the central Zn(II) are connected with six μ_3-oxo bridges of methoxide(OMe anion).

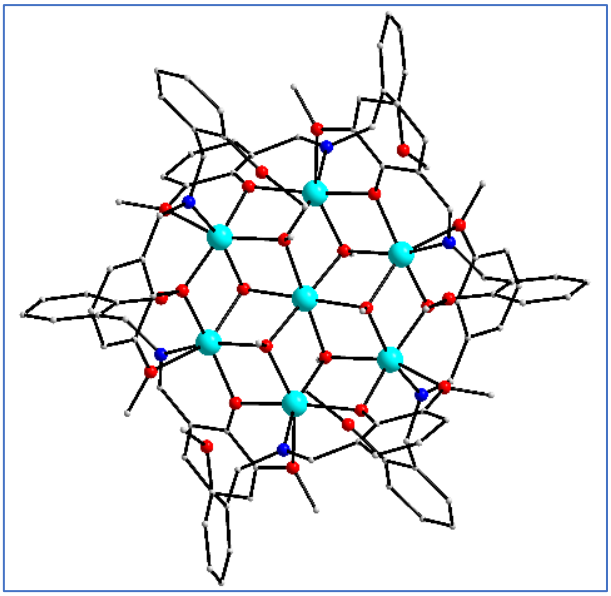

Figure 40: Structures of disk-shaped heptanuclear Schiff-base cluster $[Zn_7L_6(\mu_3\text{-}OCH_3)_6](ClO_4)_2$

J. Sanmartin et al. reported an unusual self-assembled pseudo-tetrahedral core Zn_8O_{13} containing Zn(II)-Schiff-base cluster[56] $[Zn_8(L)_4(H_2O)_3]\cdot H_2O\cdot 0.25MeCN$ was reported. (**figure 41a**) where [H_4L = N,N'-bis(3-hydroxysalicylidene)- 1,4-diaminobutane] was used as a tetra-protonated ligand to assembly the cluster where in all the Zn(II)-ions are penta-coordinated distorted environment. The SCXRD data shows that four ligand molecules assemble the Zn(II)-ions in a pseudo-tetrahedral arrangement with thirteen μ-phenoxo bridges. (**figure 41b**) The other four inner Zn-metal atoms lay on four tetrahedral edges forming a square. The Zn-atoms in the cluster are present in a perfect trigonal-bipyramidal, distorted trigonal-bipyramidal, and distorted square-pyramidal environment.

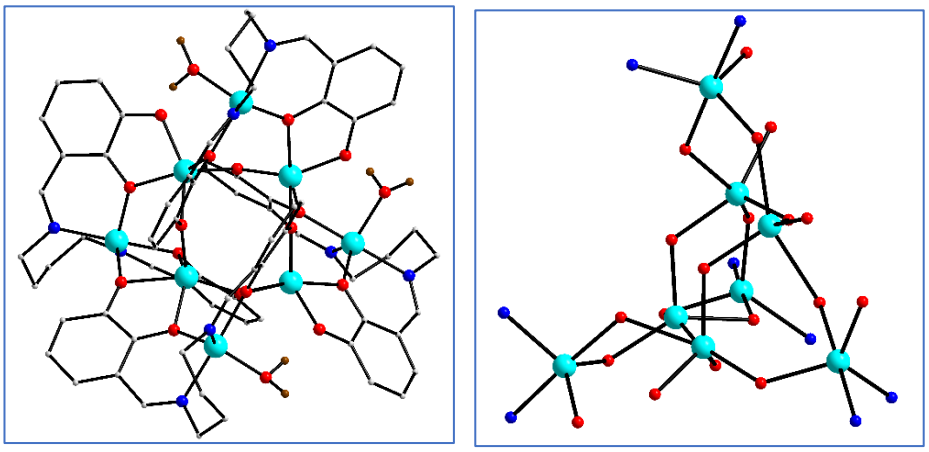

(a) **(b)**

Figure 41: (a) Structure of octa-nuclear zinc Schiff base cluster $[Zn_8(L)_4(H_2O)_3]\cdot H_2O\cdot 0.25MeCN$ **(b)** Core structure of $[Zn_8(L)_4(H_2O)_3]\cdot H_2O\cdot 0.25MeCN$

(b) Cd-related clusters:

(i) phosphinic acid clusters:

Most of the reported metal phosphinates are formed in polymeric[57]. Depending on the structure of phosphinic acid ligands 1D, 2D, and 3D structures form. Using different paramagnetic (Co, Mn, etc)/diamagnetic (Cd, Zn, Hg, etc) metal atoms variety of interesting magnetic properties containing materials, luminescent materials, and porous materials of phosphinates have been reported. In the following section, we discussed a few examples of cadmium-related phosphinate clusters and their structure in the solid state.

Peter Betz et al. reported[58] Cd-phosphinate (**figure 42a**) containing polymeric chain, $Cd(HCONH_2)_2[H(C_6H_5)PO_2]_2$ repeating unit present in the molecular structure. The SCXRD analysis shows the cadmium atom is octahedrally surrounded with O-atoms of four phosphinic acid in a square planner plane and two axial coordination satisfied with the O-atom of formamide ligand. Another polymeric Cd-phosphinate of ferrocenyl phenyl phosphinic was reported by Olivier Oms et al. in 2005.[59] From the physical measurements they proposed the structure of the compound (**figure 42b**)

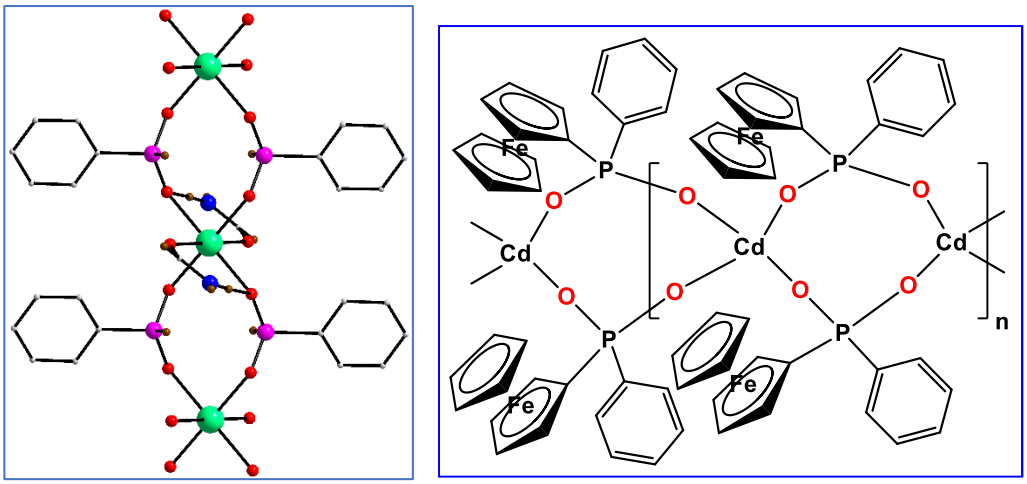

(a) **(b)**

Figure 42: (a) Structure of polymeric $Cd(HCONH_2)_2[H(C_6H_5)PO_2]_2$ **(b)** Proposed structure of polymeric Cd-phosphinate of ferrocenyl phenyl phosphinic

Li-Jie Dong et al reported[60] $[Cd(L)(bipy)(H_2O)_2]$ (**1**), a metastable 3D-Cd-coordination polymer, utilizing (2-carboxyethyl)(phenyl)phosphinate(H_2L) and 4,4'-bipyridine(bipy) at room temperature reaction. (**Figure 43a)** Hydrothermal reaction with **1** at two various temperatures, two different 2D $[Cd(L)(bipy)]$ (**2**) and 3D $[Cd(L)(bipy)0.5]\cdot 0.5H_2O$ (**3**) Cd-coordination polymer was prepared by self-assembly-disassembly and reassembly of **1**. (**Figure 43b**)

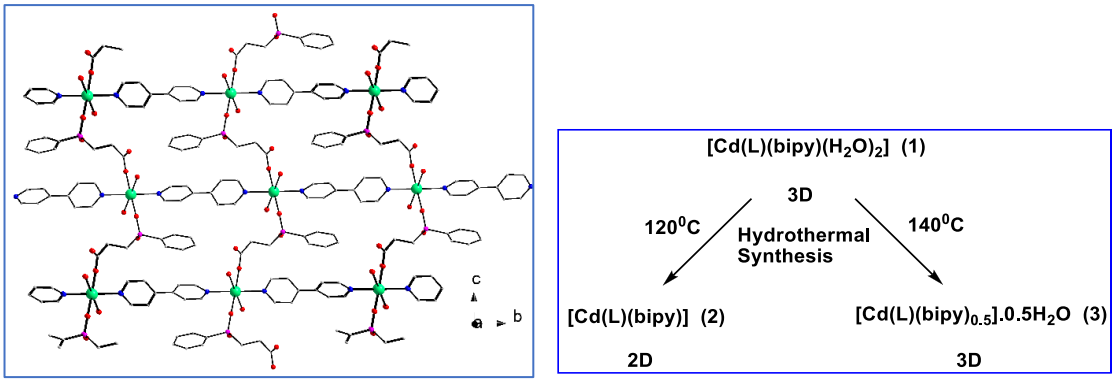

(a) **(b)**

Figure 43. (a) Structure of 3D coordination polymer $[Cd(L)(bipy)(H_2O)_2]$ **(b)** Scheme of the preparation of 2D and 3D coordination polymer [Cd(L)(bipy)] and $[Cd(L)(bipy)0.5]\cdot 0.5H_2O$

A. V. Anyushin et al. synthesized[61] yet another polymeric compound $[Na_2CdCl_2(O_2P(CH_2OH)_2)_2(H_2O)_3]$. The crystal structure is shown here (**Figure 44 a**).

Using co-ligand phenanthroline and carboxylate-phosphinate (H_2L) as ligand C.C. Zhao et al. synthesized[62] three isomeric double chain array containing supramolecular architectures of cadmium phosphinates [Cd(L)(phen)](**1**), $[Cd(L)(phen)].3(H_2O)$ (**2**), $[Cd(L)(phen)].13/6(H_2O)$ (**3**). These molecules differ in the lattice water molecule and the supramolecular architecture. From X-ray analysis of **1** (**Figure 44b**) it doesnot contain any lattice water molecule in between the double chains. The double chain assembled to form a 3D supramolecular architecture through van der Waals forces. Structure **1** contains one Cd^{2+} ion, one L^{2-} anion, and one phen ligand in the asymmetric unit. Cd-atom adopts a distorted O_h environment with two phosphinate O-atoms, one carboxylate group from three L^{2-} ligands, and the remaining two sites are coordinately saturated with phen ligand.

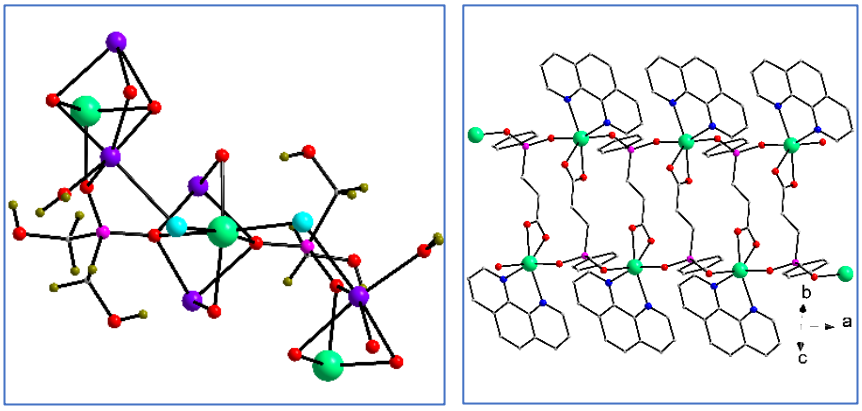

(a) **(b)**

Figure 44: (a) Core structure of coordination polymer $[Na_2CdCl_2(O_2P(CH_2OH)_2)_2(H_2O)_3]$ **(b)** Structure of polymeric [Cd(L)(phen)] (L= 2-carboxyethyl(phenyl)phosphinic acid)

Two novel Cd-compounds $[Cd(HL)_2]_n$ and $[Cd_3(L)_2(OH)_2]_n$ were reported by C.C. Xue et al.[63] in a hydrothermal reaction condition with chloride salt of cadmium and substituted phosphinic acid (H_2L) under pH 2.69 or 5.00 (**Figure 45a**). A 2D extended layer structure was prepared at pH 2.69 where only phosphinic acid hydrogen was deprotonated and the carboxylic acid hydrogen remains intact. Another 2D extended layer structure was prepared with increasing pH 5.00 and total deprotonation of the two acidic groups of the carboxy-phosphinic acid ligand (H_2L). X-ray structural analysis reveals that in both cases Cd-ions are present in a distorted octahedrally coordinated. In the latter case hydroxy group (μ_3-OH) connects three cadmium atoms to construct an inorganic chain of Cd-O-Cd along the x-axis.

Another example of a reaction with 2-carboxyethyl(phenyl)phosphinic acid (H_2L) and cadmium chloride was reported by L. Zhang et al.[64] They have synthesized one 2D layer containing dimeric motifs which are three-dimensionally supramolecular assembled $[Cd(HL)_2]$ (**Figure 45b**)and another discrete dimeric structure $[Cd(L)(phen)(H_2O)].2H_2O$(**Figure 45c**). In this case, too as in the former structure ligand is partially deprotonated and in the latter case, the ligand is fully deprotonated. In both cases Cd (II)-ion is distorted octahedrally coordinated.

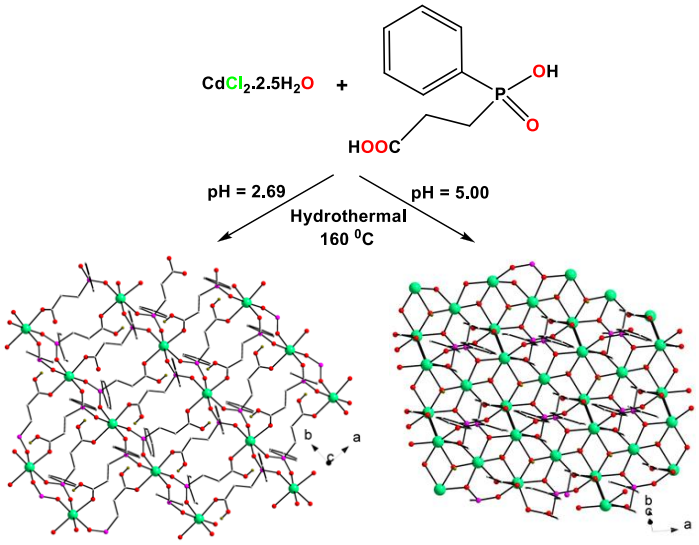

(a)

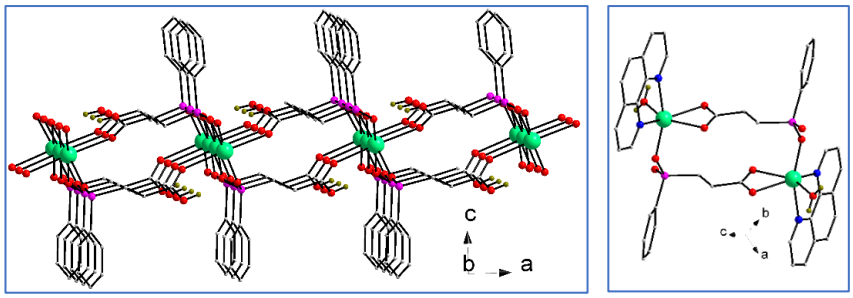

(b) **(c)**

Figure 45: (a) Preparation scheme of coordination polymer $[Cd(HL)_2]_n$ and $[Cd_3(L)_2(OH)_2]_n$ (H_2L = 2-carboxyethyl(phenyl)phosphinic acid) **(b)** 2D layer motif of $[Cd(HL)_2]_n$ **(c)** Discrete dimeric structure of $[Cd(L)(phen)\ (H_2O)].2H_2O$

R. Shekurov et al. synthesized[65] a electrochemically-active coordination polymer of ferrocene, $[Cd(H_2O)_2(Fc(PHOO)_2).2H_2O]_n$ (fc = 1,1'-ferrocenediyl). In the grown molecular structure, cadmium atoms are connected with phosphinate group to form infinite chains, these infinite chains form a 2D coordination polymer interconnecting by both side of the ferrocene-bis-phosphinate groups. (**Figure 46a**)

M. B. Garcia et al. reported[66] Cd -phosphinate-carboxylate coordination polymer $Cd[O_2P(CH_2CH_2COOH)(C_6H_5)]_2$ which displays layer topology. (**Figure 46b**) They have done a hydrothermal reaction with ligand 2-carboxyethyl(phenyl)phosphinic acid (H_2L) and $Cd(OAc)_2.2H_2O$ as a molecular precursor. Single crystal X-ray analysis shows that divalent cadmium ion is in a distorted octahedral environment consists with four oxygen atoms of phosphinate group and two carboxylate group oxygen atoms from six ligands. The CdO_6 polyhedra sheets are connected with bridging phosphinate groups.

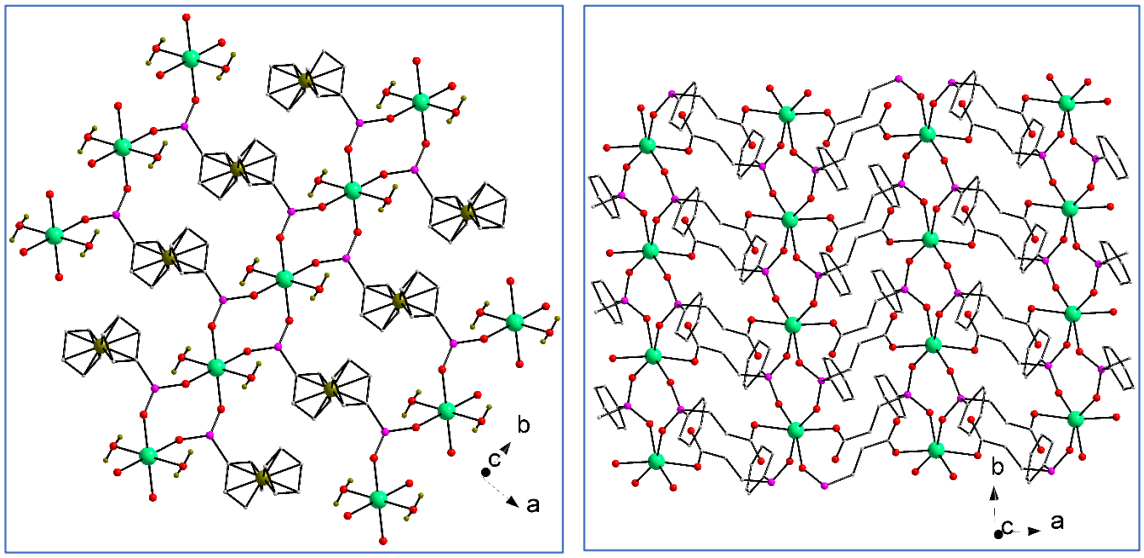

(a) **(b)**

Figure 46: (a) Structure of polymeric $[Cd(H_2O)_2(Fc(PHOO)_2).2H_2O]_n$ (fc = 1,1'-ferrocenediyl) **(b)** Structure of polymeric polymer $Cd[O_2P(CH_2CH_2COOH)(C_6H_5)]_2$

1.4. SMM- an application of lanthanide clusters:

(a) General Introduction:

Lanthanides/ Lanthanoids are the elements that have a special position bottom of the periodic table, starting from atomic number 57-71(Lanthanum-Lutetium). Sometimes these are called rare-earth elements. Though it is called rare-earth in the earth's crust it is found more than some common elements cerium is the 26th more abundant than copper. Neodymium, thulium is more abundant than gold, iodine

respectively. Promethium is the only radioactive element among them. Lanthanides are abundant in the minerals such as samarskite an oxide ore, monazite a phosphate ore. In the ore, all lanthanides are mixed, and their separation is not so easy because of the similar properties and similar ionic radius.

Magnetism and luminescence are some of the physical properties of lanthanides, which are extremely investigated and a brief introduction to magnetism is presented here.

Diamagnetic material

All the electrons inside a diamagnetic material are paired. In presence of an externally applied magnetic field, diamagnetic materials are repelling the line of force of the magnetic field. The diamagnetic material shows very weak negative magnetic susceptibility(χ). In the absence of the field, the magnetic susceptibility will not be retained.

Paramagnetic material

Paramagnetic materials have unpaired electrons for which in the presence of the externally applied magnetic field, the line-force of material attracts each other. It shows a positive magnetic susceptibility. In absence of the field, the magnetization will not be retained. A small, induced magnetization remains due to the presence of little spin present in the paramagnetic material which is not parallel to the applied field when applied external magnetic field.

Ferromagnetism

Ferromagnetic substances have electron spin parallel with san externally applied magnetic field. In absence of the magnetic field also a large magnetic moment remains. Ferromagnetic materials show ferromagnetism up to a characteristic temperature called Curie temperature.

Antiferromagnetism

Antiferromagnetic material has neighboring electron spins antiparallel and the magnitude of those electron spins is equal and opposite. So the total magnitude of the magnetic momentum is nil. At absolute 0 K, it behaves like diamagnetic material. Above a certain temperature, it behaves as paramagnetic material called Neel temperature.

Ferrimagnetism

Ferrimagnetism is a special case of antiferromagnetic material phenomena. Though all the neighboring spins are antiparallel the magnitude of those spins is not equal as a result a net magnetic moment is present in the ferrimagnetic substances. Above a certain temperature called Curie temperature ferrimagnetic material shows paramagnetism.

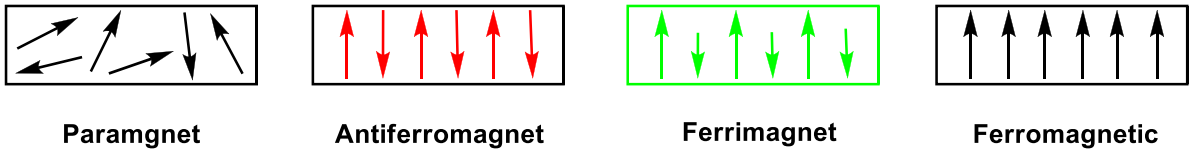

Figure 47: Spin arrangement of different types of magnetic material

Superparamagnetism

Superparamagnetism is a special case of ferromagnetic/ferrimagnetic material property that has the particle size dimension of 2-3 to 20-30 nm. At room temperature, the magnetization of this nanoparticle randomly flips, the time to flip the direction under the influence of temperature is called 'Neel relaxation time'. In absence of an externally applied magnetic field, when the measurement time of the magnetization of the nanoparticle higher than the time of Neel-relaxation, the average magnetization is zero; a superparamagnetic state of the nanoparticle is observed. In this state in presence of an external magnetic field, It is behaving similar to the paramagnet ($\chi_{superparamagner} > \chi_{paramagnet}$). Superparamagnetism occurs below Curie temperature whereas ferromagnetic/ferrimagnetic to paramagnetic state occurs above Curie temperature.

(b) SMM and working principle of SMM:

Sessoli and co-workers reported[67] the magnetic behavior of Mn_{12}-OAc for the first time in 1993. Before that magnetism was bound up to a few hundred nanometers with nanomaterials. After the discovery of the single molecular magnetism (SMM) property of Mn_{12}-OAc, this scale comes down to the molecular level to a few angstroms. Here each of the molecules behaves like a bar magnet. SMM is magnetic molecules/clusters which are constructed with spin metal ions and ligands (an organic moiety). Inside the core, metal atoms are protected by organic moiety to minimize the intermolecular interaction with the neighboring spins. SMMs exhibit magnetization after removing the magnetic field for a relatively long time at low temperatures. Unlike bulk magnets such as AlNiCo or $SmCo_5$, SMMs do not require long-range magnetic interactions, it's a molecular origin phenomenon. The hysteresis loop below a certain temperature (blocking temperature T_B) is a measure of SMM property. After the removal of the magnetic field, the bistable ground state molecule has to overcome certain energy barriers to be equilibrated which means from one spin projection to another lowest energy spin projection a minimum energy barrier (U_{eff}) or anisotropic energy barrier is required. A minimum time required to be equilibrated is called relaxation time(τ), and only because of it does the term come 'memory effect'. The relaxation process and magnetization can be described with the double-well potential energy diagram. The memory effect of the magnetic bistable state of the SMM has a potential application in the field of high-density information storage, molecular spintronics, and quantum computing.

Large negative uniaxial magnetic anisotropy and bistable non-zero ground state are the two essential requirements to exhibit SMM behavior. The energy difference (ΔE) between the two bistable ground

states is represented by the formula $S^2 \left| D \right|$ and $(S^2 - 1/4) \left| D \right|$ for integer and non-integer spin values respectively, where S denotes the ground state spin value and D denotes axial anisotropy term/ zero-field splitting (ZFS) parameter.

(c) Relaxation processes

Removing the externally applied magnetic field to reorient the magnetization through the whole excited energy levels is not the only path to overcome the energy barrier. The quantic characteristic of these single molecular magnetic materials makes various complex relaxation pathways that are very subtle towards temperature, magnetic field, hyperfine (interaction between nuclear and electronic spins), and intermolecular interactions. The relaxation processes are the spin-phonon coupled processes (Orbach, Raman, and Direct processes) or the processes caused by the quantic behavior of the material(QTM (Quantum Tunneling of Magnetization)and TA-QTM(Thermally assisted QTM)). Relaxation processes are occurring in these three regimes.

1) At a high-temperature thermal regime:

2) At a low-temperature QTM regime:

3) Thermal-assisted QTM regime:

Spin-phonon coupled process:

There are three spin-phonon coupled processes present. a) Orbach process b) Raman process and c) Direct process. Among the spin-phonon coupled processes Orbach and Raman processes are two phonon relaxation phenomena, and the Direct process is only one phonon relaxation phenomenon.

a) In an Orbach process, large phonon energy is required to overcome the entire energy barrier. First, the system absorbs the exact energy phonon to overcome the highest energy sublevel ($M_S=\pm S$) from the ground energy sublevels ($M_S=0$). Then excited state system relaxed to any of the ground states $M_S=\pm S$ with the new phonon emission. It occurs at high temperatures.

b) In the Raman process, the system absorbs phonon to reach a virtual excited state and then emits another phonon. In this case, the phonons are obsessed with the inelastic dispersion mechanism. The two phonons' energy difference corresponds to the sublevel ($\pm M_S$) energy difference in the ground state. Raman process is observed throughout the whole temperature range.

c) Direct process is a single phonon absorb or emission phenomenon. The single phonon absorption occurs relates to the energy difference of the $\pm M_S$ sublevels in the ground state. This process is field-dependent, at a higher field the relaxation behavior becomes faster which means the relaxation time decreased.

Quantum Tunneling of magnetization (QTM):

QTM is another important relaxation process that generally occurs in low temperatures between two same energy-containing ground state sub-levels. Doubly degenerated ground state ($\pm M_S$) with the same energy when coming into resonance a reversal of spin happens, is called the QTM process. This is a process where the spin reversal takes place in a shortcut path without crossing the whole excited energy levels barrier with no-cost energy. Thermally assisted quantum tunneling of magnetization (TA-QTM) is a combined process of phonon absorption by the system to populate the excited state and then from the exited state directly relaxation of one state to another state of the opposite sign of same energy sub-levels ($+M_S$ to $-M_S$ or vise-versa).

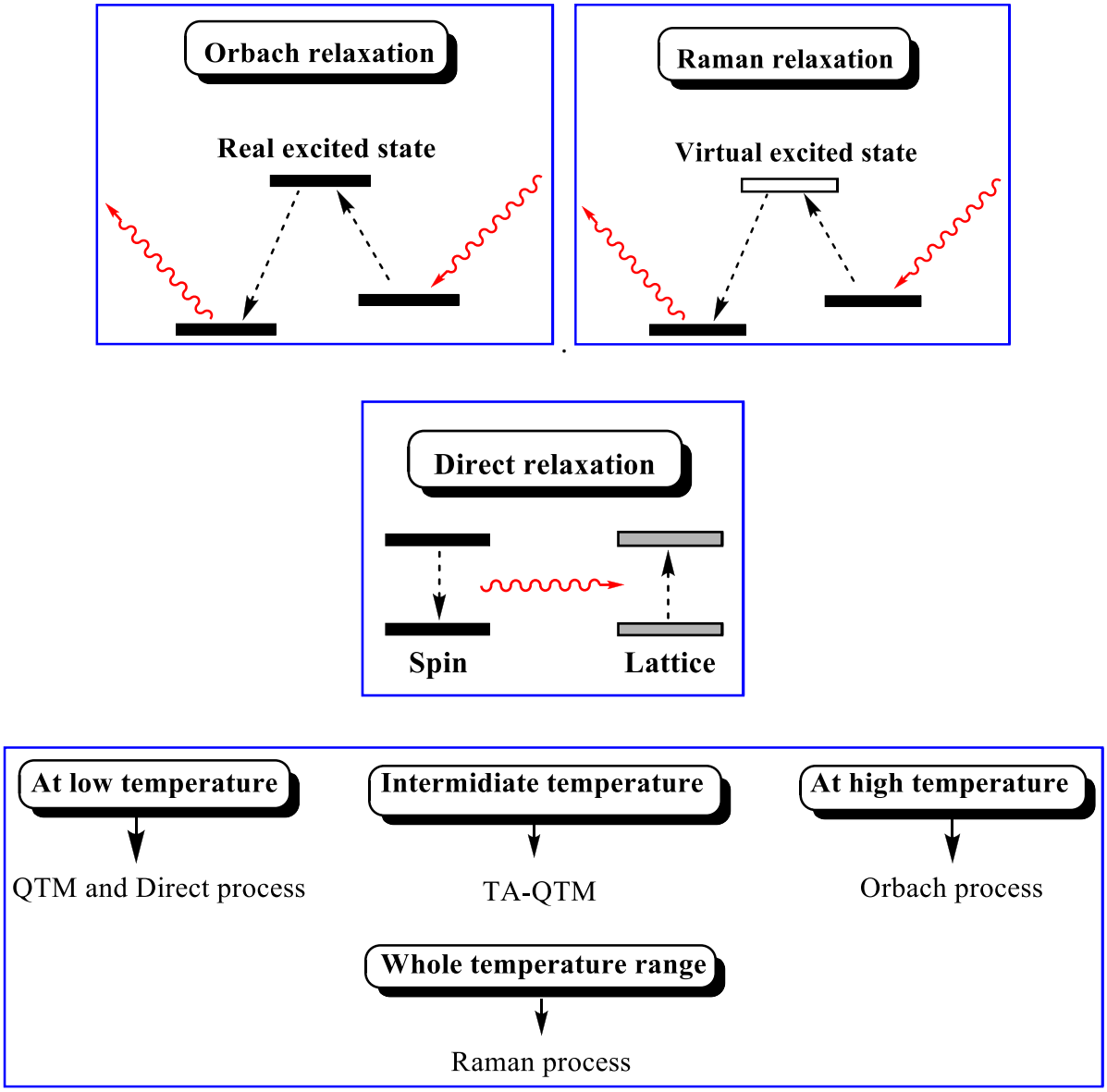

Figure 48: Types of relaxation processes

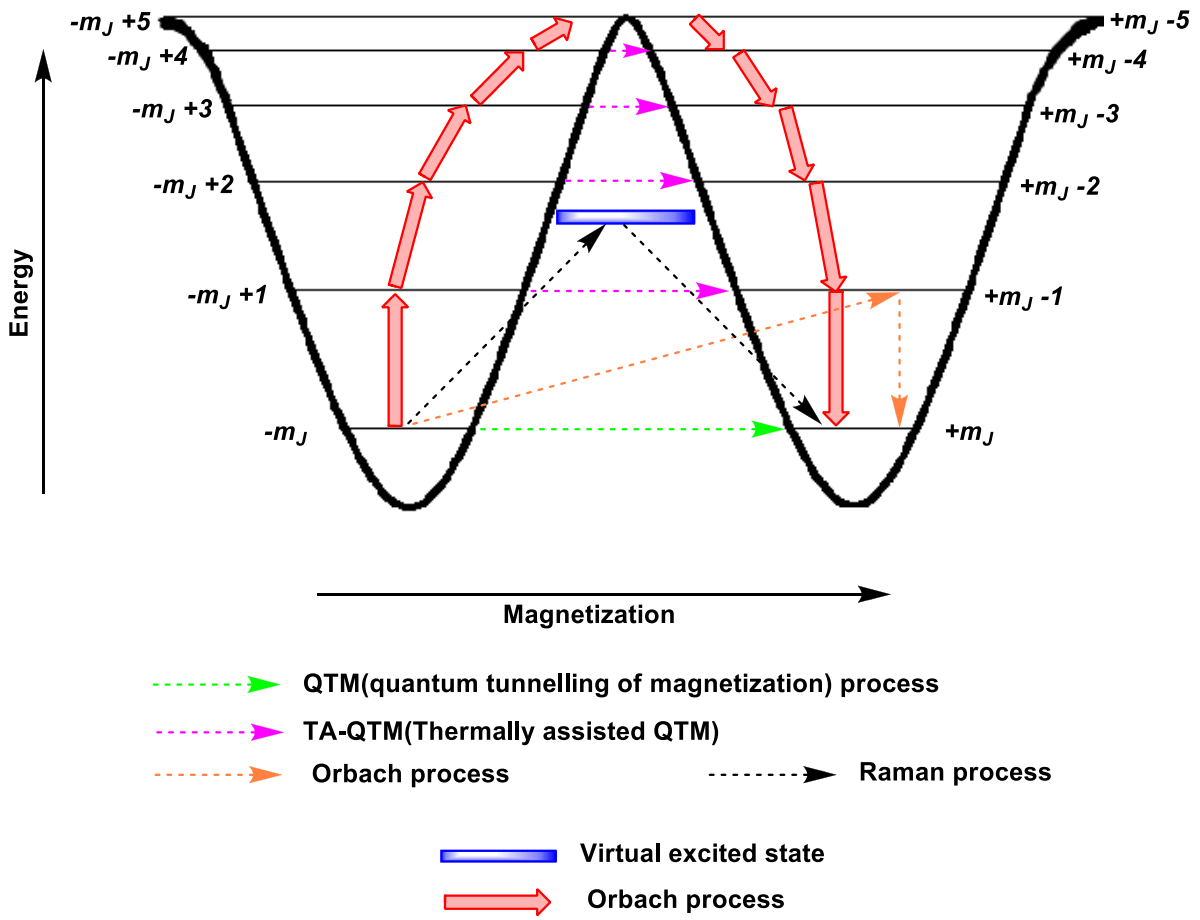

Figure 49: Double well potential diagram with relaxation processes

The time of different relaxation processes is given by the general formula

$$\tau^{-1} = \tau^{-1}_{QTM} + AT + BT^{n} + \tau^{-1}_{0} \exp(- U_{eff}/k_B T)$$

where the first,2nd,3rd, and 4th terms are the quantum tunneling of magnetization, direct process, Raman process, and Orbach processes respectively.

(d) Plot analysis of SMM detecting behavior:

AC magnetic field and DC/ Static magnetic field measurement are the two techniques that have been used to measure the SMM behavior of magnetic material.

AC magnetic susceptibility:

Out-in-phase (χ'_M) and Out-of-phase (χ''_M) susceptibility are the two techniques of the alternating magnetic susceptibility measurement.

Out-of-phase (χ''_M) susceptibility measurement measured at 2 K-300 K temperature range. There are also two types of measurement has done

1) χ''_M (T) plot, where χ''_M vs T will be plotted by varying frequency of the field. (**Figure 50a**)

2) χ''_M (ν) plot, where χ''_M vs ν will be plotted by varying temperatures. **(Figure 50b)**

In the frequency-dependent peaks in χ''_M (T) plot the frequency varies from 0-15 K.

Among these two plots, the χ''_M vs frequency(ν) plot is more informative. From this plot, we can know whether the QTM occurs or not for a magnetic material. If the position of the maxima of the χ''_M (ν) plot is not varying with the temperature change then it can be said that the process is temperature independent, so QTM phenomena are not operating for the relaxation process (which operates major at a lower temperature). The position of the maxima of this plot depends on the relaxation time (τ).

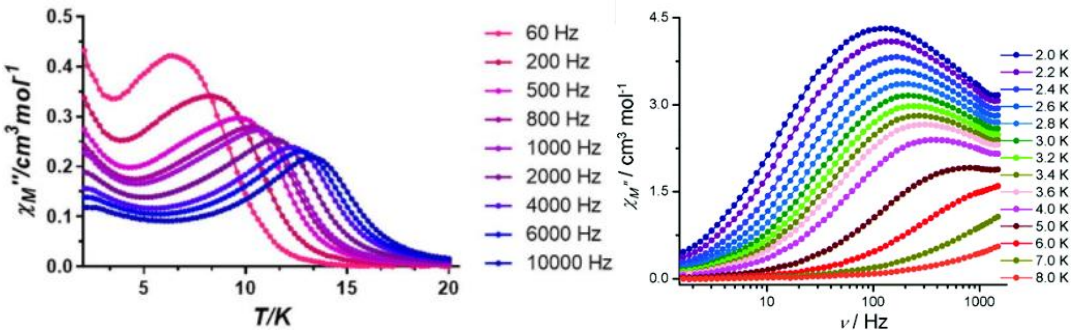

(a) **(b)**

Figure 50: (a) χ''_M vs T plot and **(b)** χ''_M vs ν plot

Cole-Cole plot

A Cole-Cole plot indicates the number of relaxation pathways. It is a χ''_M vs χ'_M plot with various temperatures. **(Figure 51)** For a particular temperature, it gives a semicircle-like graph which is fitted by the Debye model. The fitting value provides a term 'α' comes which has a value between 0 and 1. The value close to zero and more than zero indicates the single and multiple relaxation pathways respectively.

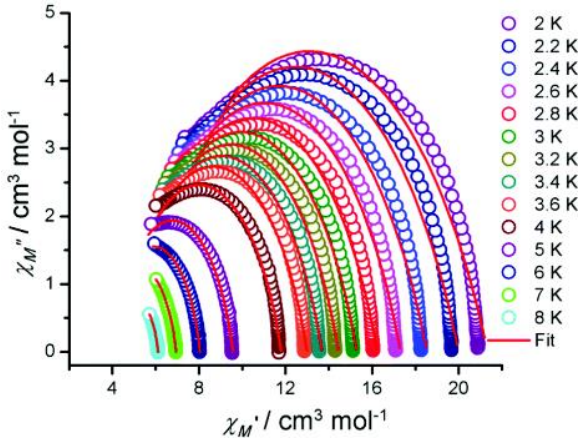

Figure 51: Cole-Cole plot

DC magnetic susceptibility:

Another technique to detect whether a magnetic material behaves SMM is the field dependence of the magnetization at various temperatures. Here plot contains M vs H where M is the magnetization term in the unit of $N\mu_B$ and H represents the magnetic field in the unit of Oresested (Oe) or Tesla (T). (**Figure 52)** The openness of the hysteresis loop is an indication of showing SMM behavior. The area under the loop is the indicator of the hardness/strongness of the SMM behavior. Greater the area under the loop greater its SMM property. Even after the presence of large U_{eff} due to lack of open hysteresis loop or presence at very low temperature (2 K) SMM property will be less. From this, an important SMM characterization parameter termed blocking-temperature (T_B) was observed. The highest temperature at which the hysteresis loop opens is called the blocking temperature.

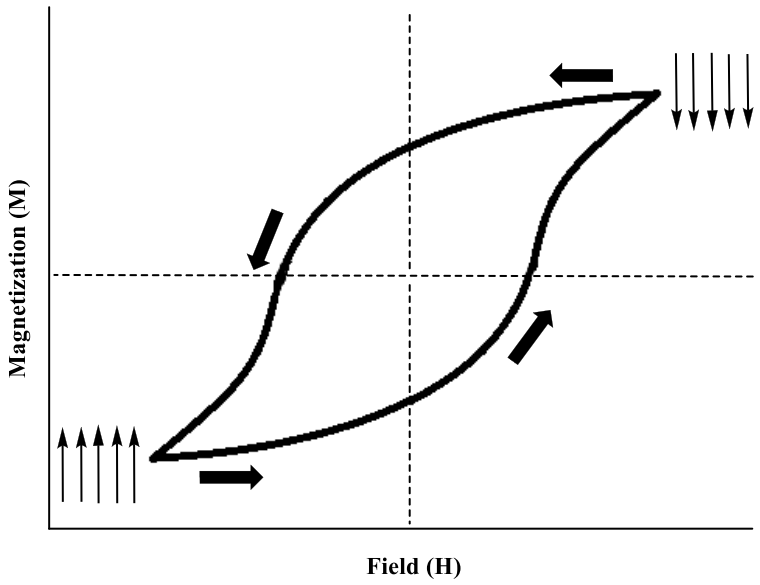

Figure 52: Hysteresis loop

(e) First SMM of transition metal:

The Famous Mn_{12}-OAc cluster is the first reported SMM among transition metal clusters (**Figure 53d**). Its fascinating magnetic property was studied by Sessoli et. al. in 1993[67] introducing a new era in magnetism. The synthesis of the Mn_{12}-OAc cluster was first reported by Caneschi et. al. in 1980.[68] In the tetragonal crystal structure of Mn_{12}-OAc, four Mn(IV) (d^3, S=3/2) present in the core as cubane and outer ring eight Mn(III) (d^4, S=2) surrounded like a crown with oxo bridges. All four Mn(IV) coupled themselves ferromagnetically and eight Mn(III) coupled themselves ferromagnetically(**Figure 53e**). Overall in the cluster, Mn(IV) and Mn(III) coupled themselves antiferromagnetically. In 1991 Gatteschi and coworkers with the help of high-field electronic paramagnetic resonance(HF-EPR) and magnetic measurement proved that the total S=10 spin state of Mn_{12}-OAc cluster.[69] An interesting observation was shown from the ac magnetic susceptibility measurement of the complex by Sessoli, Gatteschi, Christou, and Hendrickson in 1993.[70] (**Figure 53a**)The ac susceptibility measurement has been done

between 4-25 K in zero applied field and frequency range 55-500 Hz, an unusual non-zero imaginary component of susceptibility (χ''_M) was observed. The maxima of the χ''_M are frequency-dependent same as superparamagnet and spin glasses. It indicates relaxation effects associated with magnetization. Same year Gateteshi and Sessoli observed the magnetic bistability in the Mn_{12}-cluster which is useful for data storage devices at the molecular level. They have found this highly anisotropic Mn_{12}- cluster magnetically relaxed very slowly at low temperatures below 4K, showing a noticeable hysteresis loop. (**Figure 53b**)This behavior is different from the bulk ferromagnet where the hysteresis loop is observed because of the domain wall's motion. In 1996, the macroscopic QTM (quantum tunneling of magnetization) in SMM (steps in the hysteresis loop) was first observed by Frielman et. al.[71], then it was confirmed by Thomas and coworkers.[72] This special feature connected the quantum world to the macroscopic world, that's why this phenomenon of Mn_{12}-cluster is so interested among physicists and chemists.

Magnetic anisotropy of this complex is arising due to the alignment of the J-T axes (Jahn-Teller) of the Mn(III)-ions ($d^4=t_{2g}^3e_g^1$)in the same direction. The bistable ground state for S=10 is split into 21 microstates (2S+1=2*10+1) due to the axial anisotropy of the molecule itself, M_s=±10, ±9, ±8,……. ±1, 0. (**Figure 53c**) When a zero external magnetic field is applied, the two bistable groundstates are equal in energy but when a field is applied, one state has become more populated than the other viz. M_s=+10 or M_s =-10. After magnetization in the field switch-off situation again both states tried to equilibrate through an energy barrier (U_{eff}). This depends upon the axial anisotropic parameter (D) and the total number of spin values (S). $U_{eff} = S^2 \mid D \mid$ and $(S^2- 1/4) \mid D \mid$ are the equations for integer and non-integer spin values. For Mn_{12}-OAc cluster the values are S = 10 and D = -0.51 cm^{-1} so the energy barrier (U_{eff}) is 51 cm^{-1}.

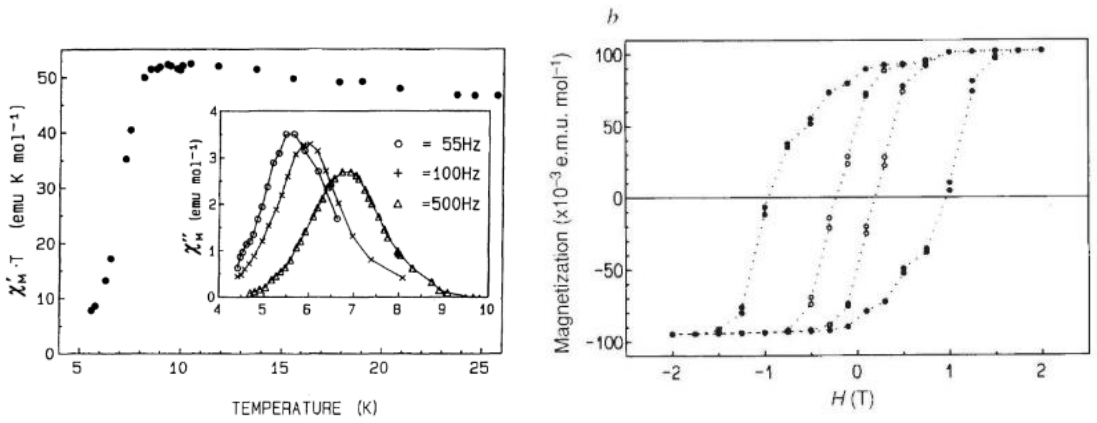

(a) **(b)**

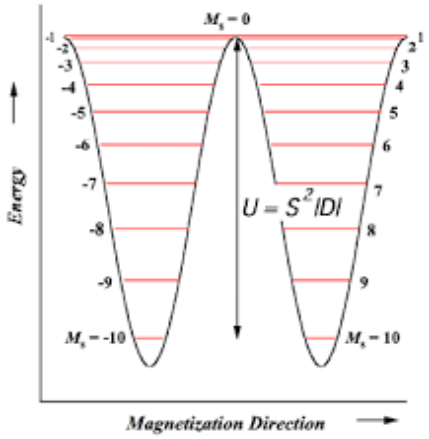

(c)

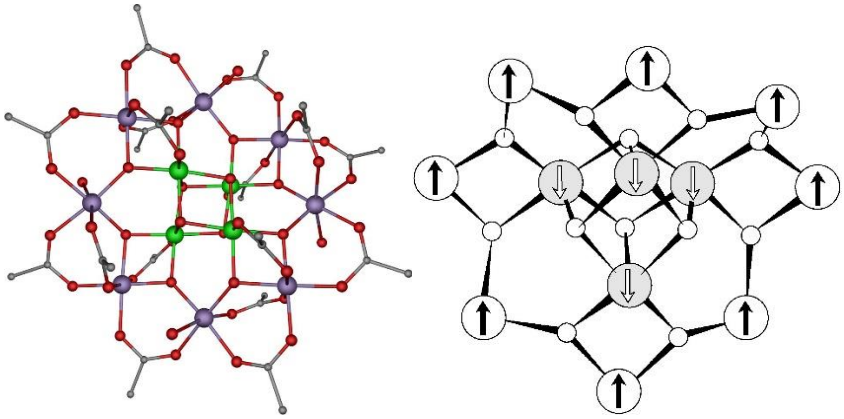

(d) **(e)**

Figure 53: (a) AC susceptibility measurement of Mn_{12}-OAc cluster **(b)** Hysteresis loop of Mn_{12}-OAc cluster **(c)** Double well energy diagram of Mn_{12}-OAc cluster **(d)** Structure of Mn_{12}-OAc cluster **(e)** Core of Mn_{12}-OAc cluster with spin orientation

(f) First SMM of Lanthanide:

Ishikawa et al. first reported lanthanide double-decker phthalocyanine complex $[Bu_4N][LnPc_2]$ (Ln = Tb, Dy and Pc = pthalocyanin) showing SMM property (**Figure 54a**).[73] This new class of complexes shows SMM with a different mechanism from the TM-SMM. Koike et al. comprehensively studied the crystal structure of these double-decker complexes.[74] The complex is a D_{4d} symmetric, square-antiprismatic eight coordination geometry sandwich lanthanide ion in between two phthalocyanine ligands and the two ligands are mutually staggered in conformation. AC magnetic measurement of $[Bu_4N][TbPc_2]$ (**Figure 54b**) and $[Bu_4N][DyPc_2]$ complexes show the slow-relaxation of SMM behavior. Magnetic susceptibility data of in-phase (χ') and out-of-phase (χ''), for the pure sample and magnetically dilute sample was collected doping with isostructural diamagnetic $[Bu_4N][Y(Pc)_2]$. The diamagnetic host lattices remove intermolecular interaction from the neighbor molecule $[Bu_4N][LnPc_2]$

(Ln=Tb, Dy) and slow down the spin-flip of the magnetic dipole. A shifting of the χ_M''/ χ_M and χ'T vs T signal peak to higher temperature was clear evidence that the SMM property of these complexes is a completely molecular origin phenomenon. (**Figure 54b**) Arrhenius analysis of the 1:4 (Ln:Y) diluted sample shows U_{eff} = 230 cm^{-1} and 31 cm^{-1} in $[Bu_4N][TbPc_2]$ and $[Bu_4N][DyPc_2]$ complexes respectively. The surrounding matrix of phthalocyanine complexes has a very much effect on the crystal-field splitting of Ln-SMM is studied by solid-state ^{1}HNMR. For undiluted and diluted $[Bu_4N][TbPc_2]$ complex with $[Bu_4N][Br]$, U_{eff} = 584 cm^{-1} and U_{eff} = 641 cm^{-1} is observed respectively.[75] A comprehensive scrutiny of ligand-field parameter and ac susceptibility measurement suggests that the relaxation pathway for Tb-complex; Orbach process dominated between 25-40 K range, and below 25 K direct or Raman-process or tunneling directly occurs from the ground state. Whereas for Dy-complex, the Orbach-process is the main pathway at 3-12 K range.[76–78] Relaxation process occurs from the lowest and 2nd-lowest sub-levels of the lanthanide ions. For A 'stepped chair hysteresis loop' for the phthalocyanine complexes is caused by a fundamentally different QTM relaxation mechanism for Ln-SMM; the nuclear and electronic spin entanglement is absent for TM-SMMs.[79] Lanthanide phthalocyanine becomes the Mn_{12}Ac for the lanthanide-SMMs due to the most frequently studied Ln-SMM.

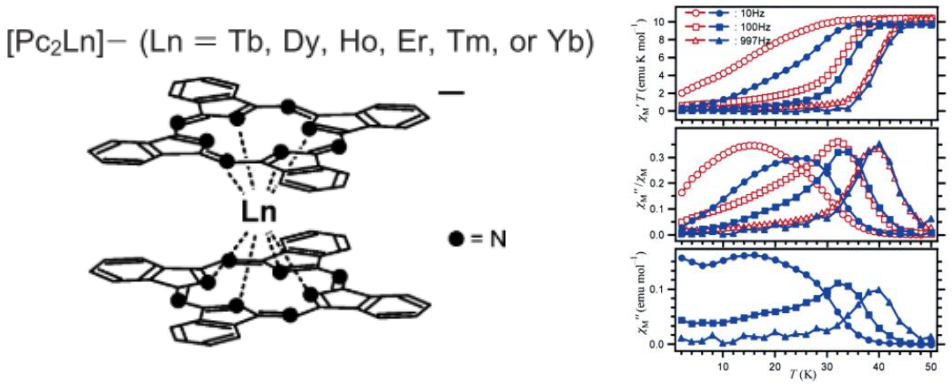

(a) **(b)**

Figure 54: (a) Structure of $[LnPc_2]$ **(b)** χ'T vs T (top), χ''/χM vs T (middle), χ'' vs T for a powdered sample of $[TbPc_2]$ (open points), and for Tb derivative diluted in diamagnetic $[Bu_4N][YPc_2]$ (filled point)

From the first Mn_{12}-SMM to recent in the field of single molecular magnetism development happened following some strategies keeping in mind to step up the energy barrier (U_{eff}) and blocking temperate (T_B). Prior stage of the SMM era, increasing the total spin (S) is the only strategy to step up the energy barrier since, concerning the energy barrier $U_{eff} = S^2 \left| D \right|$, the quadric nature of the total spin term is more pronounced. Then the race begins to obtain the highest spin value with polynuclear transition metal-based clusters. Very much promising examples of large ground spin states containing metal clusters have been synthesized such as Mn_{19} (S = 83/2), Mn_{25} (S = 61/2), and Fe_{42}(S = 45). But

unfortunately, these are not showing any SMM or very less. So, knowledge gained from the failure of the strategy that magnetic anisotropy is another important parameter in designing high-performance SMMs. After the discovery of the SMM property of $[Bu_4N][LnPc_2]$ (Ln=Tb, Dy) by Ishikawa et al. it was understood that a single lanthanide ion can be shown a better SMM property though it has a smaller spin state compared with the polynuclear TM-clusters in term of effective energy barrier (U_{eff}). Now it is more focus shifted toward increasing the magnetic anisotropy of the complexes. In this regard, lanthanide is the best choice for procedure bistable ground state which is the essential condition for the SMMs. The orbital strong orbital contribution to the ground state generates inherent magnetic anisotropy in the lanthanide complexes which is different from the observation from the TM complexes.

Here in the following section, we will discuss a few breakthrough examples of lanthanide SMMs.

(g) Few breakthrough examples of lanthanide SMM:

Powell and coworkers in 2006 were reported[80] two similar interesting trinuclear clusters $[Dy_3(\mu_3\text{-}OH)_2L_3Cl(H_2O)_5]Cl_5$ and $[Dy_3(\mu_3\text{-}OH)_2L_3Cl(H_2O)_5]Cl_3$ (**Figure 55**). SCXRD analysis shows that all the dysprosium atoms are octa-coordinated distorted geometry. This coordination geometry is pentagonal bipyramidal with one side of the pentagonal plane vacant. In the vacant pentagonal plane site above and below the plane, two μ_3-hydroxo groups are present. An unprecedented non-magnetic ground state was observed, which is not expected for an odd number of paramagnetic centers with a *J* value of half-integer and slow magnetic-relaxation. These three dysprosium centers are coupled antiferromagnetically with each-other through oxo-bridges. In 2008 Sessoli and Chibotaru et al. revealed the reason for a nonmagnetic ground state (experimentally and theoretically) that the single-ion easy axes of magnetization arranged themselves in a way noncollinear 120° on the plane of the Dy_3 triangle system. From these results, the remarkable phenomenon called 'toroidal magnetic moment' or 'vortex spin chirality came into the picture in the SMM family.

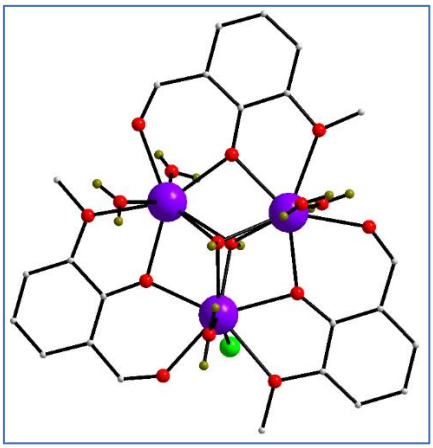

Figure 55: Structure of $[Dy_3(\mu_3\text{-}OH)_2L_3Cl(H_2O)_5]Cl_3$

A record anisotropic barrier of a tetranuclear complex $[Dy_4(\mu_3\text{-}OH)_2(bmh)_2(msh)_4Cl_2]$ (**Figure 56a**)(where H_2bmh = 1,2-bis(2-hydroxy-3-methoxybenzylidene)hydrazone and Hmsh= 3-methoxysalicylaldehyde) hydrazone was reported by Murugesu et al.[81] X-ray analysis reveals that this is centrosymmetric complex with monoclinic P21/c space group. Two types of dysprosium atoms are present. in eight-coordinated DyN_2O_5Cl and DyN_2O_6 coordinating environment with square-antiprismatic geometry. It has a defect-dicubane central core structure where all the four Dy(III) are coplanar and these four coplanar Dy(III) are connected with two μ_3-OH bridges above and below the plane. Zang et al. reported a similar Dy_4-core. Frequency-dependent ac magnetic susceptibility shows that two maxima in the peaks exist at 9 K and 30 K, stipulated two type of relaxation processes are operating in the molecular system at low and high temperatures. From Arrhenius analysis, two anisotropic energy barriers were calculated U_{eff} = 9.7 K ($\tau_0 = 3.2\times10^{-5}$ s) and U_{eff} = 170 K ($\tau_0=4\times10^{-7}$ s). At high temperatures, this slow magnetic relaxation is a very unique property. At that time, it was the record U_{eff} among the polynuclear SMMs.

In 2011 Winpenny et al. synthesized[82] square-based pyramid pentanuclear cluster $[Dy_5O(O^iPr)_{13}]$ (**Figure 56b**) which shows slow magnetic relaxation at temperature 40 K and U_{eff} =530K. At that time, it was the largest observed U_{eff} among the d and f-block compounds. SCXRD reveals that in this compound all the Dy(III)-ions are six-coordinated and the center of the cluster μ_5-oxo bridge is present. Each Dy(III)-ion has non-crystallographic C_{4v} . Among the thirteen isopropyl groups four μ_3- O^iPr, four μ_2- O^iPr, and five terminal isopropoxide at each Dy(III) are present.

Chandrasekhar et al. reported[83] two isostructural tetranuclear-rhombus-shaped clusters $[\{(LH)_2Dy_4\}(\mu_2\text{-}O)_4](H_2O)_8\cdot2CH_3OH\cdot8H_2O$ (**Figure 56c**)and $[\{(LH)_2Ho_4\}(\mu_2\text{-}O)_4](H_2O)_8\cdot6CH_3OH\cdot4H_2O$ using a hexadentate Schiff-base hydrazide ligand (6-Hydroxymethyl)-N′-((8-hydroxyquinolin-2-yl)-methylene) Picolinohydrazide (LH_3). SCXRD reveals that in this complexes lanthanide atoms and donor atoms of the ligand are present in the same plane, is the first example of this type of complex. In the structure of the complex two ligands are present. Each ligand molecule binds two lanthanide atoms in the two pockets of the ligand and forms two $[LH(Dy)_2]^{4+}$ subunits. These two subunits are connected with four μ_2-oxo bridges above and below the molecular plane to form Dy_4-assembly. Two Dy(III)-ions are eight coordinated dodecahedron and seven coordinated geometry. Among Dy4 and Ho4, only Dy4 shows slow magnetic relaxation behavior below 20 K. From the frequency-dependent χ_M'' vs temperature(T) graph it reveals that two maxima were observed at lower and higher temperature regions with U_{eff} = 16.8 K ($\tau_0 = 1.4\times10^{-6}$ s) and 54.2 K ($\tau_0= 7.2\times10^{-7}$ s) respectively. This peculiar response shows the presence of two dysprosium sites with distinct coordination spheres and geometry.

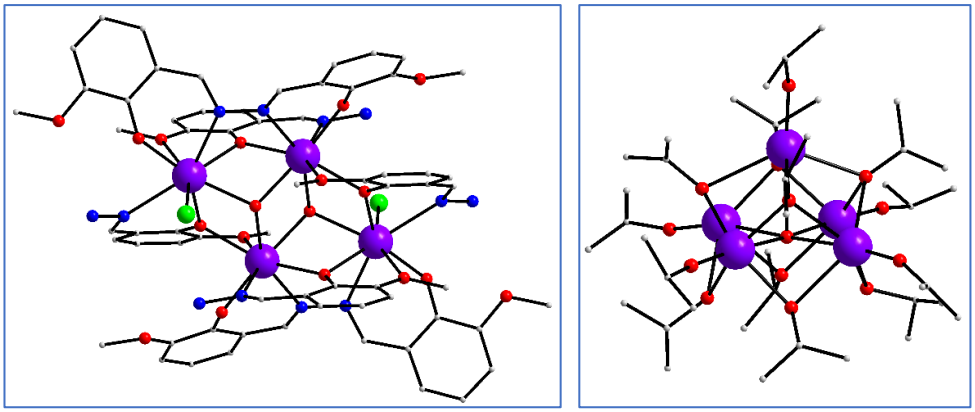

(a) **(b)**

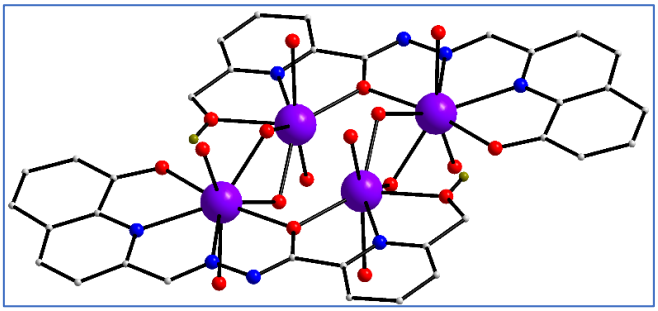

(c)

Figure 56: (a) Structure of $[Dy_4(\mu_3\text{-}OH)_2(bmh)_2(msh)_4Cl_2]$s **(b)** Structure of $[Dy_5O(O^iPr)_{13}]$ **(c)** Structure of rhombus-shaped complex $[\{(LH)_2Dy_4\}(\mu_2\text{-}O)_4](H_2O)_8\cdot 2CH_3OH\cdot 8H_2O$

Using bulky hindered phenolate ligand Gao and coworkers reported[84] another interesting cluster. They have synthesized a di-nuclear symmetric hydroxide-bridged complex $[Dy(\mu\text{-}OH)(DBP)_2(THF)]_2$ (DBP^- = 2,6-di-tert-butylphenolate) (**Figure 57a**). SCXRD reveals that both dysprosium are five coordinated square-pyramidal (C_{4v}) geometry. Two dysprosium ions are connected with two hydroxide ions each other. From magnetism data, Arrhenius fitting data at ZSF (zero static field) gave U_{eff} = 721 K (τ_0= 6.6×10^{-12} s) and dual fitting data gave U_{eff} = 754 K (τ_0= 3.5×10^{-12} s) which implies the predominate Orbach process. This result is the highest U_{eff} among 4f-only dimers up to 2017. Due to the large Dy-Dy magnetic interaction and well-separated thermal relaxation regime and quantum tunneling regime, this is an excellent model to study the relaxation pathway of SMMs with intramolecular Dy-Dy magnetic interactions.

Although polynuclear lanthanides are giving a high anisotropic energy barrier (U_{eff}), due to fast QTM very tiddly and narrow hysteresis-loops were observed. To overcome this difficulty, a strategy people are using is to make a strong coupling between lanthanide centers. Using radical ligands researchers are trying to solve this problem. A remarkable example of this was reported by Demir et al.in 2017[85]. They have synthesized di-nuclear complex $[K(crypt\text{-}222)][(Cp^{Me4H}{}_2Tb)_2(\mu\text{-}N_2^{\cdot-})]$ (**Figure 57b**); it shows the highest coercive field H_c =7.9 T at 10 K is higher than the commercial permanent magnet. It displays U_{eff} = 276 cm^{-1} and 100 s magnetic blocking temperature T_B =20 K.

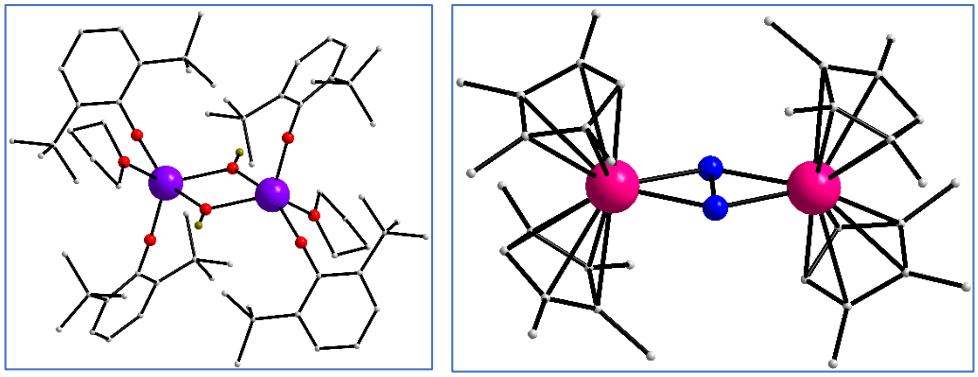

(a) **(b)**

Figure 57: (a) Structure of $[Dy(\mu\text{-}OH)(DBP)_2(THF)]_2$ **(b)** Structure of $[(Cp^{Me4H}{}_2Tb)_2(\mu{-}N_2)]$

Two examples of mononuclear lanthanide complex, so-called SIMs (Single Ion Magnet) were reported[86,87] with keeping in mind the molecular symmetry strategy which exhibits the high-performance SMMs. Murugavel et al. were synthesized[87] pentagonal-bipyramidal (PB), pseudo-D_{5h} symmetry containing $[L_2Dy(H_2O)_5]^{3+}$ (L= ^{t}BuPO(NH^{i}Pr)$_2$).(**Figure 58a**). SCXRD reveals that five water molecules are present equatorially and two phosphonic diamide ligands are present in two axial positions coordinated with the metal through phosphoryl oxygen(P=O). It shows a high anisotropic barrier (U_{eff}) 735.4 K with magnetization-blocking (T_B) previous to 12 K and magnetic-hysteresis up to 12 K (30 K) with a large-coercivity ~0.9 T (~1.5 T) at a field-sweep rate of ~0.0018 Ts^{-1} (~0.02 Ts^{-1}) .This molecule is the best observed air-stable SIM/SMM reported at that time. Another remarkable a near-perfect pentagonal bipyramidal SIM $[Dy(O^{t}Bu)_2(py)_5][BPh4]$ (**Figure 58b**)was reported[86] which shows the largest U_{eff} = 1815(1) K and blocking temp. (T_B = 14 K). Despite its high magnetic anisotropy, it has a lower T_B value than reported by Murugavel et al.[87] Until 2016 it was the example of the highest anisotropic energy barrier.

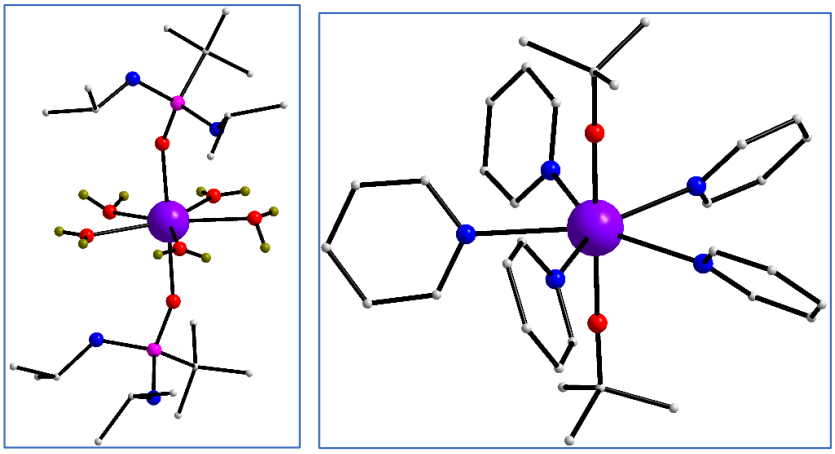

(a) **(b)**

Figure 58: (a) Structure of $[L_2Dy(H_2O)_5]^{3+}$ (L= ^{t}BuPO(NH^{i}Pr)$_2$) **(b)** Structure of $[Dy(O^{t}Bu)_2(py)_5]$

In 2018 Layfield, Tong and co-workers were reported[88] the exceptionally high anisotropic energy barrier (Ueff) 1541 cm^{-1} and highest blocking temperature (T_B) 80K displaying extraordinary example of organometallic lanthanide SMM $[(Cp^{i}Pr_5)Dy(Cp^*)][B(C_6F_5)_4]$ ($Cp^{i}Pr_5$= penta-iso-propylcyclopentadienyl; Cp*= pentamethylcyclopentadienyl)(**Figure 59**). This molecule shows golden light in the dark night in the realm of SMM which reaches towards the present drawback that all SMM molecules requirement of liquid helium colling to show magnetic memory effects by reaching above liquid nitrogen boiling point temperature.

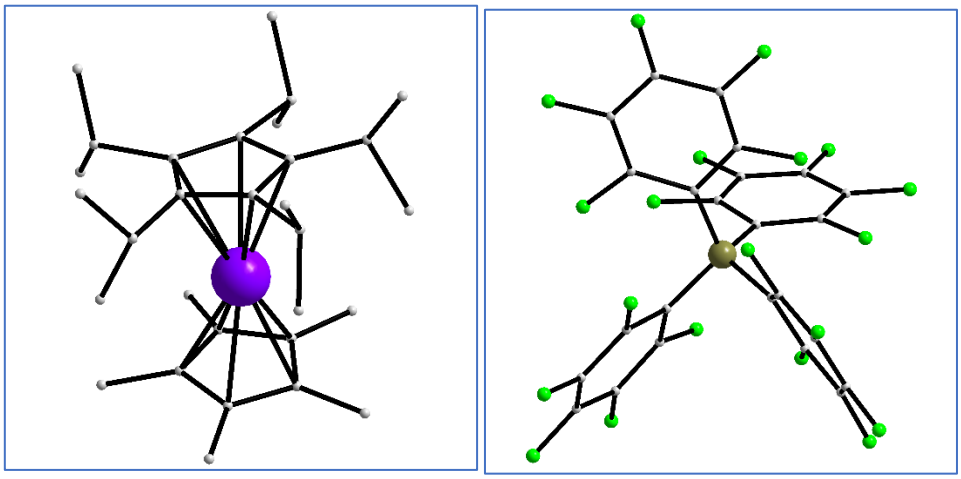

Figure 59: Structure of $[(Cp^{i}Pr_5)Dy(Cp^*)][B(C_6F_5)_4]$

Very recently Gould et al. reported[89] for the first time the mixed-valence dilanthanide complex $(Cp^{i}Pr_5)_2Dy_2I_3$ (**Figure 60**) which gives a substantial coercive magnetic field with a lower limit of 14 T at temperature 60 K. Its record coercivity at liquid nitrogen temperatures exceeds even commercial magnets $SmCo_5$ (4.3 T at 4.2 K) and $Nd_2Fe_{14}B$ (5.0 T at 80 K) and gave the name Ultrahard magnet. They have synthesized $(Cp^{i}Pr_5)_2Dy_2I_3$ from $(Cp^{i}Pr_5)_2Dy_2I_4$ by reduction with potassium graphite in hexane (**Figure 60**). Solid-state structure from SCXRD tells three iodine anions are bridges the two dysprosium centers to yield a Dy_2I_3 core; all the metal center is capped with $(Cp^{iPr5})^-$ ligand and a trigonal symmetry. The Dy…Dy bond displays 3.713Å which is within the sum of the covalent radii of the Dy-metal atom indicating the presence of Dy…Dy metal bonding. From the ac and dc magnetic data, U_{eff} = 1631(25) cm^{-1} and T_B = 72 K of the $(Cp^{i}Pr_5)_2Dy_2I_3$ complex was reported which exceeds the previous record made by Layfield et al.[88] Strong magnetic coupling between two lanthanide ions diminishes the Raman and QTM processes, resulting large H_c value. It is the first example, where the exchange interaction and the large magnetic anisotropy induced by the crystal field are collinear.

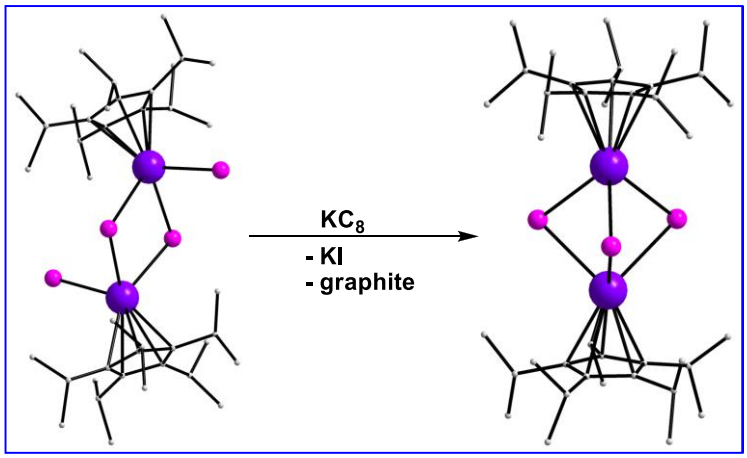

Figure 60: Scheme of the preparation of $(Cp^{i}Pr_5)_2Dy_2I_3$

(h) Lanthanide phosphinates:

Lanthanide phosphinates generally form poorly soluble complexes in aqueous and organic solvents. For this reason, a very less number of reports are present in the literature.[90,91,100–105,92–99] Maximum reports present in literature are macrocyclic-based phosphinic acid pendant arm containing ligands (**Figure 62**). The solution behaviors are mostly studied. Among them, very few have structurally characterized by single-crystal X-ray diffraction.[91,92,95,96,100,103] These complexes are used in radio-pharmaceuticals and taking advantage of their physical properties such as luminescence and magnetism used as EPR, NMR-shift probes, and MRI-contrast agents. According to CSD (Cambridge Crystallographic Database) following binding motifs (**Figure 61**) have been found with metal-phosphinates [106] To our best knowledge until now there are three coordination modes (**Figure 61(A)**) of phosphinic acid with lanthanide reported.

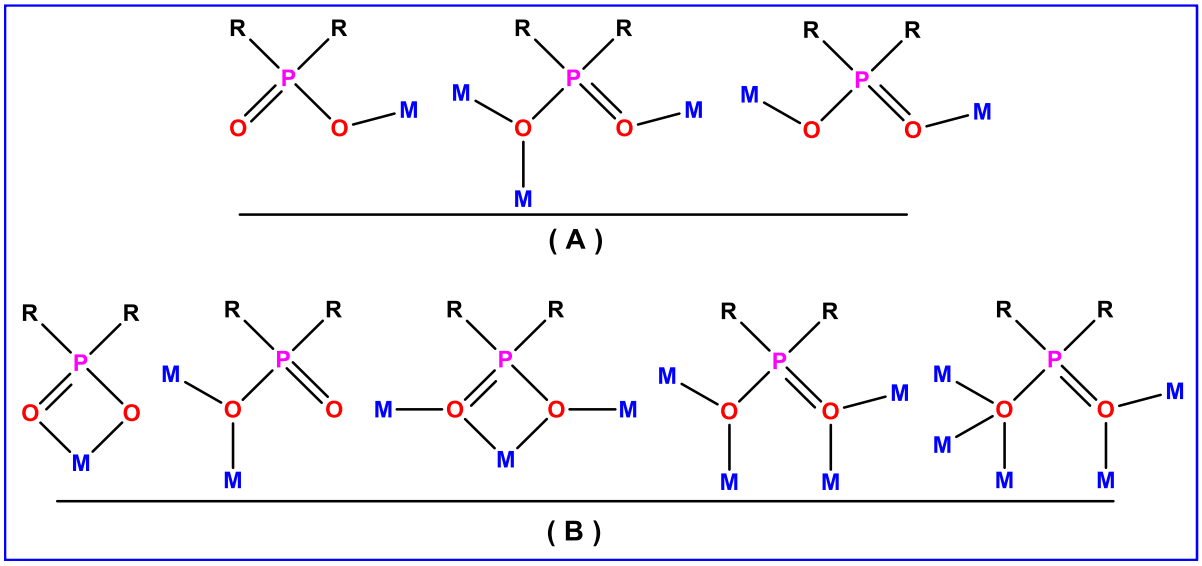

Figure 61: Binding motifs of metal-phosphinates

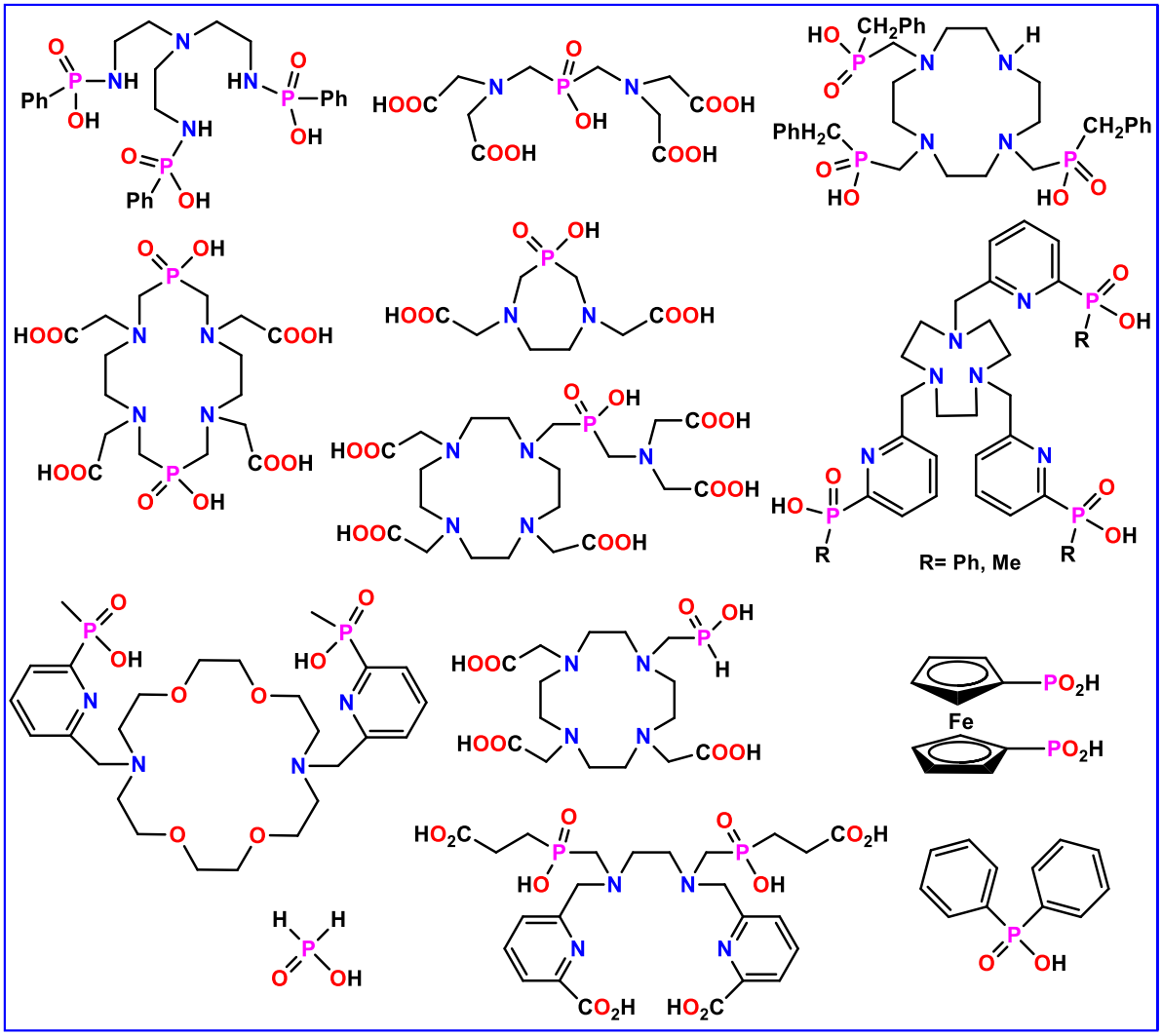

Figure 62: List of phosphinic acid ligands known with lanthanide complexes

1.5. Thesis overview:

The thesis work focuses on the synthesis of the new multinuclear cluster of 3d (Zn and Cd) and 4f-block metals with the use of Schiff base and Bis-[(α-hydroxyphenyl)methyl]-phosphinic acid.

Schiff-bases are widely used as a ligand for the synthesis of polynuclear cluster synthesis. Hence our motivation was to synthesize multinuclear clusters of zinc metal with various alkyl chain lengths containing Schiff-base ligands along with or without auxiliary ligands and how it helps to form different nuclearity of the cluster. Details of the work are presented in **chapter 2**.

In **chapter 3** we have utilized Bis[(α-hydroxy(p-methylphenyl)methyl)]-phosphinic acid with cadmium salt and yielded various geometry and architectures of cadmium complexes of 0D, 1D, and 2D coordination polymers.

Lanthanide phosphinates are rarely explored in the research field. Very few lanthanides are known structurally by single-crystal X-ray diffraction (SCXRD). Herein **chapter 4** and **chapter 5** dinuclear, trinuclear linear paddlewheel and tetranuclear [2 × 2] square grid structures were synthesized and well-characterized respectively by SCXRD using Bis[(α-hydroxy(p-methylphenyl)methyl]-phosphinic acid and Bis-[(α-hydroxy(p-bromophenyl)methyl]-phosphinic acid. From the synthetic viewpoint, these structures are very much important in the realm of phosphinic acid chemistry.

1.6. References

1 Z. M. Gyorgy Keglevich, Nora Zsuzsa kiss, *Chem. Sci. J.*, 2014, **05**, 1–14.

2 S. M. Z. and M. G. Mingkui Wang, a Xin Li, b Hong Lin, b Peter Pechy, *Dalt. Trans.*, 2009, 9952–9959.

3 J. Wang, G. Chen, S. Xu and L. Li, *Hydrometallurgy*, 2015, **154**, 129–136.

4 G. Keglevich and E. Bálint, *Molecules*, 2012, **17**, 12821–12835.

5 S. Deprèle and J. L. Montchamp, *J. Am. Chem. Soc.*, 2002, **124**, 9386–9387.

6 M. Kolb, *Synth. Commun.*, 1979, **9**, 261–266.

7 J. Dussart, N. Guedeney, J. Deschamp, M. Monteil, O. Gager, T. Legigan, E. Migianu-Griffoni and M. Lecouvey, *Org. Biomol. Chem.*, 2018, **16**, 6969–6979.

8 B. Kaboudin and N. As-Habei, *Tetrahedron Lett.*, 2004, **45**, 9099–9101.

9 B. Kaboudin and H. Haghighat, *J. Org. Chem.*, 2006, **71**, 6604–6606.

10 B. Kaboudin, H. Haghighat and T. Yokomatsu, *Tetrahedron Asymmetry*, 2008, **19**, 862–866.

11 H. Schiff, *Justus Liebigs Ann. Chem.*, 1864, **131**, 118–119.

12 V. Chandrasekhar, R. Boomishankar, P. Sasikumar, L. Nagarajan and A. W. Cordes, *Zeitschrift fur Anorg. und Allg. Chemie*, 2005, **631**, 2727–2732.

13 R. Pothiraja, S. Shanmugan, M. G. Walawalkar, M. Nethaji, R. J. Butcher and R. Murugavel, *Eur. J. Inorg. Chem.*, 2008, 1834–1845.

14 M. J. Zhou, B. Li, L. Liu, Y. L. Feng and J. Z. Guo, *CrystEngComm*, 2014, **16**, 10034–10039.

15 M.-X. L. Zhao-Xi Wang, Lin-Fei Wu, Hong-Ping Xiao, Xing-Hua Luo, *Cryst. Growth Des.*, 2016, **16**, 5184–5193.

16 S. D. Pike, E. R. White, M. S. P. Shaffer and C. K. Williams, *Nat. Commun.*, 2016, **7**, 1–11.

17 E. Oleshkevich, I. Romero, F. Teixidor and C. Viñas, *Dalt. Trans.*, 2018, **47**, 14785–14798.

18 I. Svobodová, P. Lubal, J. Plutnar, J. Havlíčková, J. Kotek, P. Hermann and I. Lukeš, *Dalt. Trans.*, 2006, 5184–5197.

19 V. Chandrasekhar, D. Sahoo and R. K. Metre, *CrystEngComm*, 2013, **15**, 7419–7422.

20 V. Chandrasekhar, S. Kingsley, B. Rhatigan, M. K. Lam and A. L. Rheingold, *Inorg. Chem.*, 2002, **41**, 1030–1032.

21 G. Anantharaman, V. Chandrasekhar, M. G. Walawalkar, H. W. Roesky, D. Vidovic, J. Magull and M. Noltemeyer, *Dalt. Trans.*, 2004, **4**, 1271–1275.

22 R. Murugavel and S. Shanmugan, *J. Chem. Soc. Dalt. Trans.*, 2008, 5358–5367.

23 V. Chandrasekhar, P. Sasikumar, R. Boomishankar and G. Anantharaman, *Inorg. Chem.*, 2006, **45**, 3344–3351.

24 D. Cao, Y. Li and L. Zheng, *Inorg. Chem.*, 2005, **44**, 2984–2985.

25 D. Sahoo, R. Suriyanarayanan, R. K. Metre and V. Chandrasekhar, *Dalt. Trans.*, 2014, **43**, 7304–7313.

26 R. Fu, S. Hu and X. Wu, *CrystEngComm*, 2013, **15**, 8937–8940.

27 H. W. R. Yu Yang, Jiri Pinkas, Mathias Noltemeyer, Hans-Georg Schmidt, *Angew. Chemie*

Int. Ed., 1999, **38**, 664–666.

28 K. Weis, M. Rombach and H. Vahrenkamp, *Inorg. Chem.*, 1998, **37**, 2470–2475.

29 B. Bauer-siebenlist, F. Meyer, E. Farkas, D. Vidovic, J. A. Cuesta-seijo, R. Herbst-irmer, H. Pritzkow, A. Institut, V. Uni, I. N. Feld and D.- Heidelberg, *Inorg. Chem.*, 2004, **43**, 4189–4202.

30 B. S. Hammes and C. J. Carrano, *J. Chem. Soc. Dalt. Trans.*, 2000, 3304–3309.

31 E. Kimura, S. Aoki, T. Koike and M. Shiro, *J. Am. Chem. Soc.*, 1997, **119**, 3068–3076.

32 R. Murugavel, M. Sathiyendiran and M. G. Walawalkar, *Inorg. Chem.*, 2001, **40**, 427–434.

33 C. G. Lugmair, T. D. Tilley and A. L. Rheingold, *Chem. Mater.*, 1997, **9**, 339–348.

34 R. Murugavel, S. Kuppuswamy, R. Boomishankar and A. Steiner, *Angew. Chemie - Int. Ed.*, 2006, **45**, 5536–5540.

35 E. K. Mishtu Dey,[a] Chebrolu Pulla Rao,*[a] Pauli Saarenketo,[b] Kari Rissanen, *Eur. J. Inorg. Chem.*, 2002, 2207–2215.

36 Y. Zhao, Z. Li, H. Li, S. Wang and M. Niu, *Inorganica Chim. Acta*, 2018, **482**, 136–143.

37 O. Tsave, E. Halevas, M. P. Yavropoulou, A. Kosmidis Papadimitriou, J. G. Yovos, A. Hatzidimitriou, C. Gabriel, V. Psycharis and A. Salifoglou, *J. Inorg. Biochem.*, 2015, **152**, 123–137.

38 M. Liu, H. Yang, D. Li, Q. Yao, H. Wang, Z. Zhang and J. Dou, *Inorganica Chim. Acta*, 2021, **522**, 120384.

39 D. Dey, G. Kaur, A. Ranjani, L. Gayathri, P. Chakraborty, J. Adhikary, J. Pasan, D. Dhanasekaran, A. R. Choudhury, M. A. Akbarsha, N. Kole and B. Biswas, *Eur. J. Inorg. Chem.*, 2014, 3350–3358.

40 D. Dey, G. Kaur, M. Patra, A. R. Choudhury, N. Kole and B. Biswas, *Inorganica Chim. Acta*, 2014, **421**, 335–341.

41 M. Mikuriya, S. Ikenoue, R. Nukada and J. W. Lim, *Bull. Chem. Soc. Jpn.*, 2001, **74**, 101–102.

42 W. Sun, X. T. Qin, G. N. Zhang, S. Ding, Y. Q. Wang and Z. L. Liu, *Inorg. Chem. Commun.*, 2014, **40**, 190–193.

43 Q. Shi, J. Yang and X. Lü, *Inorg. Chem. Commun.*, 2015, **59**, 61–62.

44 L. Jiang, D. Y. Zhang, J. J. Suo, W. Gu, J. L. Tian, X. Liu and S. P. Yan, *Dalt. Trans.*, 2016, **45**, 10233–10248.

45 M. Garai, A. Das, M. Joshi, S. Paul, M. Shit, A. R. Choudhury and B. Biswas, *Polyhedron*, 2018, **156**, 223–230.

46 E. M. Swarup Ghosh, Anke Spannenberg, *Helv. Chim. Acta*, 2017, **100**, e1700176.

47 H. Yu, M. Liu, X. Gao and Z. Liu, *Polyhedron*, 2017, **137**, 217–221.

48 A. Pravat Ghorai and [c] and Amrita Saha*[a] Paula Branda˜o,[b] Antonio Bauza´,[c] Antonio Frontera, 2018, 7697–7706.

49 E. C. Constable, C. E. Housecroft, J. A. Zampese and G. Zhang, *Polyhedron*, 2012, **44**, 150–155.

50 E. Liu, Y. Z. Zhang, J. Tan, C. Yang, L. Li, J. A. Golen, A. L. Rheingold and G. Zhang, *Polyhedron*, 2015, **102**, 41–47.

51 N. Hari, S. Ghosh and S. Mohanta, *Inorganica Chim. Acta*, 2019, **491**, 34–41.

52 S. K. Kushvaha, B. Shankar, N. V. T. S. M. Gorantla and K. C. Mondal, *ChemistrySelect*, 2019, **4**, 3334–3339.

53 S. H. Zhang and C. Feng, *J. Mol. Struct.*, 2010, **977**, 62–66.

54 W. L. Haifeng Zhang,[a, b] Jin Zhang,[a] Rui Liu,[b] Yahong Li,*[a] Wei Liu, *Eur. J. Inorg. Chem.*, 2016, 4134–4144.

55 R. Gheorghe, G. Andreea Ionita, C. Maxim, A. Caneschi, L. Sorace and M. Andruh, *Polyhedron*, 2019, **171**, 269–278.

56 J. Sanmartín, M. R. Bermejo, A. M. García-Deibe and A. L. Llamas-Saiz, *Chem. Commun.*, 2000, **8**, 795–796.

57 S. J. I. Shearan, N. Stock, F. Emmerling, J. Demel, P. A. Wright, K. D. Demadis, M. Vassaki, F. Costantino, R. Vivani, S. Sallard, I. R. Salcedo, A. Cabeza and M. Taddei, *New directions in metal phosphonate and phosphinate chemistry*, 2019, vol. 9.

58 P. Betz and A. V. I. Bino, *Inorganica Chim. Acta*, 1990, **170**, 45–51.

59 O. Oms, J. Le Bideau, A. Vioux and D. Leclercq, *J. Organomet. Chem.*, 2005, **690**, 363–370.

60 L. J. Dong, C. C. Zhao, X. Xu, Z. Y. Du, Y. R. Xie and J. Zhang, *Cryst. Growth Des.*, 2012, **12**, 2052–2058.

61 A. V Anyushin, D. A. Mainichev, N. K. Moroz, P. A. Abramov, D. Y. Naumov, M. N. Sokolov and V. P. Fedin, *Inorg. Chem.*, 2012, **51**, 9995–10003.

62 C. C. Zhao, Z. G. Zhou, X. Xu, L. J. Dong, G. H. Xu and Z. Y. Du, *Polyhedron*, 2013, **51**, 18–26.

63 C. C. Xue, M. X. Li, M. Shao and Z. X. Wang, *Russ. J. Coord. Chem. Khimiya*, 2016, **42**, 442–448.

64 L. Zhang, S. Y. Zhang, Y. N. Gong, J. X. Liu, Z. Y. Du and Y. R. Xie, *J. Chem. Crystallogr.*, 2016, **46**, 237–244.

65 R. Shekurov, M. Khrizanforov, D. Islamov, T. Gerasimova, A. Zagidullin, Y. Budnikova and V. Miluykov, *J. Organomet. Chem.*, 2020, **914**, 121233.

66 M. Bazaga-García, Á. Vílchez-Cózar, B. Maranescu, P. Olivera-Pastor, M. Marganovici, G. Ilia, A. Cabeza Díaz, A. Visa and R. M. P. Colodrero, *Dalt. Trans.*, 2021, **50**, 6539–6548.

67 D. N. H. Roberta Sessoli, Hui Lien Tsai, Ann R. Schake, Sheyi Wang, John B. Vincent, Kirsten Folting, Dante Gatteschi, George Christou, *J. Am. Chem. Soc.*, 1993, **115**, 1804–1816.

68 T. Lis, *Acta Crystallogr. Sect. B Struct. Crystallogr. Cryst. Chem.*, 1980, **36**, 2042–2046.

69 A. Caneschi, D. Gatteschi, R. Sessoli, A. L. Barra, L. C. Brunei and M. Guillot, *J. Am. Chem. Soc.*, 1991, **113**, 5873–5874.

70 M. A. Novak, R. Sessoli, D. Gatteschi and A. Caneschi, *Nature*, 1993, **365**, 141–143.

71 J. R. Friedman, M. P. Sarachik, J. Tejada and R. Ziolo, *Phys. Rev. Lett.*, 1996, **76**, 3830–3833.

72 L. Thomas, F. Lionti, R. Ballou, D. Gatteschi, R. Sessoli and B. Barbara, *Nature*, 1996, **383**, 145–147.

73 N. Ishikawa, M. Sugita, T. Ishikawa, S. Y. Koshihara and Y. Kaizu, *J. Am. Chem. Soc.*, 2003, **125**, 8694–8695.

74 N. Koike, H. Uekusa, Y. Ohashi, C. Harnoode, F. Kitamura, T. Ohsaka and K. Tokuda, *Inorg. Chem.*, 1996, **35**, 5798–5804.

75 F. Branzoli, P. Carretta, M. Filibian, G. Zoppellaro, M. J. Graf, J. R. Galan-Mascaros, O. Fuhr, S. Brink and M. Ruben, *J. Am. Chem. Soc.*, 2009, **131**, 7934–7934.

76 N. Ishikawa, M. Sugita, T. Okubo, N. Tanaka, T. Iino and Y. Kaizu, *Inorg. Chem.*, 2003, **42**, 2440–2446.

77 N. Ishikawa, M. Sugita, T. Ishikawa, S. Y. Koshihara and Y. Kaizu, *J. Phys. Chem. B*, 2004, **108**, 11265–11271.

78 N. Ishikawa, *J.Phys.Chem. A*, 2003, **107**, 5831–5835.

79 W. W. Naoto Ishikawa, Miki Sugita, *Angew. Chemie - Int. Ed.*, 2005, **44**, 2931–2935.

80 A. K. P. Jinkui Tang, Ian Hewitt, N. T. Madhu, Guillaume Chastanet, Wolfgang Wernsdorfer, Christopher E. Anson, Cristiano Benelli, Roberta Sessoli, *Angew. Chemie Int. Ed.*, 2006, **45**, 1729–1733.

81 M. M. Po-Heng Lin, Tara J. Burchell, Liviu Ungur, Liviu F. Chibotaru, Wolfgang Wernsdorfer, *Angew. Chemie*, 2009, **1221**, 9653–9656.

82 R. J. Blagg, C. A. Muryn, E. J. L. McInnes, F. Tuna and R. E. P. Winpenny, *Angew. Chemie - Int. Ed.*, 2011, **50**, 6530–6533.

83 V. Chandrasekhar, S. Hossain, S. Das, S. Biswas and J. P. Sutter, *Inorg. Chem.*, 2013, **52**, 6346–6353.

84 J. Xiong, H. Y. Ding, Y. S. Meng, C. Gao, X. J. Zhang, Z. S. Meng, Y. Q. Zhang, W. Shi, B. W. Wang and S. Gao, *Chem. Sci.*, 2017, **8**, 1288–1294.

85 S. Demir, M. I. Gonzalez, L. E. Darago, W. J. Evans and J. R. Long, *Nat. Commun.*, 2017, **8**, 1–9.

86 Y.-Z. Z. You-Song Ding, Nicholas F. Chilton,* RichardE.P.Winpenny, *Angew. Chemie - Int. Ed.*, 2016, **55**, 16071–16074.

87 S. K. Gupta, T. Rajeshkumar, G. Rajaraman and R. Murugavel, *Chem. Sci.*, 2016, **7**, 5181–5191.

88 F. S. Guo, B. M. Day, Y. C. Chen, M. L. Tong, A. Mansikkamäki and R. A. Layfield, *Science (80-.).*, 2018, **362**, 1400–1403.

89 C. A. Gould, K. R. McClain, D. Reta, J. G. C. Kragskow, D. A. Marchiori, E. Lachman, E. S. Choi, J. G. Analytis, R. D. Britt, N. F. Chilton, B. G. Harvey and J. R. Long, *Science (80-.).*, 2022, **375**, 198–202.

90 E. B. Stucchi, S. L. Scarpari, M. A. Couto Dos Santos and S. R. A. Leite, *J. Alloys Compd.*, 1998, **275**–**277**, 89–92.

91 M. P. Lowe, P. Caravan, S. J. Rettig and C. Orvig, *Inorg. Chem.*, 1998, **37**, 1637–1647.

92 A. E.- Aziz and M. Crude, *J. Chem.Soc., Dalt. Trans*, 1999, 2189–2196.

93 L. Xu, S. J. Rettig, C. Orvig, M. Mall and B. C. Vt, *Inorg. Nano-Metal Chem.*, 2001, **40**, 3734–3738.

94 B. Song, T. Storr, S. Liu and C. Orvig, *Inorg. Chem.*, 2002, **41**, 685–692.

95 K. Senanayake, A. L. Thompson, J. A. K. Howard, M. Botta and D. Parker, *J. Chem. Soc. Dalt. Trans.*, 2006, 5423–5428.

96 J. W. Walton, R. Carr, N. H. Evans, A. M. Funk, A. M. Kenwright, D. Parker, D. S. Yufit, M. Botta, S. De Pinto and K. L. Wong, *Inorg. Chem.*, 2012, **51**, 8042–8056.

97 J. H. S. K. Monteiro, A. L. B. Formiga and F. A. Sigoli, *J. Lumin.*, 2014, **154**, 22–31.

98 S. Procházková, V. Kubíček, Z. Böhmová, K. Holá, J. Kotek and P. Hermann, *Dalt. Trans.*, 2017, **46**, 10484–10497.

99 D. M. Weekes, M. De Guadalupe Jaraquemada-Peláez, T. I. Kostelnik, B. O. Patrick and C. Orvig, *Inorg. Chem.*, 2017, **56**, 10155–10161.

100 S. Procházková, V. Kubíček, J. Kotek, A. Vágner, J. Notni and P. Hermann, *Dalt. Trans.*, 2018, **47**, 13006–13015.

101 R. P. Shekurov, L. H. Gilmanova, M. N. Khrizanforov, S. O. Strekalova, Y. H. Budnikova, T. P. Gerasimova, S. A. Katsyuba and V. A. Miluykov, *Phosphorus, Sulfur Silicon Relat. Elem.*, 2019, **194**, 459–462.

102 M. N. Khrizanforov, R. P. Shekurov, L. H. Gilmanova, T. P. Gerasimova, V. A. Miluykov and Y. H. Budnikova, *Phosphorus, Sulfur Silicon Relat. Elem.*, 2019, **194**, 1010–1012.

103 N. A. Thiele, D. J. Fiszbein, J. J. Woods and J. J. Wilson, *Inorg. Chem.*, 2020, **59**, 16522–16530.

104 T. I. Kostelnik, X. Wang, L. Southcott, H. K. Wagner, M. Kubeil, H. Stephan, M. D. G. Jaraquemada-Pelaéz and C. Orvig, *Inorg. Chem.*, 2020, **59**, 7238–7251.

105 L. Pazderová, T. David, J. Kotek, V. Kubíček and P. Hermann, *Polyhedron*, 2021, **196**, 114994.

106 I. Carson, M. R. Healy, E. D. Doidge, J. B. Love, C. A. Morrison and P. A. Tasker, *Coord. Chem. Rev.*, 2017, **335**, 150–171.

In-situ Assembled Polynuclear Zinc Oxo Clusters Using modified Schiff-bases as Ligands

CHAPTER

2

A series of different core and nuclearity zinc metal clusters have been synthesized **2.1-2.5** using $Zn(ClO_4)_2.6H_2O$, Schiff-base primary ligand, and DBM or monoethanolamine(MEA) as co-ligand at room temperature reaction. The structure of the complexes characterized by single-crystal X-ray diffraction. Among this (**2.1**) $[Zn(L1)(DBM)]$ is mononuclear, (**2.2**) $[Zn(L2)_2(DBM)_4]$, (**2.3**) $[Zn_4(L2)_4(H_2O)_2(ClO_4)_2].2CH_2Cl_2$. (**2.4**) $[Zn_4(L3)_2(DBM)_4]$ has a cubane core. (**2.5**) $[Zn_4(L4)_4(MEA)_2(ClO_4)_2]$ is a ladder-like core structure. Compounds **2.1-2.5** has been also characterized by UV-Vis absorption and emission spectroscopy. For in-depth understanding of the absorption spectrum of **2.1**,**2.3** DFT (Density Functional Theory) calculations has been performed which suggests that the transitions correspond to the $\pi \rightarrow \pi^*$ intra-ligand charge transfer (ILCT) transitions.

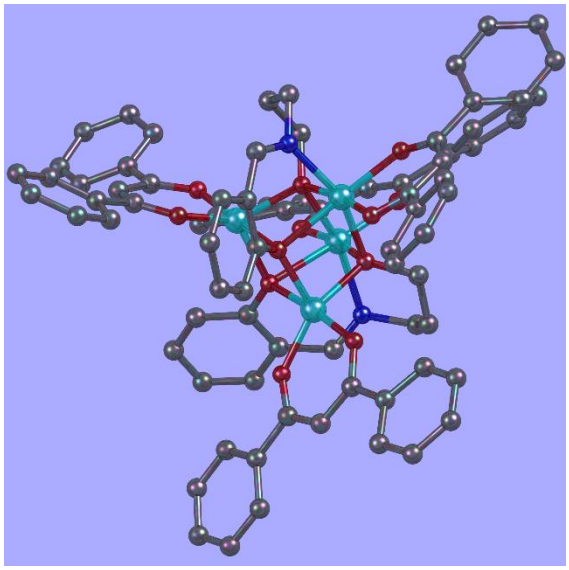

2.1 Introduction:

Multicomponent reactions of 3d and 4f elements with multidentate organic/main group elements based on ligands containing donating heteroatoms have been exploited in detail due to their interesting and complex coordination behaviors.[1] Our interest in this area has been established from a series of multinuclear clusters using phosphinate/phosphonate and organostibonate-based ligand systems which have yielded structurally fascinating molecular clusters of transition metal ions[2] and lanthanides[3], some of which have shown interesting magnetic properties like single-molecule magnet (SMM) behavior.[4] We have recently shown the assembly of titanium-based multinuclear clusters, one of which shows interesting structural properties like fluxional behavior at room temperature.[5] Moreover, we have also recently shown a designed approach for reducing bandgaps by synthesizing Ti_4Sb_2-based heteronuclear clusters from a parent Sb_6 molecular framework using solvothermal reaction conditions.[6] We have also been using multidentate donating ligands like Schiff base ligands due to their adjustable coordination properties and flexible bridging modes.[7] Using Schiff base /modified vanillin-based Schiff bases, several multinuclear complexes of d/f block elements have been reported.[8] Notable reports among them are multinuclear dysprosium-based clusters reported by Murugesu et al., who synthesized a series of tetranuclear butterfly cores containing dysprosium clusters, and the magnetic measurements revealed that some of those clusters displayed a high energy barrier for reversal of magnetization.[9] In this backdrop, Schiff base ligands have been used for synthesizing zinc-based multinuclear clusters, some of which has shown interesting applications as a polymerization catalyst,[10] reagents in organic synthesis,[11] molecular precursor for ZnO-based materials,[12] models of the active site in zinc enzymes[13] and in synthesizing functional molecule-based materials.[14] Some of the molecular clusters of zinc reported in the literature are mononuclear[15], binuclear[16], trinuclear[17], tetranuclear[18] to polynuclear clusters[19]. Some of these structural forms, like the tetranuclear core cluster, have garnered special attention, particularly the manganese-based tetranuclear clusters, which have been involved in multielectron transfer redox reactions OEC (oxygen-evolving complex) of PSII in green plants.[20]

Herein, the synthesis and structural characterization of a series of zinc-based molecular clusters have been reported. By systematically carrying out reactions of metal perchlorates in the presence/absence of the co-ligand used and varying the length of the methylene side-chain incorporated in the modified Schiff bases used, different nuclearity-based zinc clusters have been synthesized and structurally characterized. DFT calculations have been performed to

understand better the electronic absorption spectra of clusters **2.1** and **2.3**. The details of the study are presented herein.

2.2 Experimental Section:

2.2.1 General information:

2.2.1.1 Preparation of the Schiff base ligand and complex

Chemicals, solvents, and starting materials

Caution! All perchlorates, including raw materials and products, are potentially explosive. These materials should be used during the process in a fume hood and handled with care.

High purity o-vanillin (Sigma-Aldrich), salicylaldehyde (Merck), ethanolamine (Avra), 3-aminopropanol (Avra), dibenzoylmethane(DBM) (Sigma-Aldrich), zinc perchlorate hexahydrate (Sigma-Aldrich), and all other solvents were purchased from commercial sources. All solvents were used distilled, and chemicals were used without further purification.

2.2.1.2 General synthesis:

Schiff base ligands L1, L2, L3, and L4 were synthesized in-situ condensation[1] into the reaction medium.

Synthesis of complexes

For **2.1**, **2.3**, **2.4**, and **2.5** similar synthetic procedures were followed. Ligands and co-ligands were taken in a 30ml methanol-acetonitrile solvent mixture (1:1) and metal salt (zinc perchlorate hexahydrate) was added following triethylamine base dropwise addition, stirred for 6h followed by different crystallization techniques. Only **2.2** stirred for 24 h.

For **2.1** salicylaldehyde (0.082 g, 0.770 mmol), monoethanolamine (0.082 ml, 0.770 mmol) DBM (0.172 g, 0.770 mmol), zinc perchlorate (0.286 g, 0.770 mmol), triethylamine (0.321 ml, 2.31 mmol) were required. After 6 h at room temperature reaction, filtered the yellowish solution and reduce the volume to 10 ml. Yellowish crystals were obtained overnight, which were collected and analyzed. Yield: 0.310 g, 89.15% (Based on $Zn(ClO_4)_2, 6H_2O$). Anal. Calcd. (%) for $C_{24}H_{21}NO_4Zn$ (452.83): C, 63.66; H, 4.67; N, 3.09. Found: C, 63.63; H, 4.71; N, 3.12.

^{1}H NMR (500 MHz, DMSO-d_6): δ = 8.39 (s,1H, CH=N), 8.04-8.06 (m, 4H, Ar H),7.47-7.54 (m, 6H, Ar H), 7.15-7.25 (m, 2H, Ar H), 6.78 (s, 1H, CH), 6.59-6.61 (d, 1H, Ar H), 6.43-6.54 (m, 1H, Ar H), 5.07 (br,1H, CH_2OH), 3.57-3.72 (m, 4H,)

^{13}C NMR (125 MHz, DMSO-d_6): δ = 185.96, 172.54, 170.59, 140.65, 136.48, 134.64, 131.46, 128.82, 127.62, 122.76, 118.79, 113.97, 92.79, 62.43, 60.43

(Selected IR bands: $\tilde{\upsilon}(cm^{-1})$ = 3205, 1591, 1519, 1233, 1065, 744)

For **2.2** o-vanillin (0.117 g, 0.770 mmol), 3-aminopropanol (0.058 ml, 0.770 mmol), DBM (0.172 g, 0.770 mmol), zinc perchlorate (0.286 g, 0.770 mmol), triethylamine (0.321 ml, 2.31 mmol) were required. Within 30 minutes a white color precipitate was started throwing out from the reaction medium. Stirring was continued for 24h for the complete precipitation. Filtered the precipitate and kept it for crystallization in the chloroform/hexane using the diffusion method. X-ray quality crystals were obtained in one week. Yield: 0.240 g, 74.05% (Based on $Zn(ClO_4)_2$, $6H_2O$). Anal. Calcd. (%) for $C_{83}H_{71}Cl_3N_2O_{14}Zn_4$ (1688.24): C, 59.05; H, 4.24; N, 1.66. Found: C, 59.09; H, 4.32; N, 1.68.

^{1}H NMR (500 MHz, DMSO-d_6): δ = 8.23 (s,2H, CH=N), 8.05-8.06 (m, Ar H), 7.47-7.54 (m, 24H, Ar H), 6.78 (s, 4H, C=CH), 6.75-6.81 (d, 4H, Ar H), 6.36-6.39 (t, 2H, Ar H), 3.83-4.33 (m, 8H, CH_2O CH_2N), 3.69 (s, 6H, OMe), 1.83 (m, 4H, CH_2)

^{13}C NMR (125 MHz, DMSO-d_6): δ = 186.03, 172.56, 140.68, 131.43, 128.79, 127.60, 92.79, 56.12

(Selected IR bands: $\tilde{\upsilon}(cm^{-1})$ = 1596, 1452, 1222, 1066, 717)

For **2.3** o-vanillin (0.117 g, 0.770 mmol), 3-aminopropanol (0.058 ml, 0.770 mmol), zinc perchlorate (0.286 g, 0.770 mmol), triethylamine (0.321 ml, 2.31 mmol) were required. Stirring was continued for 6 h for completion of the reaction. The solvent to half the initial volume and kept it for crystallization in DCM/hexane mixture using the diffusion method. X-ray quality crystals were obtained in two weeks. Yield: 0.190 g, 66.10% (Based on $Zn(ClO_4)_2$, $6H_2O$). Anal. Calcd. (%) for $C_{46}H_{62}Cl_6N_4O_{22}Zn_4$ (1497.17): C, 36.90; H, 4.17; N, 3.74. Found: C, 36.82; H, 4.21; N, 3.70.

^{1}H NMR (500 MHz, DMSO-d_6): δ = 8.24 (s, 4H, CH=N), 6.75-6.86 (m, 8H, Ar-H), 6.37-6.43 (m, 4H, Ar-H), 3.69 (s, 12H, OMe), 3.46-3.61 (m, 16H, NCH_2 and OCH_2), 1.78 (m, 8H, CH_2)

^{13}CNMR (125 MHz, DMSO-d_6): δ = 168.60, 161.39,152.56, 152.28, 127.55, 126.71, 118.31, 118.11, 113.74, 112.22, 69.14, 62.73, 55.98, 55.72, 55.38, 36.39, 33.21

(Selected IR bands: $\tilde{\upsilon}(cm^{-1})$ = 3483, 1614, 1442, 1211, 1058, 733, 1058)

For **2.4** salicylaldehyde (0.082 g, 0.770 mmol), 3-aminopropanol (0.058 ml, 0.770 mmol), DBM (0.172 g, 0.770 mmol), zinc perchlorate (0.286 g, 0.770 mmol), triethylamine (0.321 ml, 2.31 mmol) were required. After 6 h stirring, the reaction mixture was filtered and evaporated. Kept it for crystallization in DCM/hexane layer method at 0°C. X-ray quality crystal came within two weeks. Yield: 0.200 g, 66.33% (Based on $Zn(ClO_4)_2$, $6H_2O$). Anal. Calcd. (%) for

$C_{81.50}H_{70}Cl_3N_2O_{12.50}Zn_4$ (1645.22): C, 59.50; H, 4.29; N, 1.70. Found: C, 59.61; H, 4.53; N, 1.68.

^{1}H NMR (500 MHz, DMSO-d_6): δ = 8.24 (s, 2H, CH=N), 8.04-8.05 (m, 16H, Ar-H), 7.46-7.53 (m, 24H, Ar-H), 7.13-7.17 (m,4H, Ar-H), 6.78 (s,4H, C-H), 6.57-6.61 (m,2H, Ar-H), 6.45-6.48 (m,2H, Ar-H), 3.61-3.74 (m,4H, CH_2N), 3.36-3.44 (m,4H, CH_2O), 1.67-1.69 (m,4H, CH_2),

^{13}CNMR (125 MHz, DMSO-d_6): δ = 186.03, 172.56, 170.73, 140.67, 136.57, 135.95, 134.88, 133.76, 131.44, 128.80, 127.60, 122.70, 114.29, 113.02, 92.80, 59.09, 58.07, 57.53, 55.35,34.66, 33.90,

(Selected IR bands: ῡ(cm^{-1}) = 1594, 1474, 1272, 1065, 716)

For **2.5** o-vanillin (0.117 g, 0.770 mmol), ethanolamine (0.069 ml, 1.155 mmol), zinc perchlorate (0.286 g, 0.770 mmol), triethylamine (0.321 ml, 2.31 mmol) were required. Stirring was continued for 6 h. The clear solution was filtered and evaporated. The oily residue was dissolved in DCM and kept for crystallization in DCM/hexane layer method at 0°C. X-ray quality crystal came within one week. Yield: 0.210 g, 80.58% (Based on $Zn(ClO_4)_2$, $6H_2O$). Anal. Calcd. (%) for $C_{44}H_{60}Cl_2N_6O_{22}Zn_4$ (1357.36): C, 38.93; H, 4.46; N, 6.19. Found: C, 38.87; H, 4.53; N, 6.23.

^{1}H NMR (500 MHz, DMSO-d_6): δ = 8.57 (s,2H, CH=N), 8.37 (s, 2H, CH=N), 6.8-4-6.87 (m, 8H, Ar-H), 6.42-6.46 (m, 4H, Ar-H), 5.64 (br, 4H, NH_2), 3.68 (s, 12H, OMe), 3.62 (m, 8H, CH_2N), 3.50 (m, 8H, CH_2O), 2.74 (m, 4H, CH_2N), 2.51-2.55 (m, 4H, CH_2O),

^{13}C NMR (125 MHz, DMSO-d_6): δ = 172.48, 171.39, 164.80, 162.95, 161.76, 127.92, 127.63, 118.18, 118.00, 115.49, 114.94, 113.58, 112.86, 112.64, 64.35, 62.25, 60.44, 60.13, 59.70, 58.63, 56.57, 56.07, 55.95, 55.38, 49.07, 44.99, 42.81

(Selected IR bands: ῡ(cm^{-1}) = 3538, 1627, 1449, 1212, 1054, 740)

2.2.2 Instrumentation:

Infrared spectra were recorded with a NICOLET iS5 FTIR Spectrometer. Elemental analysis was performed with a Flash EA Series 1112 CHNS analyzer. TGA was recorded with PerkinElmer STA 8000 thermogravimetric analyzer under a nitrogen gas flow rate of 20 ml/min and heating rate of 10°C/min. UV-Visible spectra were recorded in the Jasco V-750 spectrophotometer, and Emission spectra were taken in Jasco FP-8500 spectrofluorometer. Single crystal X-ray data for **2.1, 2.4, 2.5** were collected at 298K, 100K, 299K with a Bruker **APEX-II CCD** diffractometer system [λ (Mo Kα) = 0.71073Å] with a graphite

monochromator. The data were reduced using APEX-2, the structures were solved using **SHELXS-97** and **Olex2**, and the data was refined using the program **SHELXL-2018/3**.[27] All non-hydrogen atoms were refined anisotropically. The SCXRD data for **2.2, 2.3** were collected at 104K and 100K with an XtaLAB Synergy, Single source at offset/far, HyPix3000 diffractometer. Rigaku Oxford HyPix3000 CCD plate detector system [λ (Mo Kα) = 0.71073Å] with a mirror monochromator. Using **Olex2**[28], the structure was solved with the **ShelXT**[29] structure solution program using Intrinsic Phasing and refined with the **SHELXL-2018/3**[27] refinement package using Least Squares minimization. In compounds **2.2** and **2.4,** the voids contain solvent molecules. Olex2 solvent mask(similar to PLATON/SQUEEZE) was used to mask out the electron density. The details of the solvent masks used are given here

Compound 2.2: A solvent mask was calculated and 188 electrons were found in a volume of 652 $Å^3$ in 1 void. This is consistent with the presence of 1[$CHCl_3$] per formula unit which accounts for 232.0 electrons.

Compound 2.4: A solvent mask was calculated and 274 electrons were found in a volume of 1076 $Å^3$ in 1 void. This is consistent with the presence of 1.5[CH_2Cl_2], 0.5[H_2O] per formula unit which accounts for 272.0 electrons.

2.2.3 Theoretical Details:

Quantum chemical calculations were performed to investigate the experimental outcomes of the Zn(II)-Schiff base complexes. Optimization of gas-phase ground electronic state molecular structure of those complexes was accomplished using the B3LYP theoretical model without considering any symmetry restriction. For the optimization in the solvent phase, we considered the Integral Equation Formalism Polarizable Continuum Model (**IEFPCM**)[30] of DMSO solvent. All these calculations were executed at the level of Density Functional Theory using a 6-311G basis set[31] for all kinds of atoms. A time-dependent-density function theory (**TD-DFT**) simulation was performed in the same solvent phase to get an elaborate justification of UV-Vis spectra. **GAUSSIAN 09W** package[32] was used for these calculations.

2.3 Results and discussions:

The complexes **2.1**-**2.5** were synthesized as summarized in **Scheme1**. In these reactions, different chain lengths containing Schiff-base ligands have been employed with (**2.1**, **2.2**, **2.4**,

2.5) and without (**2.3**) auxiliary ligands such as DBM (dibenzoyl methane)/monoethanolamine (MEA) in a mix-solvent methanol-acetonitrile (1:1) medium and triethylamine as a base. All the Schiff-base ligands L1, L2, L3, and L4 were prepared in-situ reactions. Ligands L1 and L4 have two oxygen, one nitrogen (O_2N) as a coordinating group, and ligand L2, L3 has three oxygen / one nitrogen (O_3N) as a coordinating group. Hence these monoprotic (L1, L4) and diprotic (L2, L3) ligands have multiple pairs of electrons to form coordination complexes where ligands can bind between metal atoms as a chelating or bridging mode (**Table 2.7**). We report the synthesis and structural characterization of mononuclear and tetranuclear (cube, ladder-like) coordination complexes using these Schiff base ligands and co-ligands as mixed ligand systems.

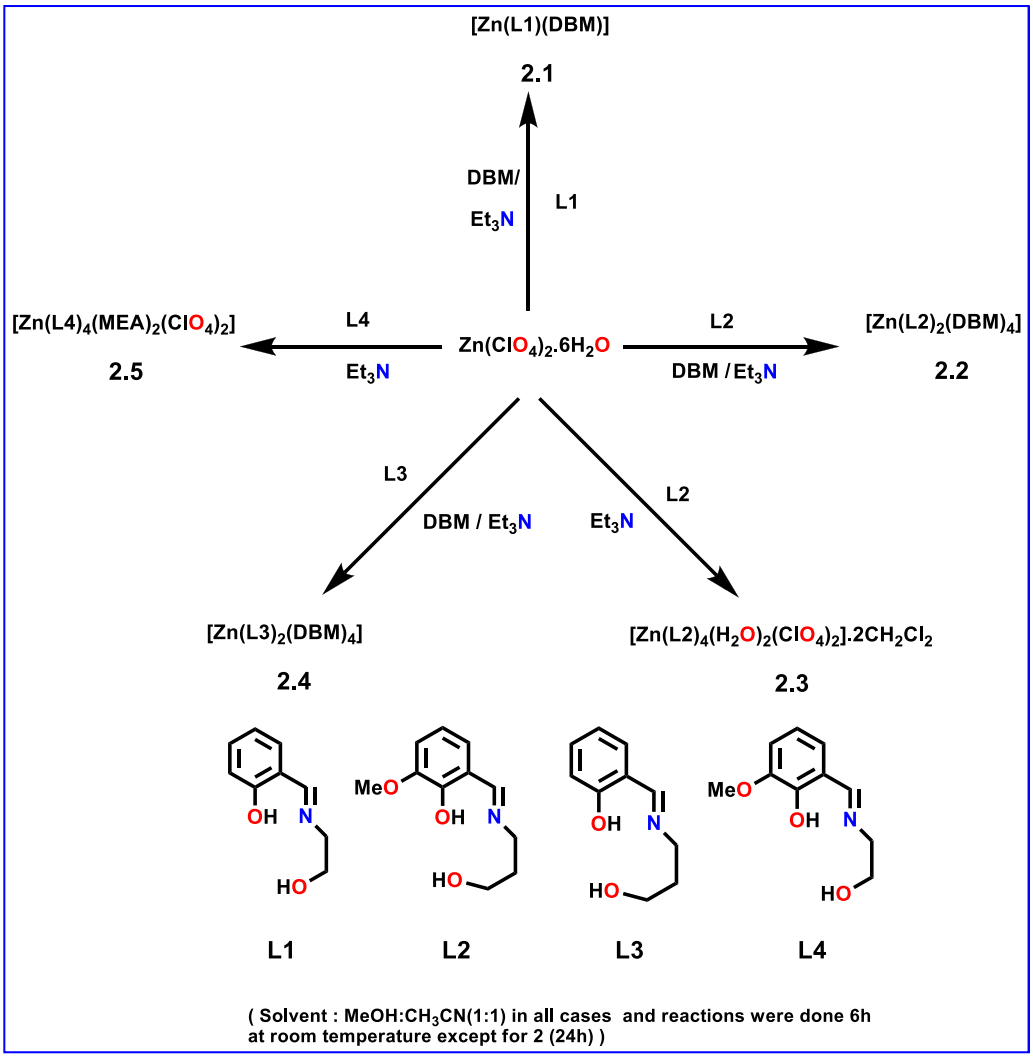

Scheme 1: Synthetic scheme of compounds **2.1-2.5**

The synthetic procedure followed for synthesizing these complexes is detailed below. In all the cases, ligands and co-ligands were taken in a solvent mixture(methanol-acetonitrile), and metal salt (zinc perchlorate hexahydrate) was added following triethylamine base dropwise addition, left for 6 h time at stirring condition except **2.2**; stirred for 24 h. The following ligands and co-ligands were used for synthesis. For **2.1** salicylaldehyde, monoethanolamine(MEA), DBM; **2.2** o-vanillin, 3-aminopropanol, DBM; **2.3** o-vanillin 3-aminopropanol; for **2.4** salicylaldehyde, 3-aminopropanol, DBM and for **2.5** o-vanillin, ethanolamine. Different methods are used for crystallization as described. **2.1** was synthesized by stirring ethanolamine, salicylaldehyde, dibenzoyl methane (DBM), zinc perchlorate hexahydrate, and triethylamine 1:1:1:1:3 molar ratio in a methanol-acetonitrile (1:1) solvent mixture for 6 h (**Scheme 1**). The clear yellowish solution was filtered and reduced the volume to half. Yellowish color rod shape crystals were obtained overnight. **2.2** was synthesized by stirring 3-aminopropanol, o-vanillin, DBM, zinc perchlorate hexahydrate, and triethylamine 1:1:1:1:3 molar ratio in methanol-acetonitrile (1:1) solvent mixture for 24h to maximize the yield of the product (**Scheme 1**). In the yellow color solution, a white color precipitate was observed. The precipitate was filtered and dried. Compound **2.2** was obtained in the chloroform/hexane diffusion method as white color good crystals in a week. **2.3** was synthesized the same as **2.2**, only here DBM was not used. A clear yellowish solution was observed at the end of the reaction, which was filtered and evaporated. After evaporating the solvent, the sticky, oily liquid was dissolved in DCM, and diffusing hexane yielded crystals of **2.3** within two weeks. Compound **2.4** was synthesized the same as compound **2.2**, the difference being salicylaldehyde was used instead of o-vanillin. Crystals were obtained by DCM/hexane layering method at 0°C. Compound **2.5** was synthesized by stirring o-vanillin, monoethanolamine, zinc perchlorate hexahydrate, and triethylamine 1:1.5:1:3 molar ratio in a methanol-acetonitrile (1:1) solvent mixture for 6h. The clear yellowish was filtered and evaporated. From DCM/hexane layering at 0°C, obtained an X-ray quality crystal.

All the compounds (**2.1-2.5**) were characterized by standard analytical and spectroscopic techniques. Thermal gravimetric analysis (TGA) was carried out under a nitrogen atmosphere to study the thermal stability of the complexes. The TGA study was done in the presence of a nitrogen gas flow rate of 20ml/min and a heating rate of 10°C/min from 30°C to 800°C. All the TGA data has been included in the **Analytical and Spectroscopic data** (**Figure 2.14- 2.18**).

In the IR spectrum of **2.1-2.5** distinct bands due to the azomethine (C=N) group are observed at 1591, 1596, 1614.49, 1594, 1627.55 cm^{-1}, whereas the same band appears at 1630.00,

1630.82, 1629.89, 1632.60 cm^{-1}, for free ligands **L1-L4** (**Analytical and Spectroscopic data Table 2.8**.). The shift of these bands towards higher and lower frequency on complexation with the metal suggests coordination via the imino nitrogen atom in all the complexes.[21] The (C-O phenolic) mode is present as a very strong band about 1211-1272 cm^{-1}. The peaks in the range 1065-1066cm^{-1} are assigned to alcoholic C-O stretches. Several weak peaks observed for the complexes in the range 3058-2859 cm^{-1} are ascribed to the aliphatic and aromatic C-H stretches, and the range 717-744 cm^{-1} is for C-H out of plane bending mode. Broad peaks are observed in the range 3205-3386 cm^{-1} due to the presence of alcoholic OH groups. Sharp, strong, single peaks at 1058.74 and 1054.61 cm^{-1} for the perchlorate ion present in complex **2.3** and **2.5**. Broadband around 3483 cm^{-1} in compound **2.3** has been assigned to the OH stretching vibration of the coordinated water molecules, which are involved in hydrogen bonding[22].

The electronic spectra for **2.1-2.5** were recorded in DMSO solvent in the range of 265-700 nm at room temperature using the same solvent as blank. The absorption maxima were observed at the region 355, 353, (279,377), 355, (280,379) respectively for **2.1-2.5 (Figure 2.1)**. **2.1, 2.2, 2.4** shows a similar kind of absorption maxima where DBM is present, and **2.3,2.5** shows a similar kind of absorption maxima where DBM is absent and only Schiff-base is present (**Analytical and Spectroscopic data Figure 2.26, 2.28**). It indicates the similar solution behavior of the compounds. The electronic transition for **2.1, 2.2, 2.4** might be due to intra-ligand charge transfer (ILCT). [23] Similarly, the electronic transition for compounds **2.3, 2.5** the two observed bands may arise from $\pi \rightarrow \pi^*$ ILCT.

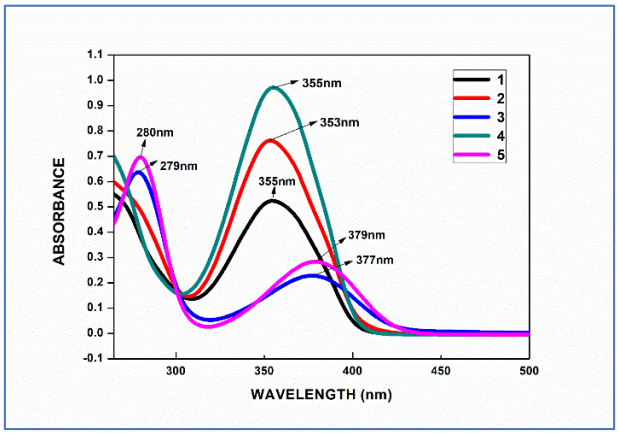

Figure 2.1. The UV-Vis spectra of **2.1-2.5** in solution state in DMSO at room temperature.

To understand in detail the electronic behavior transitions of **2.1, 2.2,** and **2.4,** DFT calculation [24] for **2.1** has been done. DFT calculations show that the transition corresponds to 352.79 nm is for the H-2→L/H-3→L/H-4→L/H-1→L/H-6→L molecular orbital (MO's) transition of an oscillator strength(f) 0.0116, which is close to the experimental value of 355nm (**Analytical and Spectroscopic data Table 2.10**). The electron cloud of H-1, H-2, H-3, H-4, H-6 MOs are mainly located on the ligand moiety (**Figure 2.2(a))**, and LUMO(L) (**Figure 2.2(a))** is also redistributed throughout the ligand moiety avoiding the metal atom Zn(II). These imply the possibility of the intra-ligand charge transfer (ILCT) phenomenon. Similarly, **2.3, 2.5**; **2.3** was taken as a case study, and DFT calculations were performed. Analysis shows that the transition corresponds to 276.77 nm and 384.22 nm are for the significant contributing orbitals (H-5→L+1/H-8→L+1/H-11→L) and (H-1→L/H-1→L+1/H→L/ H→L+1) transition of an oscillator strength(f) 0.0169 and 0.0055 respectively is close to the experimental value 279nm and 377nm (**Analytical and Spectroscopic data Table 2.10**). The electronic clouds of the MO's are mostly lying on the ligand orbitals (**Figure 2.2(b)**), which suggests that the transitions correspond to the $\pi \rightarrow \pi^*$ ILCT.

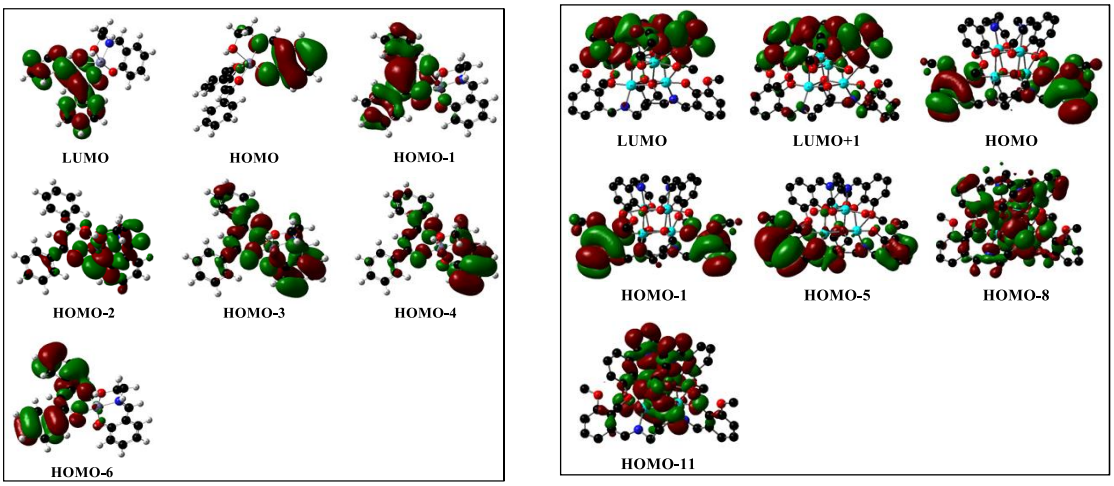

(a) **(b)**

Figure 2.2. (a): MO's of compound **2.1, (b):** MO's of compound **2.4**

The fluorescence spectra of **2.1**-**2.5** (**Figure 2.3**) were done in DMSO solvent in the region 350-700 nm by exciting at 375 nm, which implies that **2.1**, **2.2**, **2.4** have similar kinds of emission spectra, and on the other hand **2.3**, **2.5** are similar. All **2.1**-**2.5** exhibit only one emission spectrum at 447 nm, 440 nm, 481 nm, 444 nm, 483 nm, respectively. In the case of **2.1**, **2.2**, **2.4** emission spectrum are 19, 21, 7 nm blue-shifted blue color emission, and for

compound **2.3**, **2.5** emission spectrum are 20, 29nm red-shifted cyan color emission compared to free Schiff-base ligands (**Figure 2.31-2.35**).

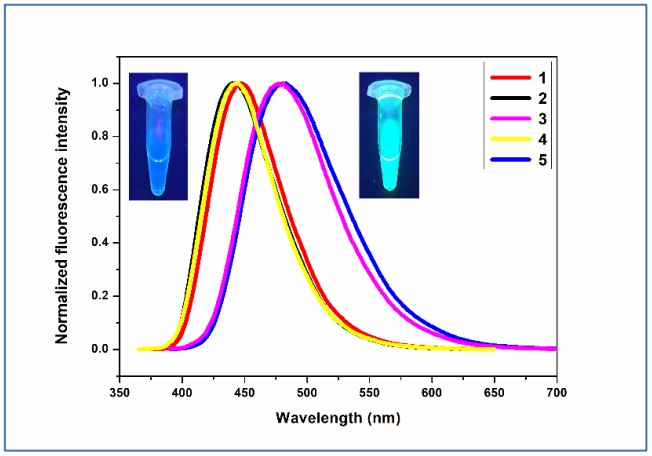

Figure 2.3. Emission Spectra of **2.1-2.5** in solution state in DMSO solvent at room temperature.

2.1 crystallizes in orthorhombic $P2_12_12_1$ space group. The molecular structure of **2.1** (**Figure 2.4**) contains one zinc (II) ion and one DBM ligand. The Penta-coordinated zinc (II) ion adopts a spherical square pyramid geometry (by SHAPE analysis) (**Analytical and Spectroscopic data Table 2.11**.) with Schiff base (L1) ligand (O1 N1 O4) and two DBM oxygen (O2 O3) doner groups. Both ligands are attached to the zinc (II) in a chelating mode; The Schiff base ligand is monoprotonated; the alkyl oxygen atom of the hydroxyl group is not deprotonated (**Figure 2.4**). The Zn1-O4 bond distance is 2.496(2)Å, which is longer than the similar distances found in the literature (literature Zn-O distance is 2.419(2)Å [2. a]]. The four-coordination number found in 1 is quite common in the literature for O, N ligated Zn (II) complexes. When the coordination number is increased from four to five, the additional coordination is weak with Zn (II)---O distances between 2.341(10) to 2.912(12)Å, and the corresponding geometry is highly distorted.[25] The selected bond lengths, bond angles, and packing diagram are given in **Analytical and Spectroscopic data** (**Table 2.2** & **Figure 2.46**), respectively.

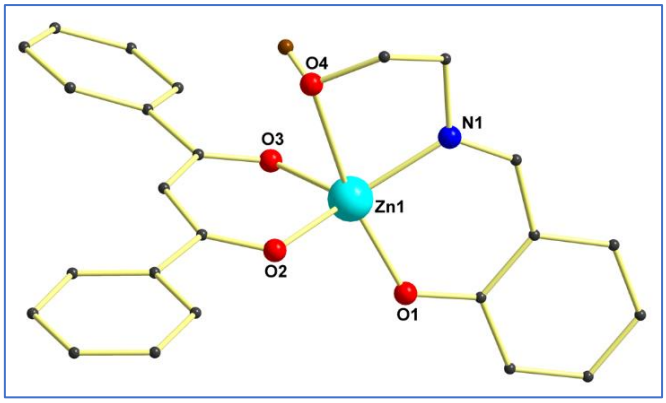

Figure 2.4. Ball and stick view of the molecular structure of 1. Hydrogen atoms are removed for clarity. Key: blue, N; red, O; black, C; brown, H; cyan, Zn.

2.2 crystallizes in I 2/a space group. The asymmetric crystallographic unit contains two zinc (II), anionic Schiff base ligand(L2), and two terminally coordinating DBM anions (**Figure 2.5(a)**). The Zn (II)-O complex adopts a cubane core (**Figure 2.5(b)**). The core structure is stabilized by two Schiff-base ligands and four DBM molecules. All the zinc (II) ions in the core are hexacoordinated with slightly distorted octahedral geometry. The Zn1 is present in a O_5N-doner environment; among these, the coordination comes from three bridging oxygen (O3 $O6^*$ $O3^*$) atoms, one nitrogen atom($N1^*$) from Schiff base, and two terminal oxygen ($O1^*$ $O2^*$) atoms from DBM. Another metal ion Zn2 is coordinated with three bridging oxygen (O6 $O3^*$ $O6^*$) atoms, one methoxy oxygen (O7) from Schiff base, and two terminal oxygen (O4 O5) atoms from DBM. The Schiff-base ligands bind to the zinc center in [4.3311] coordination mode, and DBM binds [1.11] based on Harris notation.[26] The selected bond lengths, bond angles, and packing diagram are given in **Analytical and Spectroscopic data** [**Table-2.3 & Figure 2.47**] respectively.

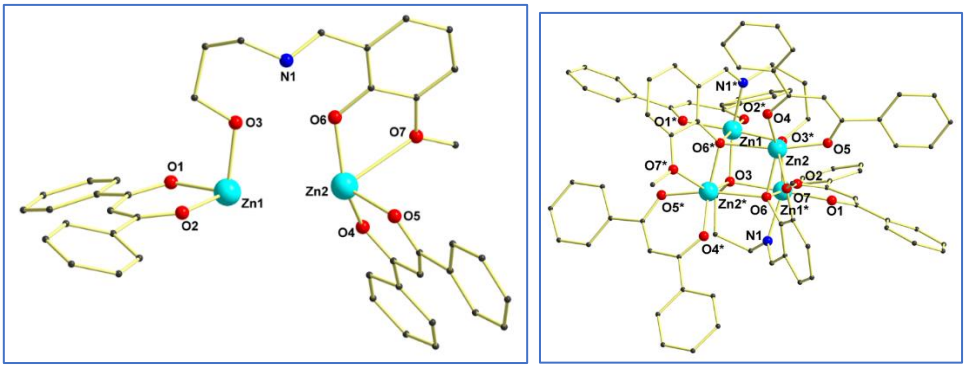

(a) **(b)**

Figure 2.5 (a) Asymmetric unit of **2.2** (b) Ball and stick view of the molecular structure of **2.2**. Hydrogen atoms are removed for clarity. Key: blue, N; red, O; black, C; cyan, Zn

2.3 crystallizes in the triclinic P-1 space group. The molecular structure of **2.3** contains four Zn (II) ions, four tridentate Schiff base ligands(L2), and two water molecules that form a distorted cubane core (**Figure 2.6(a)**). In the core, Zn1 is hexacoordinated and present in a distorted octahedral environment with three μ_3-oxo bridging oxygens (O2 O3 O4), one alcoholic oxygen (O1), one nitrogen (N1) from the Schiff base ligand, and one terminal oxygen (O6) water molecule. Zn3 also has the same hexacoordinated distorted octahedrally with three μ_3-oxo bridging oxygens (O2 O4 O5), one alcoholic oxygen (O12), one nitrogen (N3) from the Schiff base ligand, and terminal oxygen (O11) water molecule. Zn2 is Penta-coordinated and present in a distorted square pyramidal geometry with three μ_3-oxo bridging oxygens (O2 O3 O5), one nitrogen(N2), and one phenolic oxygen (O7). Zn4 hexacoordinated is found in a distorted octahedral geometry where zinc atom is surrounded by three μ_3-oxo bridging oxygens (O3 O4 O5), one nitrogen(N4), one phenolic (O9), and one methoxy (O14) oxygen. Based on Harris notation, the coordination modes found in the Schiff-base fall in these three different coordination modes [3.3111], [3.3110], [3.3110]. The molecule is dicationic, and the charge is balanced by the two perchlorate ions present in the crystal structure, confirmed by the characteristic IR peak 1058cm^{-1}. The selected bond lengths, bond angles, and packing diagram are given in **Analytical and Spectroscopic data** [**Table 2.4 & Figure 2.48**], respectively.

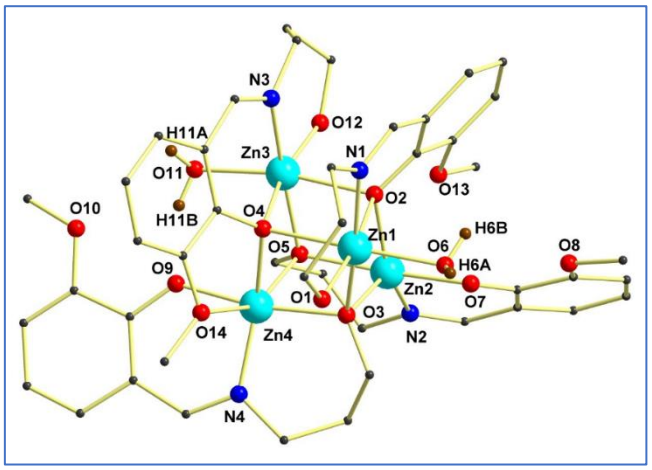

(a)

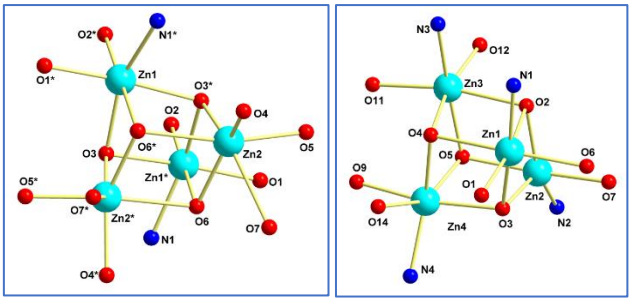

(b) (c)

Figure 2.6 (a) Ball and stick view of the molecular structure of **2.3**. Hydrogen atoms and counteranions are removed for clarity. Key: blue, N; red, O; black, C; brown, H; cyan, Zn (**b**) Ball and stick view of cubane core of **2.2 (c)** Ball and stick view of cubane core of **2.3**. Hydrogen atoms are removed for clarity. Key: blue, N; red, O; black, C; cyan, Zn

2.4 crystallizes in the triclinic P-1 space group. The molecular structure of **2.4** (**Figure 2.7(a)**) contains four Zn (II) ions, two Schiff base ligands (L3), and four DBM molecules in a distorted cubane core. Zn2 and Zn3 are penta-coordinated with three μ_3-oxo bridging oxygens (O4 O7 O8) and (O3 O4 O8), two DBM oxygen (O5 O6) and (O11 O12) respectively in a distorted square-pyramidal geometry. Zn1 and Zn4 are hexa-coordinated with three μ_3-oxo bridging oxygens (O3 O4 O7) and (O3 O7 O8), one nitrogen (N1 and N2), two DBM oxygen (O1 O2) and (O9 O10) respectively and present in a distorted octahedral geometry. In the crystal structure, the two Schiff-base binds are present in [4.331] binding mode. In the IR spectrum, the characteristic Schiff-base azomethine peak of compound 4 appears at 1645cm^{-1} and 1594cm^{-1}. The bond angles, bond lengths, and packing diagram are given in **Analytical and Spectroscopic data** [**Table 2.5 & Figure 2.49**] respectively.

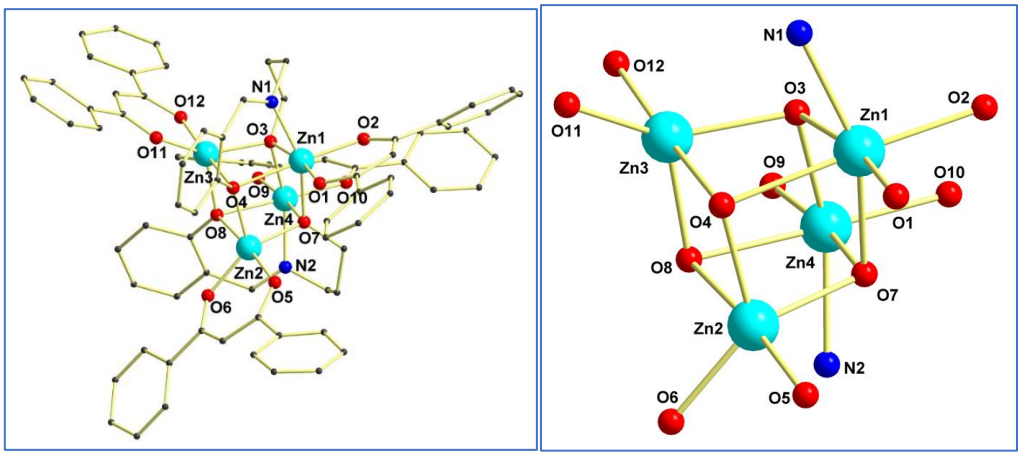

(a) (b)

Figure 2.7. (a)Ball and stick view of the molecular structure of **2.4**. (b)Cubane core of **2.4**. Hydrogen atoms are removed for clarity. Key: blue, N; red, O; black, C; cyan, Zn

2.5 crystallizes in the monoclinic P 2_1/c space group. The asymmetric crystallographic unit contains two zinc (II) ions, two di-anionic Schiff base ligand(L4), and one ethanolamine molecule (**Figure 2.8(a)**). The Zn (II)-O complex adopts a ladder-like core (**Figure 2.8(c)**). In the ladder-like core, Zn1 is present in a six-coordinated distorted octahedral geometry with one μ_3-oxo bridging oxygen(O6), one μ_2-oxo bridging oxygen(O4), one phenolic oxygen(O1), one methoxy oxygen(O2), and one nitrogen(N1). Zn2 is Penta-coordinated and is found in a distorted square-pyramidal geometry with two μ_3-oxo bridging oxygen (O6 O6*), one μ_2-oxo bridging oxygen(O4), and two nitrogens (N2, N3) as the binding sites. The binding modes of Schiff-base present are in [1.1110] and [2.2110] fashion. The two bridging ethanolamine moiety stabilizes the ladder-like core with a [3.31] binding mode. The whole moiety is dicationic in charge, balanced by the presence of two perchlorate ions characterized crystallographically and from the IR characteristic peak 1054cm^{-1}. The peak 3386-3310 cm^{-1} corresponds to two primary amines and 3517cm^{-1} for the unprotonated alcoholic peak of the Schiff-base ligand. Distinct azomethine peak appears at 1627cm^{-1} and 1599cm^{-1}. The bond lengths, bond angles, and packing diagram are given in **Analytical and Spectroscopic data** [**Table 2.6 & Figure 2.50**] respectively.

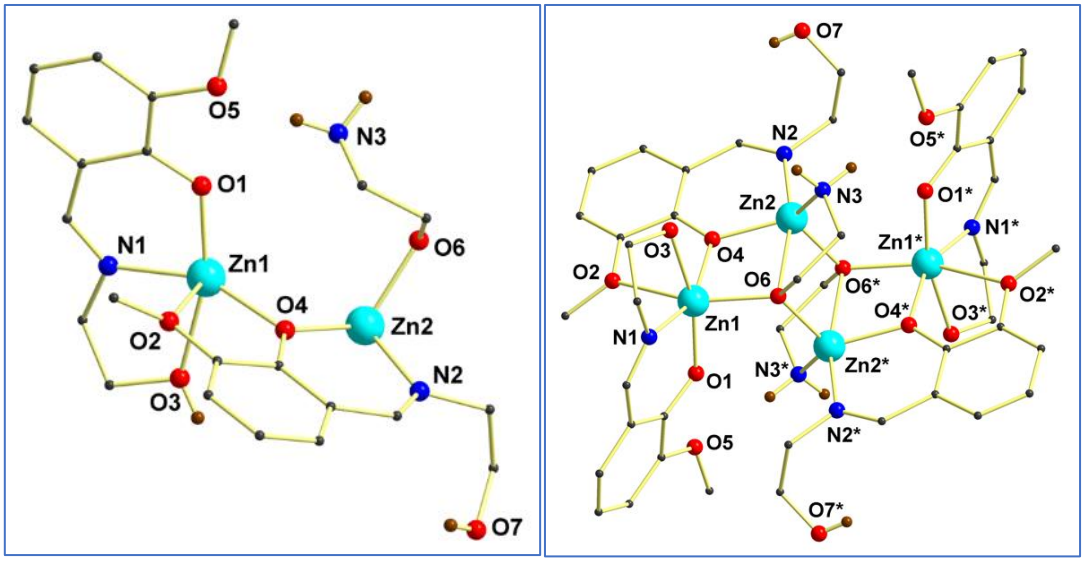

(a) (b)

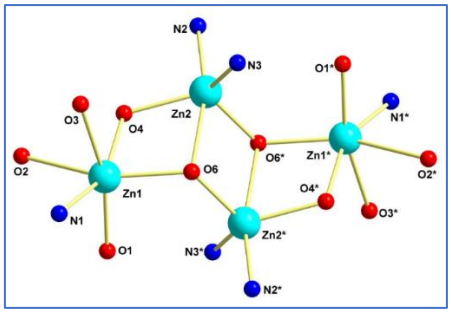

(c)

Figure 2.8. (a) Ball and stick view of the asymmetric unit of 5. (b) Ball and stick view of 5. (c) Cubane core of 5. Hydrogen atoms and counteranions are removed for clarity. Key: blue, N; red, O; black, C; brown, H; cyan, Zn

2.4 Conclusion:

Using varying chain lengths containing Schiff-base ligand and auxiliary ligands mononuclear Zn-complex to tetranuclear Zn_4 cubane, Zn_4 ladder-like core has been synthesized and characterized. The UV absorption and fluorescence property of the DBM and non-DBM containing Schiff-base complexes reveals that the UV-absorbing property of DBM is responsible for the blue-shifted absorption maxima compared to the Schiff base containing ligand which does not contain DBM. DFT study (for **2.1**) shows that the LUMO is mostly lying on the UV-absorbing DBM moiety and in the case of **2.3** LUMO is redistributed upon the Schiff-base ligands. The absorption maxima of the absorption spectra correspond to the $\pi \rightarrow \pi^*$ ILCT transition.

2.5 *Analytical and Spectroscopic Data*

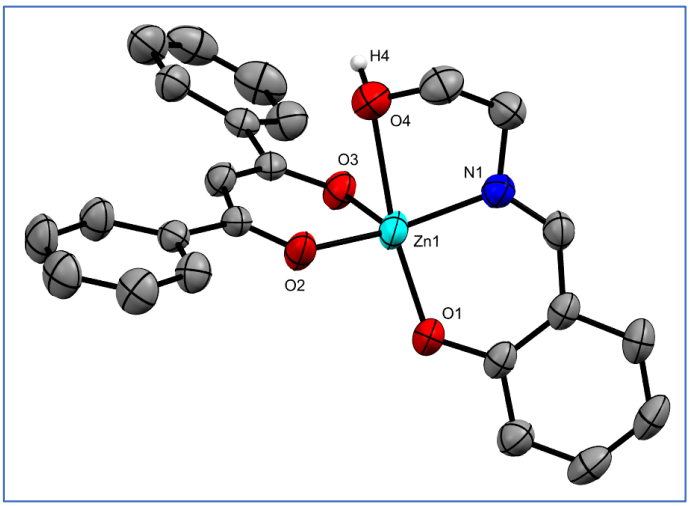

Figure 2.9. ORTEP view of **2.1** with thermal ellipsoids shown at 50%probability.

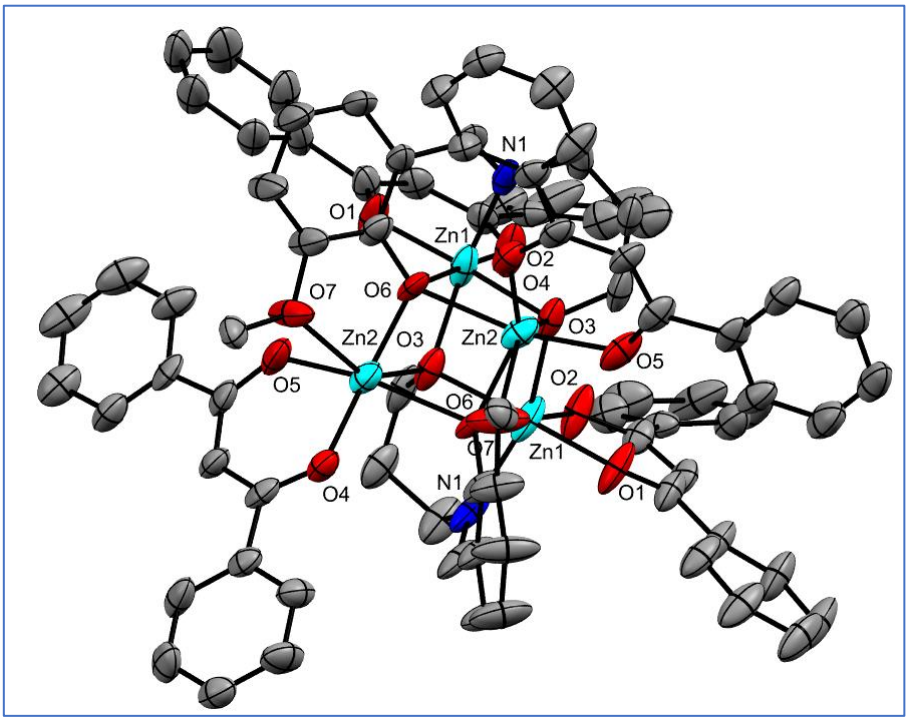

Figure 2.10. ORTEP view of **2.2** with thermal ellipsoids shown at 50%probability.

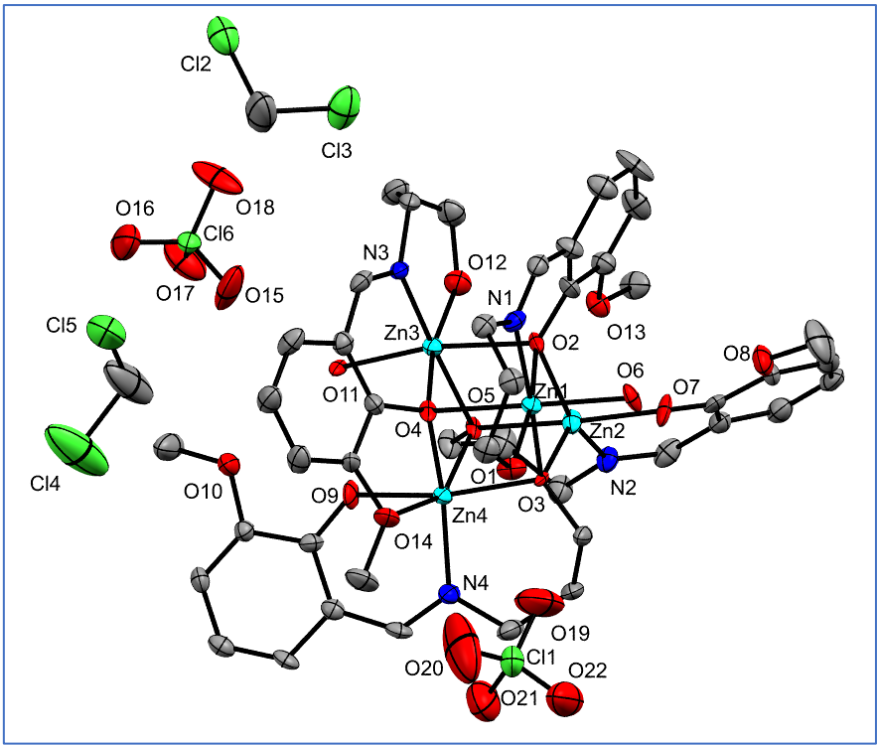

Figure 2.11. ORTEP view of **2.3** with thermal ellipsoids shown at 50%probability.

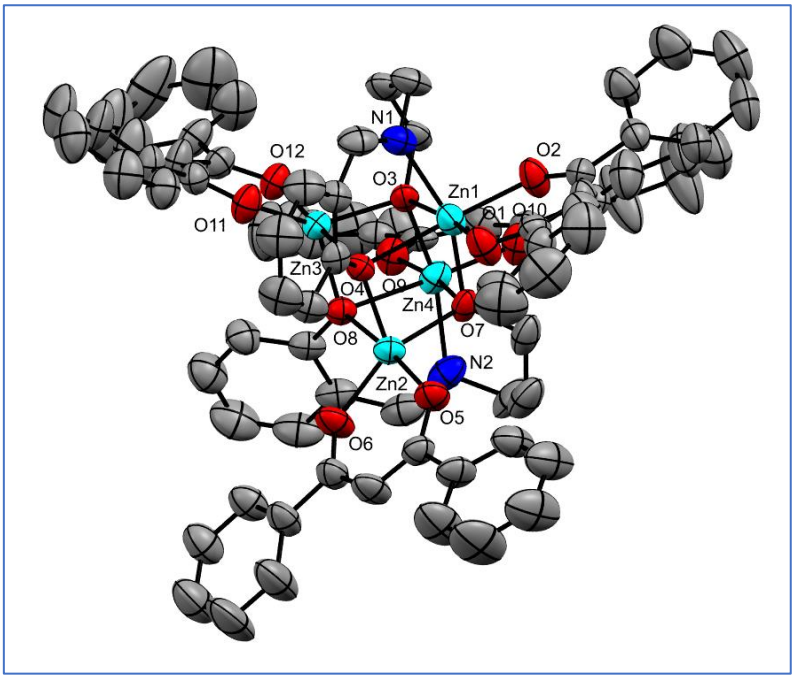

Figure 2.12. ORTEP view of **2.4** with thermal ellipsoids shown at 50%probability.

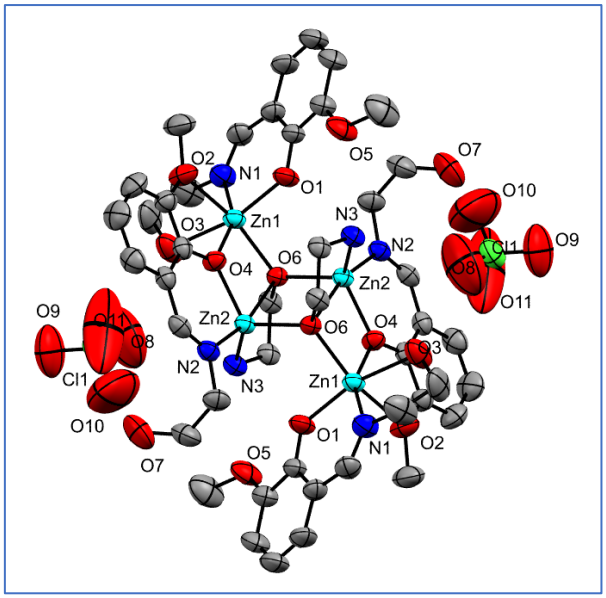

Figure 2.13. ORTEP view of **2.5** with thermal ellipsoids shown at 50%probability.

Table 2.1. Crystallographic information of compound **2.1**-**2.5**.

	2.1	2.2	2.3	2.4	2.5
Empirical formula	$C_{24}H_{21}NO_4Zn$	$C_{83}Cl_3H_{71}N_2O_{14}Zn_4$	$C_{46}H_{62}Cl_6N_4O_{22}Zn_4$	$C_{81.5}Cl_3H_{70}N_2O_{12.5}Zn_4$	$C_{44}H_{60}Cl_2N_6O_{22}Zn_4$
Formula weight	452.83	1688.24	1497.17	1645.22	1357.36
Temperature /K	298.25	104(2)	100	99.79	299(2)
Crystal system	orthorhombic	monoclinic	triclinic	triclinic	monoclinic
Space group	$P2_12_12_1$	I2/a	P-1	P-1	$P2_1/c$
a/Å	9.8362(6)	21.5371(12)	12.2590(2)	18.435(5)	12.7078(5)
b/Å	11.1097(6)	19.1267(6)	13.5320(2)	19.074(5)	14.9075(7)
c/Å	18.6066(11)	20.9374(12)	19.5839(4)	22.742(6)	14.9036(7)
α/°	90	90	87.731(2)	92.506(12)	90
β/°	90	120.883(8)	87.341(2)	92.044(12)	110.868(2)
γ/°	90	90	65.386(2)	109.169(11)	90
Volume/Å^3	2033.3(2)	7402.0(8)	2949.64(10)	7535(3)	2638.2(2)
Z	4	4	2	4	2

ρ_{calc}g/cm^3	1.4792	1.515	1.686	1.450	1.709
μ/mm^{-1}	1.239	1.457	1.957	1.428	1.984
F(000)	937.6	3464.0	1528.0	3376.0	1392.0
Crystal size/mm^3	0.07 × 0.03 × 0.02	0.06 × 0.04 × 0.02	0.04 × 0.02 × 0.01	0.06 × 0.02 × 0.01	0.03 × 0.02 × 0.01
Radiation	Mo Kα (λ = 0.71073)	MoKα (λ = 0.71073)	MoKα (λ = 0.71073)	MoKα (λ = 0.71073)	MoKα (λ = 0.71073)
2Θ range for data collection/°	5.54 to 55.14	4.26 to 53.988	3.872 to 53.926	4.39 to 62.012	4.386 to 48.34
Index ranges	-12 ≤ h ≤ 12, -14 ≤ k ≤ 14, -24 ≤ l ≤ 24	-27 ≤ h ≤ 27, -24 ≤ k ≤ 24, -26 ≤ l ≤ 26	-15 ≤ h ≤ 15, -16 ≤ k ≤ 16, -2 ≤ l ≤ 24	-23 ≤ h ≤ 24, -25 ≤ k ≤ 23, -29 ≤ l ≤ 29	-14 ≤ h ≤ 14, -17 ≤ k ≤ 17, -17 ≤ l ≤ 17
Reflections collected	20496	33028	12300	345106	86249
Independent reflections	4670 [R_{int} = 0.0309, R_{sigma} = 0.0336]	7706 [R_{int} = 0.1232, R_{sigma} = 0.1215]	12300 [R_{int} = ?, R_{sigma} = 0.0569]	35715 [R_{int} = 0.1438, R_{sigma} = 0.2035]	4211 [R_{int} = 0.0868, R_{sigma} = 0.0227]
Data/restraints/parameters	4670/0/273	7706/0/472	12300/8/759	35715/0/1765	4211/3/369
Goodness-of-fit on F^2	1.040	1.008	1.112	1.011	1.095
Final R indexes [I>=2σ (I)]	R_1 = 0.0255, wR_2 = 0.0613	R_1 = 0.0607, wR_2 = 0.1324	R_1 = 0.0754, wR_2 = 0.1903	R_1 = 0.0739, wR_2 = 0.1664	R_1 = 0.0438, wR_2 = 0.1135
Final R indexes [all data]	R_1 = 0.0311, wR_2 = 0.0635	R_1 = 0.1182, wR_2 = 0.1554	R_1 = 0.0902, wR_2 = 0.1966	R_1 = 0.1915, wR_2 = 0.2041	R_1 = 0.0617, wR_2 = 0.1229
Largest diff. peak/hole / e Å^{-3}	0.21/-0.43	0.49/-1.01	1.93/-1.15	0.57/-0.45	1.34/-0.40

Flack parameter	0.027(9)				

Table 2.2. Selected bond lengths (Å) and bond angle (deg) parameters of **2.1**

Zn1- O2	1.953(1)	O2- Zn1- N1	136.39(6)
Zn1- O3	1.969(1)	O3- Zn1- O1	111.84(5)
Zn1- O1	1.973(1)	O3- Zn1- O4	86.02(5)
Zn1- O4	2.496(2)	O3- Zn1- N1	118.46(6)
Zn1- N1	1.992(2)	O1- Zn1- O4	162.09(5)
O2- Zn1- O3	95.12(5)	O1- Zn1- N1	93.74(6)
O2- Zn1- O1	98.82(5)	O4- Zn1- N1	75.65(6)
O2- Zn1- O4	80.19(5)		

Table 2.3. Selected bond lengths (Å) and bond angle (deg) parameters of **2.2**

Zn2-Zn1^{1}	3.0877(7)	O5-Zn2-O3^{1}	93.03(13)
Zn2-O6^{1}	2.353(3)	O3-Zn1-O6^{1}	79.75(10)
Zn2-O6	2.010(3)	O3^{1}-Zn1-O6^{1}	80.97(10)
Zn2-O4	1.954(3)	O3-Zn1-O3^{1}	81.81(14)
Zn2-O3^{1}	2.027(3)	O3-Zn1-N1^{1}	158.73(13)
Zn2-O5	2.014(3)	O1-Zn1-O6^{1}	91.26(11)
Zn1-Zn1^{1}	3.1095(10)	O1-Zn1-O3^{1}	172.23(12)
Zn1-O6^{1}	2.214(3)	O1-Zn1-O3	96.84(13)
Zn1-O3^{1}	2.122(3)	O1-Zn1-N1^{1}	96.36(14)
Zn1-O3	2.042(3)	O2-Zn1-O6^{1}	178.55(12)
Zn1-O1	2.033(3)	O2-Zn1-O3	98.87(13)
Zn1-O2	2.022(3)	O2-Zn1-O3^{1}	98.44(12)
Zn1-N1^{1}	2.076(4)	O2-Zn1-O1	89.33(12)
O6-Zn2-O6^{1}	79.64(10)	O2-Zn1-N1^{1}	97.88(15)
O6-Zn2-O3^{1}	85.15(11)	N1^{1}-Zn1-O6^{1}	83.37(13)
O6-Zn2-O5	110.88(12)	N1^{1}-Zn1-O3^{1}	82.85(13)
O4-Zn2-O6^{1}	85.02(11)	Zn2-O6-Zn2^{1}	100.34(10)
O4-Zn2-O6	141.89(12)	Zn2-O6-Zn1^{1}	93.82(11)
O4-Zn2-O3^{1}	126.11(11)	Zn1^{1}-O6-Zn2^{1}	92.91(10)

O4-Zn2-O5	90.63(13)	Zn2[1] -O3-Zn1[1]	105.88(13)
O3[1] -Zn2-O6[1]	79.63(11)	Zn2[1] -O3-Zn1	98.73(12)
O5-Zn2-O6[1]	166.80(11)	Zn1-O3-Zn1[1]	96.63(13)

[1]1/2-X,+Y,1-Z

Table 2.4. Selected bond lengths (Å) and bond angle (deg) parameters of **2.3**

Zn1- O3	2.053(6)	O1-Zn1-N1	93.9(4)
Zn1- O2	2.168(6)	O5-Zn2-O3	82.5(3)
Zn1- O4	2.26(1)	O5-Zn2-O2	82.1(3)
Zn1- O6	2.075(9)	O5-Zn2-O7	173.4(3)
Zn1- O1	2.091(7)	O5-Zn2-N2	95.6(4)
Zn1- N1	2.058(8)	O3-Zn2-O2	84.6(3)
Zn2- O5	2.073(9)	O3-Zn2-O7	94.4(3)
Zn2- O3	2.030(7)	O3-Zn2-N2	122.7(4)
Zn2- O2	2.107(6)	O2-Zn2-O7	91.8(3)
Zn2- O7	2.01(1)	O2-Zn2-N2	152.2(4)
Zn2- N2	2.01(1)	O7-Zn2-N2	91.0(4)
Zn3- O5	2.071(6)	O5-Zn3-O11	93.0(3)
Zn3- O11	2.089(9)	O5-Zn3-O2	79.1(3)
Zn3- O2	2.24(1)	O5-Zn3-O4	83.7(3)
Zn3- O4	2.155(6)	O5-Zn3-O12	93.4(3)
Zn3- O12	2.093(8)	O5-Zn3-N3	171.3(3)
Zn3- N3	2.065(8)	O11-Zn3-O2	169.9(3)
Zn4- O5	2.135(7)	O11-Zn3-O4	95.2(3)
Zn4- O3	2.102(9)	O11-Zn3-O12	95.8(3)
Zn4- O4	2.068(6)	O11-Zn3-N3	92.2(3)
Zn4- O9	1.99(1)	O2-Zn3-O4	77.8(3)
Zn4- O14	2.523(7)	O2-Zn3-O12	90.9(3)
Zn4- N4	2.02(1)	O2-Zn3-N3	94.9(3)
O3-Zn1-O2	82.6(3)	O4-Zn3-O12	168.7(3)
O3-Zn1-O4	78.6(3)	O4-Zn3-N3	88.9(3)
O3-Zn1-O6	93.7(3)	O12-Zn3-N3	92.9(3)
O3-Zn1-O1	94.7(3)	O5-Zn4-O3	79.3(3)
O3-Zn1-N1	169.7(3)	O5-Zn4-O4	84.3(3)
O2-Zn1-O4	77.0(3)	O5-Zn4-O9	91.3(3)
O2-Zn1-O6	92.7(3)	O5-Zn4-O14	150.2(3)
O2-Zn1-O1	170.8(3)	O5-Zn4-N4	121.9(4)
O2-Zn1-N1	88.1(3)	O3-Zn4-O4	82.1(3)
O4-Zn1-O6	167.8(3)	O3-Zn4-O9	169.5(3)
O4-Zn1-O1	93.9(3)	O3-Zn4-O14	102.8(3)
O4-Zn1-N1	95.1(3)	O3-Zn4-N4	97.5(4)
O6-Zn1-O1	96.2(3)	O4-Zn4-O9	92.4(3)
O6-Zn1-N1	91.1(3)	O4-Zn4-O14	66.8(3)
O4-Zn4-N4	153.4(4)	Zn1-O3-Zn4	101.9(3)
O9-Zn4-O14	83.0(3)	Zn2-O3-Zn4	100.1(3)
O9-Zn4-N4	91.5(4)	Zn1-O2-Zn2	91.5(3)
O14-Zn4-N4	87.6(4)	Zn1-O2-Zn3	102.7(3)
Zn2-O5-Zn3	102.4(3)	Zn2-O2-Zn3	95.9(3)
Zn2-O5-Zn4	97.7(3)	Zn1-O4-Zn3	102.3(3)
Zn3-O5-Zn4	94.2(3)	Zn1-O4-Zn4	96.2(3)
Zn1-O3-Zn2	97.2(3)	Zn3-O4-Zn4	93.8(3)

Table 2.5. Selected bond lengths (Å) and bond angle (deg) parameters of **2.4**

Zn3-O3	1.966(3)	Zn1-O4	2.219(3)
Zn3-O4	2.393(3)	Zn1-O7	2.091(3)
Zn3-O8	1.985(3)	Zn1-O1	2.034(4)
Zn3- O12	2.020(4)	Zn1-O2	2.016(4)
Zn3-O11	1.941(3)	Zn1-N1	2.099(4)
Zn2-O4	1.994(3)	Zn4-O3	2.100(3)
Zn2-O7	1.991(3)	Zn4-O7	2.137(4)
Zn2-O8	2.337(3)	Zn4-O8	2.245(3)
Zn2-O6	1.937(4)	Zn4-O9	2.002(4)
Zn2-O5	2.007(4)	Zn4- O10	2.008(4)
Zn1-O3	2.146(3)	Zn4-N2	2.089(6)
O3-Zn3-O4	82.7(1)	O7-Zn1-O1	97.6(1)
O3-Zn3-O8	88.7(1)	O7-Zn1-O2	99.9(1)
O3-Zn3-O12	99.2(1)	O7-Zn1-N1	155.4(1)
O3-Zn3-O11	138.0(1)	O1-Zn1-O2	89.2(1)
O4-Zn3-O8	79.7(1)	O1-Zn1-N1	97.5(2)
O4-Zn3-O12	173.0(1)	O2-Zn1-N1	99.6(2)
O4-Zn3-O11	82.9(1)	O3-Zn4-O7	80.9(1)
O8-Zn3-O12	106.9(1)	O3-Zn4-O8	78.9(1)
O8-Zn3-O11	126.9(1)	O3-Zn4-O9	97.0(1)
O12-Zn3-O11	91.3(2)	O3-Zn4-O10	99.6(1)
O4-Zn2-O7	87.4(1)	O3-Zn4-N2	155.7(2)
O4-Zn2-O8	81.0(1)	O7-Zn4-O8	82.1(1)
O4-Zn2-O6	124.4(1)	O7-Zn4-O9	169.6(1)
O4-Zn2-O5	107.2(1)	O7-Zn4-O10	99.7(1)
O7-Zn2-O8	83.0(1)	O7-Zn4-N2	82.1(2)
O7-Zn2-O6	142.8(2)	O8-Zn4-O9	87.5(1)
O7-Zn2-O5	98.3(1)	O8-Zn4-O10	177.4(1)
O8-Zn2-O6	83.8(1)	O8-Zn4-N2	81.7(2)
O8-Zn2-O5	171.7(1)	O9-Zn4-O10	90.6(2)
O6-Zn2-O5	90.3(2)	O9-Zn4-N2	96.6(2)
O3-Zn1-O4	83.2(1)	O10-Zn4-N2	100.3(2)
O3-Zn1-O7	80.9(1)	Zn3-O3-Zn1	103.9(1)
O3-Zn1-O1	172.3(1)	Zn3-O3-Zn4	97.7(1)
O3-Zn1-O2	98.5(1)	Zn1-O3-Zn4	97.8(1)
O3-Zn1-N1	81.6(1)	Zn3-O4-Zn2	98.5(1)
O4-Zn1-O7	79.3(1)	Zn3-O4-Zn1	89.1(1)
O4-Zn1-O1	89.2(1)	Zn2-O4-Zn1	93.7(1)
O4-Zn1-O2	178.1(1)	Zn2-O7-Zn1	97.9(1)
O4-Zn1-N1	81.5(1)	Zn2-O7-Zn4	103.5(1)
Zn1-O7-Zn4	98.4(1)	Zn3- O8- Zn4	92.5(1)
Zn3-O8-Zn2	100.6(1)	Zn2- O8- Zn4	90.1(1)

Table 2.6. Selected bond lengths (Å) and bond angle (deg) parameters of compound **2.5**

Zn2-O4	1.993(3)	Zn1-O6[1]	2.072(3)
Zn2-O6	2.000(3)	Zn1-O1	1.981(3)
Zn2-O6[1]	2.395(3)	Zn1-O2	2.378(4)
Zn2-N2	2.058(4)	Zn1-O3	2.231(4)
Zn2-N3[1]	2.021(4)	Zn1-N1	2.071(4)
Zn1-O4	2.056(3)	Zn1[1]-O6-Zn2[1]	94.64(12)
O4-Zn2-O6	112.30(13)	O4-Zn1-O3	83.70(15)
O4-Zn2-O6[1]	74.88(12)	O4-Zn1-N1	154.85(17)
O4-Zn2-N2	91.72(15)	O6[1]- Zn1-O2	151.95(13)
O4-Zn2-N3[1]	122.73(16)	O6[1]-Zn1-O3	96.29(16)
O6-Zn2-O6[1]	85.25(12)	O1-Zn1-O4	108.54(14)
O6-Zn2-N2	100.29(14)	O1-Zn1-O6[1]	95.62(14)
O6-Zn2-N3[1]	114.35(15)	O1-Zn1-O2	87.10(16)
N2-Zn2-O6[1]	166.60(14)	O1-Zn1-O3	164.11(15)
N3[1] -Zn2-O6[1]	77.77(14)	O1-Zn1-N1	90.29(16)
N3[1]-Zn2-N2	110.35(16)	O3-Zn1-O2	87.32(18)
O4-Zn1-O6[1]	81.20(12)	N1-Zn1-O6[1]	114.24(16)
O4-Zn1-O2	71.54(13)	N1-Zn1-O2	93.61(17)
N1-Zn1-O3	75.22(17)	N1-Zn1-O3	75.22(17)
Zn2-O4-Zn1	108.75(14)	Zn2-O4-Zn1	108.75(14)
Zn2-O6-Zn2[1]	94.75(12)	Zn2-O6-Zn2[1]	94.75(12)
Zn2-O6-Zn1[1]	119.33(15)		

[1]1-X,1-Y,1-Z

Table 2.7. Ligand coordination mode of **2.1**-**2.5**.

Compound	Ligands binding mode	Auxiliary ligand binding mode
2.1	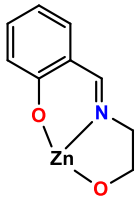	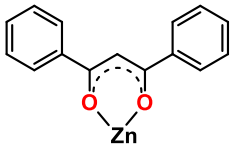
2.2	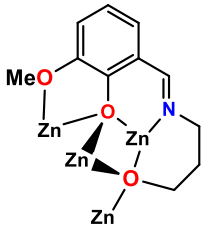	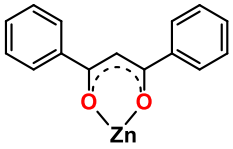
2.3	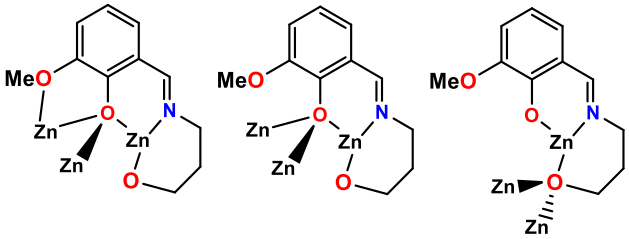	
2.4	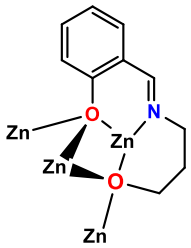	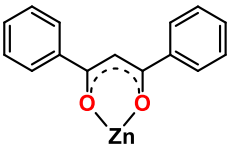
2.5	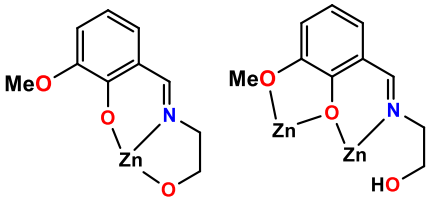	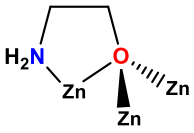

TGA data:

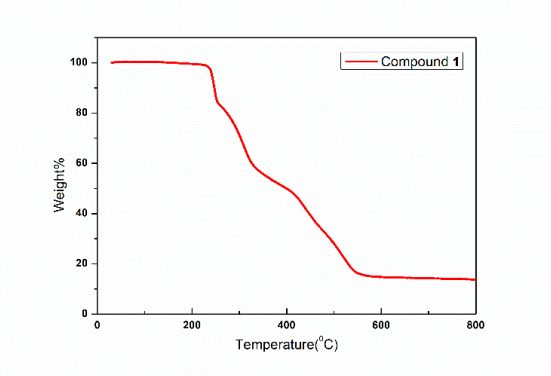

Figure 2.14. TGA of compound **2.1**

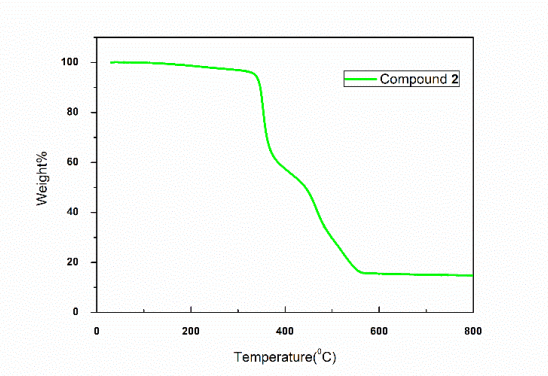

Figure 2.15. TGA of compound **2.2**

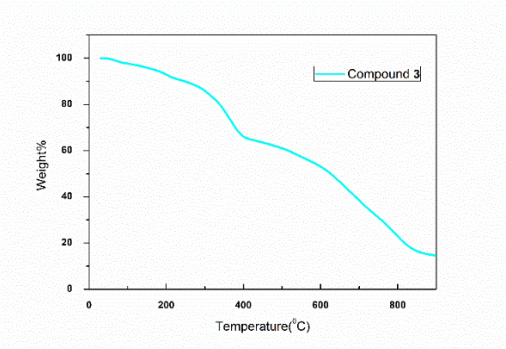

Figure 2.16. TGA of compound **2.3**

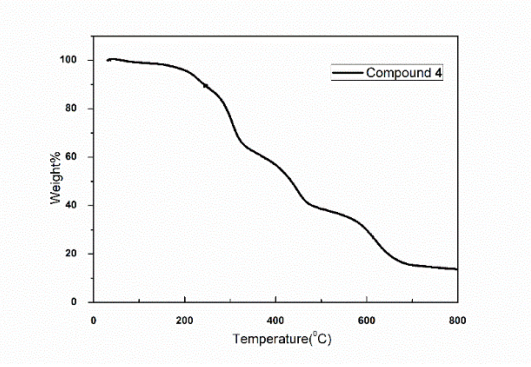

Figure 2.17. TGA of compound **2.4**

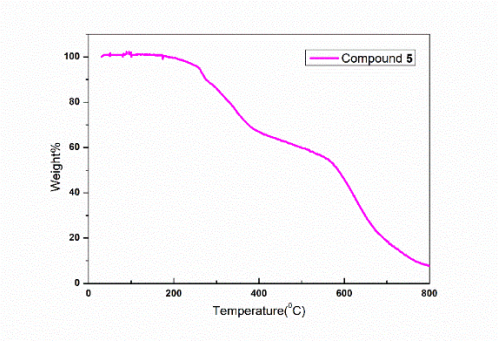

Figure 2.18. TGA of compound **2.5**

IR data:

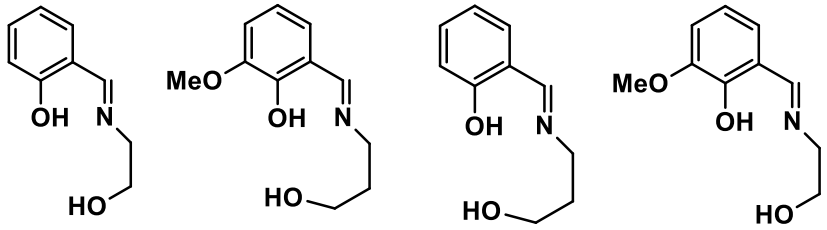

L1 **L2** **L3** **L4**

Ligand 1-4

Table 2.8. IR stretching frequency(ῡ)(cm^{-1}) of ligands **L1-L4**

L1	**L2**	**L3**	**L4**	Streatching.frequency (ῡ) of group
3338.96	3354.72	3354.50	3357.90	(O-H----N) Intramolecular H-bonding
1630.00	1630.82	1629.89	1632.60	(C=N)azomithine
1526	1463	1494	1464	C=C
1338	1340	1337	1341	(C-OH)phenolic
1275	1224	1276	1221	C-O phenolic
1060	1076	1060	1071	C-O alcoholic
753	735	754	735	C-H out of plane bending

Table 2.9. Comparison of IR stretching frequency(ῡ)(cm^{-1}) of ligand **L1-L4** & compound **2.1-2.5.**

Ligand(L)/ compound	**(O-H----N)** Intramolecular H-bonding/ **H_2O**	**(C=N)**	**(C=C)**	**(C-OH)**	**C-O** phenolic	**C-O** alcoholic	**C-H** out of plane bending	**ClO_4^-**
L1	3338	1630	1526	1338	1275	1060	753	
Compound**1**	3205	1591	1519		1233	1065	744	
L2	3354	1630	1463	1340	1224	1076	735	
Compound**2**	------	1596	1452		1222	1066	717	
Compound**3**	3483	1614	1442		1211	1058	733	1058
L3	3354	1629	1494	1337	1276	1060	754	
Compound**4**	------	1594	1474		1272	1065	716	
L4	3357	1632	1464	1341	1221	1071	735	
Cmpound**5**	3538	1627	1449		1212	1054	740	1054

IR spectra of compound **2.1-2.5**.

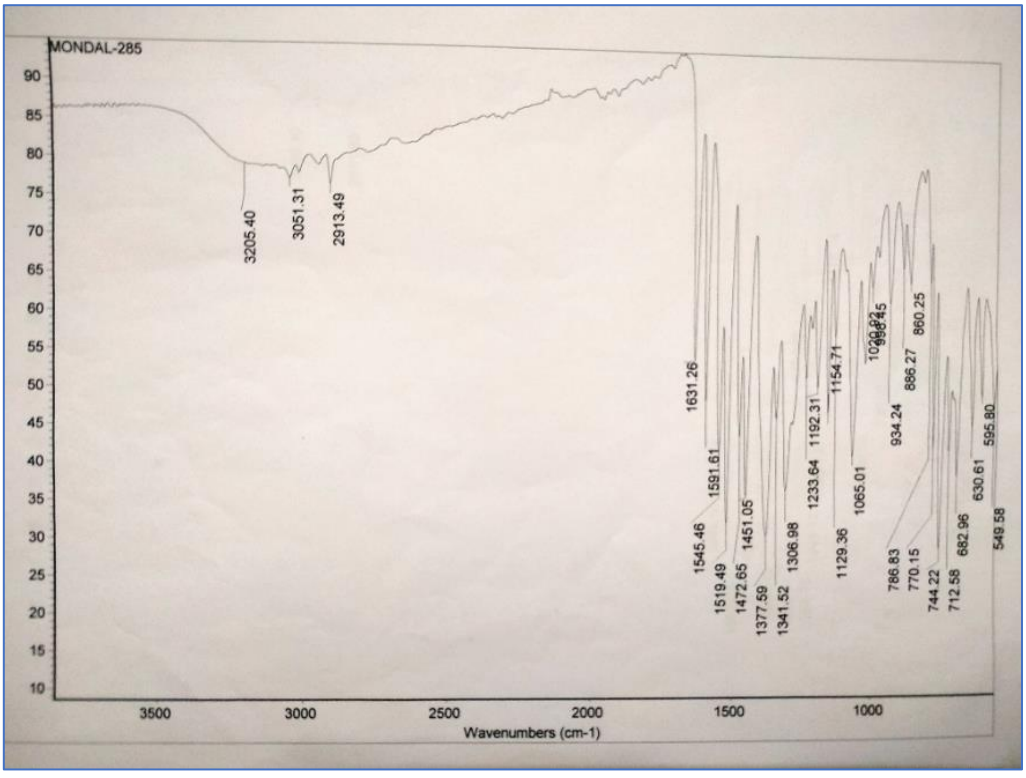

Figure 2.19. IR spectra of compound **2.1.**

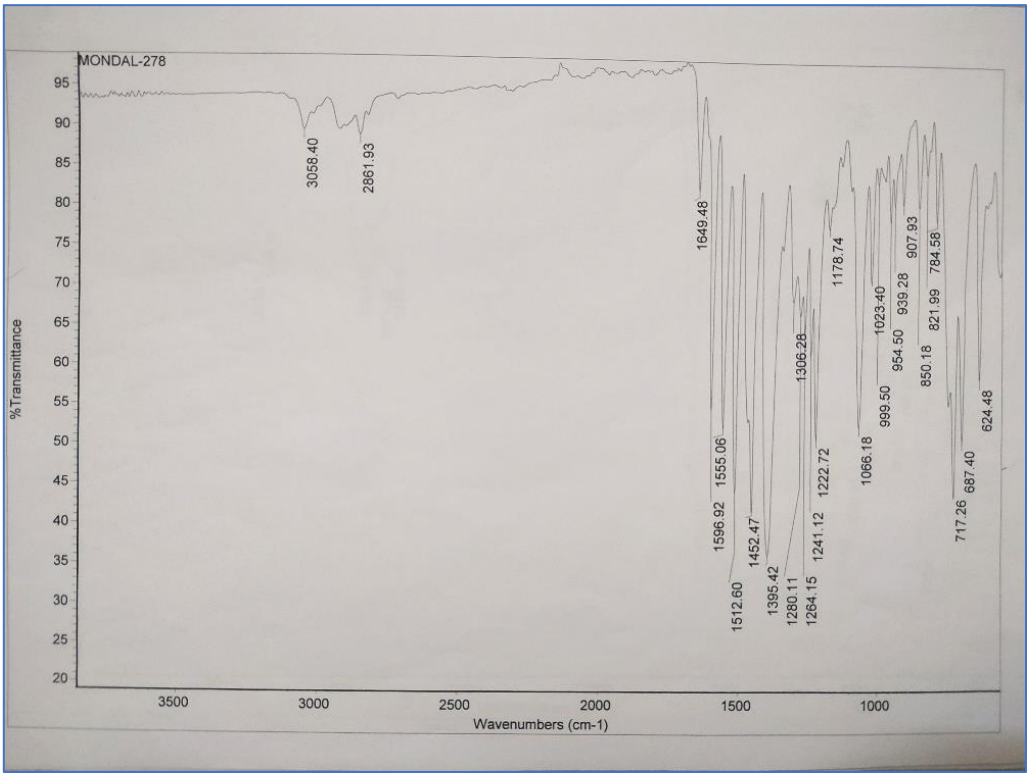

Figure 2.20. IR spectra of compound **2.2.**

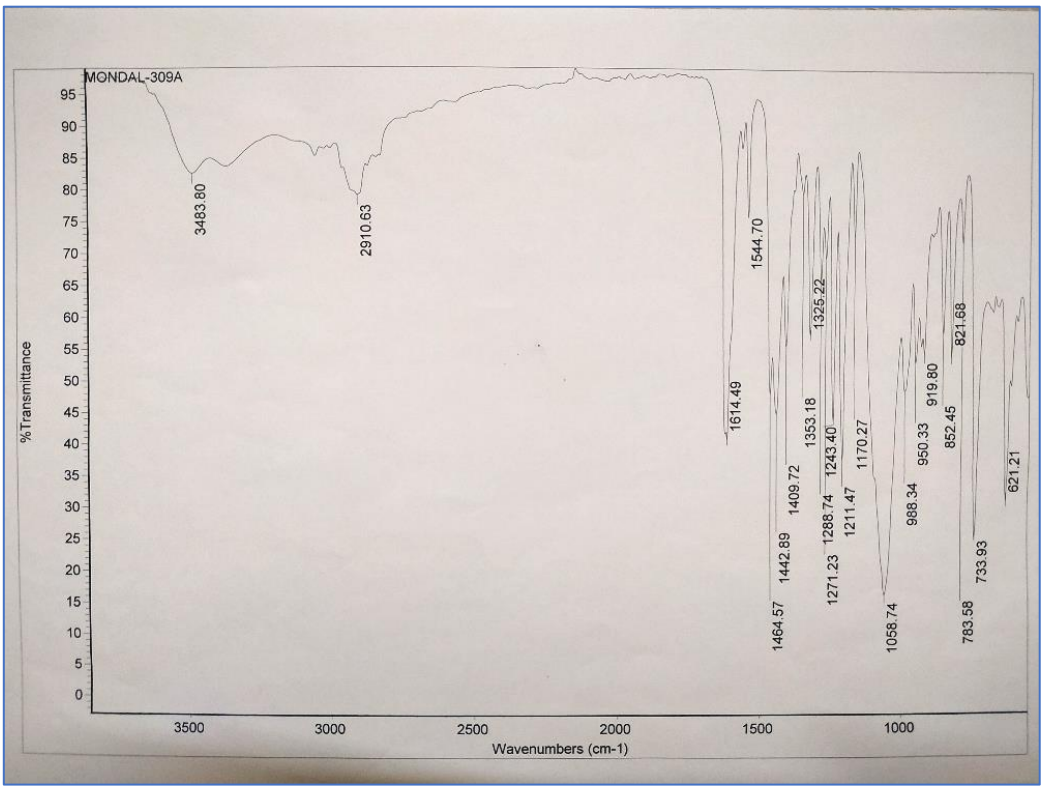

Figure 2.21. IR spectra of compound **2.3.**

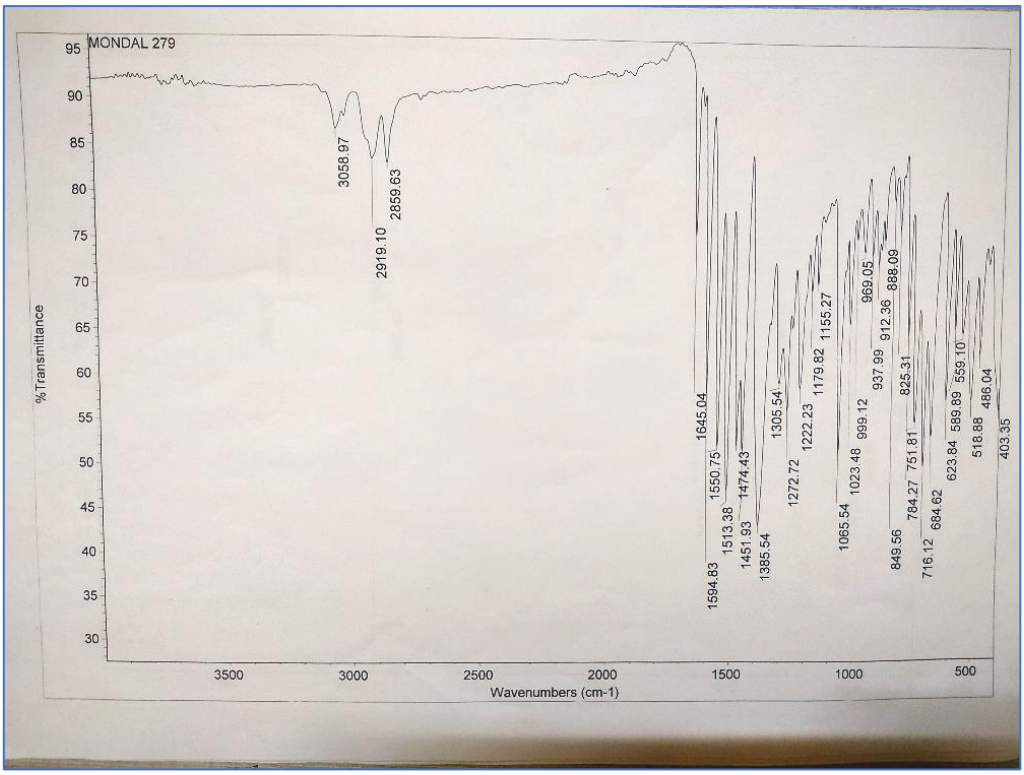

Figure 2.22. IR spectra of compound **2.4.**

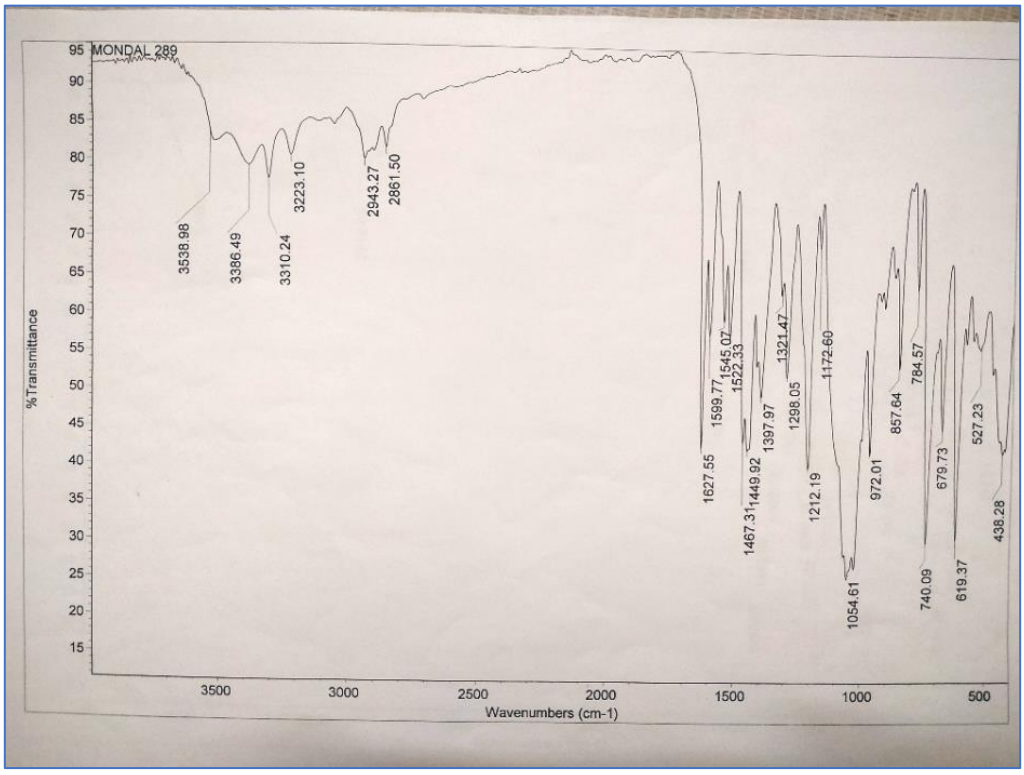

Figure 2.23. IR spectra of compound **2.5.**

UV-VIS absorption spectra of compound **2.1-2.5**.

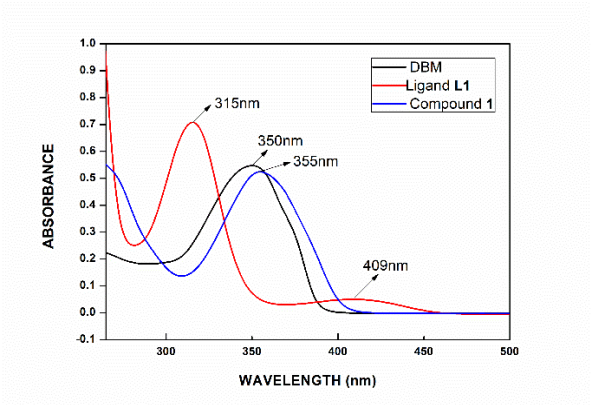

Figure 2.24

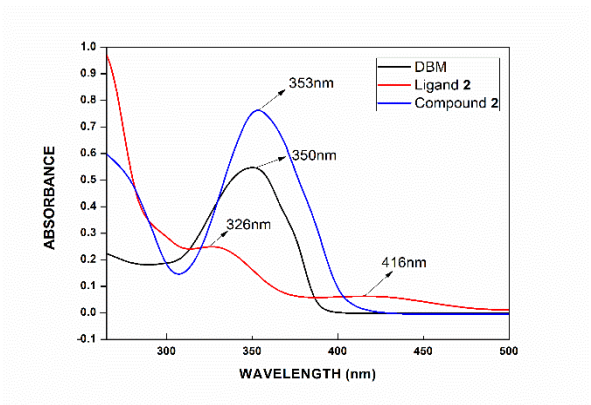

Figure 2.25

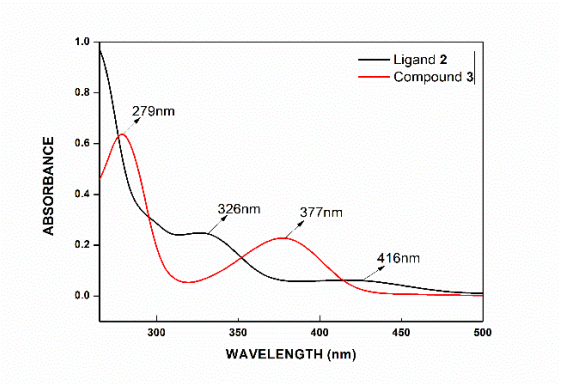

Figure 2.26

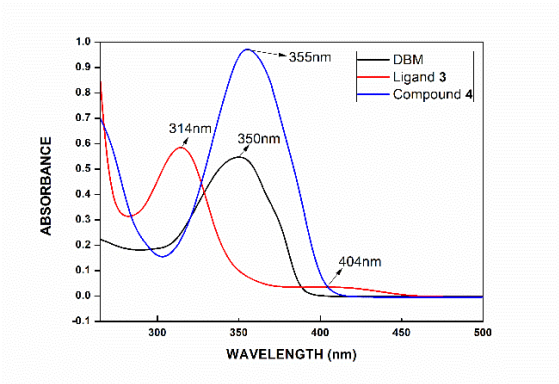

Figure 2.27

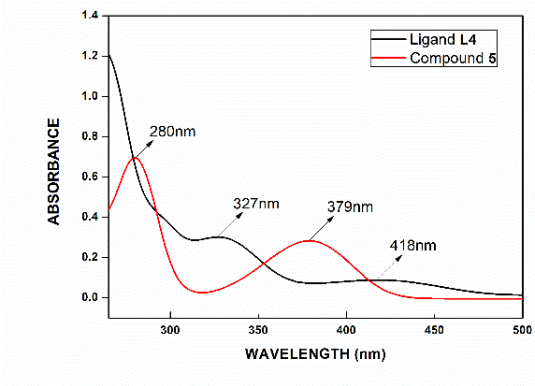

Figure 2.28

Table 2.10. Experimental and calculated electronic transition, oscillator strength (f), contributing orbitals for compound 2.1 and compound 2.4

System	Calculated λ(nm)	Experimental λ(nm)	Major Contribution	f (oscillator strength)
Compound 2.1	420.65	----------	H → L (98.88%)	0.0062
	352.79	355	H-2 → L (43.02%) H-3 → L (29.59%) H-4 → L (15.67%) H-1 → L (5.07%) H-6 → L (3.77%)	0.0116
	352.39	----------	H → L+1(95.97%)	0.1364
	339.35	----------	H-3 → L(3.74%) H-1 → L(90.02%)	0.6177
	323.44	----------	H-3 → L(3.01%) H-3 → L+1(2.47%) H-2 → L(5.61%) H-2 → L+1(64.97%) H-1 → L+1(2.96%)	0.0244
Compound 2.4	384.22	377	H-1→ L(33.88%) H-1 → L+1(4.13%) H → L(42.17%) H → L+1(19.53%)	0.0055
	365.85	----------	H → L+2(44.85%) H → L+1(19.3%) H-1 → L+2(12.44%)	0.0767
	364.19	----------	H-1 → L+2(34.43%) H → L+3(24.6%) H-1 → L+1(17.05%)	0.065

			H-1 → L+2(12.48%)	
	362.36	**----------**	**H → L+1(50.49%)** **H → L+2(20.85%)** **H-1 → L(10.61%)**	**0.0179**
	346.53	**----------**	**H-2 → L(90.17%)** **H-1→ L+2(3.00%)**	**0.0609**
	276.77	**279**	**H-5 → L+1(33.10%)** **H-8 → L+1(23.62%)** **H-11 → L(12.50%)**	**0.0169**
	272.59	**----------**	**H-3 → L(3.01%)** **H-3 → L+1(2.47%)** **H-2 → L(5.61%)** **H-2 → L+1(64.97%)** **H-1 → L+1(2.96%)**	**0.5783**
	271.85	**----------**	**H-6 → L+2(4.45%)** **H-5 → L+2(3.96%)** **H-5 → L+3(46.91%)** **H-4→ L+3(38.35%)**	**0.019**
	270.98	**----------**	**H-8 → L+2(4.45%)** **H-5 → L+2(42.98%)** **H-5 → L+3(32.33%)** **H-4 → L+2(17.70%)**	**0.0507**
	270.56	**----------**	**H-4 → L+3(83.72%)** **H-6 → L+3(4.16%)**	**0.0372**

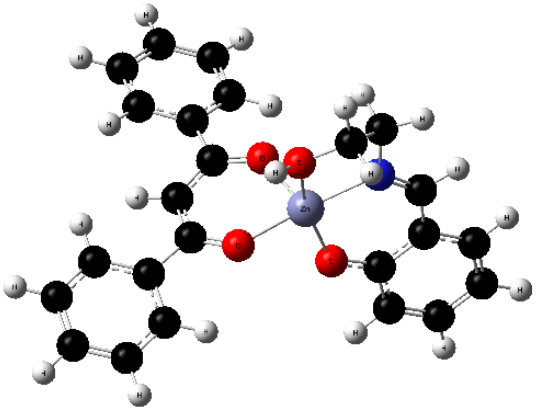

Figure 2.29. Compound 2.1 Optimized Structure

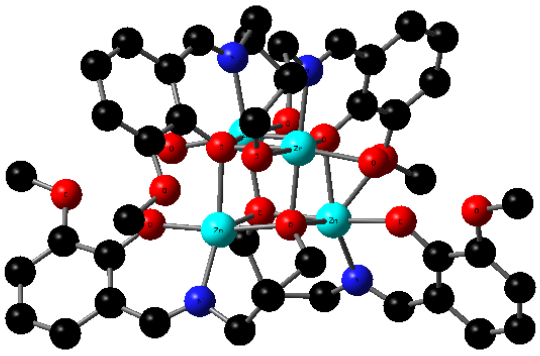

Figure 2.30. Compound 2.4 Optimized Structure

Emission spectra of compound **2.1-2.5**.

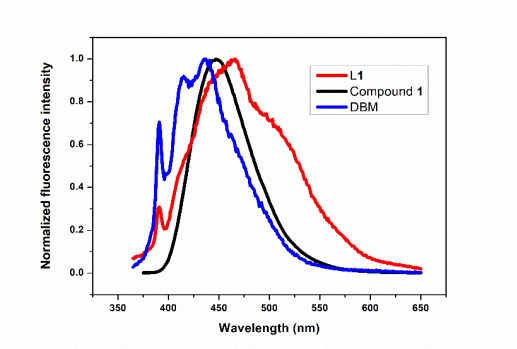

Figure 2.31

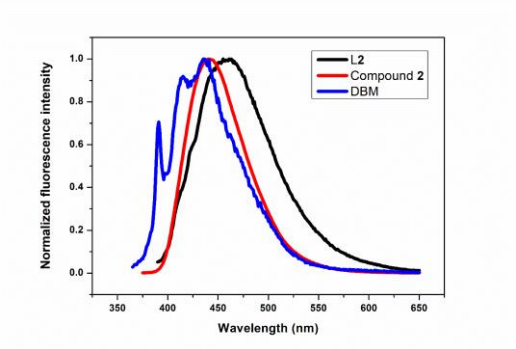

Figure 2.32

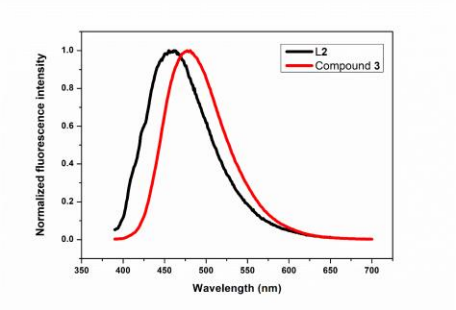

Figure 2.33

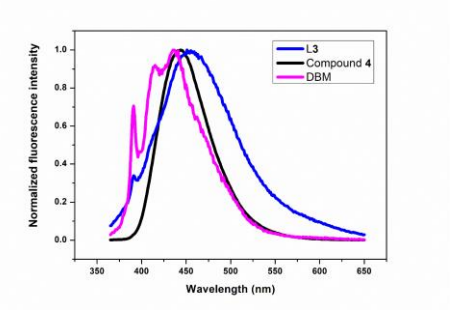

Figure 2.34

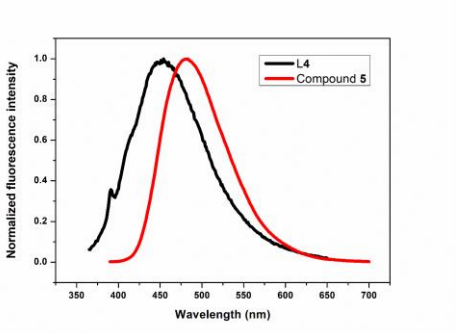

Figure 2.35

^{1}H NMR and ^{13}C NMR of compound **2.1-2.5:**

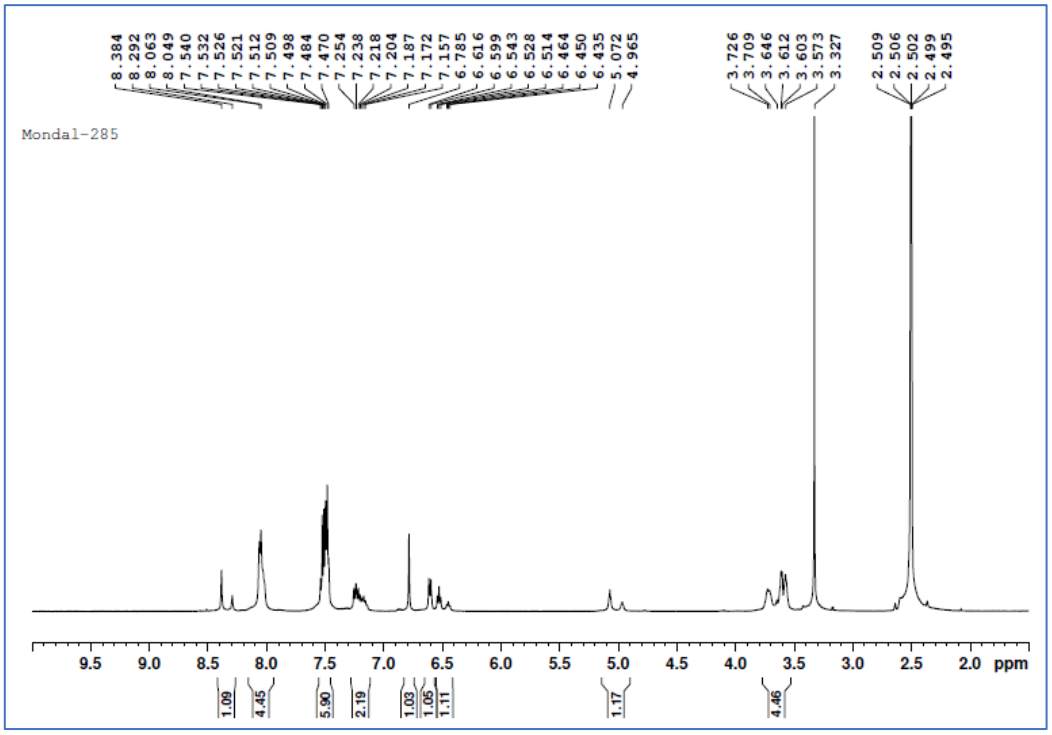

Figure 2.36. ^{1}H NMR of compound **2.1**

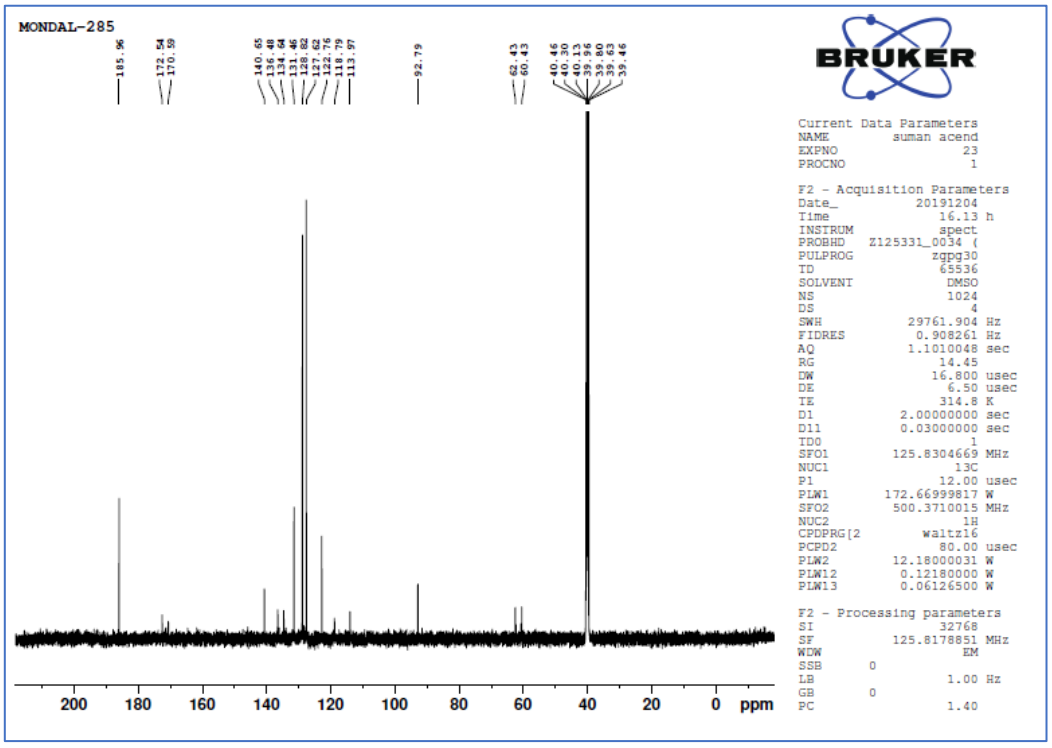

Figure 2.37. ^{13}C NMR of compound **2.1**

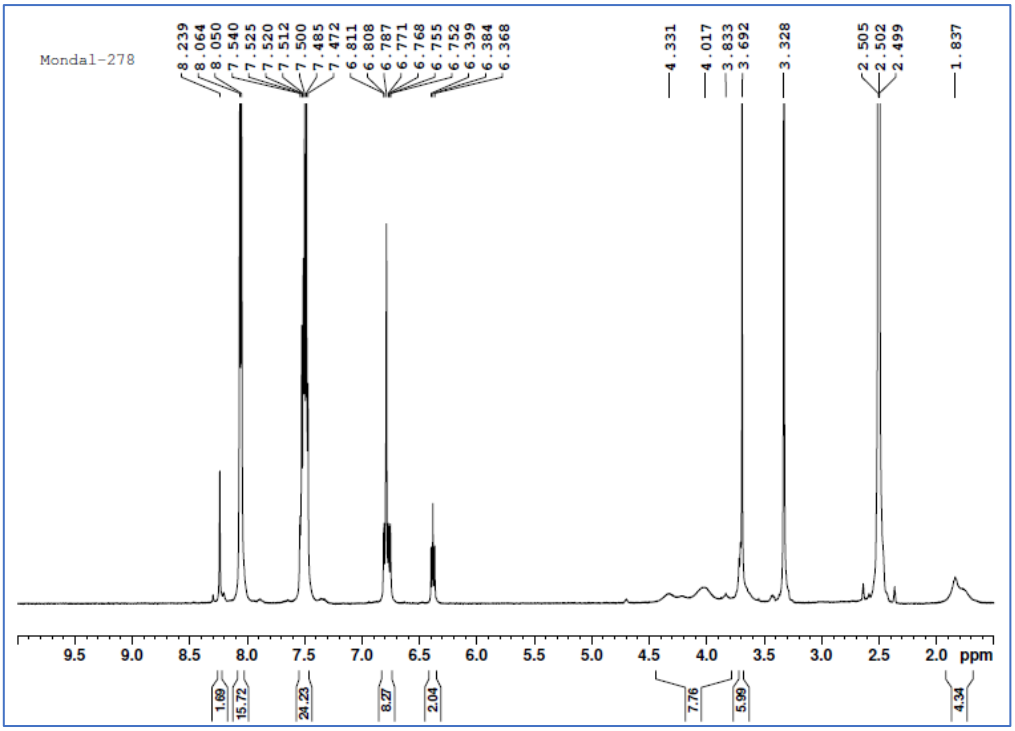

Figure 2.38. ^{1}H NMR of compound **2.2**

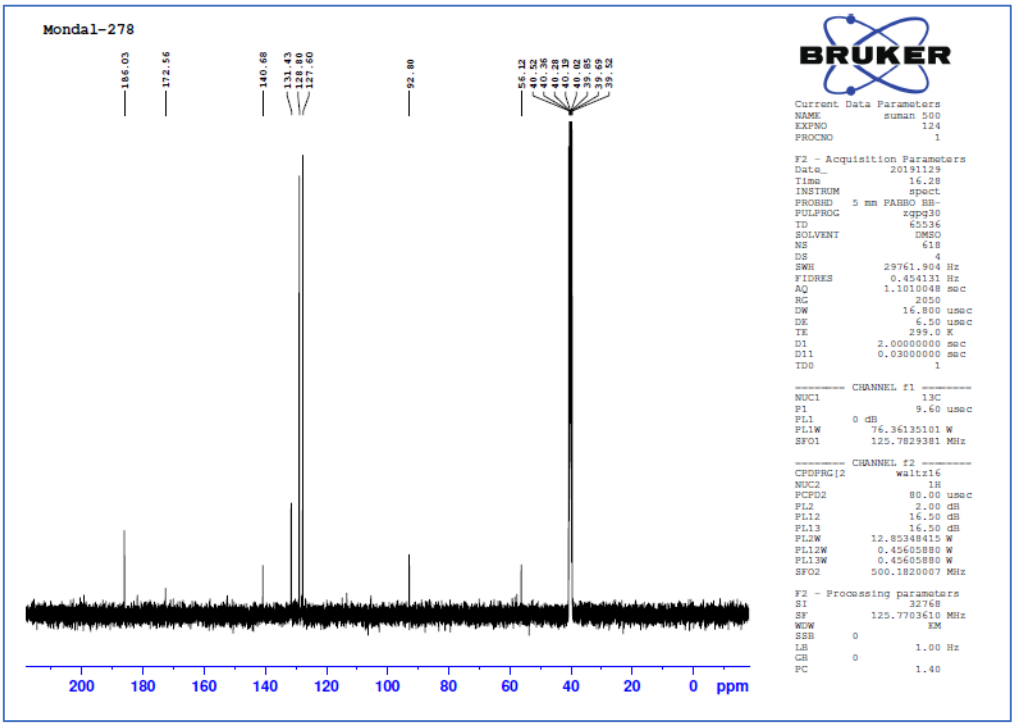

Figure 2.39. ^{13}C NMR of compound **2.2**

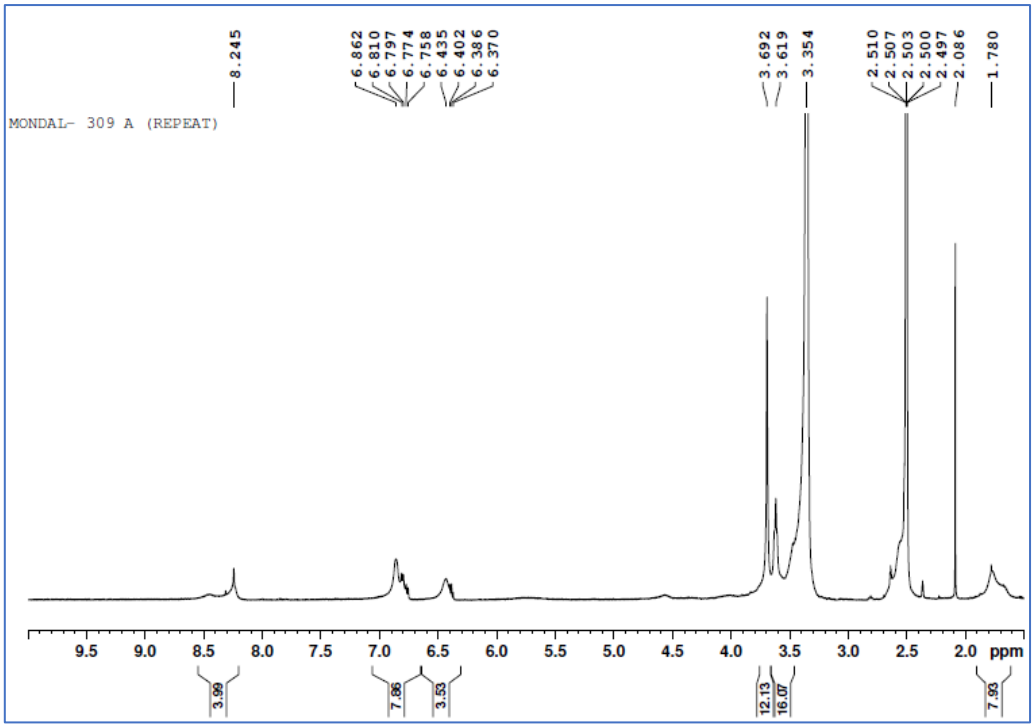

Figure 2.40. ^{1}H NMR of compound **2.3**

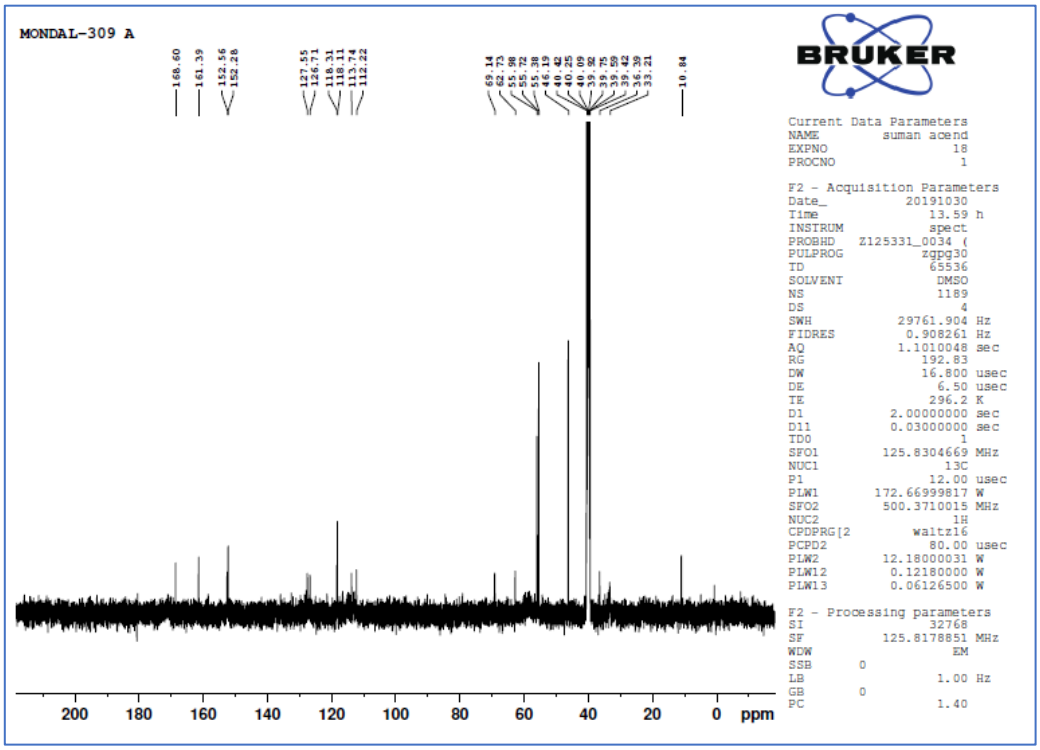

Figure 2.41. ^{13}C NMR of compound **2.3**

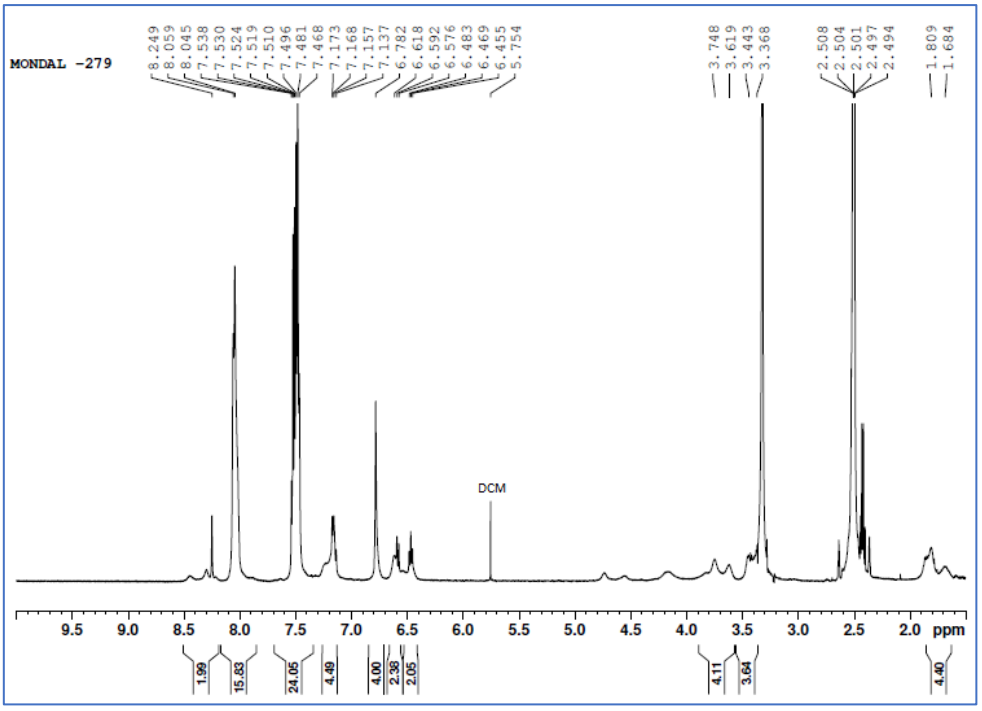

Figure 2.42. ^{1}H NMR of compound **2.4**

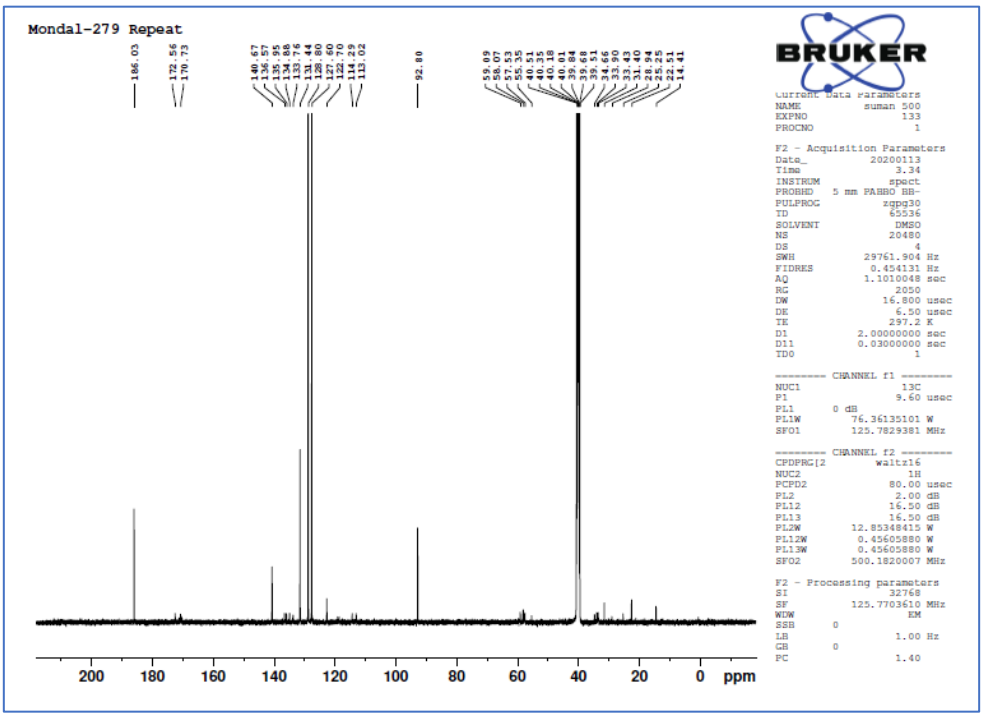

Figure 2.43. ^{13}C NMR of compound **2.4**

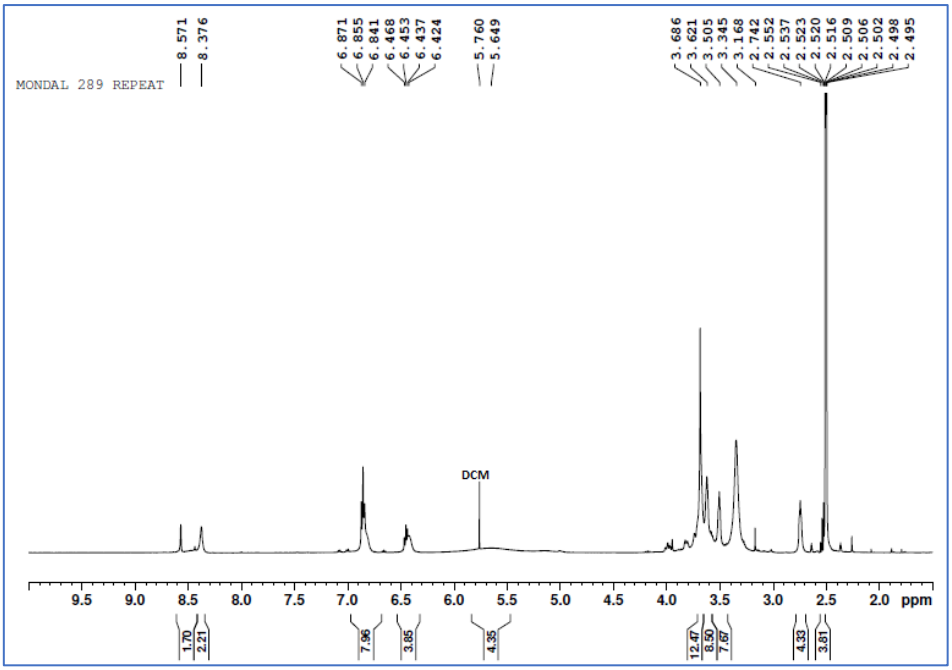

Figure 2.44. ^{1}H NMR of compound **2.5**

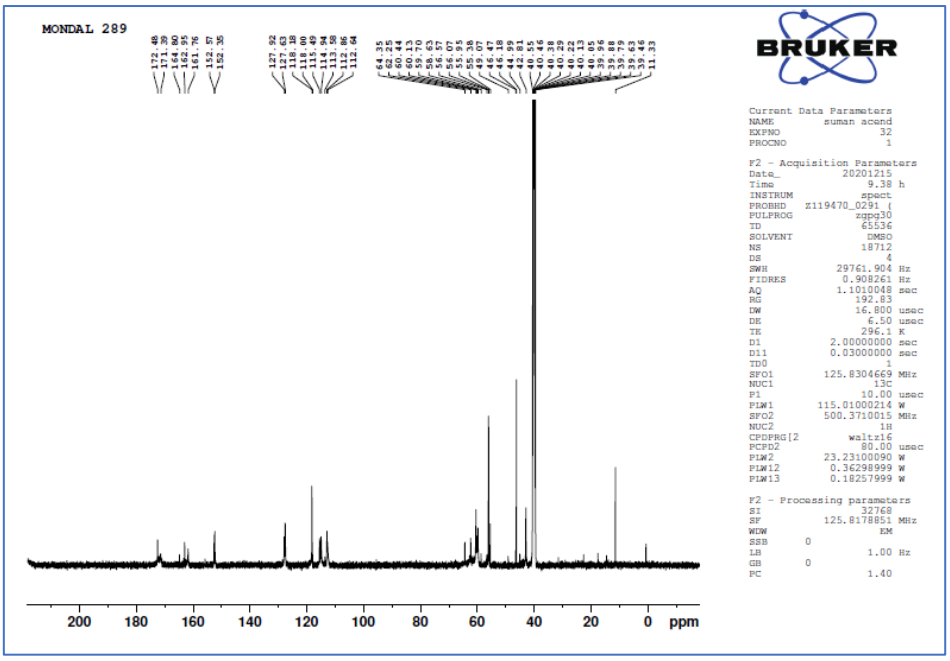

Figure 2.45. ^{13}C NMR of compound **2.5**

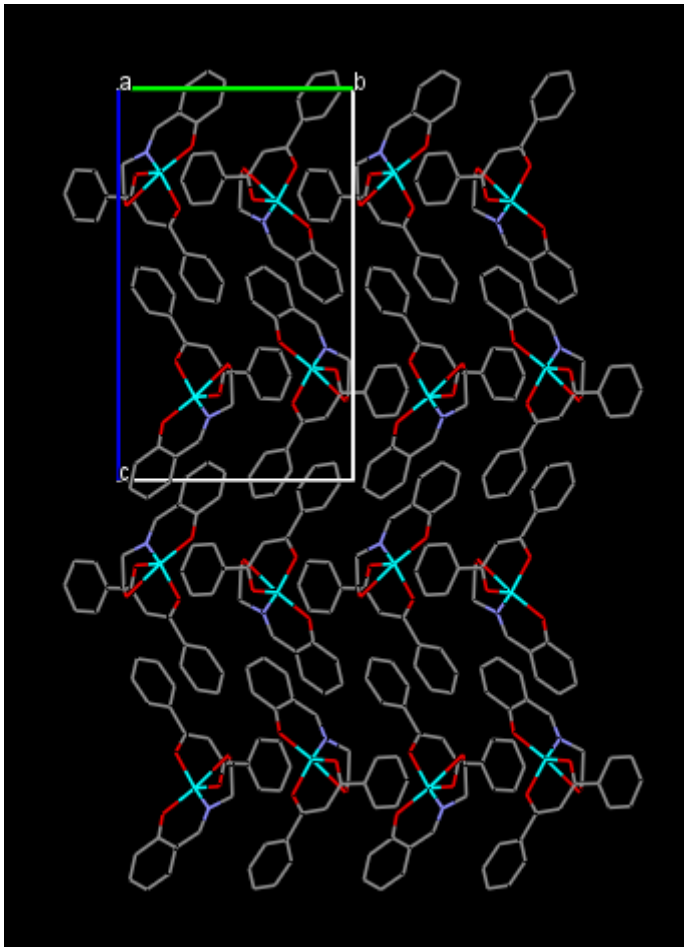

Figure 2.46. Packing diagram of **2.1**

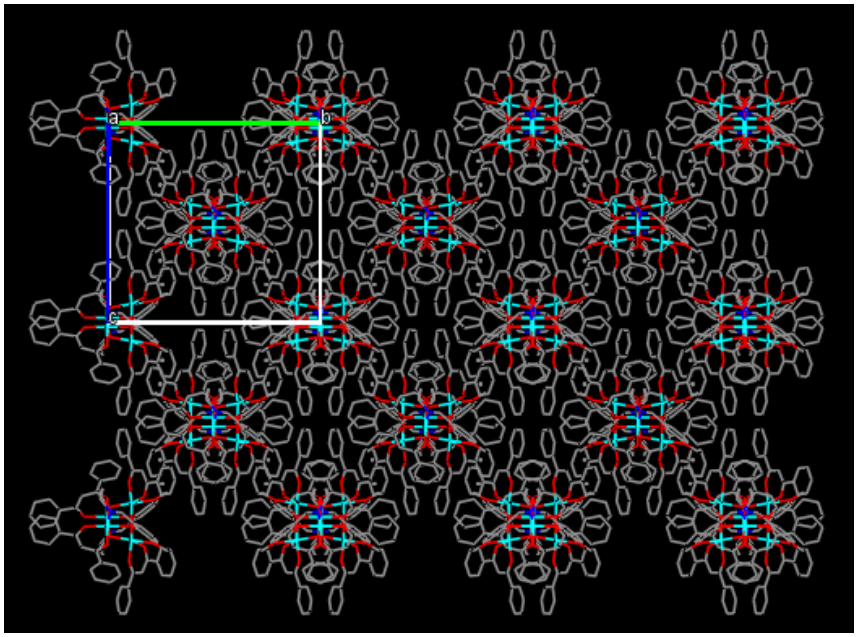

Figure 2.47. Packing diagram of **2.2**

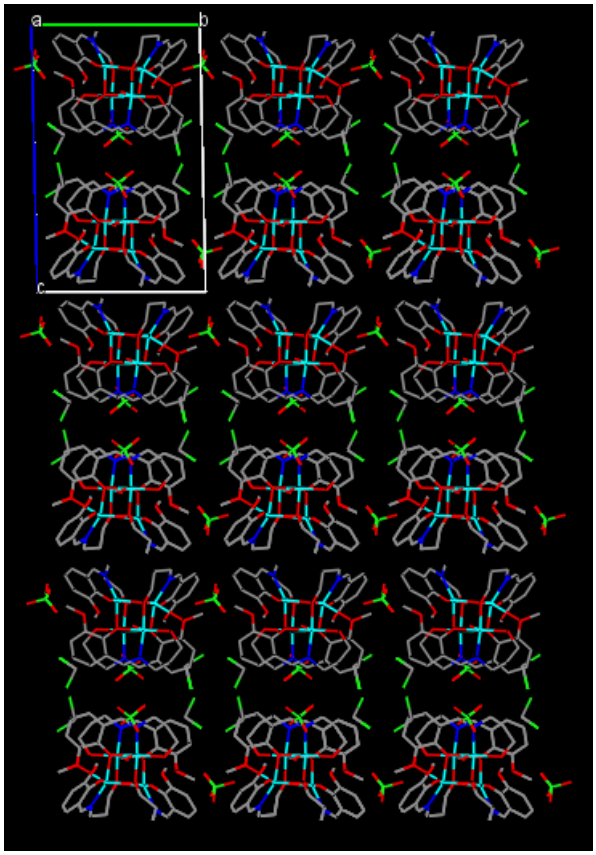

Figure 2.48. Packing diagram of **2.3**

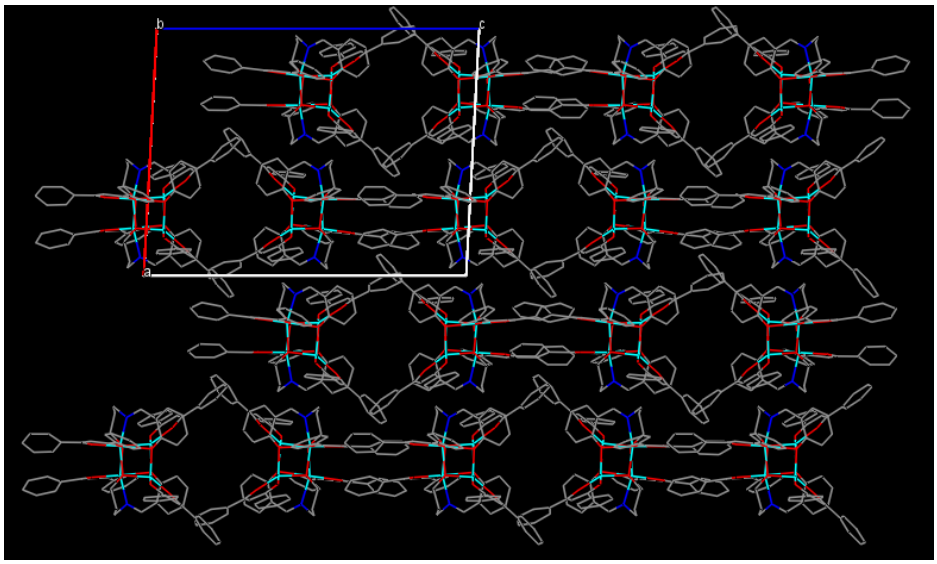

Figure 2.49. Packing diagram of **2.4**

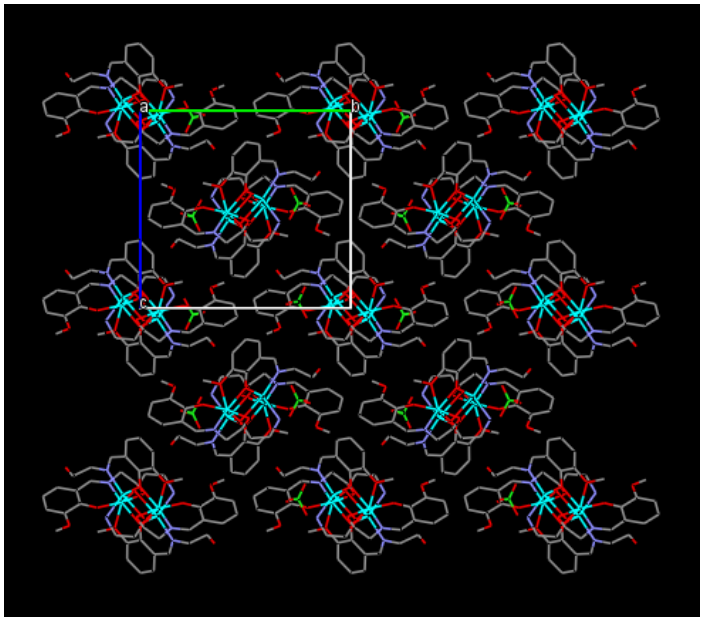

Figure 2.50. Packing diagram of **2.5**

SHAPE ANALYSIS DATA

S H A P E v2.1 Continuous Shape Measures calculation(Cshm)

(c) 2013 Electronic Structure Group, Universitat de Barcelona

Contact: llunell@ub.edu

Table 2.11. Shape calculation of compound **2.1.**

S.No.	Geometry			Cshm value for Zn1
1	PP-5	D5h	Pentagon	28.654
2	vOC-5	C4v	Vacant octahedron	3.332
3	TBPY-5	D3h	Trigonal bipyramid	3.693
4	**SPY-5**	**C4v**	**Spherical square pyramid**	**2.281**
5	JTBPY-5	D3h	Johnson trigonal bipyramid J12	4.159

Table 2.12, 2.13. Shape calculation of compound **2.2.**

S.No.	Geometry			Cshm value for Zn1
1	HP-6	D6h	Hexagon	31.550
2	PPY-6	C5v	Pentagonal pyramid	26.577
3	**OC-6**	**Oh**	**Octahedron**	**0.717**
4	TPR-6	D3h	Trigonal prism	14.882
5	JPPY-6	C5v	Johnson pentagonal pyramid J2	30.381

S.No.	Geometry			Cshm value for Zn2
1	HP-6	D6h	Hexagon	32.161
2	PPY-6	C5v	Pentagonal pyramid	17.230
3	OC-6	Oh	Octahedron	7.452
4	**TPR-6**	**D3h**	**Trigonal prism**	**3.891**
5	JPPY-6	C5v	Johnson pentagonal pyramid J2	20.646

Table 2.14-2.17. Shape calculation of compound **2.3.**

S.No.	Geometry			Cshm value for Zn1
1	HP-6	D6h	Hexagon	30.940
2	PPY-6	C5v	Pentagonal pyramid	27.760
3	OC-6	Oh	Octahedron	**0.568**
4	**TPR-6**	**D3h**	**Trigonal prism**	14.976
5	JPPY-6	C5v	Johnson pentagonal pyramid J2	31.587

S.No.	Geometry			Cshm value for Zn2
1	PP-5	D5h	Pentagon	28.171
2	**vOC-5**	**C4v**	**Vacant octahedron**	**2.696**
3	TBPY-5	D3h	Trigonal bipyramid	3.462
4	SPY-5	C4v	Spherical square pyramid	3.094
5	JTBPY-5	D3h	Johnson trigonal bipyramid J12	5.706

S.No.	Geometry			Cshm value for Zn3
1	HP-6	D6h	Hexagon	31.214
2	PPY-6	C5v	Pentagonal pyramid	27.289
3	OC-6	Oh	Octahedron	**0.494**
4	**TPR-6**	**D3h**	**Trigonal prism**	14.477
5	JPPY-6	C5v	Johnson pentagonal pyramid J2	31.205

S.No.	Geometry			Cshm value for Zn4
1	HP-6	D6h	Hexagon	31.955
2	PPY-6	C5v	Pentagonal pyramid	21.514
3	OC-6	Oh	Octahedron	**3.810**
4	**TPR-6**	**D3h**	**Trigonal prism**	8.407
5	JPPY-6	C5v	Johnson pentagonal pyramid J2	24.582

Table 2.18-2.21. Shape calculation of compound **2.4.**

S.No.	Geometry			Cshm value for Zn1
1	HP-6	D6h	Hexagon	32.248
2	PPY-6	C5v	Pentagonal pyramid	25.384
3	OC-6	Oh	Octahedron	**0.918**
4	**TPR-6**	**D3h**	**Trigonal prism**	13.884
5	JPPY-6	C5v	Johnson pentagonal pyramid J2	29.244

S.No.	Geometry			Cshm value for Zn2
1	PP-5	D5h	Pentagon	26.033
2	vOC-5	C4v	Vacant octahedron	3.599
3	TBPY-5	D3h	Trigonal bipyramid	3.665
4	**SPY-5**	**C4v**	**Spherical square pyramid**	**3.301**
5	JTBPY-5	D3h	Johnson trigonal bipyramid J12	4.385

S.No.	Geometry			Cshm value for Zn3
1	PP-5	D5h	Pentagon	26.357
2	vOC-5	C4v	Vacant octahedron	4.491
3	TBPY-5	D3h	Trigonal bipyramid	**3.303**
4	**SPY-5**	**C4v**	**Spherical square pyramid**	4.114
5	JTBPY-5	D3h	Johnson trigonal bipyramid J12	3.714

S.No.	Geometry			Cshm value for Zn4
1	HP-6	D6h	Hexagon	32.381
2	PPY-6	C5v	Pentagonal pyramid	25.890
3	**OC-6**	**Oh**	**Octahedron**	**0.876**
4	TPR-6	D3h	Trigonal prism	14.093
5	JPPY-6	C5v	Johnson pentagonal pyramid J2	29.726

Table 2.22-2.23. Shape calculation of compound **2.5.**

S.No.	Geometry			Cshm value for Zn1
1	HP-6	D6h	Hexagon	33.895
2	PPY-6	C5v	Pentagonal pyramid	20.001
3	**OC-6**	**Oh**	**Octahedron**	**3.300**
4	TPR-6	D3h	Trigonal prism	9.135
5	JPPY-6	C5v	Johnson pentagonal pyramid J2	24.323

S.No.	Geometry			Cshm value for Zn2
1	PP-5	D5h	Pentagon	32.114
2	vOC-5	C4v	Vacant octahedron	5.889
3	**TBPY-5**	**D3h**	**Trigonal bipyramid**	**1.613**
4	SPY-5	C4v	Spherical square pyramid	4.556
5	JTBPY-5	D3h	Johnson trigonal bipyramid J12	2.546

PXRD data:

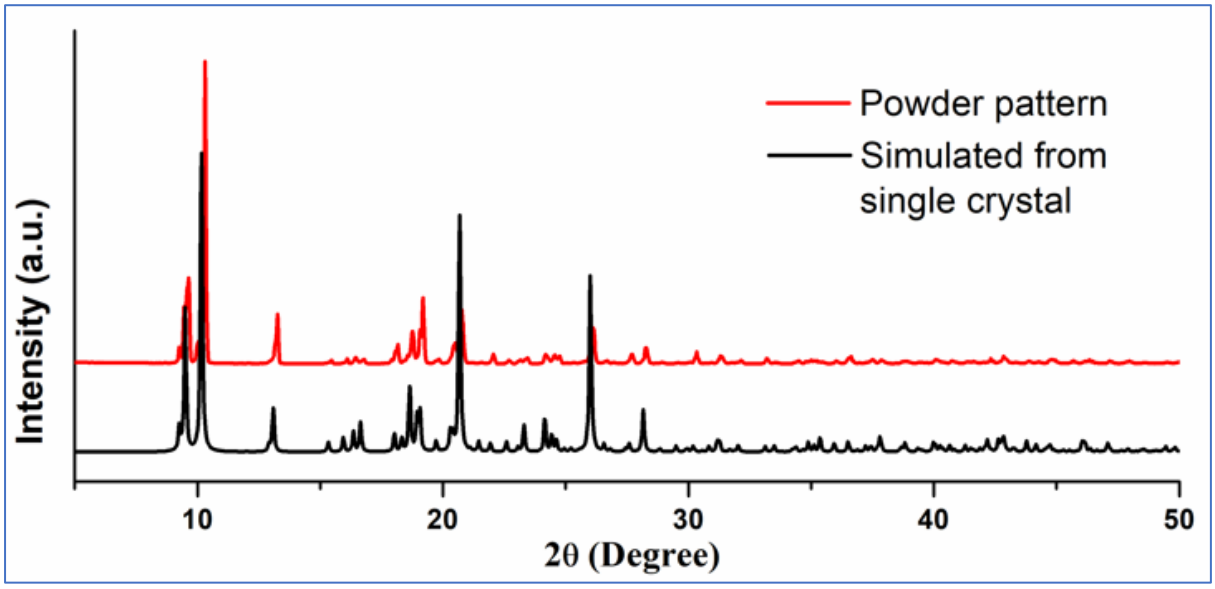

Figure 2.51. Powder X-ray diffraction pattern of a bulk sample of **2.1** compared to the simulated powder pattern extracted from single crystal diffraction data.

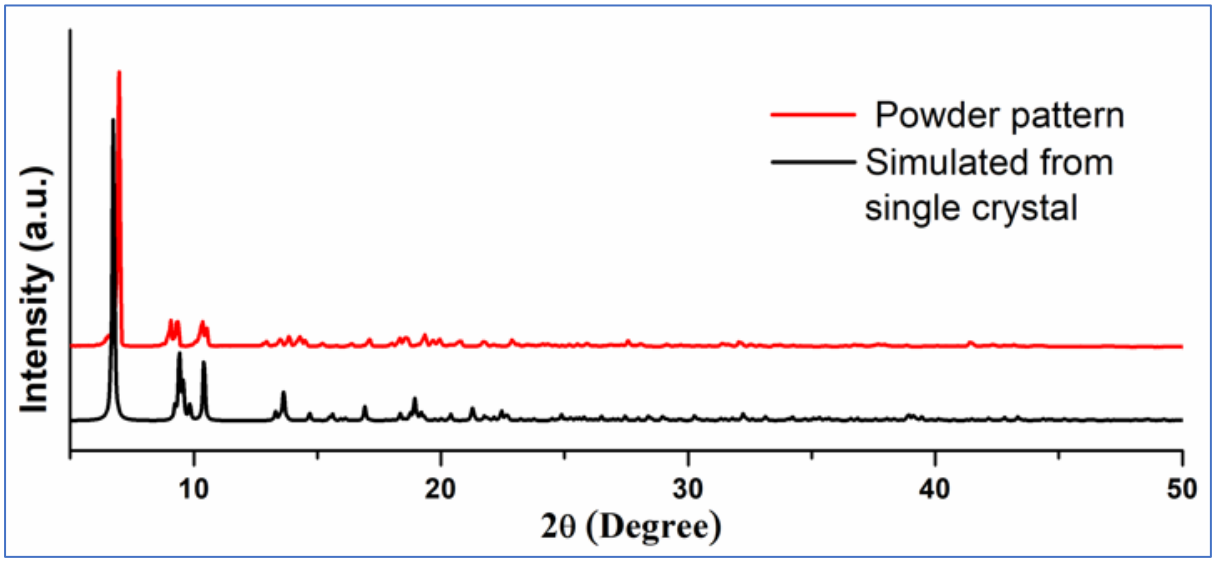

Figure 2.52. Powder X-ray diffraction pattern of a bulk sample of **2.2** compared to the simulated powder pattern extracted from single crystal diffraction data.

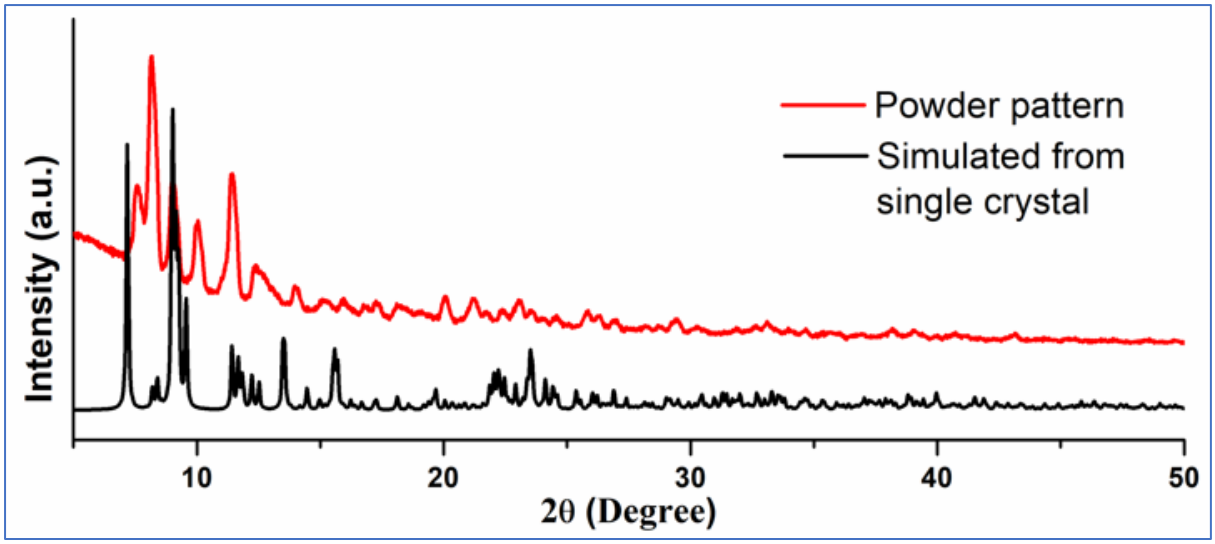

Figure 2.53. Powder X-ray diffraction pattern of a bulk sample of **2.3** compared to the simulated powder pattern extracted from single crystal diffraction data.

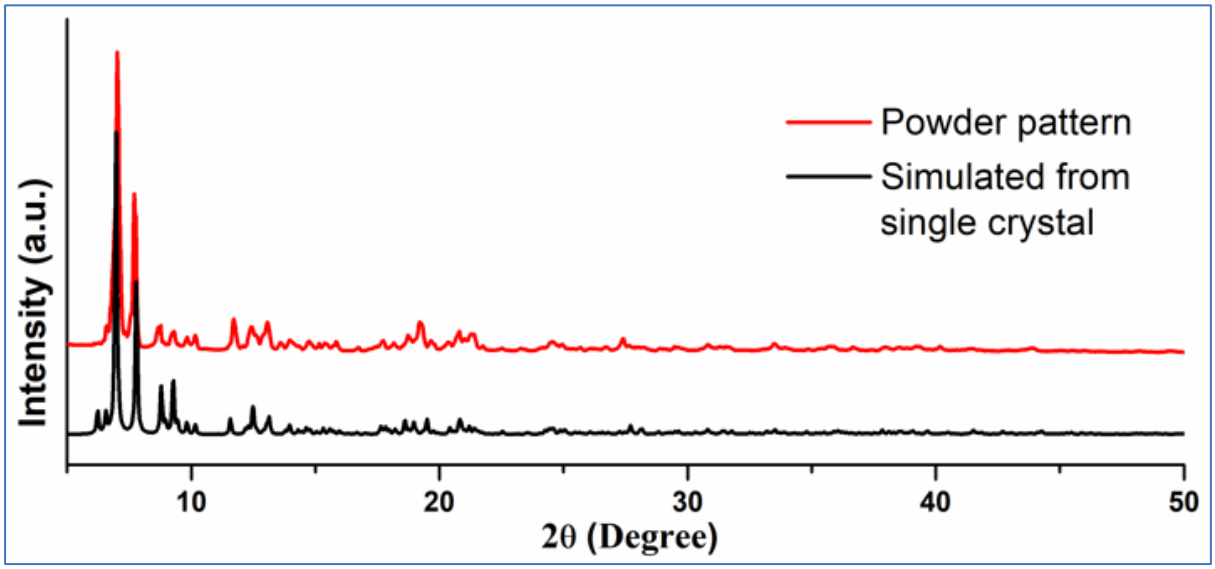

Figure 2.54. Powder X-ray diffraction pattern of a bulk sample of **2.4** compared to the simulated powder pattern extracted from single crystal diffraction data.

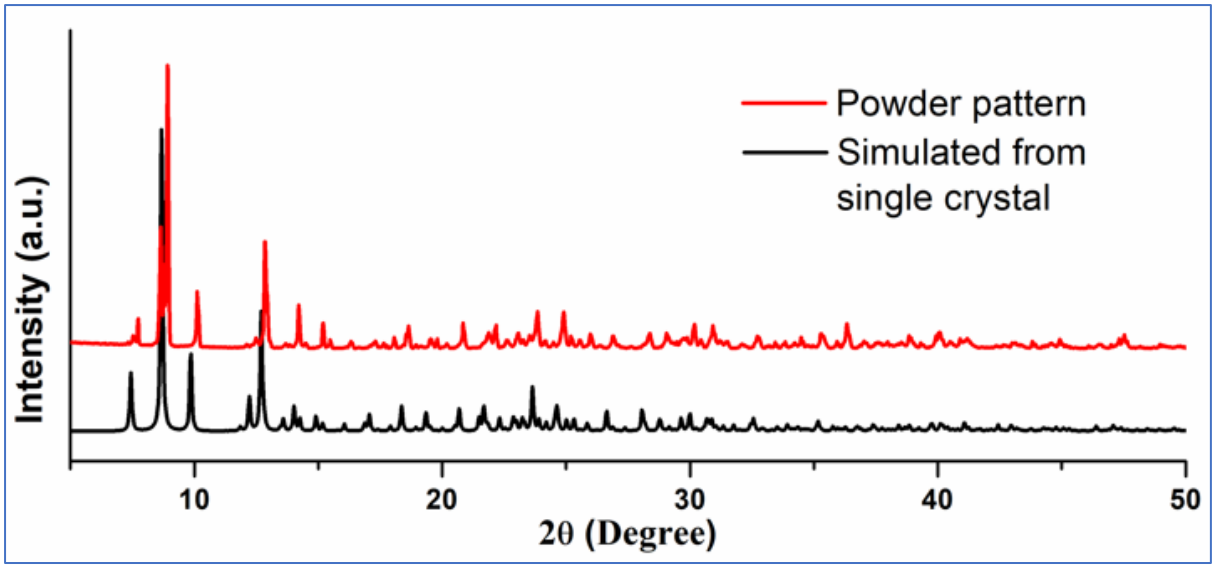

Figure 2.55. Powder X-ray diffraction pattern of a bulk sample of **2.5** compared to the simulated powder pattern extracted from single crystal diffraction data.

2.6. References:

(1) (a) R. Murugavel, S. Kuppuswamy, R. Boomishankar and A. Steiner, *Angew. Chem. Int. Ed.,* 2006, **45,** 5536-5540.

(b) A. A. Dar, S. Sen, S. K. Gupta, G. N. Patwari and R. Murugavel, *Inorg. Chem.*, 2015, **54,** 9458-9469.

(c) A. K. Bar, P. Kalita, J. P. Sutter and V. Chandrasekhar, *Inorg. Chem.*, 2018, **57,** 2398-2401.

(d) M. Yadav, A. Mondal, V. Mereacre, S. K. Jana, A. K. Powell and P. W. Roesky, *Inorg. Chem.*, 2015, **54,** 7846-7856.

(e) L. Li, J. Gou, D. F. Wu, Y. J. Wang, Y. Y. Duan, H. H. Chen, H. L. Gao and J. Z. Cui, *New J. Chem.*, 2020, **44,** 3912-3921.

(2) (a) V. Baskar, M. Shanmugam, E. C. Sañudo, M. Shanmugam, D. Collison, E. J. McInnes, Q. Wei and R. E. Winpenny, *Chem. Comm.*, 2007, 37-39.

(b) S. Ali, V. Baskar, C. A. Muryn and R. E. Winpenny, *Chem. Comm.*, 2008, **47,** 6375-6377.

(3) V. Chandrasekhar, L. Nagarajan, K. Gopal, V. Baskar and P. Kögerler, *Dalt. Trans.*, 2005,**19,** 3143-3145.

(4) V. Baskar, K. Gopal, M. Helliwell, F. Tuna, W. Wernsdorfer and R. E. Winpenny, *Dalt. Trans.*, 2010, **39,** 4747-4750.

(5) J. Ali, T. Navaneetha, V. Baskar, *Inorg. Chem.*, 2019, **59,** 741-747.

(6) U. Ugandhar, T. Navaneetha, J. Ali, S. Mondal, G. Vaitheeswaran and V. Baskar, *Inorg. Chem.*, 2020, **59,** 6689-6696.

(7) (a) M. Dey, C.P. Rao, P. Saarenketo, K. Rissanen and E. Kolehmainen, *Eur. J. Inorg. Chem.*, 2002, **8,** 2207-2215.

(b) S. Akine, W. Dong and T. Nabeshima, *Inorg. Chem.*, 2006, **45,** 4677-4684.

(c) M. Nihei, A. Yoshida, S. Koizumi and H. Oshio, *Polyhedron*, 2007, **26,** 1997-2007.

(d) Q. Gao, Y. Qin, Y. Chen, W. Liu, H. Li, B. Wu, Y. Li and W. Li, *RSC Advances*, 2015, **5,** 43195-43201.

(e) S. K. Kushvaha, S. Arumugam, B. Shankar, R. S. Sarkar, V. Ramkumar and K. C. Mondal, *Eur. J. Inorg. Chem.*, 2019, **24,** 2871-2882.

(8) (a) H. Xiang, Y. Lan, L. Jiang, W. X. Zhang, C. E. Anson, T. B. Lu, A. K. Powell, *Inorg. Chem. Comm.*, 2012, **16,** 51-54.

(b) M. N. Ahamad, K. Iman, M. K. Raza, M. Kumar, A. Ansari, M. Ahmad and M. Shahid, *Bioorg. Chemi*, 2020, **95,** 103561.

(c) E. C. Constable, C. E. Housecroft, J. A. Zampese and G. Zhang, *Polyhedron*, 2012, **44,** 150-155.

(d) Z. Y. Liu, H. H. Zou, R. Wang, M. S. Chen and F. P. Liang, *RSC advances*, 2018, **8,** 767-774.

(e) S. Shit, M. Nandy, G. Rosair, M. S. El Fallah, J. Ribas, E. Garribba and S. Mitra, *Polyhedron*, 2013, **52,** 963-969.

(f) S. T. Tsantis, D. I. Tzimopoulos, M. Holynska and S. P. Perlepes, *Int. J. Mol. Sci.*, 2020, **21,** 555.

(g) R. Biswas, M. G. Drew and A. Ghosh, *Inorg. Chem. Comm.*, 2012, **24,** 1-3.

(h) K. Griffiths, I. A. Kühne, G. J. Tizzard, S. J. Coles, G. E. Kostakis and A. K. Powell, *Inorg. Chem.*, 2019, **58,** 2483-2490.

(i) A. N. Georgopoulou, M. Pissas, V. Psycharis, Y. Sanakis and C. P. Raptopoulou, *Molecules*, 2020, **25,** 2280.

(9) (a) P. H. Lin, T. J. Burchell, L. Ungur, L. F. Chibotaru, W. Wernsdorfer and M. Murugesu, *Angew. Chem.*, 2009. **121,** 9653-9656.

(b) W. B. Sun, B. L. Han, P. H. Lin, H. F. Li, P. Chen, Y. M. Tian, M. Murugesu and P. F. Yan, *Dalt. Trans.*, 2013, **42,** 13397-13403.

(10) (a) B. Gao, R. Duan, X. Pang, X. Li, Z. Qu, H. Shao, X. Wang and X. Chen, *Dalt. Trans.*, 2013, **42,** 16334-16342.

(b) R. Duan, B. Gao, X. Li, X. Pang, X. Wang, H. Shao and X. Chen, *Polymer*, 2015, **71,** 1-7.

(c) A. Virachotikul, N. Laiwattanapaisarn, P. Wongmahasirikun, P. Piromjitpong, K. Chainok and K. Phomphrai, *Inorg. Chem.*, 2020, **59,** 8983-8994.

(d) S. Ghosh, A. Spannenberg and E. Mejía, *Helvetica Chimica Acta*, 2017, **100,** 1-17.

(11) (a) K. Bernardo, S. Leppard, A. Robert, G. Commenges, F. Dahan and B. Meunier, *Inorg. Chem.*, 1996, **35,** 387-396.

(12) (a) M. H. Chisholm, J. C. Gallucci, H. Zhen and J. C. Huffman, *Inorg. Chem.*, 2001, **40,** 5051-5054.

(b) A. S. Orabi, K. M. Abou El-Nour, M. F. Youssef and H. A. Salem, *Arab. J. Chem.*, 2020, **13,** 2628-2648.

(c) V. Pushpanathan and D. S. Kumar, *J. Nano. Chem.*, 2014, **4,** 95-101.

(13) (a) T. Chowdhury, S. Dasgupta, S. Khatua, K. Acharya and D. Das, *ACS Appl. Bio Mat.*, 2020, **3,** 4348-4357.

(b) O. Tsave, E. Halevas, M. P. Yavropoulou, A. K. Papadimitriou, J. G. Yovos, A. Hatzidimitriou, C. Gabriel, V. Psycharis and A. Salifoglou, *J. Inorg. Biochem.*, 2015, **152,** 123-137.

(c) D. Dey, G. Kaur, A. Ranjani,; L. Gayathri, P. Chakraborty, J. Adhikary, J. Pasan, D. Dhanasekaran, A. R. Choudhury, M. A. Akbarsha and N. Kole, *Eur. J. Inorg. Chem.*, 2014, **21,** 3350-3358.

(d) S. Das, A. Sahu, M. Joshi, S. Paul, M. Shit, A. R. Choudhury and B. Biswas, *Chem. Select*, 2018, **3,** 10774-10781.

(e) M. Garai, A. Das, M. Joshi, S. Paul, M. Shit, A. R. Choudhury and B. Biswas, *Polyhedron*, 2018, **156,** 223-230.

(14) (a) W. Sun, X. T. Qin, G. N. Zhang, S. Ding, Y. Q. Wang and Z. L. Liu, *Inorg. Chem. Comm.*, 2014, **40,** 190-193.

(b) T. K. Ghosh, S. Jana and A. Ghosh, *Inorg. Chem.*, 2018, **57,** 15216-15228.

(c) H. Yu, M. Liu, X. Gao and Z. Liu, *Polyhedron*, 2017, **137,** 217-221.

(15) (a) S. Dasgupta, S. Karim, S. Banerjee, M. Saha, K.D. Saha and D. Das, *Dalt. Trans.*, 2020, **49,** 1232-1240.

(b) M. Strinoiu, M. Răducă and A. M. Mădălan, *J. Coord. Chem.*, 2020, **73,** 2786-2800.

(16) (a) T. H. Sanatkar, A. Khorshidi and J. Janczak, *Appl. Organomet. Chem.* 2020, **34,** 5493.

(17) (a) M. Karmakar and S. Chattopadhyay, *Polyhedron*, 2020, **187,** 114639.

(b) M. Fondo, N. Ocampo, A.M. García-Deibe and J. Sanmartín, *Inorg. Chem.*, 2009, **48,** 4971-4979.

(18) C. Yang, Y. Peng, J. Wang, P. Chen and X. Gong, *Inorg. Chem. Comm.*, 2020, **119,** 108136.

(19) (a) S. K. Kushvaha, B. Shankar, N. S. M. Gorantla and K. C. Mondal, *Chem. Select*, 2019, **4,** 3334-3339.

(b) P. Roy, M. Manassero, K. Dhara and P. Banerjee, *Polyhedron*, 2009, **28,** 1133-1137.

(c) R. Gheorghe, G.A. Ionita, C. Maxim, A. Caneschi, L. Sorace and M. Andruh, *Polyhedron*, 2019, **171,** 269-278.

(20) (a) G. C. Dismukes, *Photochem. and photobio.*, 1986, **43,** 99-115.

(b) G. Renger, *Angew. Chem. Int. Ed. in English*, 1987, **26,** 643-660.

(c) H. B. Lee, D. A. Marchiori, R. Chatterjee, P. H. Oyala, J. Yano, R. D. Britt and T. Agapie, *J. Am. Chem. Soc.*, 2020, **142,** 3753-3761.

(d) J. Wang, X. Meng, W. Xie, X. Zhang, Y. Fan and M. Wang, *J. Bio. Inorg. Chem.*, 2021, 1-12.

(21) M. Dolaz, M. Tümer and M. Diğrak, *Trans. Met. Chem.*, 2004, **29,** 528-536.

(22) (a) S. Chattopadhyay, M. S. Ray, M. G. Drew, A. Figuerola, C. Diaz and A. Ghosh, *Polyhedron*, 2006, **25,** 2241-2253.

(b) M. Sinha Ray, S. Chattopadhyay, M.G. Drew, A. Figuerola, J. Ribas, C. Diaz and A. Ghosh, *Cr2yst. Struc., Spec. and Mag. Properties*. 2005, 4562-4571.

(23) (a) C. K. Pal, S. Mahato, M. Joshi, S. Paul, A. R. Choudhury and B. Biswas, *Inorg. Chim. Acta*, 2020, **506,** 119541.

(b) L. Jiang, D. Y. Zhang, J. J. Suo, W. Gu, J. L. Tian, X. Liu and S. P. Yan, *Dalt. Trans.*, 2016, **45,** 10233-10248.

(c) H. Wang, D. Zhang, Z.H. Ni, X. Li, L. Tian and J. Jiang, *Inorg. Chem.*, 2009, **48,** 5946-5956.

(24) (a) K. G. Vladimirova, A. Y. Freidzon, O. V. Kotova, A. A. Vaschenko, L. S. Lepnev, A. A. Bagatur'yants, A. G. Vitukhnovskiy, N. F. Stepanov, M. V. Alfimov, *Inorg. Chem.*, 2009, **48,** 11123-11130.

(b) A. Sarkar, A. Chakraborty, T. Chakraborty, S. Purkait, D. Samanta, S. Maity and D. Das, *Inorg. Chem.*, 2020,**59,** 9014-9028.

(25) (a) P. Orioli, R. Cini, D. Donati and S. Mangani, *J. Am. Chem. Soc.*, 1981, **103,** 4446-4452.

(b) M. T. Harding and S. J. Cole, *Acta Crystallographica*, 1963, **16,** 643-650.

(c) R. H. Kretsinger, F. A. Cotton and R. F. Bryan, *Acta Crystallographica*, 1963, **16,** 651-657.

(d) S. C. Rawle, A. J. Clarke, P. Moore and N. W. Alcock, *Dalt. Trans.*, 1992, **18,** 2755-2757.

(e) A. B. Charette, J. F. Marcoux and F. Bélanger-Gariépy, *J. Am. Chem. Soc.*, 1996, **118,** 6792-6793.

(26) R. A. Coxall, S. G. Harris, D. K. Henderson, S. Parsons, P. A. Tasker and R. E. Winpenny, *J. Chem. Soc.*, *Dalt. Trans.*, 2000, **14,** 2349-2356.

(27) (a) L. J. Bourhis, O. V. Dolomanov, R. J. Gildea, J. A. K. Howard and H. Puschmann, *Acta Cryst.* 2015, **A71**,59-75.

(b) G.M. Sheldrick, *Acta Cryst.* 2015, **A71,** 3-8.

(28) O. V. Dolomanov, L. J. Bourhis, R. J Gildea, J. A. K. Howard and H. Puschmann, *J. Appl. Cryst.* 2009, **42,** 339-341.

(29) G.M. Sheldrick, Crystal structure refinement with SHELXL. *Acta Crystallographica Section C: Structural Chemistry*, 2015, **71,** 3-8.

(30) S. Miertuš, E. Scrocco and J. Tomasi, *Chem. Phys.*, 1981, **55,** 117-29.

(31) (a) A. J. H. Wachters, "Gaussian basis set for molecular wave functions containing third-row atoms," *J. Chem. Phys.*,1970, **52 ,**1033.

(b) P. J. Hay, "Gaussian basis sets for molecular calculations – representation of 3D orbitals in transition-metal atoms," *J. Chem. Phys.*, 1977, **66 ,**4377-84.

(c) A. D. McLean and G. S. Chandler, "Contracted Gaussian-basis sets for molecular calculations. 1. 2nd row atoms, Z=11-18," *J. Chem. Phys.*, 1980, **72,**5639-48.

(d) K. Raghavachari, J. S. Binkley, R. Seeger and J. A. Pople, "Self-Consistent Molecular Orbital Methods. 20. Basis set for correlated wave-functions," *J. Chem. Phys.*, 1980, **72,** 650-54.

(32) M. J. Frisch, G. W. Trucks and H. B. Schlegel et al. Gaussian 09, Revision C.01, Gaussian, Inc., Wallingford, CT, 2010.

Aza-donor ligands- A key to synthesizing mononuclear to coordination polymers of cadmium phosphinates.

CHAPTER

3

Four cadmium phosphinate complexes were synthesized based on Bis-[α-hydroxy(p-methylphenyl)methyl]phosphinic acid (L) ligand. These complexes $[Cd(L)_2(H_2O)_2]$ **(3.1),** $[Cd(L)_2(py)_3].py$ **(3.2),** $[Cd(L)_2(4,4'\text{-bpy})_4]_n$ **(3.3),** $[Cd(L)_4(4,4'\text{-azo-bpy})(H_2O)]_n$ **(3.4),** were well characterized by single crystal X-ray diffraction, IR spectroscopy, powder X-ray diffraction, elemental analysis and TGA. **3.1** and **3.2** are zero-dimensional(0D) structures while **3.3** and **3.4** are two dimensional net-like(2D), one dimensional chain-like(1D) structures, respectively. N-donor co-ligands(py, 4,4'-bpy, 4,4'-azo-bpy) contribute to the formation of these architectures.

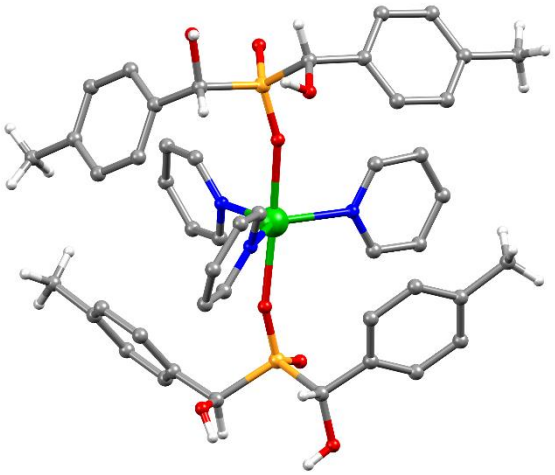

3.1 Introduction:

Metal-organic framework(MOF) and coordination polymers(CPs) are the most attractive and continuously explored research topics in the modern era.[1] This is due to the great potential application of MOF, CPs in gas adsorption,[2,3] catalysis,[4–7] ion-exchange,[8–10] magnetic property,[11–14] luminescence,[15,16] gas storage[17], separation technology,[18–20] nanotechnology,[21,22] sensors in the field of material science.[23–25] Along with this, the beautiful architectures of metal ions with multi-functional ligands are quite fascinating.[26] Proper design and synthesis of a determined structure are very challenging in the field of MOF and CPs. Desired structures can be obtained only by fine-tuning the natural interactions between the reactants through continuous efforts. A small modification in the synthetic process (metal-ion, ligand, solvent, temperature, pH, etc.) can dramatically change the framework structure. The use of multifunctional carboxylate ligands such as terephthalic acid,[27–33] trimesic acid,[34–42] benzene tetracarboxylic acids[1,43–48] with different metal species is widely reported in MOF synthesis by researchers. Phosphates and phosphinates which are analogous to these carboxylic acids have also greatly contributed to the synthesis of multidimensional architectures with their coordinating sites.[49–69] Reports of metal phosphonates and phosphates are quite prevalent when compared to metal phosphinates which are rarely investigated and not well explored. From simple crystallization to hydrothermal conditions, different strategies have been followed to obtain MOF and CPs. Room temperature synthesis is a low-cost synthetic strategy for MOF/CPs preparation. To construct coordination polymers, the self-assembly of metal ions and polycarboxylate /phosphonates cooperating with the N-donor ligand is one of the most effective approaches.[70] Bipyridine derivatives such as 4,4'-bpy, 2,2'-bpy are multifunctional ligands largely used in the assembly of CPs.[71–78] They act as bridging/chelating ligands to connect the metal ions.[79,80] and form coordination compounds with established properties; it is known as a spacer when they act as a bridging ligand.

In this regard, we have synthesized different geometries and architectures of cadmium complexes and coordination polymer by room temperature synthetic strategy. The ligand [(Bis-[α-hydroxy(p- methylphenyl)methyl]phosphinic acid] {(R_2PO_2H)[R= CH(OH)PhMe]}, for the first time has been utilized in the coordination polymer field. With this alpha-hydroxy phosphinic acid, mononuclear octahedral, mononuclear tbp, and 1D, 2D coordination polymer of cadmium compounds were synthesized and characterized.

3.2 Experimental Section:

3.2.1 General information:

High purity cadmium acetate dihydrate (Finar), 4-methylbenzaldehyde (Sigma Aldrich), Hypophosphorous acid (50% w/w in aqueous solution) (Avra), pyridine (Avra), 4,4'-bipyridine (Sigma Aldrich), 4,4'-azo-bipyridine (Sigma Aldrich), and all other chemicals were purchased from commercial sources. All solvents were used distilled, and chemicals were used without further purification.

3.2.2 Synthesis:

The ligand [Bis-[α-hydroxy(p-methylphenyl)methyl]phosphinic acid] (L) was synthesized using the literature procedure.[81,82] The synthetic procedures of the compounds are given in the following-

Compound 3.1: A mixture of ligand (L) (0.054 g, 0.179 mmol) and $Cd(OAc)_2.2H_2O$ (0.047 g, 0.179 mmol) were taken in 15 ml of distilled methanol. To it, triethylamine (0.716 mmol,0.099 ml) was added dropwise. The reaction mixture was stirred for 24 h at room temperature. The volume of the solvent was reduced under vacuum to about 7 ml, this was filtered and kept for crystallization at room temperature by slow evaporation. After 10 days colorless crystals suitable for X-ray analysis were obtained. Yield: 0.110 g (82.21% based on $Cd(OAc)_2.2H_2O$); major decomposition temperature: 213°C. $^{31}P\{^1H\}$ NMR (202 MHz, DMSO-d_6, ppm): δ 31.50. Anal. Calcd. for $C_{32}H_{40}CdO_{10}P_2$ (758.98) C 50.64 H 5.31. Found: C 51.03% H 6.01%. IR(cm^{-1}): 3566(s), 3385(m), 3021(m), 2917(m), 2583(m), 1631(s), 1509(s), 1462(s), 1457(w), 1408(w), 1376(w), 1260(w), 1207(w), 1125(s), 1037(s), 1007(s), 856(w), 829(m), 746(s), 726(s), 616(w), 583(w), 511(s), 473(w), 433(w).

Compound 3.2: To a 15 ml methanolic solution of ligand (L) (0.054 g, 0.179 mmol) and $Cd(OAc)_2.2H_2O$ (0.047 g, 0.179 mmol) triethylamine (0.716 mmol, 0.099 ml) was added dropwise. The reaction mixture was stirred for 24 h at room temperature. The volume of the solvent was reduced under vacuum to about 7 ml, this was filtered to it 0.1 ml of pyridine was added and kept for crystallization at room temperature by slow evaporation. After 2 weeks colorless crystals suitable for X-ray analysis were obtained. Yield: 0.150 g (81.87% based $Cd(OAc)_2.2H_2O$); major decomposition temperature: 208°C. $^{31}P\{^1H\}$ NMR (202 MHz, DMSO-d_6, ppm): δ 31.38. Anal. Calcd. for $C_{52}H_{56}CdN_4O_8P_2$ (1039.34) C 60.09 H 5.43 N 5.39. Found: C 71.20% H 6.91% N 5.52%. IR(cm^{-1}): 3221(m), 3024(w), 2961(m), 2921(m),

2857(w), 2360(m), 1599(s), 1573(w), 1510(s), 1484(w), 1442(s), 1259(s), 1216(s), 1147(s), 1064(s), 1017(s), 858(w), 789(s), 739(w), 698(s), 629(w), 544(s), 500(s), 457(m), 416(m).

Compound 3.3: A mixture of ligand (L) (0.054 g, 0.179 mmol) and $Cd(OAc)_2.2H_2O$ (0.047 g, 0.179 mmol) were taken in 15 ml of distilled methanol. To it 4,4'-bipyridine (0.027 g, 0.179 mmol) was added following triethylamine (0.716 mmol, 0.099 ml) dropwise. The reaction mixture was stirred for 24 h at room temperature. This was filtered and kept for crystallization at room temperature by slow evaporation. After 3 weeks colorless crystals suitable for X-ray analysis were obtained. Yield: 0.120 g (65.75% based on $Cd(OAc)_2.2H_2O$); major decomposition temperature: 233 °C. $^{31}P\{^1H\}$ NMR (202 MHz, DMSO-d_6, ppm): δ 30.87. Anal. Calcd. for $C_{52}H_{52}CdN_4O_8P_2$ (1035.31) C 60.32 H 5.06 N 5.41. Found: C 61.56% H 6.01% N 6.32%. IR(cm^{-1}): 3367(s), 1601(s), 1537(w), 1510(m), 1412(s), 1323(w), 1236(w), 1205(s), 1166(s), 1078(s), 1035(s), 1018(s), 858(w), 811(s), 721(w), 704(w), 625(s), 501(s), 445(w).

Compound 3.4: A mixture of ligand (L) (0.054 g, 0.179 mmol) and $Cd(OAc)_2.2H_2O$ (0.047 g, 0.179 mmol) were taken in 15 ml of distilled methanol. To it 4,4'-azo-pyridine (0.032 g, 0.179 mmol) was added following triethylamine (0.716 mmol, 0.099 ml) dropwise. The reaction mixture was stirred for 24 h at room temperature. This was filtered and kept for crystallization at room temperature by slow evaporation. After 3 weeks colorless crystals suitable for X-ray analysis were obtained. Yield: 0.120 g (73.80% based on $Cd(OAc)_2.2H_2O$); major decomposition temperature: 217°C. $^{31}P\{^1H\}$ NMR (202 MHz, DMSO-d_6, ppm): δ 31.25. Anal. Calcd. for $C_{42}H_{43}CdN_4O_9P_2$ (922.14) C 54.70 H 4.70 N 6.08 Found: C 55.10% H 5.71% N 6.16%. IR(cm^{-1}): 3319(s), 1648(w), 1559(s), 1411(s), 1221(s), 1128(s), 1041(m), 1014(s), 933(w), 836(s), 662(m), 613(m), 567(w), 545(w), 519(m), 489(w), 464(w).

3.2.3 Instrumentation:

Infrared spectra were recorded with a NICOLET iS5 FTIR Spectrometer. Elemental analysis was performed with a Flash EA Series 1112 CHNS analyzer. TGA was recorded with a PerkinElmer STA 8000 thermogravimetric analyzer under a nitrogen gas flow rate of 20 ml/min and a heating rate of 10°C/min. The ^{31}P {H}NMR spectra were recorded in DMSO-d_6 solution on a Bruker spectrometer operating at 202 MHz. **3.1, 3.3** were collected at 298K, and 100K with a Bruker **APEX-II CCD** diffractometer system [λ (Mo Kα) = 0.71073 Å] with a graphite monochromator using the φ-ω scan technique. The data were reduced using the Bruker SAINT package. Absorption correction was performed using the SADABS program. The structures were solved by the direct methods and refined on F^2 by full-matrix least-squares using the

program **SHELXL-2018/3**. The Single crystal X-ray data (SCXRD) data for **3.2, and 3.4** were collected at 105K, and 111K with an XtaLAB Synergy, Single source at offset/far, HyPix3000 diffractometer. Rigaku Oxford HyPix3000 CCD plate detector system [λ (Mo Kα) = 0.71073 Å] with a mirror monochromator. Using **Olex2**[83], the structure was solved with the **ShelXT**[84] structure solution program using Intrinsic Phasing and refined with the **SHELXL-2018/3**[85,86] refinement package using Least Squares minimization. All non-hydrogen atoms were refined anisotropically, hydrogen atoms were fixed at calculated positions and refined as a riding model. Graphics of the crystal structures have been done with Diamond (version 2.1e) and Mercury (version 3.10.3) software. Details of the data have been given in the analytical and spectroscopic data section.

3.3 Results and discussions:

A methanolic solution of a mixture of ligand [Bis-[α-hydroxy(p-methylphenyl)methyl]phosphinic acid] (L), $Zn(OAc)_2.6H_2O$, and an aza-donor ligand gave compounds **3.1-3.4** as described in **Scheme1**. When we varied small aza-donor molecule to long spacer aza-donor group we got two different kinds of coordination polymer two dimensional (2D) and one dimensional (1D). Analysis and characterization of the compounds were carried out by FT-IR and single-crystal X-ray diffraction (SCXRD) techniques.

Infrared Spectroscopy Study:

In the IR spectra of **3.1-3.4,** (Fig.**3.14-3.17**)the characteristic Cd-O-P band appears in the region 1007-1078 cm^{-1}, and O-H stretching of CH_2OH moiety is seen in the region 3221-3385 cm^{-1}. Aromatic C=C and C=N (pyridyl) bands are seen in the region 1408-1601 cm^{-1}. The aromatic and aliphatic C-H stretching and the out-of-plane bending band appear at 2703-3096 cm^{-1} and 662-779 cm^{-1} respectively. The characteristic band of P=O for **3.1**-**3.3** appears in the region 1125–1166cm^{-1} while for compound **3.4** the peak appears at 1128 cm^{-1} due to the PO_2^- asymmetric stretching. In cases **3.1** and **3.4** the presence of H_2O molecule shows O-H stretching frequency at 3566, 3319 cm^{-1} and bending frequency at 1631, 1648 cm^{-1} respectively.

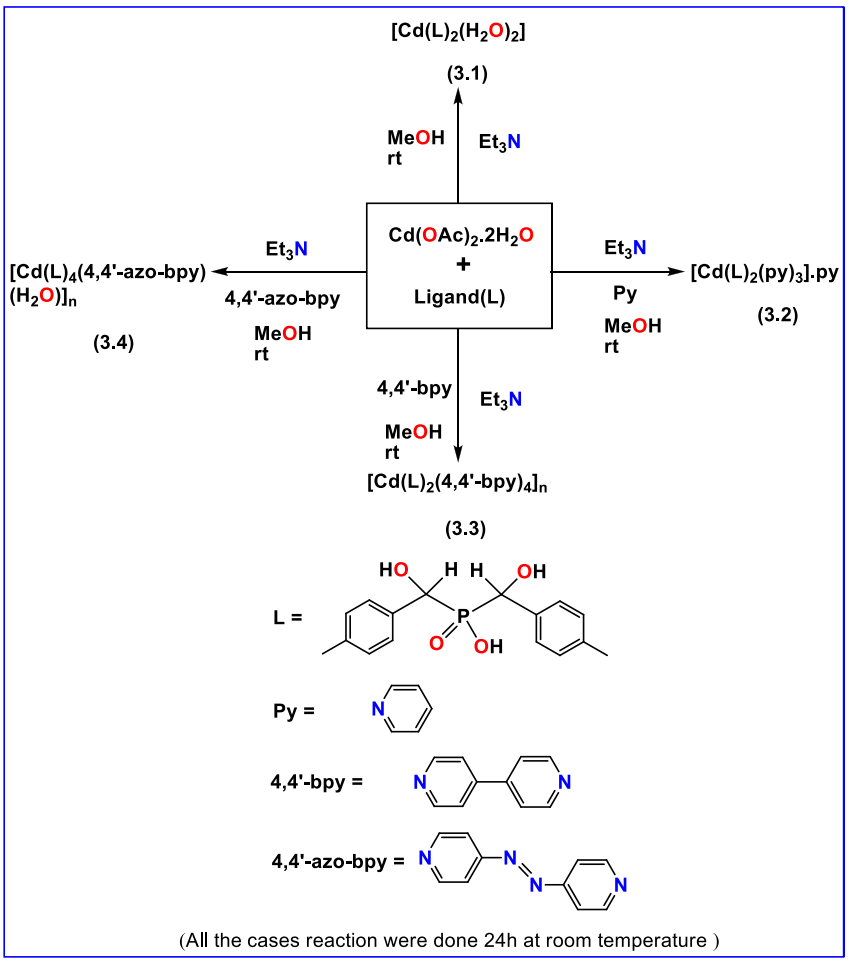

Scheme 1

PXRD and Thermogravimetric Analysis(TGA) and $^{31}P\{H\}$ NMR :

For checking the purity of **3.1-3.4** compounds at room temperature we studied the sample with PXRD (**Figure 3.22-3.25**). The experimental peaks and simulated peaks are well-matched implying the bulk purity of samples. The thermal studies of **3.1-3.4** were examined in a nitrogen atmosphere with thermogravimetric analysis (TGA) in the range of 25-800°C. TGA plots (**Figure 3.1**) show that the major weight loss occurs at 213, 208, 233, and 217°C for **3.1-3.4** respectively. Compound **3.1** shows a 5.33% weight loss due to the two coordinated water molecules in the temperature range of 30-170°C. Weight losses of compound **3.1** takes place up to 800°C. Among these weight losses, the major weight loss due to partial ligand(L) decomposition starts from 170°C to 390°C and is approximately 45.46%(Fig.**3.34**). For compound **3.2** the first two weight loss overlapped partially. Among these two weight losses, the first 15.26% is due to the lattice pyridine and coordinated pyridine molecules in the region 30-175°C. 51.88% weight loss takes place between temperatures of 175-564°C(Fig.**3.35**).

Major weight loss for ligand(L) decomposition takes place with a weight loss of 38.24% at 175-368°C. In the case of compound **3.3,** total weight loss obtained 63.17% up to 30-567°C in the gradual decomposition of 4,4'-bipyridine, Ligand (L), and two-dimensional structural breakdown(Fig.**3.36**). Major weight loss of 53.10% occurs between 30-346°C. For compound **3.4**, 5.42% weight loss due to the surface moisture and coordinated water molecule at 30-140°C region. In the temperature region of 140-556°C, 59.99% total weight loss occurs due to the decomposition of 4,4'-azo-bipyridine, ligand(L), and one-dimensional chain structure collapse. The major weight loss of ca. 33.01% occurs between 140-289°C(Fig.**3.37**). After TGA the residue sample for each case was analyzed by PXRD(Fig.**3.38**). The patterns revealed that all the residual solids are amorphous in nature. $^{31}P\{H\}$ NMR was taken in DMSO-d_6 solution, showing the solution stability of compounds **3.1-3.4.** Only one peak was observed for compounds **3.1-3.4** at 31.50, 31.38, 30.87, and 31.25 ppm respectively (supporting info. Fig.**3.18-3.21**). It indicates the presence of a similar electronic environment around the phosphorus atoms in the complexes.

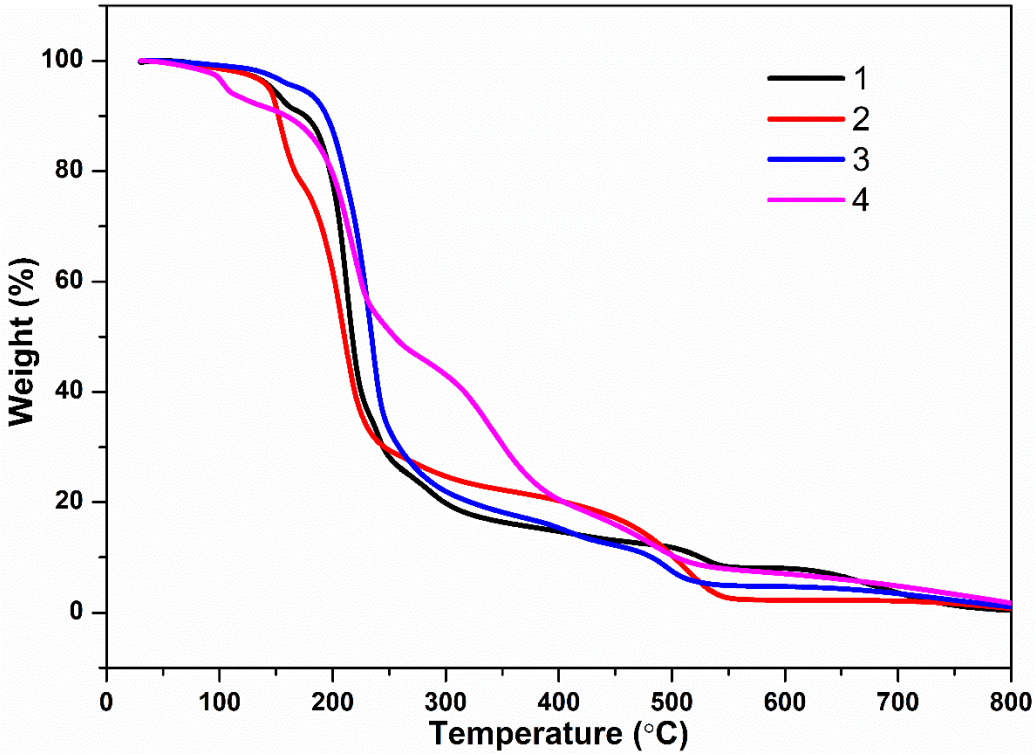

Figure 3.1. TGA curves for compounds **3.1-3.4**

X-ray Crystallographic Study:

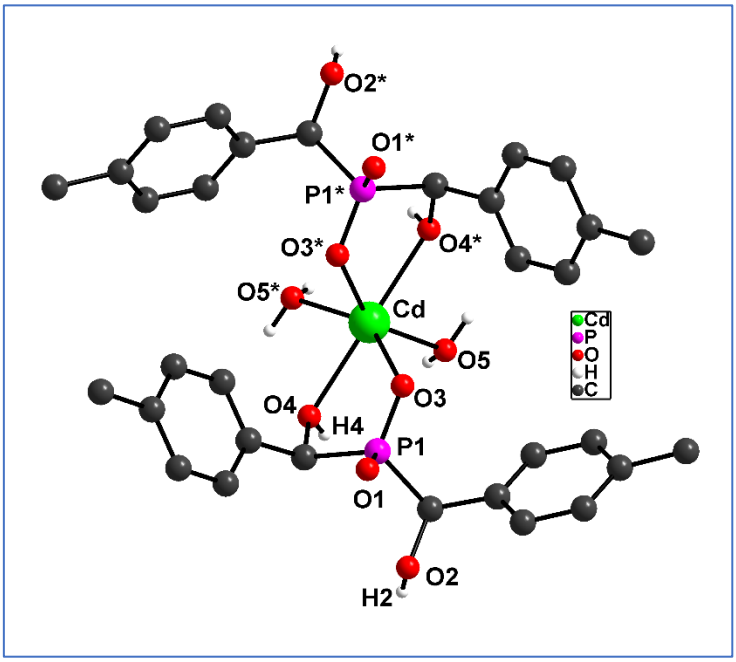

Figure 3.2. Ball and stick view of the molecular structure of **3.1**. Hydrogen atoms are removed for clarity. Key: pink, P; red, O; black, C; white, H; green, Cd.

Structure 1:

Compound **3.1** crystallizes in the monoclinic centrosymmetric C2/c space group and shows a mononuclear complex. There are two Bis-[α-hydroxy(p-methylphenyl)methyl]phosphinic acid ligand(LH_3) in the molecular structure in **Figure 3.2**. In the ligand three labile protons are present, one from the phosphinic acid and another two from the alpha positioned hydroxyl group. In the molecular structure, the central cadmium atom (**Cd**) hexacoordinated with a distorted octahedral geometry confirmed from the bond angles around the cadmium. The octahedral coordination was satisfied with two phosphinic acid oxygen atoms (**O3** and **O3***), two hydroxyl group oxygen atoms (**O4** and **O4***), and two water molecule oxygen (**O5** and **O5***). Here in the ligands, the alpha-positioned hydroxyl group remains protonated. The water molecule present in the structure and the phosphinic acid oxygen remains in a cis manner[O5-Cd-O5* (98.90°) and O3-Cd-O3* (89.0°)] and both the hydroxyl groups are in a trans manner[O4-Cd-O4* (163.50°)]. The bond lengths of Cd-O around the cadmium coordination environment fall in the range of 2.224-2.399 Å.

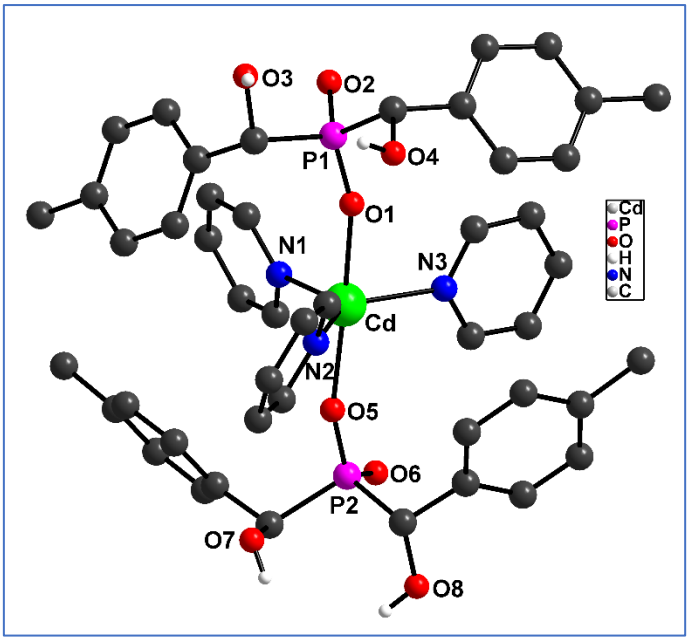

Figure 3.3. Ball and stick view of the molecular structure of **3.2**. Hydrogen atoms are removed for clarity. Key: blue N; pink, P; red, O; black, C; white, H; green, Cd.

Structure 2:

When aza donor pyridine was added to react with Bis-[α-hydroxy(p-methylphenyl)methyl]phosphinic acid ligand and $Cd(OAc)_2.2H_2O$, compound **3.2** was obtained. Compound **3.2** crystallizes in the monoclinic $P2_1/c$ space group and shows a mononuclear complex (**Figure 3.3**). In the complex, the central cadmium atom shows penta-coordinated distorted trigonalbipyramidal (tbp) geometry, where the **Cd** atom is surrounded by three pyridine nitrogen (**N1**, **N2**, **N3**) in the equatorial basal plane and two phosphinic acid oxygen atoms (**O1**, **O5**) axially. To the basal plane bond angles between three pyridine molecules are N1-Cd-N2 (130.60°), N2-Cd-N3 (134.30°), N1-Cd-N3 (94.92°) and the bond angle between the two axial atoms is O1-Cd-O5 (170.80°) reveals the distorted tbp geometry. From the bond lengths around the cadmium atom Cd-N1 (2.290 Å), Cd-N2 (2.306 Å), Cd-N3 (2.315 Å), Cd-O1 (2.226 Å), Cd-O5 (2.211 Å) it observed that the axial bonds are shorter than the equatorial bonds i.e., z-in manner.

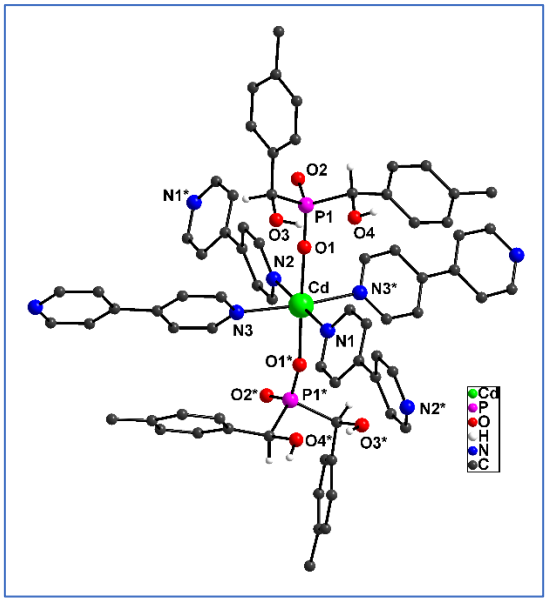

Figure 3.4. Ball and stick view of the molecular structure of **3.3**. Hydrogen atoms are removed for clarity. Key: blue N; pink, P; red, O; black, C; white, H; green, Cd.

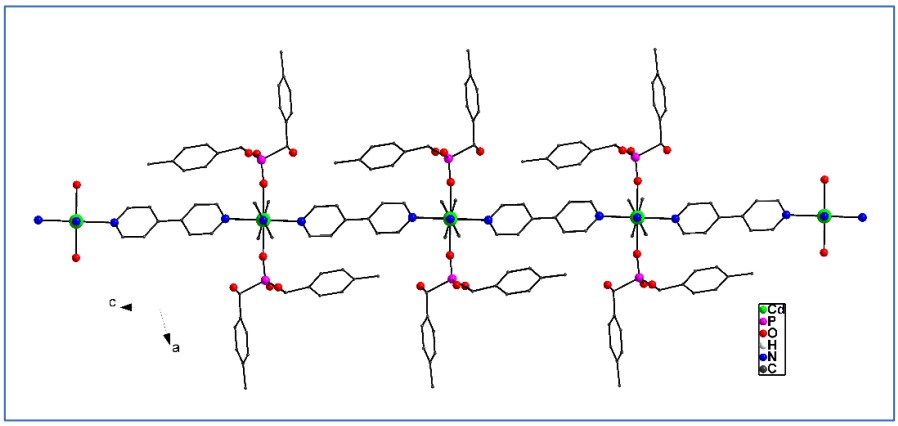

Figure 3.5. 1D infinite chain structure formed by Cd(II), L^{3-}, and bpy along the c-axis. Hydrogen atoms are removed for clarity. Key: blue N; pink, P; red, O; black, C; white, H; green, Cd.

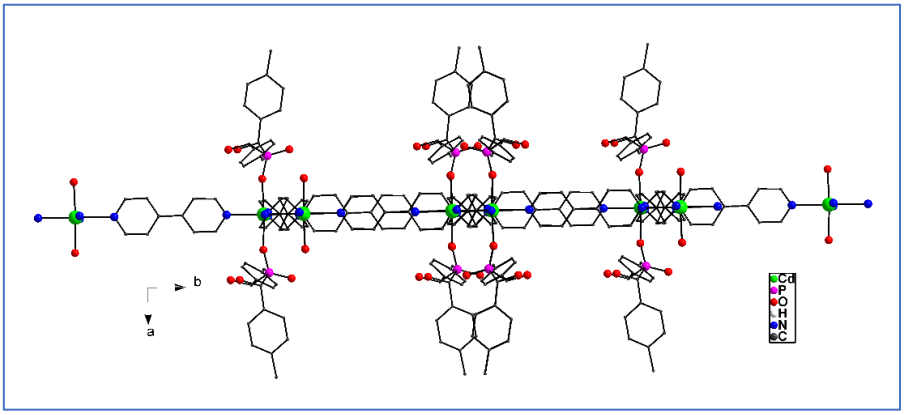

Figure 3.6. Ball and stick view of **3.3** along ab-plane. Hydrogen atoms are removed for clarity. Key: blue N; pink, P; red, O; black, C; white, H; green, Cd.

Structure 3:

Compound **3.3** crystallizes in the monoclinic C2/c space group and has a 2D structure. The coordination environment around the **Cd** atom is embodied by two Ligand (L^-) anions and four bipyridine (bpy) moieties (**Figure 3.4**). Here the **Cd** atom generating a [CdO_2N_4] coordination sphere distorted octahedral geometry. The two ligands (L^-) anions are present in trans to each other with **O1** and **O1*** atom connectivity [O1-Cd-O1(176.40Å)]and four 4,4'-bpy molecules connected with Cd through N atoms (**N1**, **N2**, **N3**, **N3***) in the same basal plane [N3-Cd-N1(96.32 Å), N1-Cd-N3* (96.32 Å), N3*-Cd-N2 (83.68 Å), N2-Cd-N3 (83.68 Å), N1-Cd-N2 (180.00 Å), N3-Cd-N3* (167.30 Å)]. The mononuclear unit is connected through a bidentate 4,4'-bpy ligand to form a 1D chain along the c-axis (**Figure 3.5**). These 1D layers are interconnected with another 1D layer molecule by 4,4'-bpy linker to construct a 2D network along bc-plane (**Figure 3.7**). Bond length around the Cd atom is Cd-N3 (2.345 Å), Cd-N1 (2.354 Å), Cd-N3* (2.345 Å), Cd-N2 (2.441 Å), Cd-O1 (2.235 Å), Cd-O1* (2.235 Å). Along c-axis inter-cadmium distance is 11.71 Å. Along b-axis inter-cadmium distance is 11.87 Å.

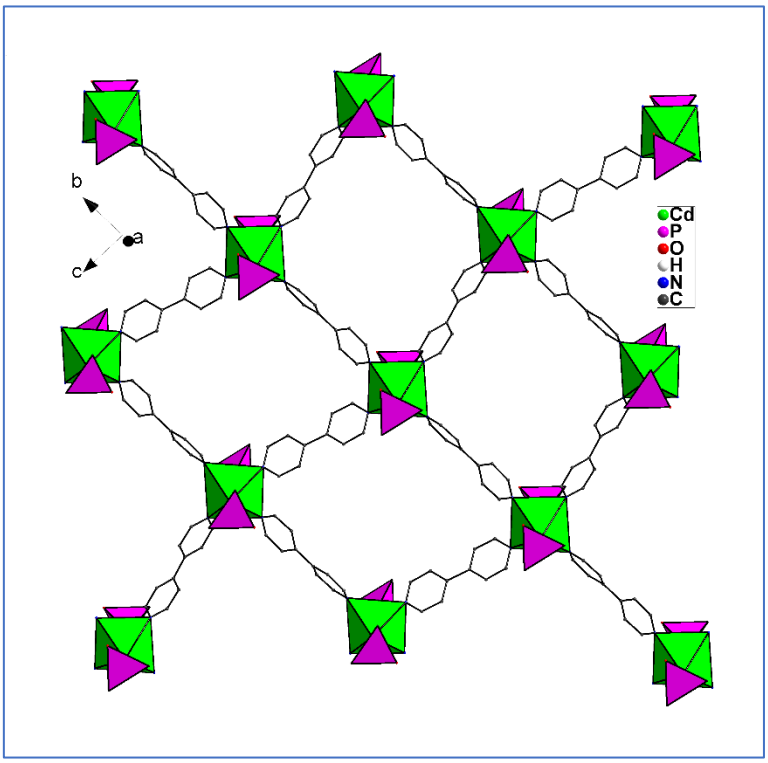

Figure 3.7. 2D structure formed by Cd(II), L^{3-} and bpy along bc-plane. Hydrogen atoms are removed for clarity. Key: blue N; pink, P; red, O; black, C; white, H; green, Cd.

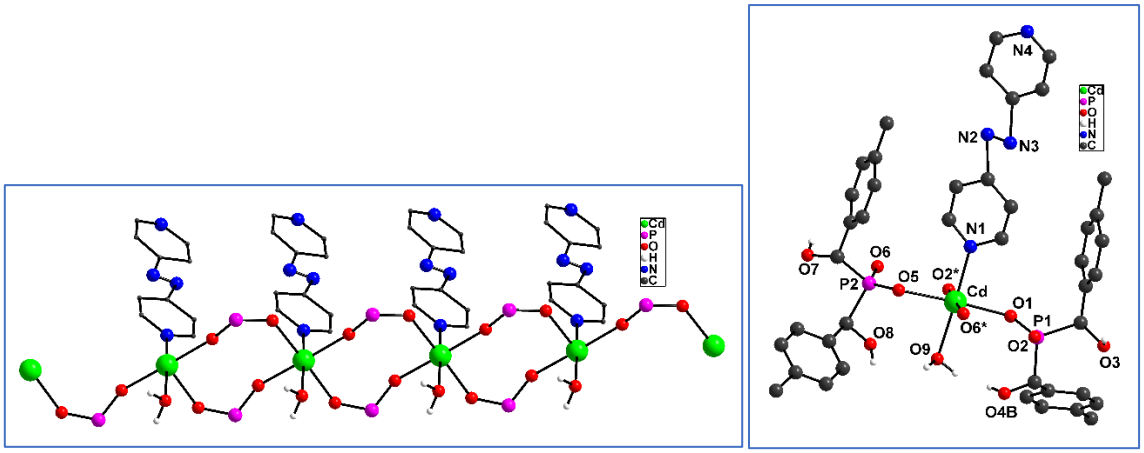

(a) **(b)**

Figure 3.8. (a) 1D structure formed by Cd(II), $L^{3-,}$ and aza-bpy along the b-axis. **(b)** Ball and stick view asymmetric unit of **3.4**. Hydrogen atoms are removed for clarity. Key: blue N; pink, P; red, O; black, C; white, H; green, Cd.

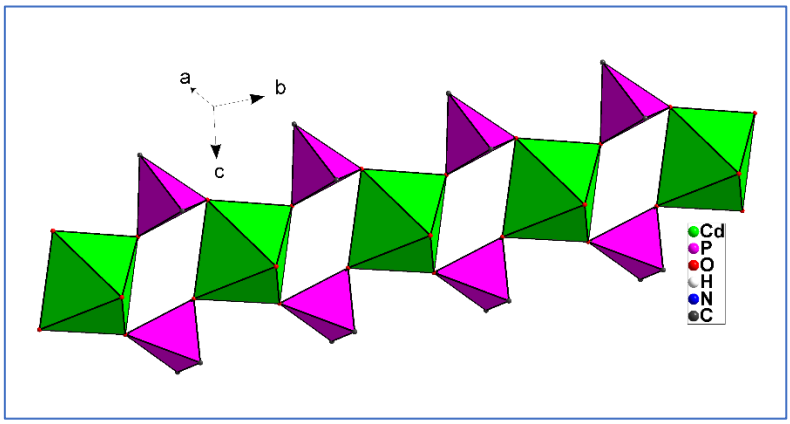

Figure 3.9. 1D infinite chain of **3.4** along the b-axis. Hydrogen atoms are removed for clarity. Key: blue N; pink, P; red, O; black, C; white, H; green, Cd.

Structure 4:

Replacing the 4,4'-bpy with a 4,4'-azo-bipyridine(4,4'-azo-bpy) and keeping all conditions same compound **3.4** was isolated. Compound **3.4** crystallizes in the monoclinic $P2_1$ space group and has a 1D structure. The coordination environment of the **Cd** atom consists of four phosphinic acid oxygen atoms (**O1**, **O5**, **O2***, **O6***), one aza-bpy nitrogen atom (**N1**), and one water molecule oxygen atom (**O9**) in a hexacoordinate distorted octahedral geometry. In the structure, the water molecule and aza-bpy are trans to each other [N1-Cd-O9 (174.4°)]. (**Figure 3.8 (b)**) To the basal plane, two phosphinic acids are bridges between two cadmium atoms constructing a 1D infinite chain structure along the b-axis. (**Figure 3.8 (a)**) The angle between the Cd atom and oxygen atoms in the basal plane is [O5-Cd-O6 (87.82°), O1-Cd-O6 (93.3°), O2-Cd-O5 (91.56°), O1-Cd-O2 (87.34°)]. Bond length around the cadmium atom environment

is Cd-O1 (2.213 Å), Cd-O2 (2.288 Å), Cd-O5 (2.202 Å), Cd-O6 (2.325 Å), Cd-O9 (2.373 Å), Cd-N1 (2.296 Å). The inter-cadmium distance along the b-axis is 10.89 Å.

3.4 Conclusion:

In summary, we have successfully synthesized and characterized cadmium phosphinate compounds .2D-network like coordination polymer and 1D-infinite chain like coordination polymer by varying the aza-donor co-ligand. The aza donor atoms have a crucial role to form these architectures in the presence of the Bis-[α-hydroxy(p-methylphenyl)methyl]phosphinic acid ligand.

3.5 *Analytical and Spectroscopic Data*

Table 3.1. Crystallographic information of compound **3.1-3.4**.

	3.1	3.2	3.3	3.4
Empirical formula	$C_{32}H_{40}CdO_{10}P_2$	$C_{52}H_{56}CdN_4O_8P_2$	$C_{52}H_{52}CdN_4O_8P_2$	$C_{42}H_{43}CdN_4O_9P_2$
Formula weight	758.98	1039.34	1035.31	922.14
Temperature/K	298.4	105(8)	100.15	111(1)
Crystal system	monoclinic	monoclinic	monoclinic	monoclinic
Space group	C2/c	$P2_1/c$	C2/c	$P2_1$
a/Å	22.0196(10)	10.8590(2)	18.8699(14)	16.4002(10)
b/Å	5.4537(2)	17.3061(3)	11.8843(8)	5.4482(5)
c/Å	28.3235(13)	26.6128(5)	22.8914(17)	22.0809(14)
α/°	90	90	90	90
β/°	98.186(3)	98.697(2)	105.234(3)	93.283(6)
γ/°	90	90	90	90
Volume/Å^3	3366.7(3)	4943.76(16)	4953.1(6)	1969.7(3)
Z	4	4	4	2
ρ_{calc}g/cm^3	1.497	1.396	1.388	1.555
μ/mm^{-1}	0.798	0.564	0.563	0.699
F(000)	1560.0	2152.0	2136.0	946.0
Crystal size/mm^3	0.06 × 0.02 × 0.01	0.2 × 0.15 × 0.1	0.2 × 0.1 × 0.03	0.07 × 0.04 × 0.02
Radiation	MoKα (λ = 0.71073)	MoKα (λ = 0.71073)	MoKα (λ = 0.71073)	MoKα (λ = 0.71073)
2Θ range for data collection/°	4.396 to 52.822	3.794 to 54.034	4.092 to 55.004	4.572 to 53.974
Index ranges	$-27 \le h \le 27$, $-6 \le k \le 6$, $-35 \le l \le 35$	$-11 \le h \le 13$, $-21 \le k \le 22$, $-33 \le l \le 33$	$-24 \le h \le 24$, $-15 \le k \le 15$, $-29 \le l \le 29$	$-20 \le h \le 20$, $-6 \le k \le 6$, $-27 \le l \le 27$
Reflections collected	42079	43320	138163	18878
Independent reflections	3442 [R_{int} = 0.0943, R_{sigma} = 0.0357]	10327 [R_{int} = 0.0583, R_{sigma} = 0.0560]	5627 [R_{int} = 0.0495, R_{sigma} = 0.0153]	7206 [R_{int} = 0.1089, R_{sigma} = 0.1310]
Data/restraints/parameters	3442/0/212	10327/0/612	5627/0/305	7206/1/494
Goodness-of-fit on F^2	1.076	1.019	1.284	1.020
Final R indexes [I>=2σ (I)]	R_1 = 0.0335, wR_2 = 0.0631	R_1 = 0.0467, wR_2 = 0.1183	R_1 = 0.0422, wR_2 = 0.1193	R_1 = 0.0889, wR_2 = 0.2082
Final R indexes [all data]	R_1 = 0.0462, wR_2 = 0.0661	R_1 = 0.0583, wR_2 = 0.1240	R_1 = 0.0431, wR_2 = 0.1198	R_1 = 0.1134, wR_2 = 0.2295
Largest diff. peak/hole / e Å^{-3}	0.42/-0.51	2.47/-1.02	1.58/-0.51	2.28/-1.77
Flack parameter				-0.04(5)

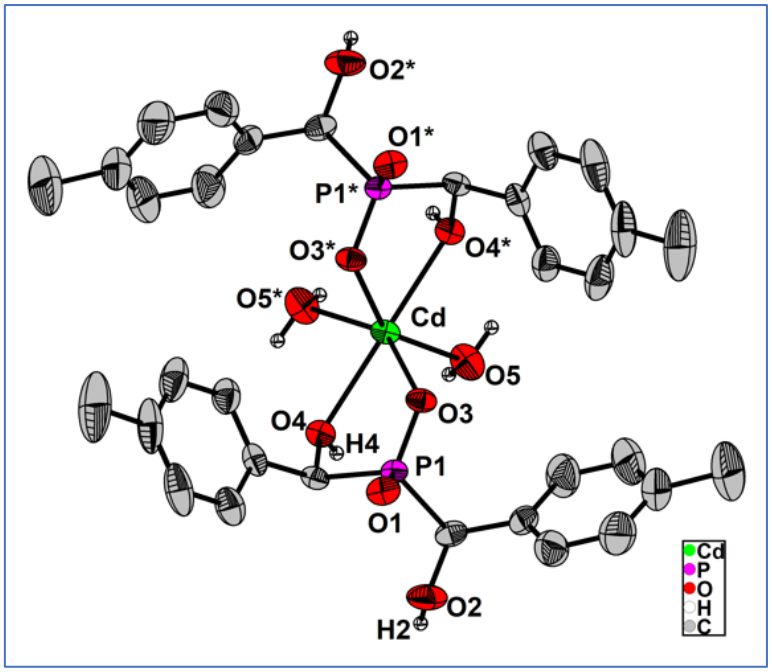

Figure 3.10. ORTEP view of **3.1** with thermal ellipsoids shown at 50%probability

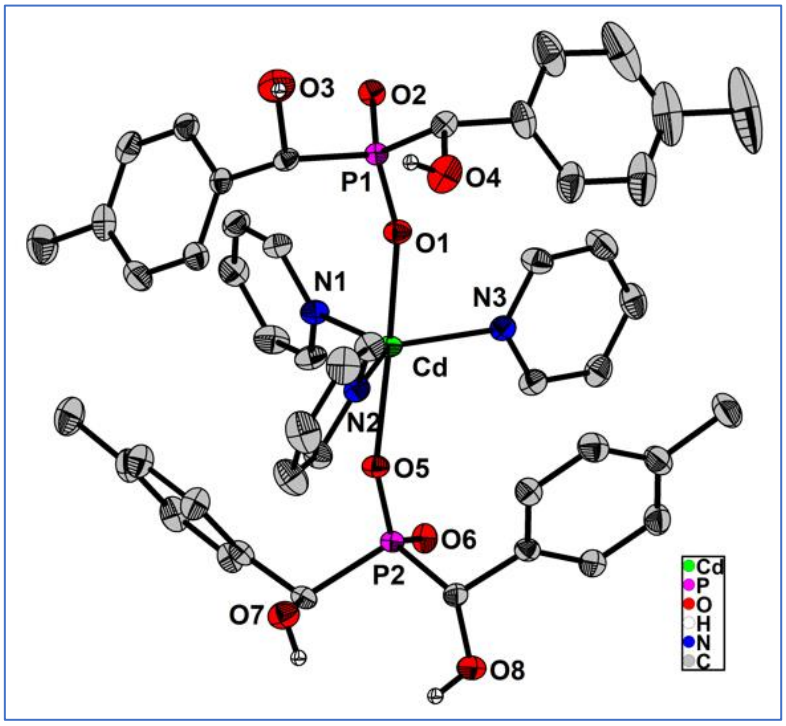

Figure 3.11. ORTEP view of **3.2** with thermal ellipsoids shown at 50%probability

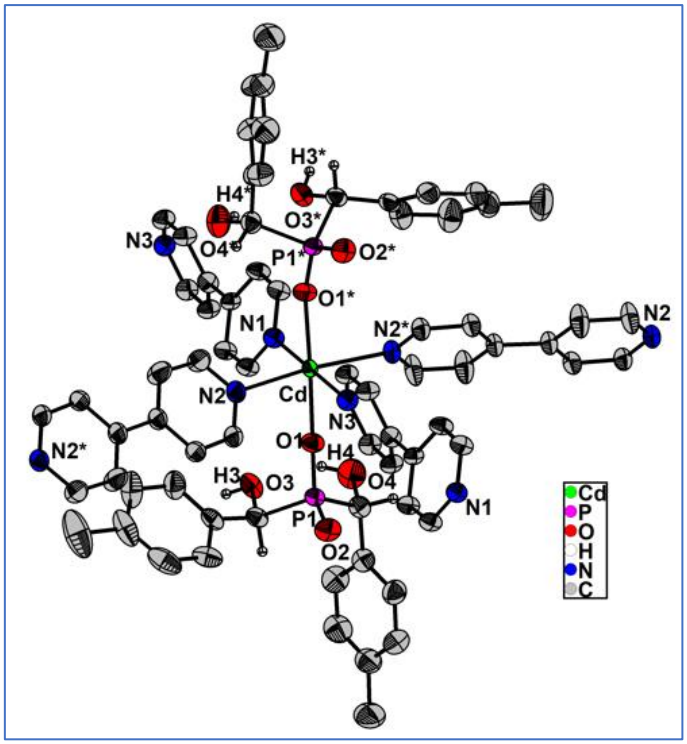

Figure 3.12. ORTEP view of **3.3** with thermal ellipsoids shown at 50%probability

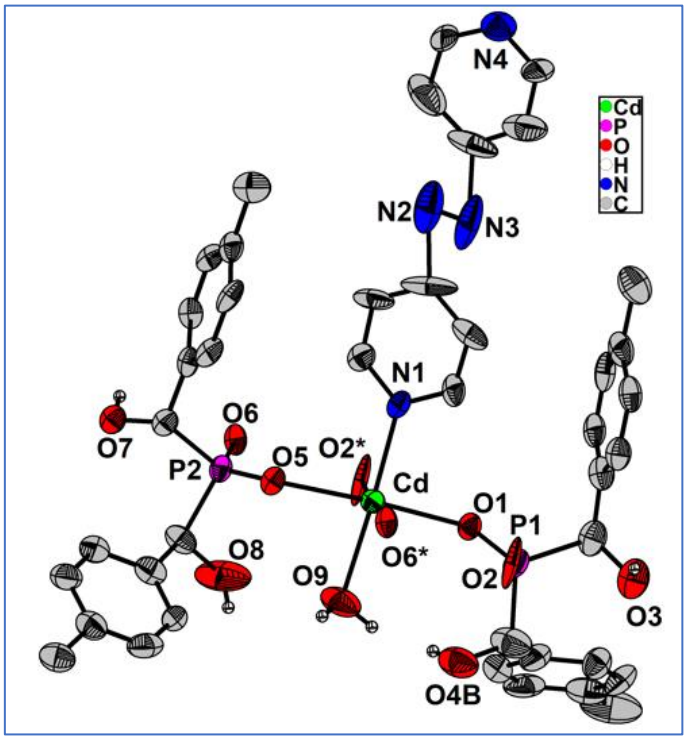

Figure 3.13. ORTEP view of **3.4** with thermal ellipsoids shown at 50%probability

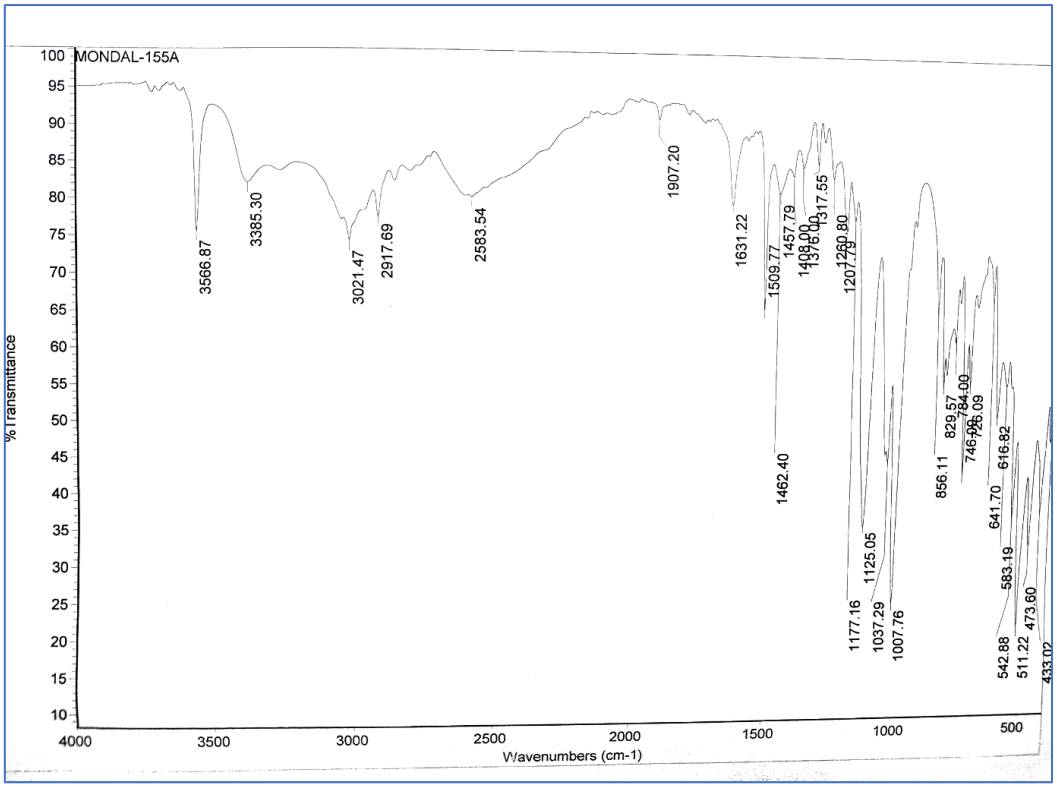

Figure 3.14. IR spectra of compound **3.1.**

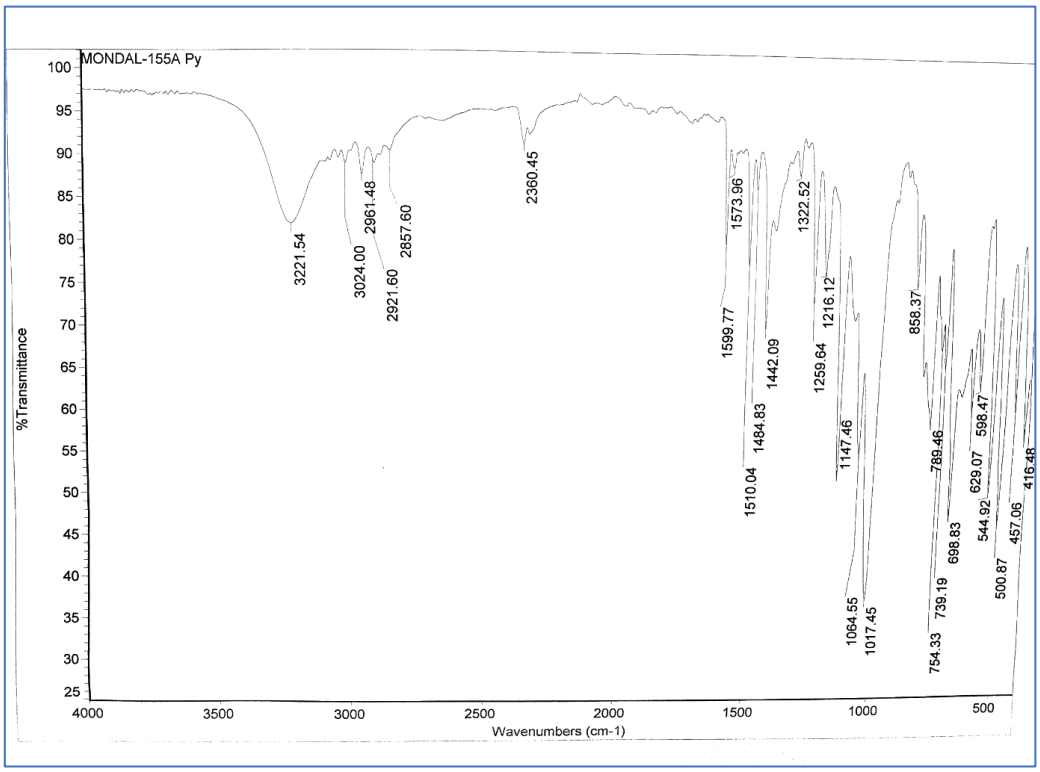

Figure 3.15. IR spectra of compound **3.2.**

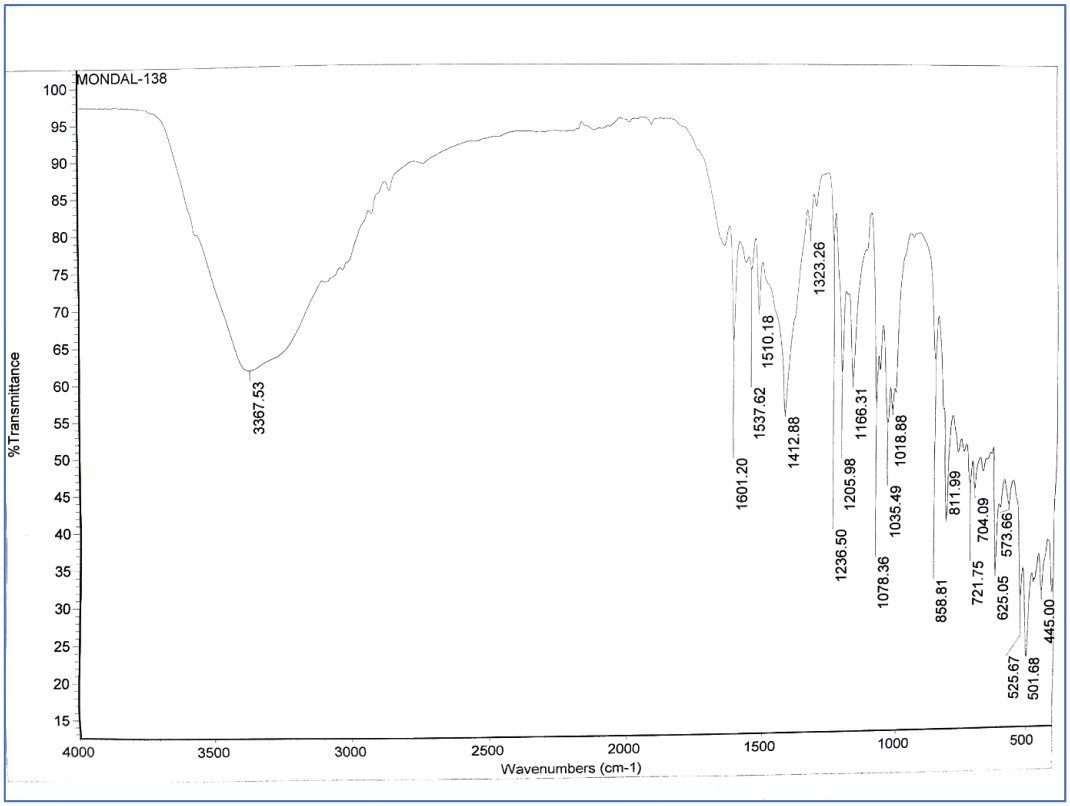

Figure 3.16. IR spectra of compound **3.3.**

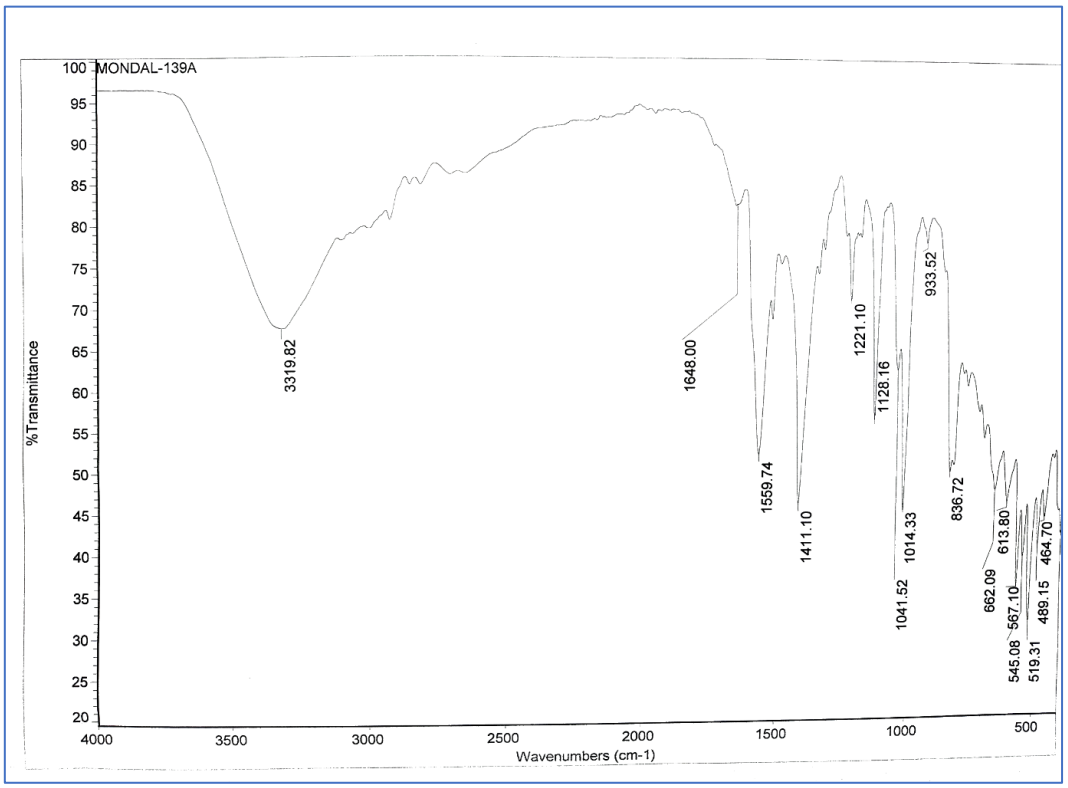

Figure 3.17. IR spectra of compound **3.4.**

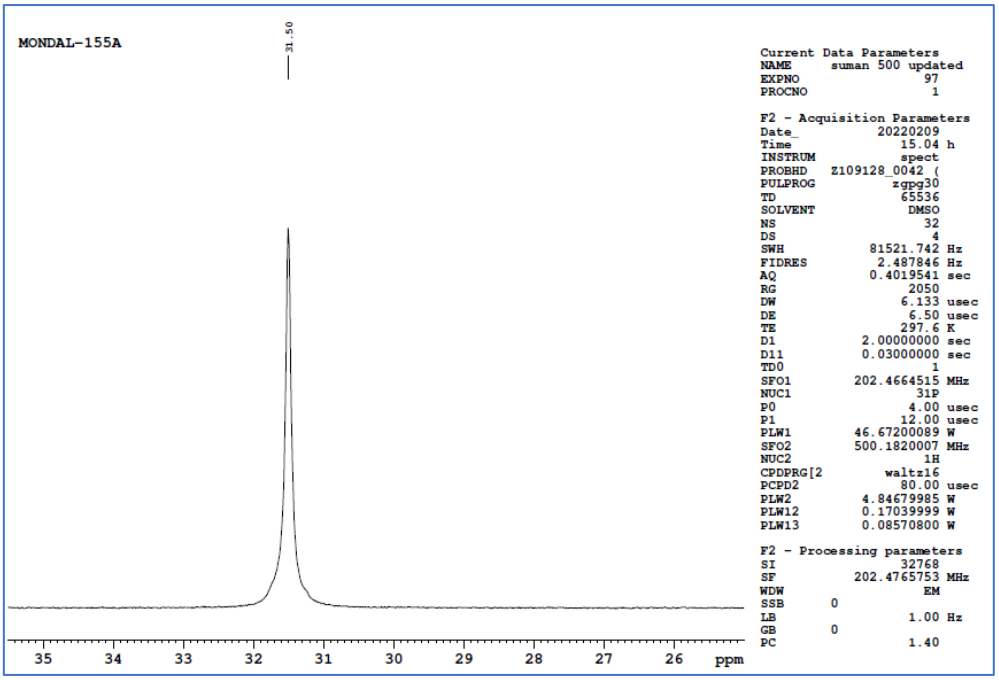

Figure 3.18. $^{31}P\{H\}$ NMR of compound **3.1.**

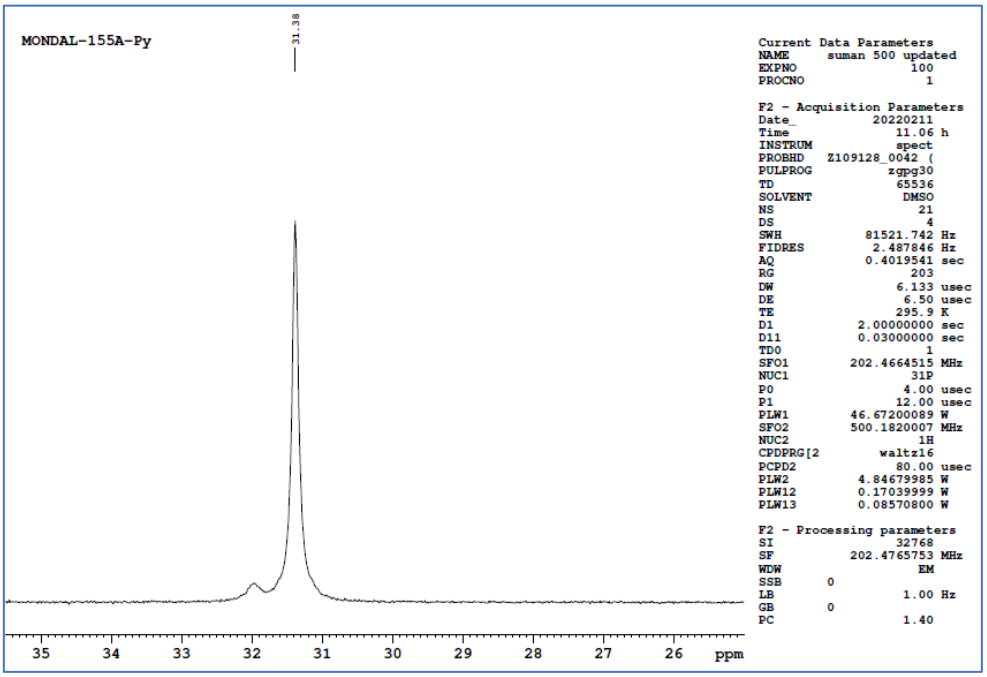

Figure 3.19. $^{31}P\{H\}$ NMR of compound **3.2.**

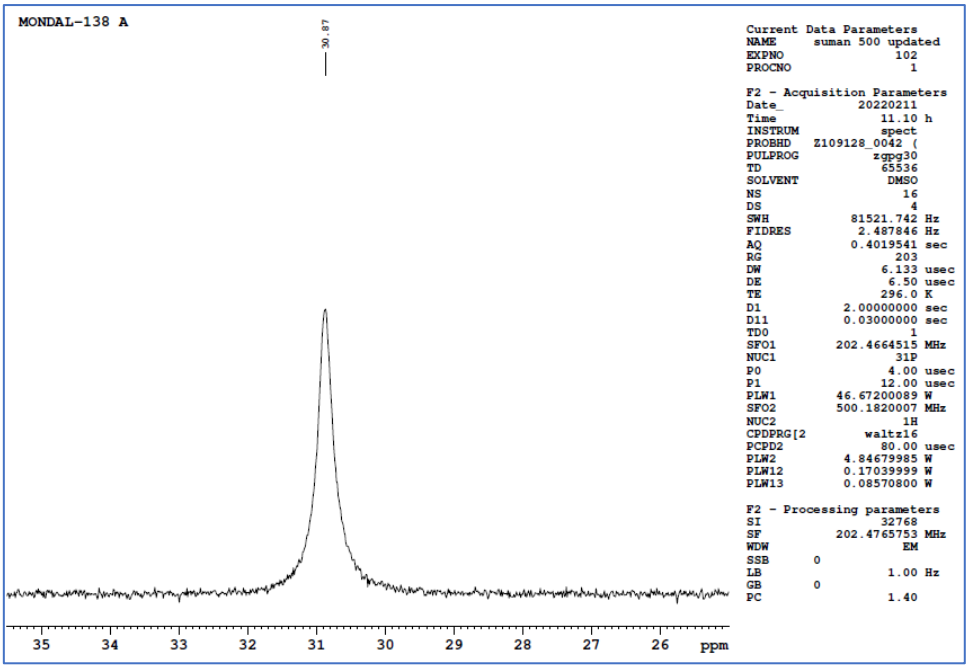

Figure 3.20. $^{31}P\{H\}$ NMR of compound **3.3.**

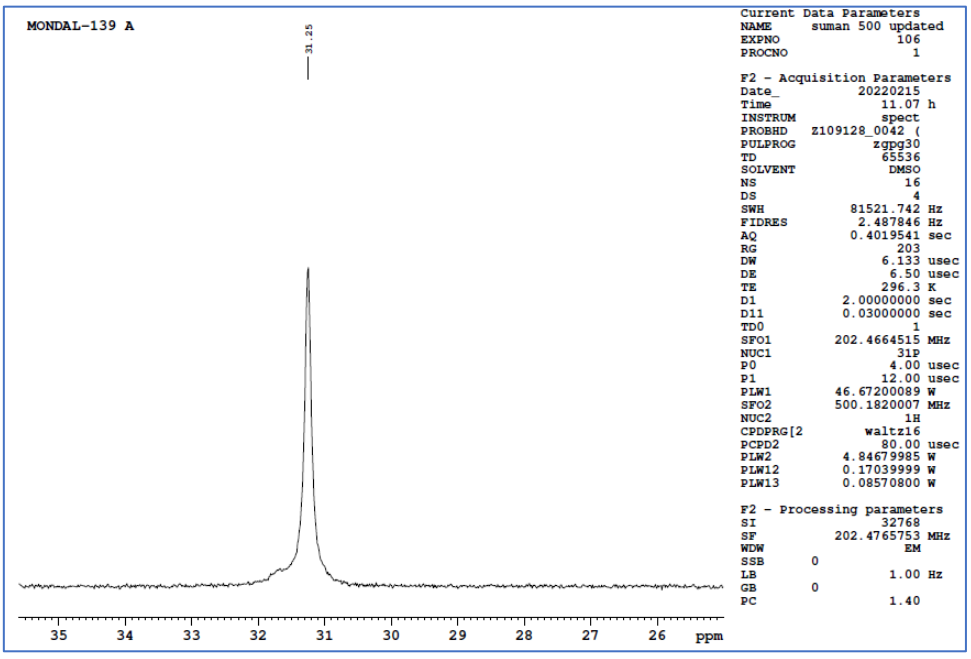

Figure 3.21. $^{31}P\{H\}$ NMR of compound **3.4.**

Table 3.2 and **3.3.** Selected bond lengths (Å) and bond angle (deg) parameters of compound **3.1.**

Cd1-O4	2.3991(19)	Cd1 O3	2.2243(17)
Cd1-O4[1]	2.3990(19)	Cd1 O5	2.2698(19)
Cd1 O3[1]	2.2242(17)	Cd1 O5[1]	2.2698(19)

[1]1-X, +Y,3/2-Z

O4[1] -Cd1-O4	163.52(9)	O3-Cd1-O5	147.42(7)
O3[1] -Cd1-O4[1]	75.23(6)	O3-Cd1-O5[1]	94.86(7)
O3-Cd1-O4[1]	117.35(6)	O5-Cd1-O4[1]	94.84(7)
O3[1]-Cd1-O4	117.35(6)	O5[1] -Cd1-O4	94.83(7)
O3-Cd1-O4	75.23(6)	O5[1] -Cd1-O4[1]	74.30(7)
O3[1] -Cd1-O3	89.00(9)	O5-Cd1-O4	74.29(7)
O3[1] -Cd1-O5	94.86(7)	O5-Cd1-O5[1]	98.90(10)
O3[1] -Cd1-O5[1]	147.42(7)		

[1]1-X, +Y,3/2-Z

Table 3.4 and **3.5.** Selected bond lengths (Å) and bond angle (deg) parameters of compound **3.2.**

Cd1-O5	2.211(2)	Cd1-N2	2.306(3)
Cd1-O1	2.226(2)	Cd1-N3	2.315(3)
Cd1-N1	2.290(3)		

O5-Cd1-O1	170.89(8)	O1-Cd1-N2	86.59(9)
O5-Cd1-N1	89.03(9)	O1-Cd1-N3	90.86(9)
O5-Cd1-N2	84.30(9)	N1-Cd1-N2	130.65(10)
O5-Cd1-N3	95.63(9)	N1-Cd1-N3	94.91(10)
O1-Cd1-N1	96.79(9)	N2-Cd1-N3	134.36(10)

Table 3.6 and **3.7.** Selected bond lengths (Å) and bond angle (deg) parameters of compound **3.3.**

Cd1-O1[1]	2.2412(19)	Cd1-N1	2.446(3)
Cd1-O1	2.2413(19)	Cd1-N2	2.344(2)
Cd1-N3	2.354(3)	Cd1-N2[1]	2.344(2)

[1]2-X, +Y,3/2-Z; [2]+X,1+Y, +Z; [3]2-X,1+Y,3/2-Z; [4]2-X,1-Y,2-Z

O1[1] -Cd1-O1	176.25(9)	O1-Cd1-N2[1]	91.77(8)
O1[1] -Cd1-N3	88.12(5)	N3-Cd1-N1	180.0
O1-Cd1-N3	88.12(5)	N2[1] -Cd1-N3	96.46(6)
O1[1] -Cd1-N1	91.88(5)	N2-Cd1-N3	96.46(6)
O1-Cd1-N1	91.88(5)	N2-Cd1-N1	83.54(6)
O1[1] -Cd1-N2[1]	88.66(8)	N2[1] -Cd1-N1	83.54(6)

O1[1] -Cd1-N2	91.77(8)	N2-Cd1-N2[1]	167.07(12)
O1-Cd1-N2	88.66(8)		

[1]2-X, +Y,3/2-Z; [2]+X,1+Y, +Z; [3]2-X,1+Y,3/2-Z; [4]+X, -1+Y, +Z; [5]2-X,1-Y,2-Z

Table 3.8 and **3.9.** Selected bond lengths (Å) and bond angle (deg) parameters of compound **3.4.**

Cd1-O6[1]	2.325(8)	Cd1-O9	2.368(9)
Cd1-O5	2.201(10)	Cd1-N1	2.306(9)
Cd1-O2[2]	2.294(9)	Cd1-O1	2.211(10)

[1]+X, -1+Y, +Z; [2]+X,1+Y, +Z

O6[1] -Cd1-O9	86.0(5)	O2[2] -Cd1-N1	92.3(4)
O5-Cd1-O6[1]	88.1(3)	N1-Cd1-O6[1]	90.9(4)
O5-Cd1-O2[2]	91.8(3)	N1-Cd1-O9	174.6(5)
O5-Cd1-O9	88.4(6)	O1-Cd1-O6[1]	93.2(3)
O5-Cd1-N1	87.1(5)	O1-Cd1-O2[2]	86.9(3)
O5-Cd1-O1	178.7(3)	O1-Cd1-O9	91.7(6)
O2[2] -Cd1-O6[1]	176.8(3)	O1-Cd1-N1	92.9(5)
O2[2] -Cd1-O9	90.9(5)		

[1]+X,-1+Y,+Z; [2]+X,1+Y,+Z

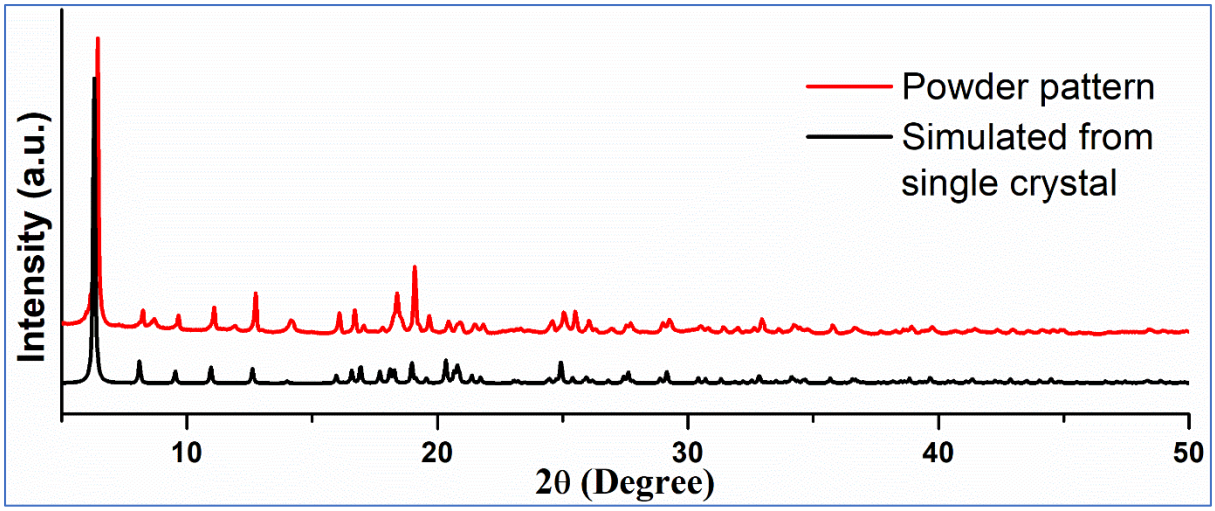

Figure 3.22. Powder X-ray diffraction pattern of a bulk sample of **3.1** compared to the simulated powder pattern extracted from single crystal diffraction data.

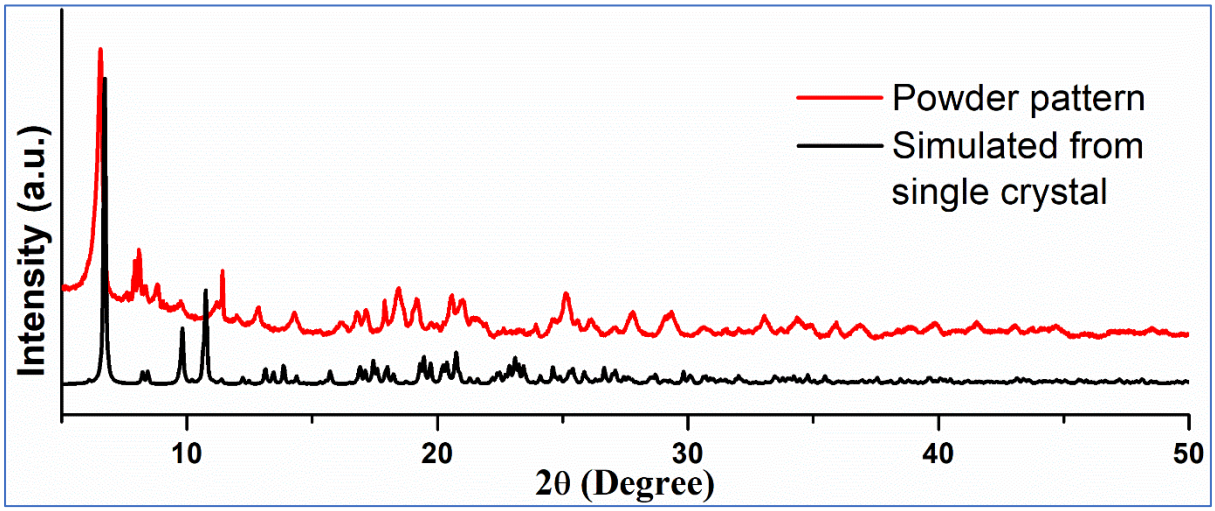

Figure 3.23. Powder X-ray diffraction pattern of a bulk sample of **3.2** compared to the simulated powder pattern extracted from single crystal diffraction data.

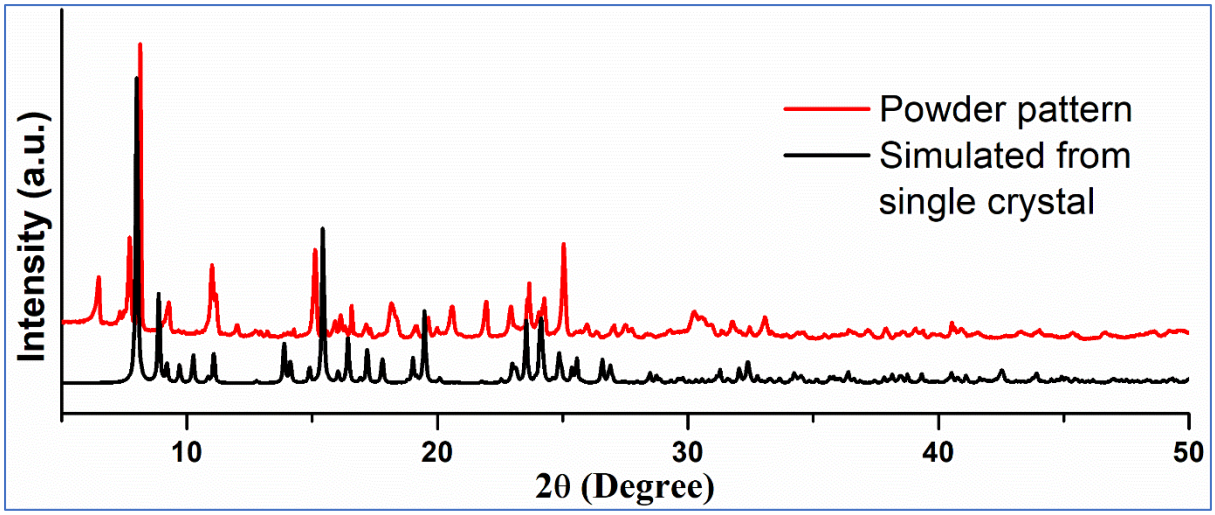

Figure 3.24. Powder X-ray diffraction pattern of a bulk sample of **3.3** compared to the simulated powder pattern extracted from single crystal diffraction data.

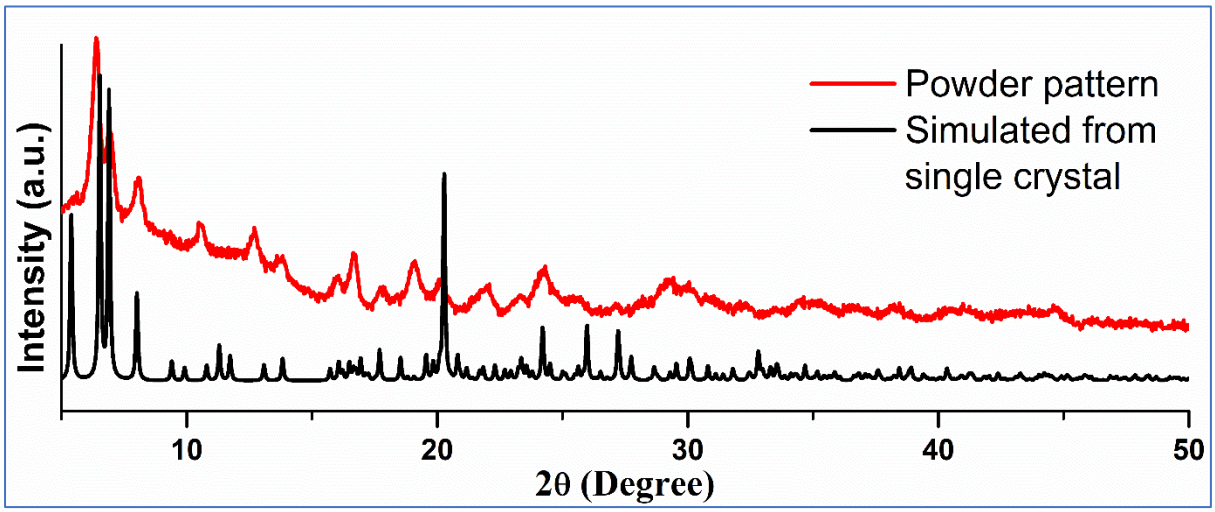

Figure 3.25. Powder X-ray diffraction pattern of a bulk sample of **3.4** compared to the simulated powder pattern extracted from single crystal diffraction data.

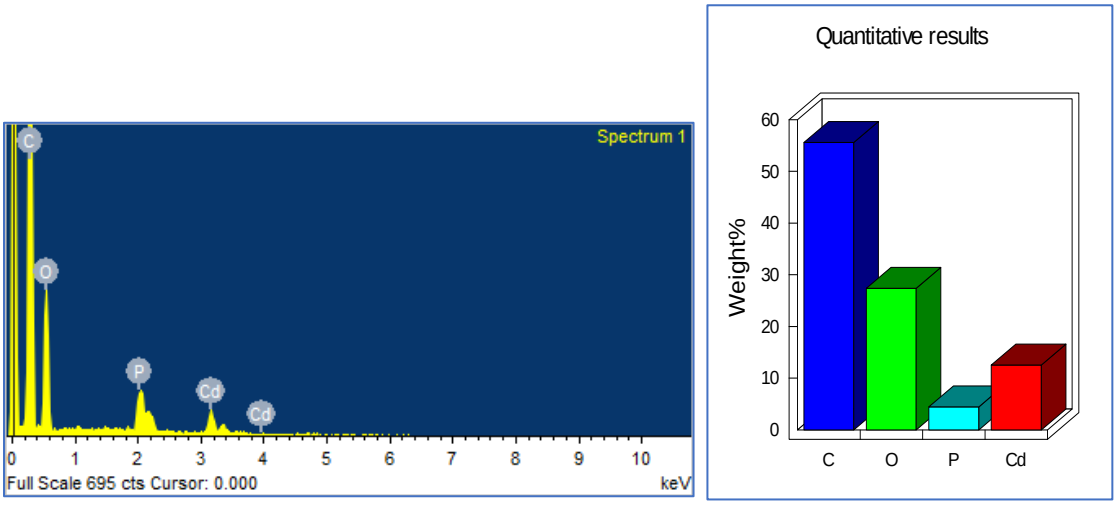

Figure 3.26. EADX spectrum of compound **3.1**

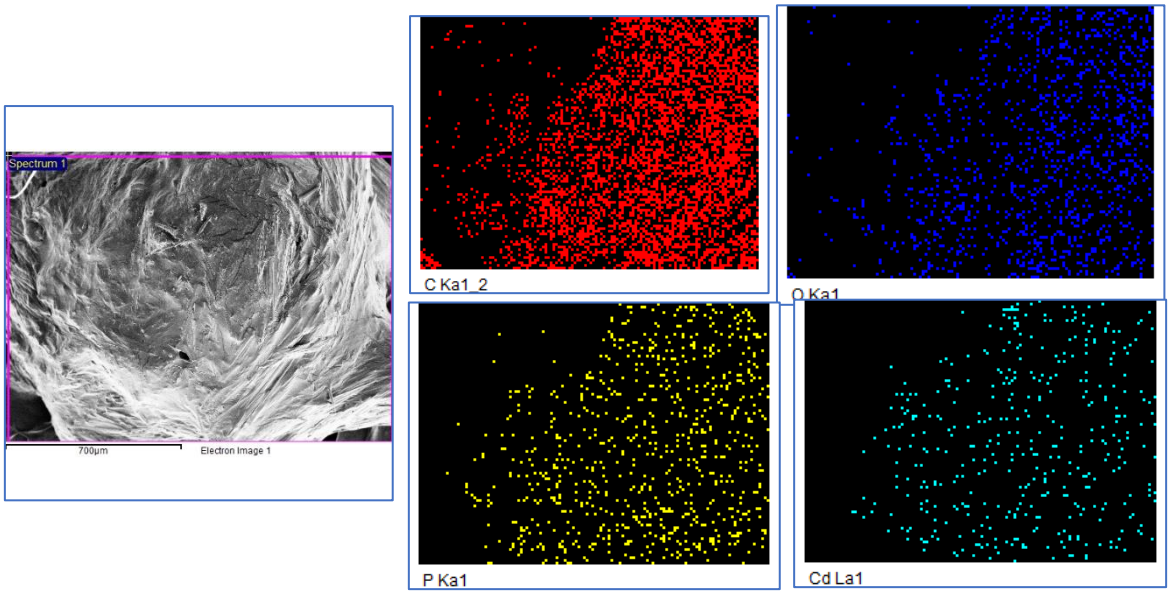

Figure 3.27. Elemental mapping of compound **3.1**

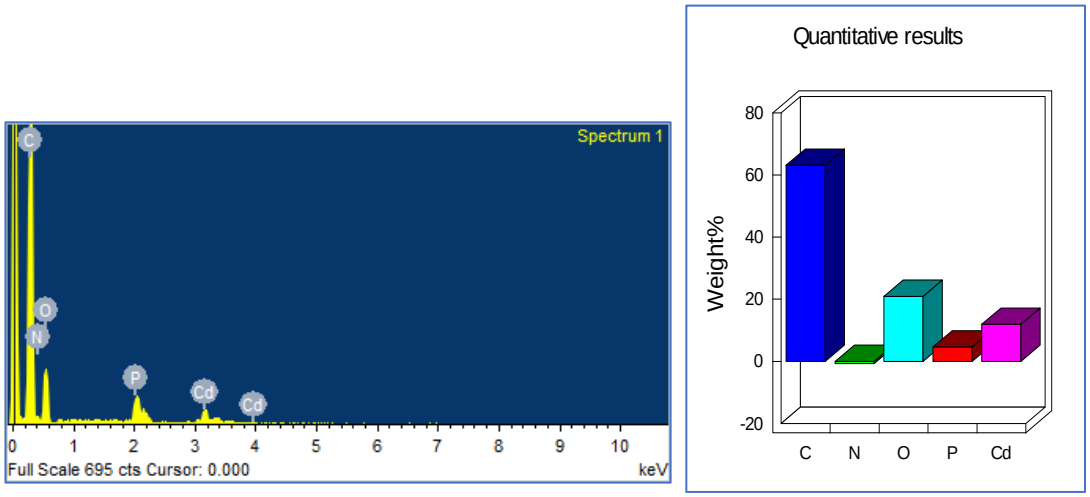

Figure 3.28. EADX spectrum of compound **3.2**

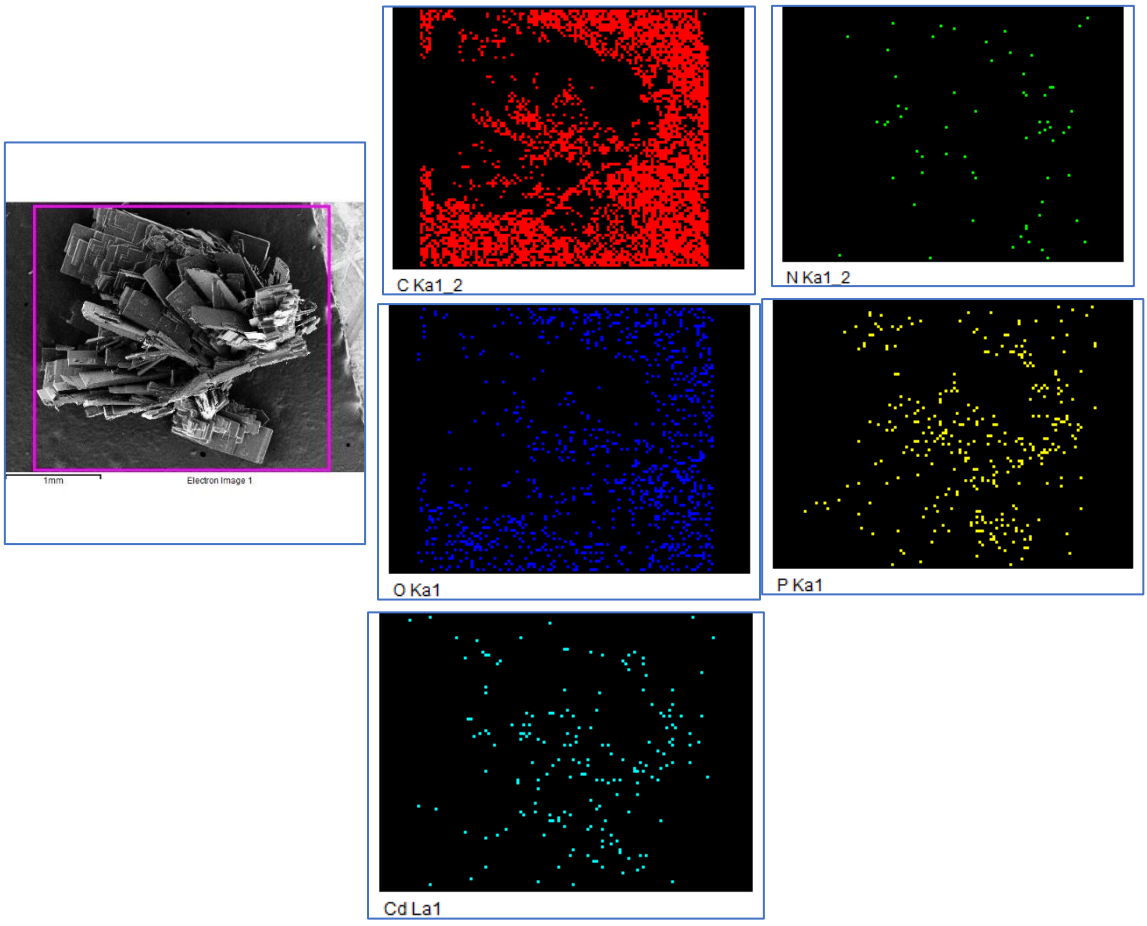

Figure 3.29. Elemental mapping of compound **3.2**

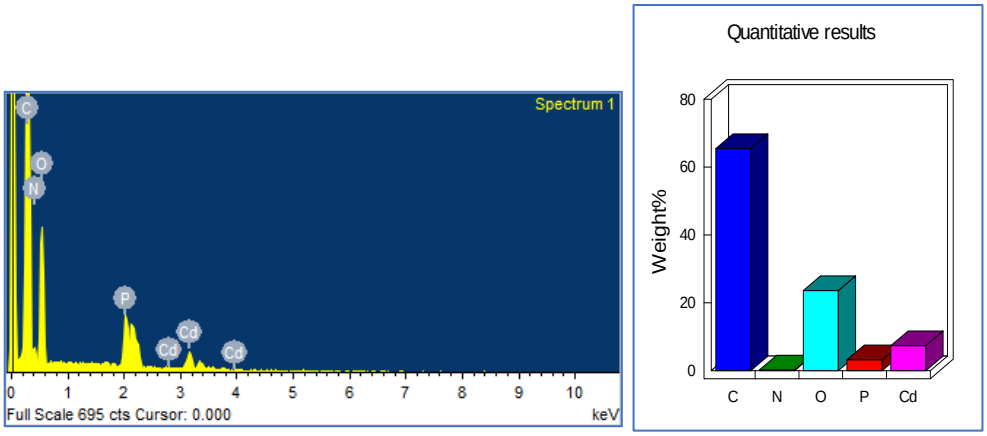

Figure 3.30. EADX spectrum of compound **3.3**

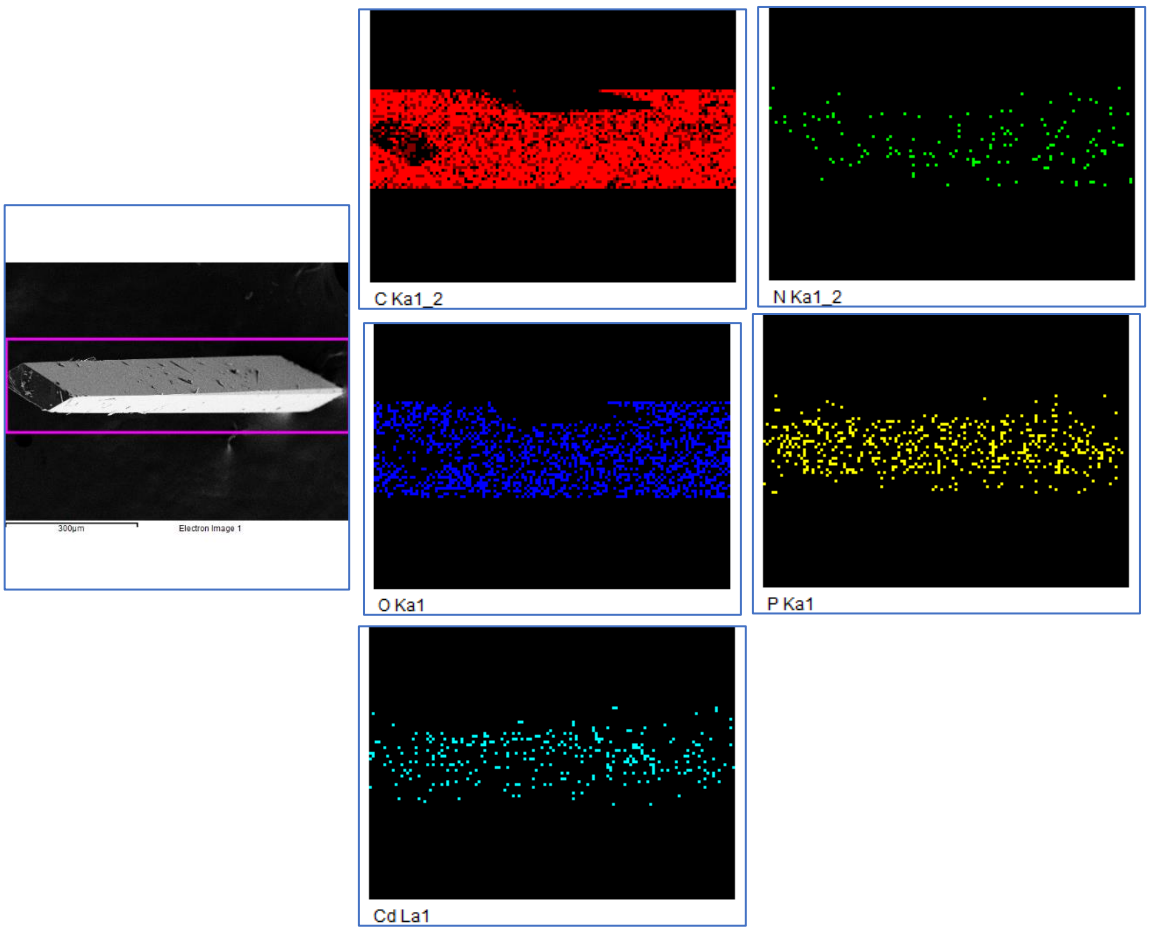

Figure 3.31. Elemental mapping of compound **3.3**

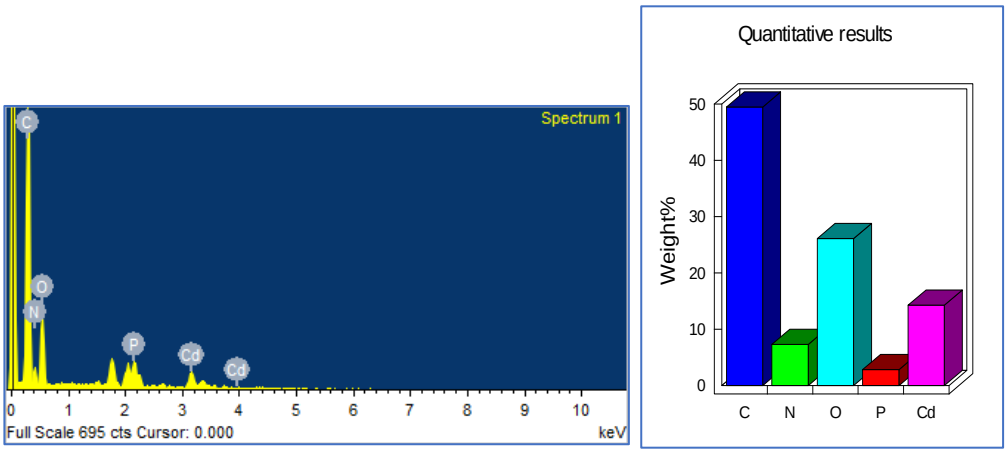

Figure 3.32. EADX spectrum of compound **3.4**

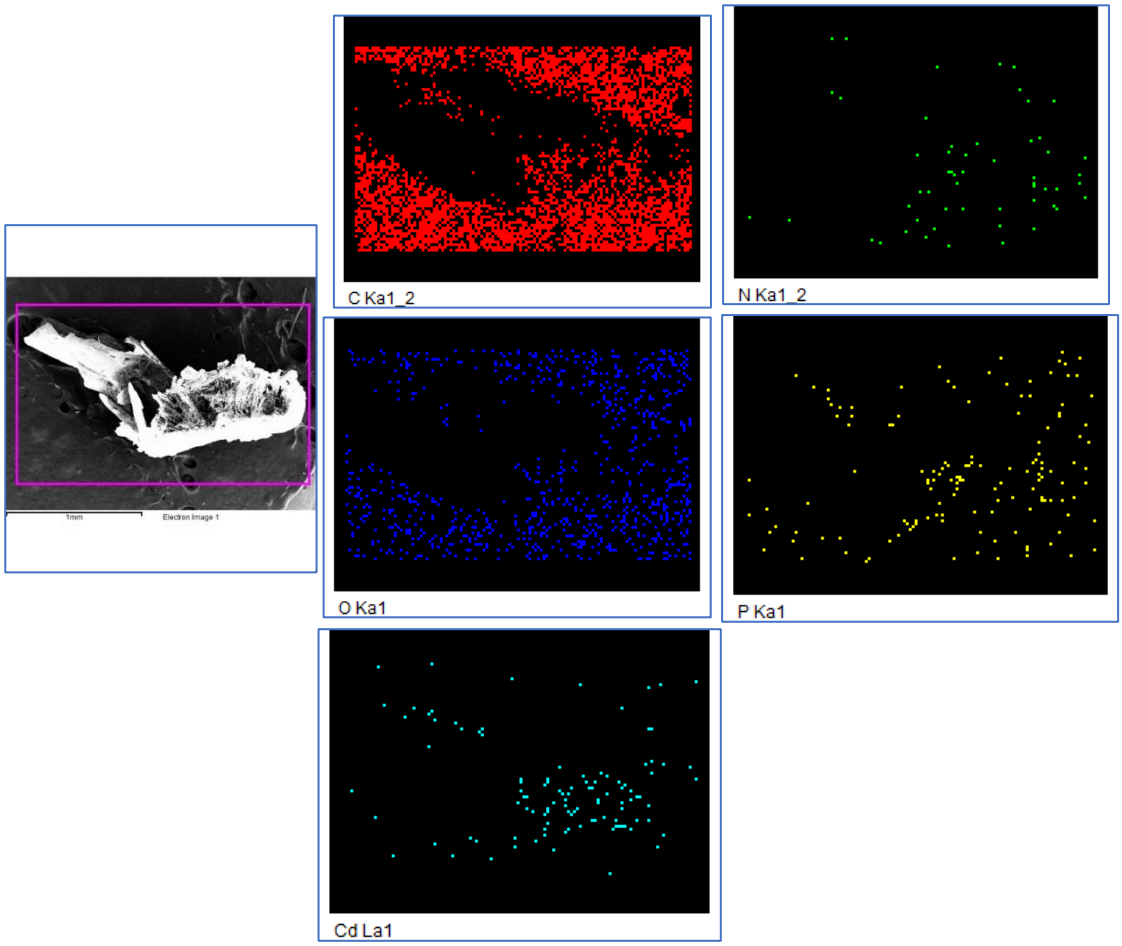

Figure 3.33. Elemental mapping of compound **3.4**

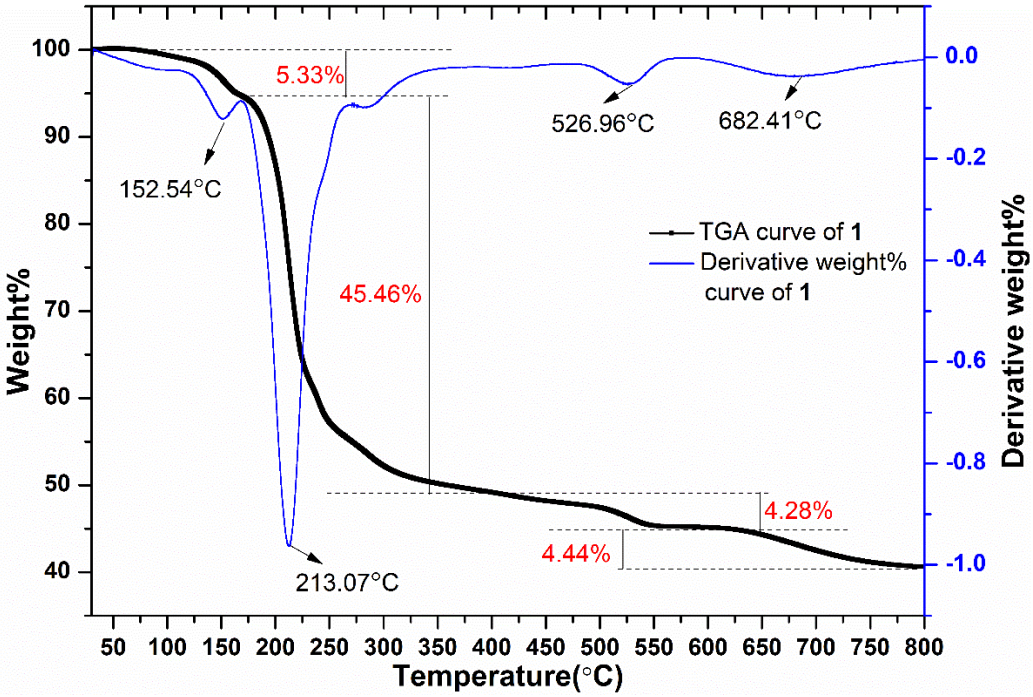

Figure 3.34: TGA curve of compound **3.1.**

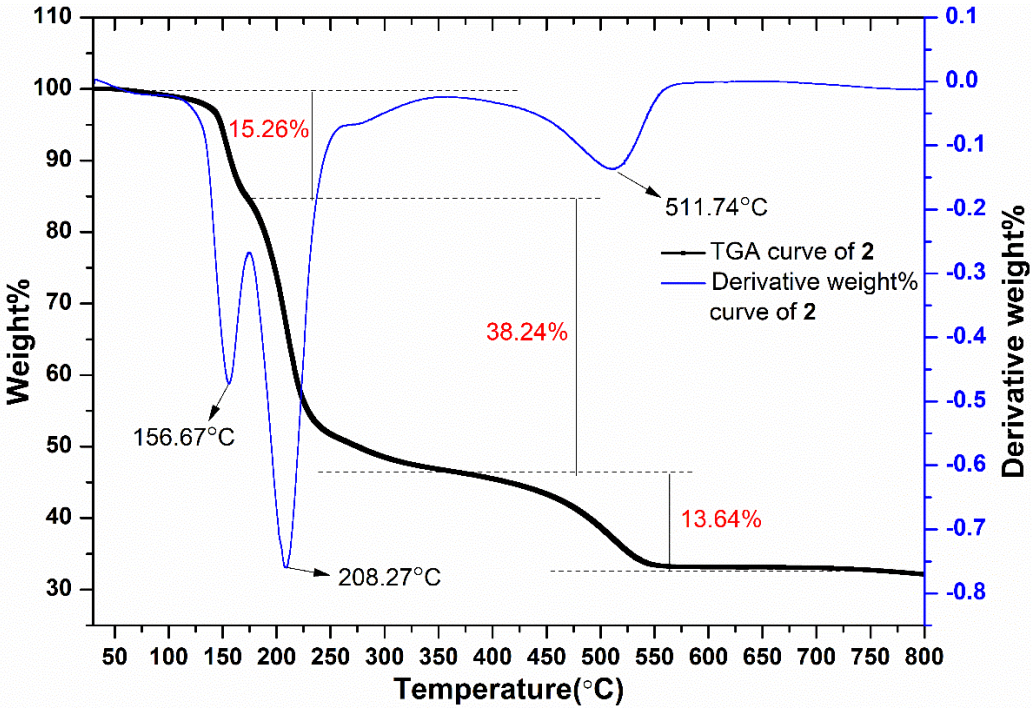

Figure 3.35: TGA curve of compound **3.2.**

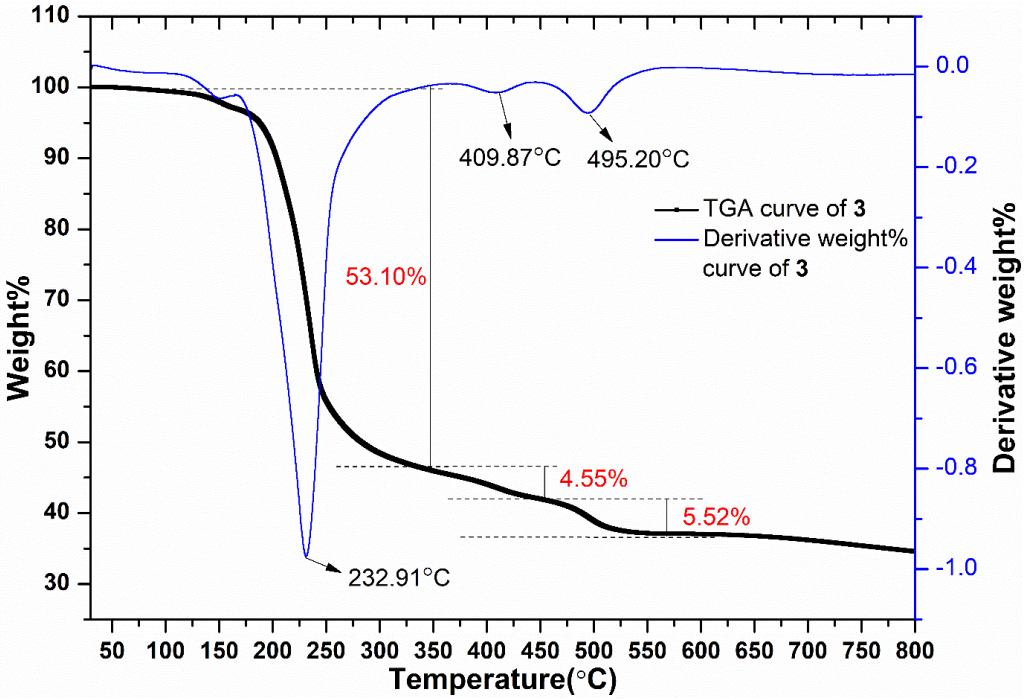

Figure 3.36: TGA curve of compound **3.3.**

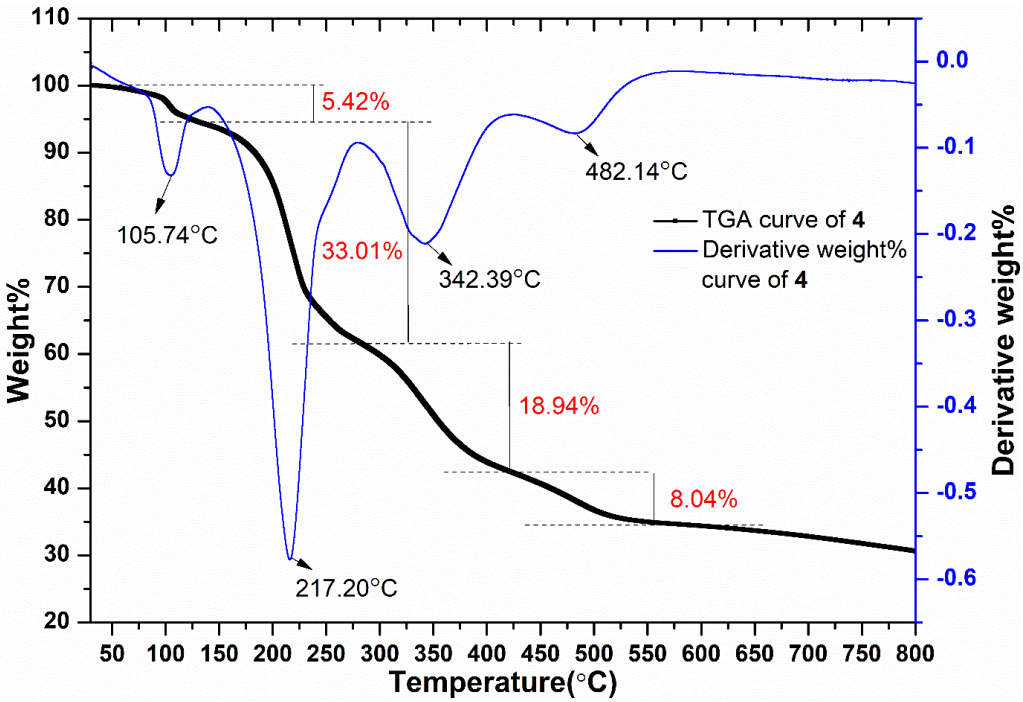

Figure 3.37: TGA curve of compound **3.4.**

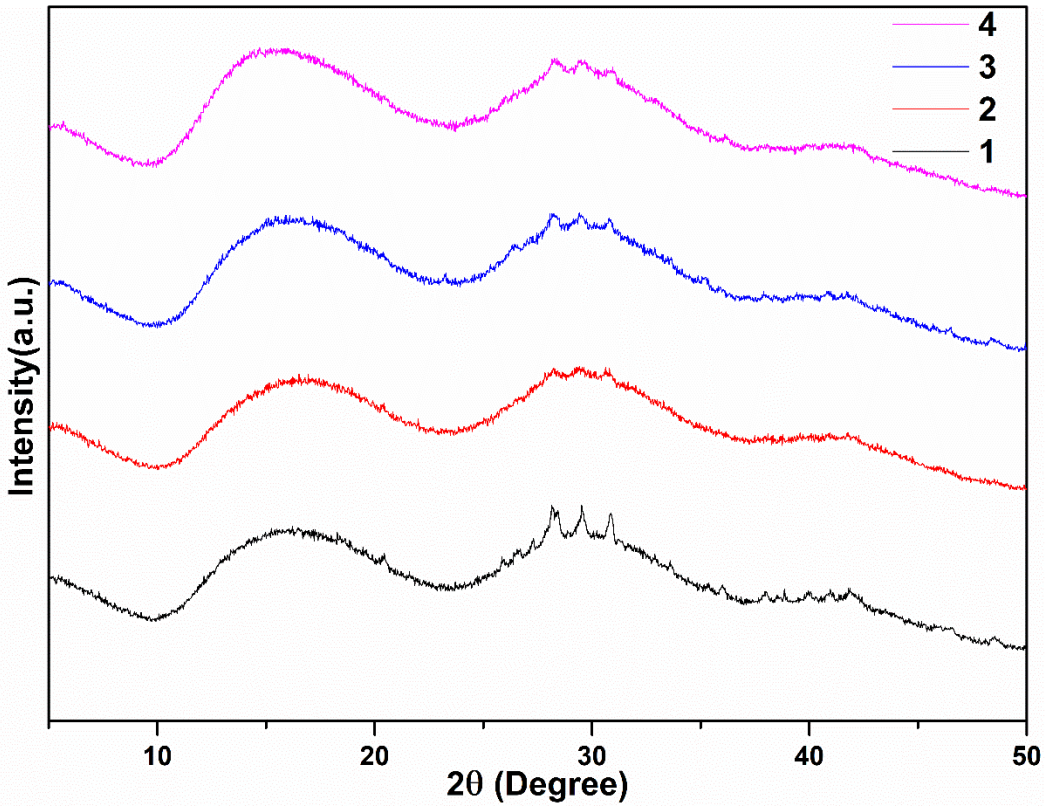

Figure 3.38: PXRD of TGA residue of compound **3.1-3.4.**

S H A P E v2.1 Continuous Shape Measures calculation(Cshm)

(c) 2013 Electronic Structure Group, Universitat de Barcelona

Contact: llunell@ub.edu

Table 3.10-3.11. SHAPE analysis for compounds **3.1-3.4.**

S.No.	Geometry			Cshm value for Cd for 3.1	Cshm value for Cd for 3.3	Cshm value for Cd for 3.4
1	HP-6	1 D6h	Hexagon	33.153	33.010	31.857
2	PPY-6	2 C5v	Pentagonal pyramid	16.716	26.943	28.568
3	**OC-6**	**3 Oh**	**Octahedron**	**6.141**	**0.467**	**0.171**
4	TPR-6	4 D3h	Trigonal prism	6.435	14.569	15.690
5	JPPY-6	5 C5v	Johnson pentagonal pyramid J2	20.261	30.243	31.674

S.No.	Geometry			Cshm value for Cd for 3.2
1	PP-5	1 D5h	Pentagon	26.562
2	vOC-5	2 C4v	Vacant octahedron	5.401
3	**TBPY-5**	**3 D3h**	**Trigonal bipyramid**	**2.177**
4	SPY-5	4 C4v	Spherical square pyramid	4.108
5	JTBPY-5	5 D3h	Johnson trigonal bipyramid J12	5.447

3.6. References:

1 X. Y. Yu, J. Lu, J. H. Yu, X. Zhang, J. Q. Xu and T. G. Wang, *Zeitschrift fur Anorg. und Allg. Chemie*, 2007, **633**, 490–494.

2 Y. Fu, J. Su, Z. Zou, S. Yang, G. Li, F. Liao and J. Lin, *Cryst. Growth Des.*, 2011, **11**, 3529–3535.

3 S. Krause, V. Bon, I. Senkovska, U. Stoeck, D. Wallacher, D. M. Többens, S. Zander, R. S. Pillai, G. Maurin, F. X. Coudert and S. Kaskel, *Nature*, 2016, **532**, 348–352.

4 S. Hasegawa, S. Horike, R. Matsuda, S. Furukawa, K. Mochizuki, Y. Kinoshita and S. Kitagawa, *J. Am. Chem. Soc.*, 2007, **129**, 2607–2614.

5 M. K. Sharma, P. P. Singh and P. K. Bharadwaj, *J. Mol. Catal. A Chem.*, 2011, **342**–**343**, 6–10.

6 Z. H. Li, L. P. Xue, Q. P. Qin, J. Zhang, J. M. Wang, X. Y. Zhang and B. T. Zhao, *J. Solid State Chem.*, 2019, **274**, 81–85.

7 J. W. Shin, J. M. Bae, C. Kim and K. S. Min, *Inorg. Chem.*, 2013, **52**, 2265–2267.

8 J. Pan, D. Zhang, M. M. Shang, Y. Mu, S. De Han and G. M. Wang, *J. Lumin.*, 2019, **210**, 70–74.

9 L. L. Lv, J. Yang, H. M. Zhang, Y. Y. Liu and J. F. Ma, *Inorg. Chem.*, 2015, **54**, 1744–1755.

10 H. Erer, O. Z. Yeşilel and M. Arici, *Cryst. Growth Des.*, 2015, **15**, 3201–3211.

11 H. Y. Wang, Y. Wu, C. F. Leong, D. M. D'Alessandro and J. L. Zuo, *Inorg. Chem.*, 2015, **54**, 10766–10775.

12 T. Gong, X. Yang, Q. Sui, Y. Qi, F. G. Xi and E. Q. Gao, *Inorg. Chem.*, 2016, **55**, 96–103.

13 Q. Liu, X. Liu, C. Shi, Y. Zhang, X. Feng, M. L. Cheng, S. Su and J. Gu, *Dalt. Trans.*, 2015, **44**, 19175–19184.

14 C. Lochenie, K. Schötz, F. Panzer, H. Kurz, B. Maier, F. Puchtler, S. Agarwal, A. Köhler and B. Weber, *J. Am. Chem. Soc.*, 2018, **140**, 700–709.

15 J. Zhang, M. Zhao, W. Xie, J. Jin, F. Xie, X. Song, S. Zhang, J. Wu and Y. Tian, *New J. Chem.*, 2017, **41**, 9152–9158.

16 Z. Hu, W. P. Lustig, J. Zhang, C. Zheng, H. Wang, S. J. Teat, Q. Gong, N. D. Rudd

and J. Li, *J. Am. Chem. Soc.*, 2015, **137**, 16209–16215.

17 L. Pan, M. B. Sander, X. Huang, J. Li, M. Smith, E. Bittner, B. Bockrath and J. K. Johnson, *J. Am. Chem. Soc.*, 2004, **126**, 1308–1309.

18 Z. R. Jiang, J. Ge, Y. X. Zhou, Z. U. Wang, D. Chen, S. H. Yu and H. L. Jiang, *NPG Asia Mater.*, , DOI:10.1038/am.2016.22.

19 J. Duan, W. Jin and R. Krishna, *Inorg. Chem.*, 2015, **54**, 4279–4284.

20 Q. Q. Xiao, G. Y. Dong, Y. H. Li and G. H. Cui, *Inorg. Chem.*, 2019, **58**, 15696–15699.

21 L. Tang, J. Shi, X. Wang, S. Zhang, H. Wu, H. Sun and Z. Jiang, *Nanotechnology*, , DOI:10.1088/1361-6528/aa7379.

22 Q. Jin, W. Zhu, D. Jiang, R. Zhang, C. J. Kutyreff, J. W. Engle, P. Huang, W. Cai, Z. Liu and L. Cheng, *Nanoscale*, 2017, **9**, 12609–12617.

23 L. Li, Q. Chen, Z. Niu, X. Zhou, T. Yang and W. Huang, *J. Mater. Chem. C*, 2016, **4**, 1900–1905.

24 X. Zhou, H. Li, H. Xiao, L. Li, Q. Zhao, T. Yang, J. Zuo and W. Huang, *Dalt. Trans.*, 2013, **42**, 5718–5723.

25 B. Dutta, R. Jana, A. K. Bhanja, P. P. Ray, C. Sinha and M. H. Mir, *Inorg. Chem.*, 2019, **58**, 2686–2694.

26 F. Costantino, A. Ienco, S. Midollini, A. Orlandini, A. Rossin and L. Sorace, *Eur. J. Inorg. Chem.*, 2010, 3179–3184.

27 Z. Li, J., Dun, L., Zeng, F., Li, C. and Su, *Crystals*, 2021, **11**, 1294.

28 Y. M. Dai and M. J. Liu, *Inorg. Nano-Metal Chem.*, 2021, **0**, 1–8.

29 F. Liu, Q. Jia and G. Wang, *ChemistrySelect*, 2021, **6**, 2939–2941.

30 Z. L. Ma, M. C. Wang, J. Y. Shi and L. Tian, *J. Mol. Struct.*, 2021, **1229**, 129804.

31 L. Dun, B. Zhang, J. Wang, H. Wang, X. Chen and C. Li, *Crystals*, 2020, **10**, 1–13.

32 J. P. Vizuet, T. S. Howlett, A. L. Lewis, Z. D. Chroust, G. T. Mccandless and K. J. Balkus, *Inorg. Chem.*, 2019, **58**, 5031–5041.

33 J. Hunger, H. Krautscheid and J. Sieler, *Cryst. Growth Des.*, 2009, **9**, 4613–4625.

34 S. M. Lo, S. S. Chui, L. Shek, Z. Lin, X. X. Zhang, G. Wen and I. D. Williams, *J. Am. Chem. Soc.*, 2000, **122**, 6293–6294.

35 S. Konar, P. S. Mukherjee, E. Zangrando, M. G. B. Drew, C. Diaz, J. Ribas and N. R. Chaudhuri, *Inorganica Chim. Acta*, 2005, **358**, 29–35.

36 J. J. Ryoo, J. W. Shin, H. S. Dho and K. S. Min, *Inorg. Chem.*, 2010, **49**, 7232–7234.

37 J. Ma, A. G. Wong-Foy and A. J. Matzger, *Inorg. Chem.*, 2015, **54**, 4591–4593.

38 J. Carlos Rendón-Balboa, L. Villanueva-Sánchez, L. David Rosales-Vázquez, J. Valdes-García, A. R. Vilchis-Nestor, D. Martínez-Otero, S. Martínez-Vargas and A. Dorazco-González, *Inorganica Chim. Acta*, 2018, **483**, 235–240.

39 A. Tahli, Ü. Köc, R. F. M. Elshaarawy, A. C. Kautz and C. Janiak, *Crystals*, 2016, **6**, 1–10.

40 J. X. Chen, S. X. Liu and E. Q. Gao, *Polyhedron*, 2004, **23**, 1877–1888.

41 G. Liang, Y. Liu, X. Zhang and Z. Wei, *Synth. React. Inorganic, Met. Nano-Metal Chem.*, 2016, **46**, 251–256.

42 A. Karmakar and C. L. Oliver, *Zeitschrift fur Krist.*, 2013, **228**, 330–334.

43 M. Tabatabaee, M. A. Sharif, F. Vakili and S. Saheli, *J. Rare Earths*, 2009, **27**, 356–361.

44 X. Y. Yu, X. B. Cui, X. Zhang, L. Jin, Y. N. Luo, J. J. Yang, H. Zhang and X. Zhao, *Inorg. Chem. Commun.*, 2011, **14**, 848–851.

45 M. Tabatabaee, R. Mohammadinasab and M. Aghaie, *J. Inorg. Organomet. Polym. Mater.*, 2016, **26**, 127–133.

46 M. A. Sharif, M. Tabatabaee, A. Shokrollahi and M. Refahi, *J. Chem. Crystallogr.*, 2015, **45**, 103–113.

47 L. Chu, D.Q., Xu, J.Q., Duan, L.M., Wang, T.G., Tang, A.Q. and Ye, *Eur. J. Inorg. Chem.*, 2001, 1135–1137.

48 D. C. Zhong, W. G. Lu and J. H. Deng, *CrystEngComm*, 2014, **16**, 4633–4640.

49 A. Pal, S. C. Pal, K. Otsubo, D. W. Lim, S. Chand, H. Kitagawa and M. C. Das, *Chem. - A Eur. J.*, 2020, **26**, 4607–4612.

50 V. Luca, J. J. Tejada, D. Vega, G. Arrachart and C. Rey, *Inorg. Chem.*, 2016, **55**, 7928–7943.

51 A. Q. Zhang, N. Liu and Z. H. Liu, *Inorg. Chem. Commun.*, 2015, **60**, 107–110.

52 B. Santra, V. Kumar, P. Kalita, V. Gupta, D. Mandal, A. Chandra, M. Joshi, A. R. Choudhury, A. Jana and V. Chandrasekhar, *Polyhedron*, 2019, **172**, 216–225.

53 E. Fernández-Zapico, I. Da Silva, R. Mendoza-Meroño, J. Montejo-Bernardo, D. Martínez-Blanco, S. García-Granda and J. R. García, *Inorganica Chim. Acta*, 2016, **448**, 78–85.

54 Z. X. Wang, L. F. Wu, H. P. Xiao, X. H. Luo and M. X. Li, *Cryst. Growth Des.*, 2016, **16**, 5184–5193.

55 M. Q. He, Y. Xu, M. X. Li, M. Shao and Z. X. Wang, *Cryst. Growth Des.*, 2019, **19**, 2892–2898.

56 E. Oleshkevich, C. Viñas, I. Romero, D. Choquesillo-Lazarte, M. Haukka and F. Teixidor, *Inorg. Chem.*, 2017, **56**, 5502–5505.

57 K. Gholivand, N. Fallah, A. A. Ebrahimi Valmoozi, A. Gholami, M. Dusek, V. Eigner, M. Pooyan and F. Mohammadpanah, *J. Mol. Struct.*, 2020, **1202**, 127369.

58 A. Guerri, M. Taddei, T. Bataille, S. Moneti, M. E. Boulon, C. Sangregorio, F. Costantino and A. Ienco, *Cryst. Growth Des.*, 2018, **18**, 2234–2242.

59 Z. X. Wang, L. F. Wu, X. Zhang, F. Xing and M. X. Li, *Dalt. Trans.*, 2016, **45**,

19500–19510.

60 E. Oleshkevich, I. Romero, F. Teixidor and C. Viñas, *Dalt. Trans.*, 2018, **47**, 14785–14798.

61 L. Guan, H. F. Sheng and Y. Wang, *Phosphorus, Sulfur Silicon Relat. Elem.*, 2015, **190**, 372–379.

62 W. Yang, D. Wu, C. Liu, Q. J. Pan and Z. M. Sun, *Cryst. Growth Des.*, 2016, **16**, 2011–2018.

63 Z. Hassanzadeh Fard, N. E. Wong, C. D. Malliakas, P. Ramaswamy, J. M. Taylor, K. Otsubo and G. K. H. Shimizu, *Chem. Mater.*, 2018, **30**, 314–318.

64 L. J. Qiu, C. L. Lin, C. Y. Chen, X. Wang and T. H. Yang, *Inorg. Chem. Commun.*, 2020, **119**, 108123.

65 R. K. Metre, S. Kundu, R. S. Narayanan and V. Chandrasekhar, *Phosphorus, Sulfur Silicon Relat. Elem.*, 2015, **190**, 2134–2141.

66 J. Ali, T. Navaneetha and V. Baskar, *Inorg. Chem.*, 2020, **59**, 741–747.

67 J. Rohlíček, D. Bůžek, P. Brázda, L. Kobera, J. Hynek, J. Brus, K. Lang and J. Demel, *Crystals*, 2019, **9**, 1–11.

68 L. Guan and Y. Wang, *J. Solid State Chem.*, 2015, **228**, 9–13.

69 K. Krekić, E. Käkel, D. Klintuch, D. Bloß and R. Pietschnig, *Zeitschrift fur Anorg. und Allg. Chemie*, 2018, **644**, 149–154.

70 L. Guan, Y. Chen and Z. Shi, *Phosphorus, Sulfur Silicon Relat. Elem.*, 2019, **194**, 1126–1133.

71 N. N. Adarsh and P. Dastidar, *Chem. Soc. Rev.*, 2012, **41**, 3039–3060.

72 S. D. Burd, S. Ma, J. A. Perman, B. J. Sikora, R. Q. Snurr, P. K. Thallapally, J. Tian, L. Wojtas and M. J. Zaworotko, *J. Am. Chem. Soc.*, 2012, **134**, 3663–3666.

73 F. Y. Ju and S. Li, *Russ. J. Gen. Chem.*, 2020, **90**, 1083–1087.

74 S. H. Li and Y. Zhao, *Inorg. Nano-Metal Chem.*, 2017, **47**, 256–259.

75 K. Das, A. Datta, C. Massera and C. Sinha, *J. Mol. Struct.*, 2019, **1179**, 618–622.

76 J. Tan, M. Pan, S. Li and X. Yang, *Inorg. Chem. Commun.*, 2018, **87**, 36–39.

77 R. X. Yuan, R. G. Xiong, Y. L. Xie, X. Z. You, S. M. Peng and G. H. Lee, *Inorg. Chem. Commun.*, 2001, **4**, 384–387.

78 K. Dungkaew, W., Jiajaroen, S., Theppitak, C., Sertphon, D. and Chainok, *JCST*, 2019, **9**, 29–39.

79 M. Ballesteros-Rivas, A. Ota, E. Reinheimer, A. Prosvirin, J. Valdés-Martinez and K. R. Dunbar, *Angew. Chemie*, 2011, **123**, 9877–9881.

80 J. H. Lim, J. H. Yoon, H. C. Kim and C. S. Hong, *Angew. Chemie - Int. Ed.*, 2006, **45**, 7424–7426.

81 B. Kaboudin and N. As-Habei, *Tetrahedron Lett.*, 2004, **45**, 9099–9101.

82 B. Kaboudin and H. Haghighat, *J. Org. Chem.*, 2006, **71**, 6604–6606.

83 O. V. Dolomanov, L. J. Bourhis, R. J. Gildea, J. A. K. Howard and H. Puschmann, *J. Appl. Crystallogr.*, 2009, **42**, 339–341.

84 G. M. Sheldrick, *Acta Crystallogr. Sect. C Struct. Chem.*, 2015, **71**, 3–8.

85 L. J. Bourhis, O. V. Dolomanov, R. J. Gildea, J. A. K. Howard and H. Puschmann, *Acta Crystallogr. Sect. A Found. Crystallogr.*, 2015, **71**, 59–75.

86 G. M. Sheldrick, *Acta Crystallogr. Sect. A Found. Crystallogr.*, 2015, **71**, 3–8.

Synthesis and Characterization of Paddlewheel dinuclear and trinuclear lanthanide phosphinate clusters.

CHAPTER

4

A series of isostructural dinuclear and trinuclear paddlewheel Ln(III) clusters have been synthesized in reaction with chiral phosphinic acid ligand [(Bis-[α-hydroxy(p-methylphenyl)methyl]phosphinic acid] and [Bis-[α-hydroxy(p-bromophenyl)methyl]phosphinic acid] {(R^1_2/$R^2_2PO_2H$)[R^1= CH(OH)PhMe], [R^2= CH(OH)PhBr]}. The complexes represented as [$Ln_2(\mu_2\text{-}\eta^1\text{:}\eta^1$ PO_2 $R^1_2)_3(NO_3)_6](HNEt_3)_3$ where Ln= Dy(**4.1**), Ho(**4.2**), Nd(**4.3**), Y(**4.4**) and [$Ln_3(\mu_2\text{-}\eta^1\text{:}\eta^1$ PO_2 $R^2_2)_6(NO_3)_6](HNEt_3)_3$ where Ln= Nd(**4.5**), Pr(**4.6**), Dy(**4.7**), $NdLa_2$(**4.8**), characterized by SCXRD. Synthesis, structural interpretation are discussed in this chapter.

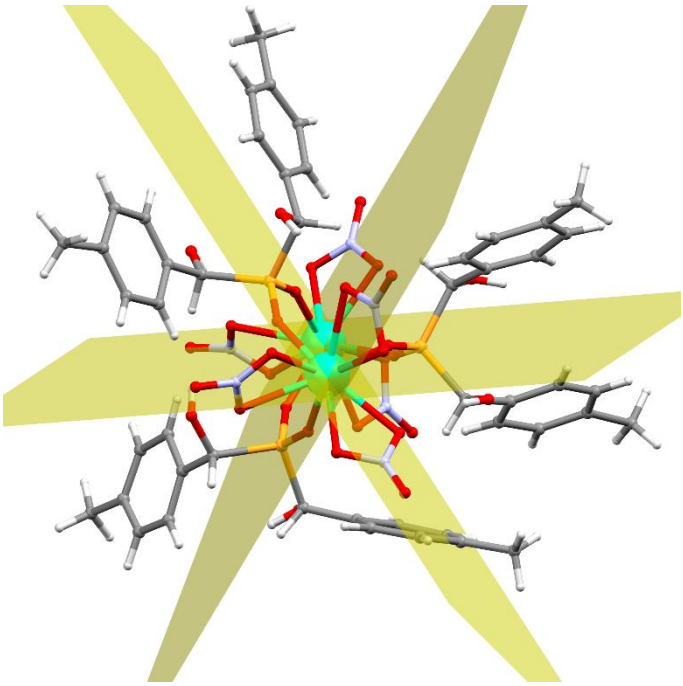

4.1 Introduction:

1993 after the discovery of the famous Mn_{12}-cluster, $[Mn_{12}O_{12}(OAc)_{16}(H_2O)_4]$ by Sessoli et al., begins the era of SMM(single molecular magnet).[1] ($Mn_{12}Ac$) retains magnetization for a long period relatively at liquid Helium temperature after removing the externally applied field, a molecular origin phenomenon.[2] Though it started with a transition metal atom, a vast number of 3d, 4f, and mixed metal (3d-4f) clusters using various ligands such as Schiff-base, diketone, carboxylates, calixarenes, alkoxide, amino acids, phosphate, phosphonates SMM properties are reported.[3] Lanthanide atoms are most useful in SMM [4] compared to transition metal due to the large single-ion anisotropy,[5] which causes a large anisotropic barrier; the greater SMM property. Among the lanthanides, Tb, Dy, Ho, and Er are the most commonly used lanthanide ions in SMM. $[Tb(Pc)_2]^-$ is the first reported SIM (single-ion magnet) with a very high energy barrier for the magnetization-reversal by Ishikawa et. al. in 2003.[6] Dy-SMM is widely used because of the Kramer's ion (odd number of f-electron $4f^9$) Dy(III) has a large magnetic anisotropy, a large energy-gap between the ground and first excited m_J levels, and a bistable ground state disregarding to the symmetry of ligand fields.[7] SMMs are contemplated as the molecular analogous of bulk-ferromagnets used such as NdFeB, AlNiCo, and $SmCo_5$. They can be used as storage devices, quantum computing, molecular spintronics, magneto-optical switches, etc.[8] in chemistry, physics, material science, and nanoscience.

Phosphorous-based ligands are an interesting research topic for the past few decades. Several phosphorous lanthanide complexes/clusters are reported in the literature using phosphine oxide, phosphonic acid, and organophosphate ligands[9]. Lanthanides with phosphinic acid ligands are not that well explored due to the insoluble nature of phosphinate compounds. Increasing the steric hindrance or substitution in the ligands lanthanide phosphinate complexes can be solubilized in a variety of organic solvents/water. Introducing the hydroxy group in phosphinic acid increases the solubility of lanthanide compounds in polar solvents like methanol, acetonitrile, etc. Dinuclear paddlewheel structures are common for transition metals (Ti, V, Cr, Mn, Fe, Co, Ni, Cu, and Zn).[10] Several paddlewheel-type structures with lanthanide and carboxylic acid[11] and linear trinuclear lanthanides[12] are reported but with carboxylic acid analogous phosphinic acid, no report except our lab's lanthanide-tritylphosphinates which shows weak ferromagnetic interaction between two Gd(III)ions (dinuclear complex) and Dy(III), Ho(III) (linear trinuclear complex) are shown anti-ferromagnetic interaction (**unpublished results**). This work is the second paddlewheel-type result with phosphinic acid from our lab.

In this work, we have synthesized four dinuclear paddle-wheel type lanthanide complexes of Dy_2, Ho_2, Nd_2, and Y_2 using a chiral phosphinic acid ligand [Bis-[α-hydroxy(p-methylphenyl)methyl]phosphinic acid] and three linear trinuclear paddle-wheel type lanthanide complexes of Nd_3, Pr_3, Dy_3 and $NdLa_2$ using [Bis-[α-hydroxy(p-bromophenyl)methyl]phosphinic acid]. These complex structures are characterized by SCXRD, PXRD, IR, and TGA studies. The details of the crystal synthesis and characterization of **4.1-4.4** and **4.5-4.8** are discussed below.

4.2 Experimental Section:

4.2.1 General information:

All the general chemicals were purchased commercially and used without further purification. Bis-[α-hydroxy(p-methylphenyl)methyl]phosphinic acid and [Bis-[α-hydroxy(p-bromophenyl)methyl]phosphinic acid] were prepared by the reported procedure.[13] Hydrated lanthanide nitrate salts were prepared from their corresponding oxides by neutralizing them with concentrated HNO_3, followed by evaporation to dryness.

4.2.2 Synthesis:

To a 15 ml methanolic solution of Bis-[α-hydroxy(p-methylphenyl)methyl]phosphinic acid($R^1{}_2PO_2H$) [R^1 = CH(OH)PhMe] (for **4.1-4.4**) or R^1 = [Bis-[α-hydroxy(p-bromophenyl)methyl]phosphinic acid] (for **4.5-4.8**), $Ln(NO_3)_3.6H_2O$ was added and stirred for 1-2 minutes following triethylamine base dropwise. The solution was stirred at room temperature for 5 h. After the reaction, methanol was evaporated with rotor-vapor and the residue was redissolved in acetonitrile for crystallization. X-ray quality crystals suitable for SCXRD were obtained by slow evaporation of the solvent mixture.

Compound 4.1: $R^1{}_2PO_2H$ (0.050 g, 0.163 mmol), $Dy(NO_3)_3.6H_2O$ (0.074 g, 0.163 mmol), Et_3N (0.06 ml, 0.489 mmol). Yield: 0.125 g, 68.64% (Based on $Dy(NO_3)_3.6H_2O$). IR(cm^{-1}): 3486.16(m), 3046.74(m), 2989.59(m), 2735.39(w), 1470.75(m), 1392.36(m), 1296.87(s), 1198.32(s), 1154.27(m), 1066.64(s), 1034.96(s), 816.06(s), 744.08(w), 606.56(w), 536.94(w), 461.09(w), 417.32(w).

Compound 4.2: $R^1{}_2PO_2H$ (0.050 g, 0.163 mmol), $Ho(NO_3)_3.6H_2O$ (0.074 g, 0.163 mmol), Et_3N (0.06 ml, 0.489 mmol). Yield: 0.120 g, 66.15% (Based on $Ho(NO_3)_3.6H_2O$). IR(cm^{-1}): 3491.95(m), 3033.88(m), 2992.76(m), 2926.04(m), 2722.87(w), 1472.25(m), 1390.27(m),

1299.89(s), 1199.32(m), 1154.71(m), 1067.39(s), 1035.90(s), 826.13(s), 745.41(w), 607.43(w), 541.04(w), 461.73(w), 414.85(w).

Compound 4.3: $R^1_2PO_2H$ (0.050 g, 0.163 mmol), $Nd(NO_3)_3.6H_2O$ (0.071 g, 0.163 mmol), Et_3N (0.06 ml, 0.489 mmol). Yield: 0.105 g, 63.36% (Based on $Nd(NO_3)_3.6H_2O$). IR(cm^{-1}): 3504.75(m), 3034.35(m), 2989.59(m), 2716.33(w), 1441.30(m), 1394.87(m), 1290.53(s), 1200.71(m), 1176.13(s), 1062.86(s), 1031.18(s), 818.06(s), 736.66(w), 609.23(w), 537.47(w), 462.22,(w) 416.53(w).

Compound 4.4: $R^1_2PO_2H$ (0.050 g, 0.163 mmol), $Y(NO_3)_3.6H_2O$ (0.062 g, 0.163 mmol), Et_3N (0.06 ml,0.489 mmol). Yield: 0.112 g, 65.88% (Based on $Y(NO_3)_3.6H_2O$). IR(cm^{-1}): 3247.69(m), 3031.00(m), 2986.41(m), 2922.86(m), 2716.33(w), 1440.79(w), 1398.82(m), 1302.48(s), 1181.64(m), 1148.57(s), 1066.11(s), 1035.00(s), 824.47(s), 746.69(w), 702.90(w), 607.47(w), 540.38(w), 479.04(w), 415.64(w).

Compound 4.5: $R^2_2PO_2H$ (0.050 g, 0.114 mmol), $Nd(NO_3)_3.6H_2O$ (0.049 g, 0.114 mmol), Et_3N (0.045 ml,0.344 mmol). Yield: 0.100 g, 48.30% (Based on $Nd(NO_3)_3.6H_2O$). IR(cm^{-1}): 3410.67(m), 3048.00(m), 2986.47(m), 2948.40(m), 2710.28(w), 1638.35(s), 1590.25(w), 1441.44(s), 1398.03(s), 1297.58.(s), 1197.58(m), 1153.70(s), 1062.45(s), 1030.79(s), 1007.47(s), 822.66(s), 735.51(w), 705.09(w), 657.58(w), 554.43(m), 507.34(s), 427.34(w).

Compound 4.6: $R^2_2PO_2H$ (0.050 g, 0.114 mmol), $Pr(NO_3)_3.6H_2O$ (0.049 g, 0.114 mmol), Et_3N (0.045 ml,0.344 mmol). Yield: 0.080 g, 57.55% (Based on $Pr(NO_3)_3.6H_2O$). IR(cm^{-1}): 3386.15(m), 3056.71(m), 2986.74(m), 2951.60(m), 2708.76(w), 1647.19(w), 1593.61(w), 1439.31(s), 1397.44(s), 1298.78.(s), 1152.08(s), 1060.82(s), 1032.55(s), 1006.85(s), 819.74(s), 733.46(w), 704.31(w), 652.69(w), 555.10(m), 510.35(s), 424.51(w).

Compound 4.7: $R^2_2PO_2H$ (0.050 g, 0.114 mmol), $Dy(NO_3)_3.6H_2O$ (0.052 g, 0.114 mmol), Et_3N (0.045 ml,0.344 mmol). Yield: 0.090 g, 59.21% (Based on $Dy(NO_3)_3.6H_2O$). IR(cm^{-1}): 3382.90(m), 3047.76(m), 2983.55(m), 2948.40(m), 2710.59(w), 1638.35(w), 1587.22(w), 1481.93(s), 1397.30(s), 1300.57.(s), 1154.33(s), 1065.58(s), 1034.35(s), 1007.89(s), 821.15(s), 731.03(w), 703.44(w), 652.79(w), 555.09(m), 509.27(s), 456.96(w).

Compound 4.8: $R^2_2PO_2H$ (0.050 g, 0.114 mmol), $Nd(NO_3)_3.6H_2O$ (0.016 g, 0.037 mmol), $La(NO_3)_3.6H_2O$ (0.032 g, 0.075 mmol), Et_3N (0.045 ml,0.344 mmol). Yield: 0.080 g, 57.55% (Based on $Nd(NO_3)_3.6H_2O$). IR(cm^{-1}): 3395.74(m), 3049.33(m), 2986.74(m), 2948.40(m), 2702.37(w), 1638.35(w), 1589.59(w), 1438.78(s), 1398.00(s), 1299.00.(s), 1153.76(s),

1060.91(s), 1031.46(s), 1007.23(s), 820.16(s), 733.30(w), 704.80(w), 653.04(w), 554.34(m), 506.69(s), 433.91(w).

4.2.3 Instrumentation:

Infrared spectra were recorded with a NICOLET iS5 FTIR Spectrometer. Elemental analysis was performed with a Flash EA Series 1112 CHNS analyzer. TGA was recorded with a PerkinElmer STA 8000 thermogravimetric analyzer under a nitrogen gas flow rate of 20 ml/min and a heating rate of 10°C/min. The SCXRD data for **4.1-4.8** were collected at 114 K, 141 K, 110 K, 119 K, 299 K, 298 K, 298 K and 299 K, respectively with an XtaLAB Synergy, Single source at offset/far, HyPix3000 diffractometer. Rigaku Oxford HyPix3000 CCD plate detector system [λ (Mo Kα)= 0.71073 Å] with a mirror monochromator. The structure was solved with the **Olex2**[14], **ShelXT**[15] structure solution program using Intrinsic Phasing and refined with the **SHELXL**[16]**- 2018/3** refinement package using Least Squares minimization. All non-hydrogen atoms were refined anisotropically and hydrogen atoms were fixed at calculated positions and refined as riding horse models. EADP, RIGU, SIMU, DELU, SADI, and FLAT constrained/restrained commands were used to fix the disordered atoms. For **4.1-4.4**, the Olex2 solvent mask (similar to PLATON/SQUEEZE) was used to mask out the electron density of disordered counterions. The details of the solvent masks used are given below-

For **4.1**, a solvent mask was calculated and 354 electrons were found in a volume of 1305 $Å^3$ in 1 void. This is consistent with the presence of 3[$C_6H_{16}N$] per formula unit which accounts for 354.0 electrons. For **4.2**, a solvent mask was calculated and 352 electrons were found in a volume of 1359 $Å^3$ in 1 void. This is consistent with the presence of 3[$C_6H_{16}N$] per formula unit which accounts for 354.0 electrons. For **4.3**, a solvent mask was calculated and 492 electrons were found in a volume of 2466 $Å^3$ in 1 void. This is consistent with the presence of 4[$C_6H_{16}N$], and 1[NO_3] per formula unit which account for 534.0 electrons. For **4.4**, a solvent mask was calculated and 270 electrons were found in a volume of 944 $Å^3$ in 2 voids. This is consistent with the presence of 1[$C_6H_{16}N$], and 1[$C_6H_{16}N$] per formula unit which account for 236.0 electrons. For **4.5**, a solvent mask was calculated and 454 electrons were found in a volume of 10460 $Å^3$ in 1 void. This is consistent with the presence of 3[$C_6H_{16}N$] per formula unit which accounts for 531.0 electrons. For **4.6**, a solvent mask was calculated and 531 electrons were found in a volume of 10540 $Å^3$ in 1 void. This is consistent with the presence of 3[$C_6H_{16}N$] per formula unit which accounts for 531.0 electrons. For **4.7**, A solvent mask was

calculated and 902 electrons were found in a volume of 10346 $Å^3$ in 1 void. This is consistent with the presence of 3[$C_6H_{16}N$], 6[CH_3CN] per formula unit which account for 927.0 electrons. For **4.8**, a solvent mask was calculated and 706 electrons were found in a volume of 10581 $Å^3$ in 1 void. This is consistent with the presence of 3[$C_6H_{16}N$], 6[H_2O] per formula unit which accounts for 711.0 electrons.

4.3 Results and discussions:

The ligand was synthesized according to the literature procedure[13]. The hydrated lanthanide nitrates were reacted in a methanolic solution of the ligand (Bis-[α-hydroxy(p-methylphenyl)methyl]phosphinic acid($R^1_2PO_2H$)[R^1= CH(OH)PhMe] (for **4.1-4.4**) or [Bis-[α-hydroxy(p-bromophenyl)methyl]phosphinic acid] (for **4.5-4.8**)) following the addition of the base triethylamine in a 1:1:3 ratio. (**scheme 1**) A clear solution was obtained after 5 hrs at room temperature. The clear solution was evaporated with rotor vapor and crystallized in acetonitrile. X-ray quality crystals were obtained after slow evaporation of the solution. Only for **4.8,** we have used two lanthanide metal ratios 1:2 (Nd/La) keeping the same condition as the synthesis procedure. Standard-analytical and spectroscopic techniques were used to characterize the products. IR spectra of **4.1-4.8** show the characteristic peaks of aromatic and aliphatic C-H stretching of the ligand around 2922-3034 cm^{-1}, O-H stretching band shows in between 3427-3504 cm^{-1}, inorganic nitrate appears in the region 1440-1472 cm^{-1} and 816-826 cm^{-1}, P-O and P-O-M stretching observed in the range 1031-1200 cm^{-1}. (**figure 4.15-4.22**) TGA studies reveal the decomposition temperature range for **4.1-4.8** is 240 °C, 236 °C, 238 °C, 238 °C, 246 °C, 260 °C, 254 °C and 246 °C respectively (**figure 4.13-4.14**). The ^{31}P-NMR spectrum of diamagnetic **4.4** shows the equivalent environment around the metal atom at 30.82 ppm. (**figure 4.31**) The crystallinity and phase purity of the bulk samples for **4.1-4.8** is represented by the PXRD data. (**figure 4.23-4.30**)

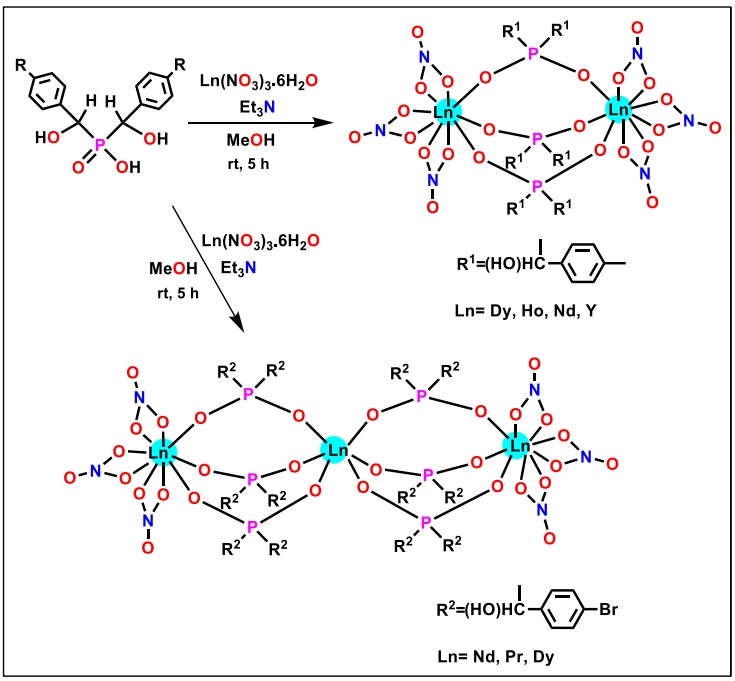

Scheme 1: Synthetic scheme of compounds **4.1-4.8**

4.1-4.4 compounds are isostructural dinuclear complexes (**scheme 1**), crystallized in the triclinic P-1 space group. As all the complexes are structurally similar, only complex **4.1 i**s described in detail. The crystal structure of **4.1** is dinuclear, consisting of two Dy(III) ions, three monoanionic ligands [Bis-[α-hydroxy(p-methylphenyl)methyl]phosphinic acid)], and six nitrate anions. (**figure 4.1(a)**) The complex is tri-negative which is charged-balanced by three monocationic triethylammonium cations. Each of the Dy atoms is nine coordinated.(**figure 4.2(b)**) Among these nine coordination, three are from the phosphinic acid oxygen atom, and another six are from three nitrate anions. Three phosphinic acids bridge the two dysprosium (III) ions in a [2.11] mode (Harris notation). Nitrate ions are attached to bidentate [1.11] mode with Dy(III) ions. SHAPE analysis shows the coordination geometry of the Dy(III) is a spherical tricapped trigonal prism(D_{3h}) (**table 4.11**). Important bond metric parameters are listed as follows; Dy-$O_{(R2PO2H)}$, and Dy-$O_{(nitrate)}$ distances are of the order of 2.227(3)-2.257(3) Å, 2.475(5)-2.528(4) Å respectively. Dy(III)…Dy(III) intranuclear bond distance in the structure is 5.258 Å. Selected bond distances and bond angles for **4.1-4.4** are given in **tables 4.3-4.6.**

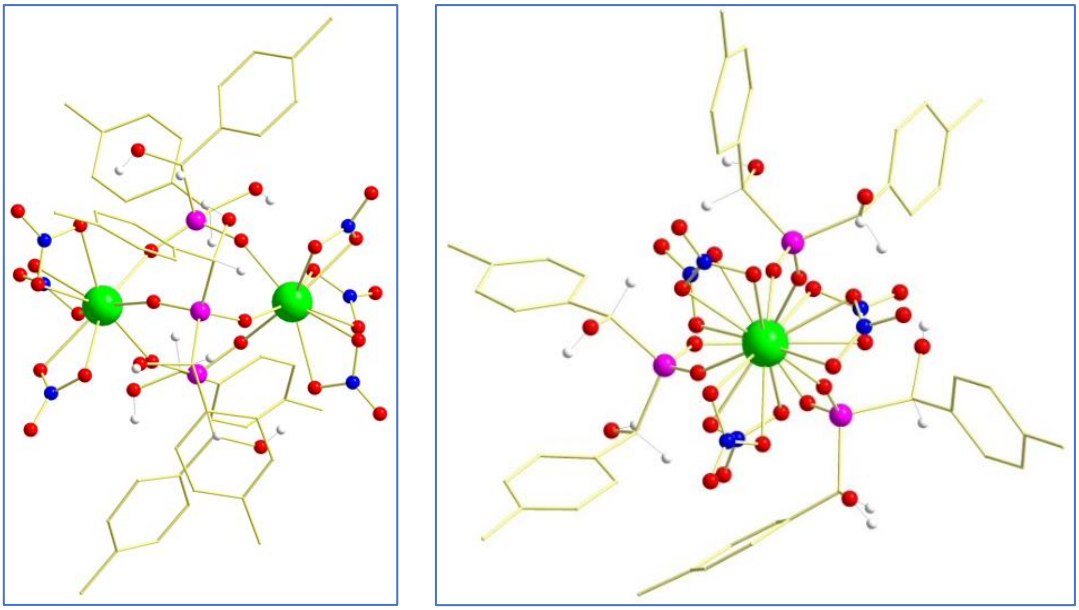

(a) **(b)**

Figure 4.1. (a) Ball and stick view showing solid-state structure side view of **4.1** and **(b)** Ball and stick view showing solid-state structure along the metal axis view of **4.1**

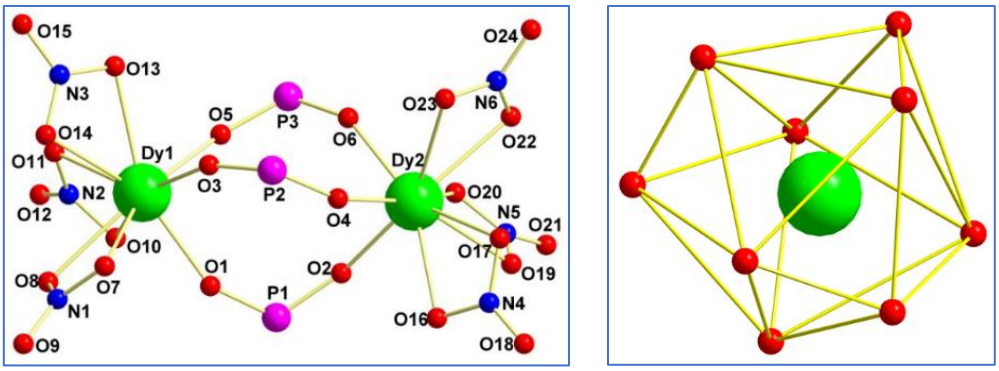

(a) **(b)**

Figure 4.2. (a) Ball and stick view showing solid state metal-oxo core structure of **4.1** and **(b)** representation of coordination geometry of dysprosium atoms in **4.1**

Two types of structural conformation of the lanthanide coordinated phosphinic acid ligand were captured in the crystal structure as shown in **figure 4.3.**

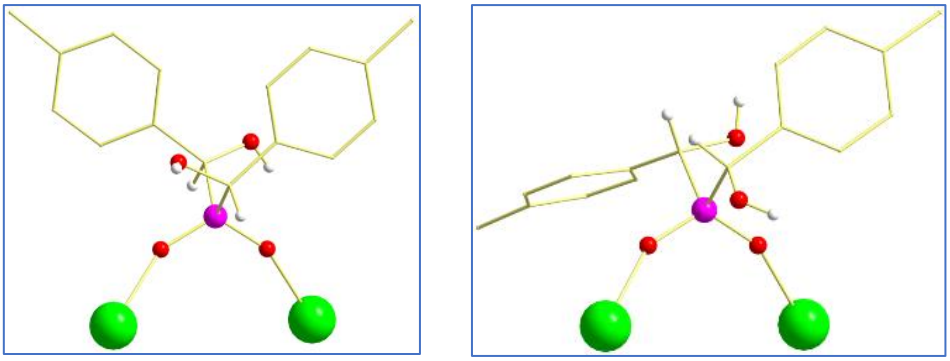

(a) **(b)**

Figure 4.3. (a) and **(b)** Ball and stick view of two types of conformation of the dysprosium coordinated phosphinic acid ligand in **4.1**

All the crystal structures are similar for **4.5-4.8**. The crystal structure of **4.5** was described in detail as representative of all other crystals (**4.6-4.8**). The crystal of **4.5** was crystallized in the trigonal R-3 space group. The trinuclear crystal contains three Nd-atoms, six phosphinic acid ligands, and six nitrate anions (**figure 4.4(a)**). The overall crystal is tri-anionic, to charge balance three triethylammonium cation is required which is truly seen from the electron density in the crystal data using the solvent mask. From the core structure, (**figure 4.4(c)**) it has been seen that three Nd-atoms are situated in exactly linear arrangements. Two terminal Nd-atoms are nine coordinated and the central Nd-atom is six coordinated. The two terminal Nd-atoms has similar environment. The coordination environment of the central Nd-atom is six, all come from the phosphinic acid ligand oxygen atoms. Terminal Nd-atoms connected with the central Nd-atom with three phosphinic acid ligands in a [2.11] (Harris notation) coordination manner. In the terminal Nd-atoms nine coordination filled with three phosphinic acid oxygen atoms and three nitrate anions six oxygen atoms in a bidentate [1.11] mode. SHAPE analysis shows the central and terminal Nd-atoms are octahedron (O_h) and spherical tricapped trigonal prism(D_{3h}) geometry. (**table 4.15-4.16**)

Another important aspect seen in the crystal structure is that all the hydroxy groups of the phosphinic acids (each phosphinic acid has two hydroxy groups) are towards the central Nd-atom (**figure 4.4(f)**). Each phosphinic acid hydroxy group two H-bonded with opposite phosphinic acid ligands hydroxy group and oxygen atom which connected with Nd-atom forming a five-membered ring. Important bond metric parameters are listed as follows; Nd-$O_{(R2PO2H)}$, and Nd-$O_{(nitrate)}$ distances are of the order of 2.219(5)-2.339(4), 2.519(4)-2.603(4) Å

respectively. Nd(III)…Nd(III) intranuclear bond distance in the structure is 5.341 Å. Selected bond distances and bond angles for **4.5-4.8** are given in **tables 4.7-4.10.**

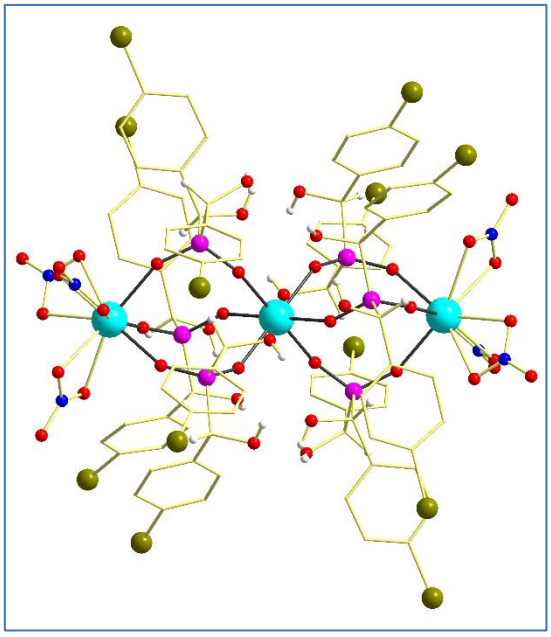

(a)

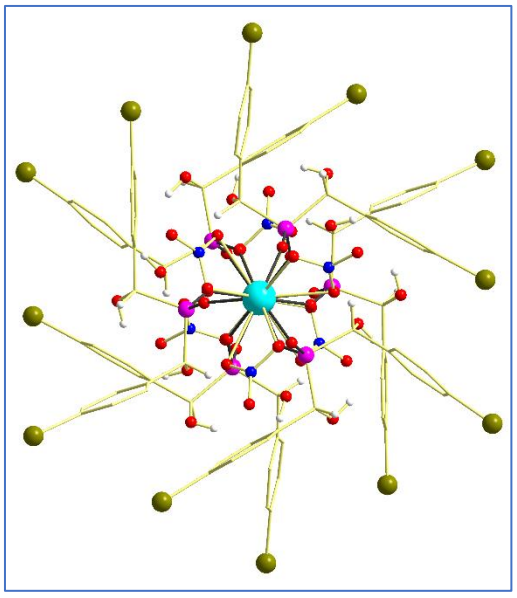

(b)

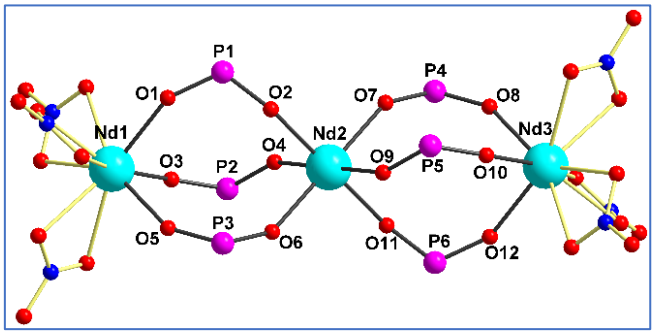

(c)

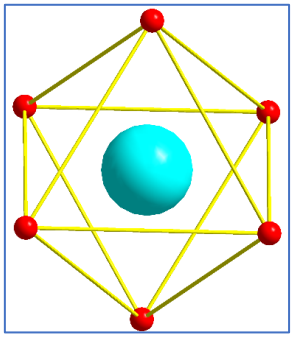

(d)

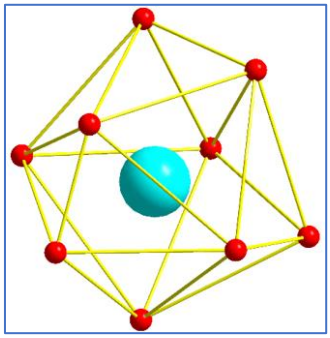

(e)

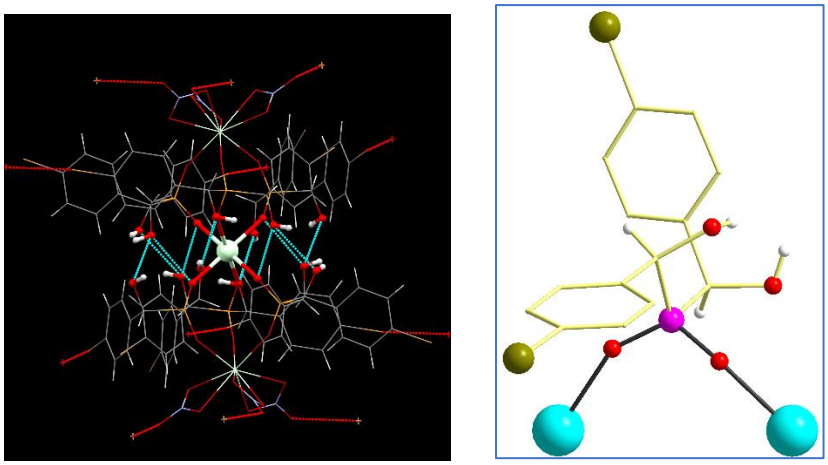

(f) (g)

Figure 4.4. Ball and stick view **(a)** showing solid-state structure side view of **4.5**, **(b)** solid-state structure along the metal axis view of **4.5**, **(c) (**solid state metal-oxo core structure of **4.5**, **(d)** and **(e)** representation of coordination geometry of neodymium atoms in **4.5**, **(f)** H-bonding interactions in **4.5**, **(g)** conformation of the dysprosium coordinated phosphinic acid ligand in **4.5.**

In the case of **4.8,** we have used two lanthanide metal ratios 1:2 (Nd/La) keeping the same condition as the synthesis procedure of **4.5-4.7. (scheme 2)** With this dilution with diamagnetic La-ions we obtained the same structural complexes as **4.5-4.7** but terminal two La-atoms and the central Nd-atom which was confirmed by SCXRD and supported by the EADX results. (**figure 4.34**)

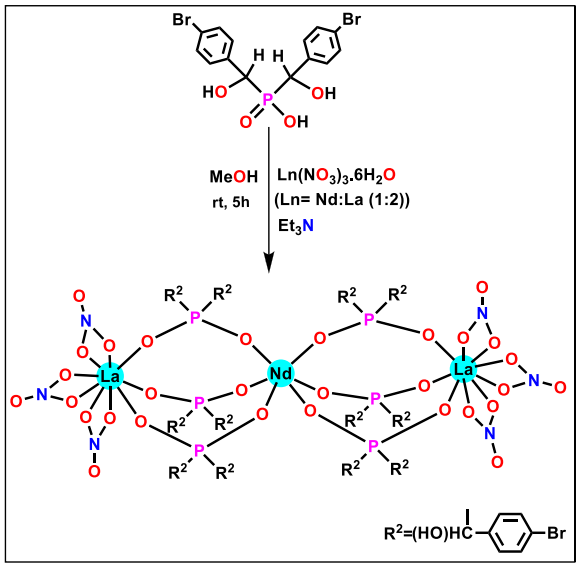

Scheme 2: Synthetic scheme of compound **4.7**

Only one type of structural conformation of the lanthanide coordinated phosphinic acid ligand was captured in the crystal structure as shown in **figure 4.4(g).**

4.4 Conclusion:

In conclusion, we have synthesized and structurally confirmed four dinuclear isostructural lanthanide phosphinates of Dy_2, Ho_2, Nd_2, and Y_2 (**4.1-4.4**) and four trinuclear lanthanide phosphinates of Nd_3, Pr_3, Dy_3 and $NdLa_2$ (**4.5-4.8**)complexes. Among these $NdLa_2$ (**4.8**) is a magnetically diluted crystal structure. All these dinuclear and trinuclear lanthanide clusters show paddlewheel-type structures which is probably the second example in the lanthanide phosphinate realm. These structures are very unique for solid-state structural reason.

4.5 *Analytical and Spectroscopic Data*

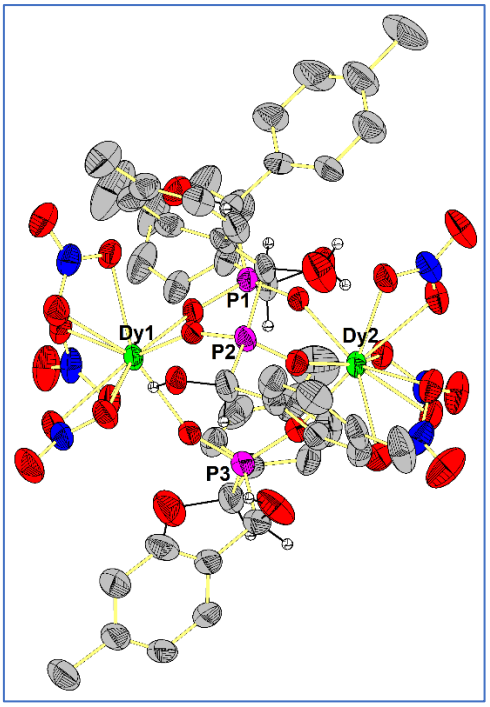

Figure 4.5. ORTEP view of **4.1** with thermal ellipsoids shown at 30%probability.

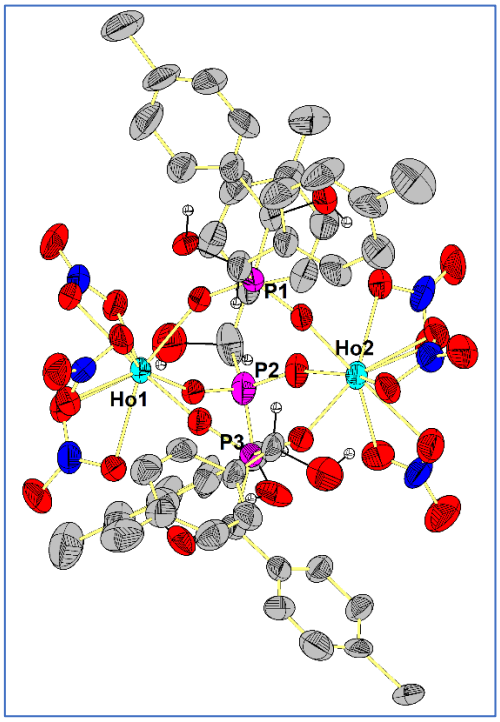

Figure 4.6. ORTEP view of **4.2** with thermal ellipsoids shown at 30%probability.

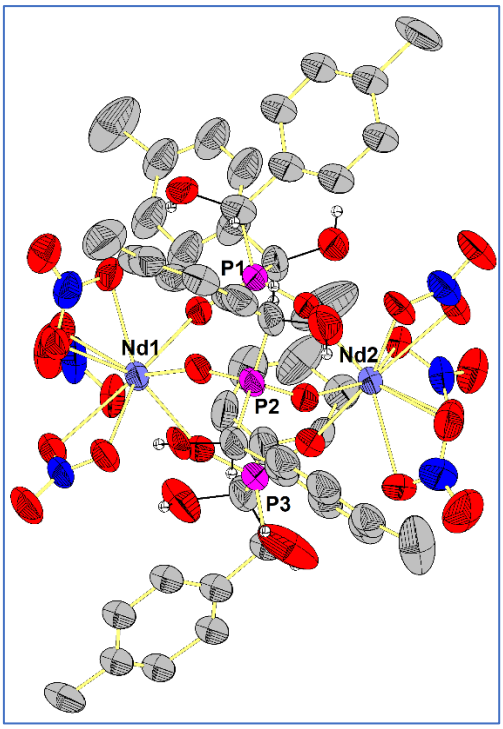

Figure 4.7. ORTEP view of **4.3** with thermal ellipsoids shown at 30%probability.

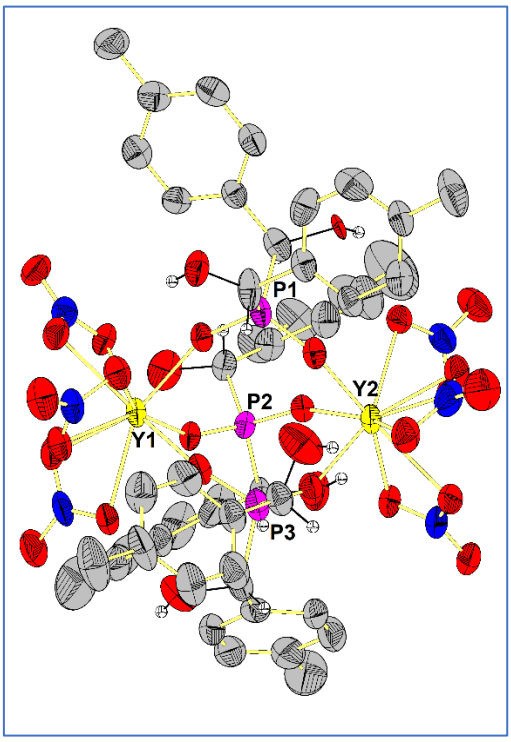

Figure 4.8. ORTEP view of **4.4** with thermal ellipsoids shown at 30%probability.

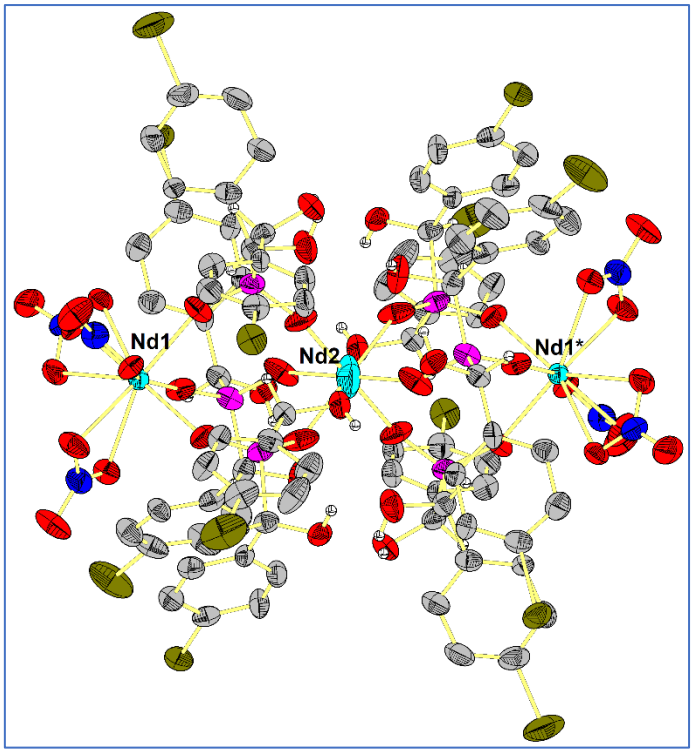

Figure 4.9. ORTEP view of **4.5** with thermal ellipsoids shown at 30%probability

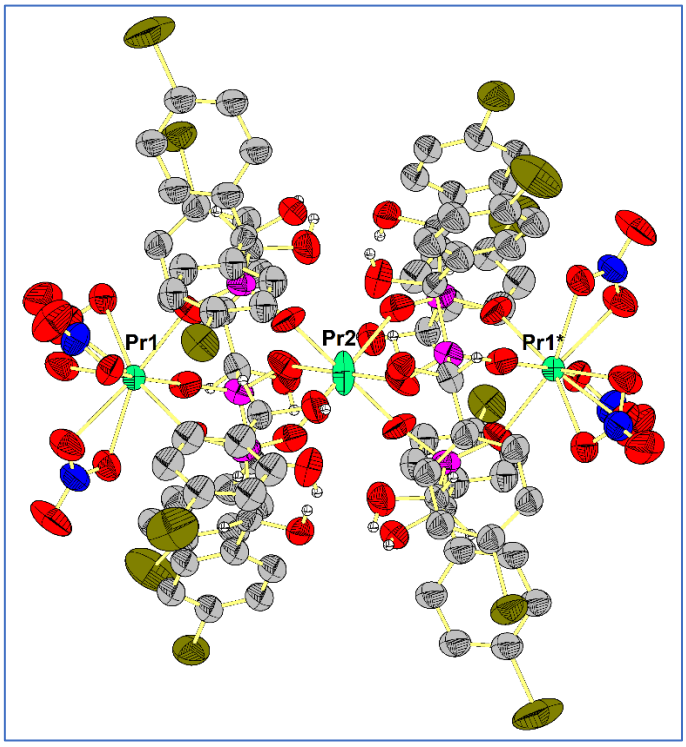

Figure 4.10. ORTEP view of **4.6** with thermal ellipsoids shown at 30%probability

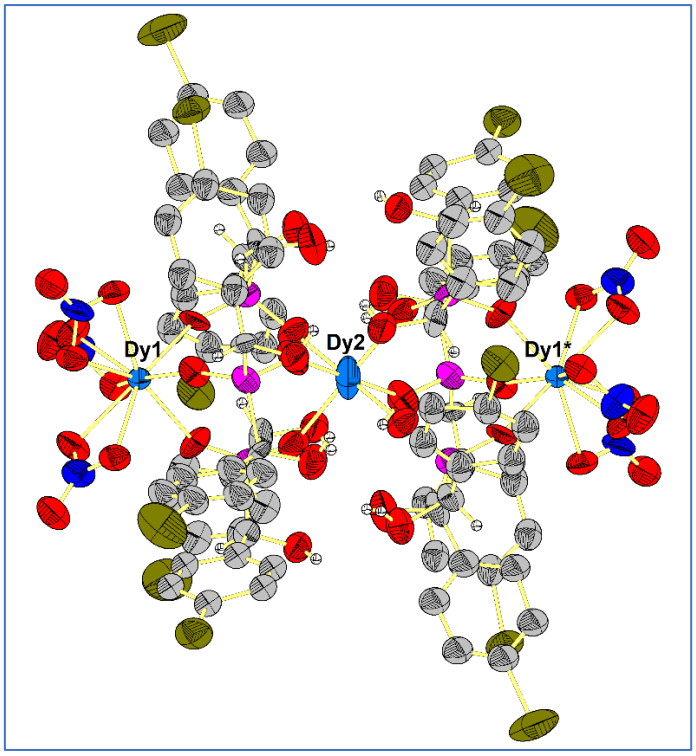

Figure 4.11. ORTEP view of **4.7** with thermal ellipsoids shown at 30%probability

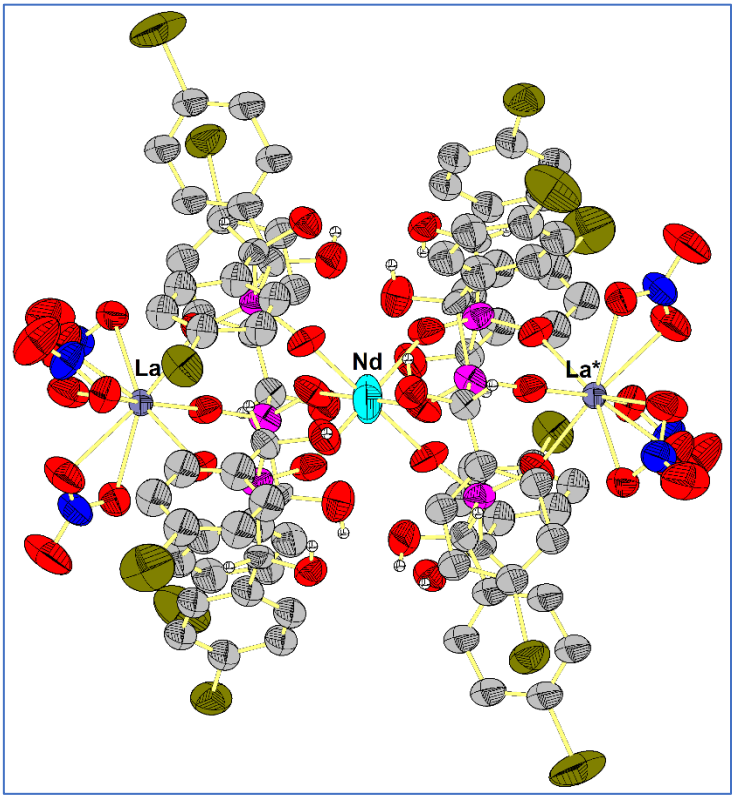

Figure 4.12. ORTEP view of **4.8** with thermal ellipsoids shown at 30%probability

Table 4.1. Crystallographic information of compound **4.1-4.4**.

	4.1	4.2	4.3	4.4
Empirical formula	$C_{78}H_{134}N_{13}O_{36}P_3Dy_2$	$C_{78}H_{133.39}N_{13}O_{35.95}P_3Ho_2$	$C_{72}H_{118}N_{11}O_{33}P_3Nd_2$	$C_{78}H_{134}N_{13}O_{36}P_3Y_2$
Formula weight	2247.88	2251.33	2047.16	2100.70
Temperature/K	114(3)	141(50)	110(3)	119(4)
Crystal system	Triclinic	Triclinic	Triclinic	Triclinic
Space group	P-1	P-1	P-1	P-1
a/Å	15.0251(2)	15.0249(5)	14.9424(2)	15.0320(2)
b/Å	15.0383(2)	15.0536(3)	15.0364(2)	15.0419(2)
c/Å	23.4198(3)	23.5177(6)	23.7599(5)	23.3613(4)
α/°	83.9970(10)	83.735(2)	82.678(2)	73.7140(10)
β/°	73.7210(10)	73.922(3)	73.969(2)	84.0260(10)
γ/°	85.3300(10)	85.275(2)	85.1240(10)	85.2800(10)
Volume/Å^3	5044.21(12)	5073.0(2)	5081.99(15)	5034.92(13)
Z	2	2	2	2
ρ_{calc}g/cm^3	1.480	1.474	1.338	1.386
μ/mm^{-1}	1.603	1.681	1.134	1.280
F(000)	2316.0	2318.0	2112.0	2208.0
Crystal size/mm^3	0.04 × 0.03 × 0.02	0.05 × 0.04 × 0.02	0.03 × 0.02 × 0.01	0.35 × 0.33 × 0.02
Radiation	Mo Kα (λ = 0.71073)	Mo Kα (λ = 0.71073)	Mo Kα (λ = 0.71073)	Mo Kα (λ = 0.71073)
2Θ range for data collection/°	3.758 to 54.068	3.744 to 54.28	3.744 to 54.07	3.646 to 54.14
Index ranges	$-19 \le h \le 18$, $-18 \le k \le 19$, $-29 \le l \le 29$	$-18 \le h \le 19$, $-19 \le k \le 19$, $-30 \le l \le 29$	$-18 \le h \le 19$, $-18 \le k \le 19$, $-30 \le l \le 29$	$-19 \le h \le 19$, $-19 \le k \le 19$, $-29 \le l \le 29$
Reflections collected	117952	90766	93905	120992
Independent reflections	21089 [R_{int} = 0.1014, R_{sigma} = 0.0731]	21215 [R_{int} = 0.1682, R_{sigma} = 0.1571]	21216 [R_{int} = 0.0614, R_{sigma} = 0.0719]	21138 [R_{int} = 0.1022, R_{sigma} = 0.1336]
Data/restraints /parameters	21089/0/1048	21215/114/1020	21216/11/708	21138/10/1093
Goodness-of	1.051	0.928	1.037	1.030

-fit on F^2				
Final R indexes [I>=2σ (I)]	R_1 = 0.0537, wR_2 = 0.1411	R_1 = 0.0714, wR_2 = 0.1774	R_1 = 0.0773, wR_2 = 0.2381	R_1 = 0.0852, wR_2 = 0.2158
Final R indexes [all data]	R_1 = 0.0884, wR_2 = 0.1582	R_1 = 0.1509, wR_2 = 0.2168	R_1 = 0.1274, wR_2 = 0.2723	R_1 = 0.1765, wR_2 = 0.2534
Largest diff. peak/hole / e $Å^{-3}$	1.53/-1.07	1.31/-1.10	1.47/-0.72	0.84/-0.59

Table 4.2. Crystallographic information of compound **4.5-4.8**.

Identification code	**4.5**	**4.6**	**4.7**	**4.8**
Empirical formula	$Br_{12}C_{102}H_{120}N_9Nd_3O_{42}P_6$	$Br_{12}C_{102}H_{120}N_9O_{42}P_6Pr_3$	$Br_{12}C_{114}H_{138}N_{15}O_{42}P_6Dy_3$	$Br_{12}C_{102}H_{132}N_9O_{48}P_6NdLa_2$
Formula weight	3721.52	3711.53	4022.63	3818.96
Temperature/K	299.15	298.0(4)	298.15	299.15
Crystal system	trigonal	trigonal	trigonal	trigonal
Space group	R-3	R-3	R-3	R-3
a/Å	23.6571(4)	23.6924(8)	23.6097(9)	23.6597(7)
b/Å	23.6571(4)	23.6924(8)	23.6097(9)	23.6597(7)
c/Å	35.8664(7)	35.9212(13)	35.6028(15)	36.1153(14)
α/°	90	90	90	90
β/°	90	90	90	90
γ/°	120	120	120	120
Volume/$Å^3$	17383.7(7)	17462.2(13)	17186.8(15)	17508.1(12)
Z	3	3	3	3
ρ_{calc}g/cm^3	1.066	1.059	1.166	1.087
μ/mm^{-1}	2.819	2.765	3.154	2.724
F(000)	5463.0	5454.0	5913.0	5625.0
Crystal size/mm^3	0.31 × 0.27 × 0.24	0.28 × 0.26 × 0.18	0.26 × 0.25 × 0.24	0.27 × 0.26 × 0.24
Radiation	Mo Kα (λ = 0.71073)	Mo Kα (λ = 0.71073)	MoKα (λ = 0.71073)	MoKα (λ = 0.71073)
2Θ range for data collection/°	4.58 to 54.112	4.128 to 54.044	4.146 to 54.218	4.132 to 54.084
Index ranges	-29 ≤ h ≤ 30, -30 ≤ k ≤ 30, -45 ≤ l ≤ 45	-29 ≤ h ≤ 29, -29 ≤ k ≤ 30, -45 ≤ l ≤ 38	-29 ≤ h ≤ 29, -29 ≤ k ≤ 29, -44 ≤ l ≤ 45	-30 ≤ h ≤ 29, -30 ≤ k ≤ 30, -43 ≤ l ≤ 44
Reflections collected	134535	43371	136389	46935
Independent reflections	8303 [R_{int} = 0.1989, R_{sigma} = 0.1380]	8165 [R_{int} = 0.1005, R_{sigma} = 0.1531]	8210 [R_{int} = 0.4714, R_{sigma} = 0.2988]	8208 [R_{int} = 0.1555,R_{sigma} = 0.2362]

Data/restraints /parameters	8303/0/201	8165/0/172	8210/0/171	8208/195/171
Goodness-of -fit on F^2	0.971	0.953	1.012	0.931
Final R indexes [I>=2σ (I)]	R_1 = 0.0927, wR_2 = 0.2174	R_1 = 0.0950, wR_2 = 0.2170	R_1 = 0.1628, wR_2 = 0.3625	R_1 = 0.0992, wR_2 = 0.1935
Final R indexes [all data]	R_1 = 0.1619, wR_2 = 0.2465	R_1 = 0.1809, wR_2 = 0.2512	R_1 = 0.2429, wR_2 = 0.4009	R_1 = 0.1981, wR_2 = 0.2259
Largest diff. peak/hole / e $Å^{-3}$	0.93/-1.52	1.45/-1.42	2.00/-1.27	0.69/-0.89

Table 4.3. Selected bond lengths (Å) and bond angle (deg) parameters of compound **4.1**

Dy1-O1	2.242(4)	Dy2-O6	2.239(3)
Dy1-O5	2.227(3)	Dy2-O2	2.257(3)
Dy1-O9	2.248(3)	Dy2-O10	2.246(3)
Dy1-O16	2.475(4)	Dy2-O29	2.516(4)
Dy1-O17	2.519(4)	Dy2-O23	2.503(4)
Dy1-O14	2.528(4)	Dy2-O26	2.501(4)
Dy1-O20	2.497(4)	Dy2-O28	2.521(4)
Dy1-O13	2.511(4)	Dy2-O25	2.496(4)
Dy1-O19	2.503(4)	Dy2-O22	2.491(4)
O1-Dy1-O9	85.40(14)	O6-Dy2-O2	86.62(12)
O1-Dy1-O16	155.00(11)	O6-Dy2-O10	86.67(12)
O1-Dy1-O17	149.15(15)	O6-Dy2-O29	74.74(12)
O1-Dy1-O14	75.32(12)	O6-Dy2-O23	83.13(12)
O1-Dy1-O20	84.95(13)	O6-Dy2-O26	156.20(12)
O1-Dy1-O13	125.48(14)	O6-Dy2-O28	124.71(14)
O1-Dy1-O19	78.55(14)	O6-Dy2-O25	148.23(14)
O5-Dy1-O1	84.15(12)	O6-Dy2-O22	78.64(13)
O5-Dy1-O9	87.44(12)	O2-Dy2-O29	78.64(12)
O5-Dy1-O16	74.16(12)	O2-Dy2-O23	148.13(15)
O5-Dy1-O17	124.44(15)	O2-Dy2-O26	73.14(12)
O5-Dy1-O14	78.33(12)	O2-Dy2-O28	85.85(13)
O5-Dy1-O20	145.91(15)	O2-Dy2-O25	123.63(13)
O5-Dy1-O13	87.74(13)	O2-Dy2-O22	154.41(12)
O5-Dy1-O19	154.64(13)	O10-Dy2-O2	86.04(12)
O9-Dy1-O16	81.42(14)	O10-Dy2-O29	156.43(11)
O9-Dy1-O17	84.73(13)	O10-Dy2-O23	123.18(14)
O9-Dy1-O14	156.98(13)	O10-Dy2-O26	79.71(13)
O9-Dy1-O20	123.70(16)	O10-Dy2-O28	146.94(14)
O9-Dy1-O13	148.00(16)	O10-Dy2-O25	86.15(13)
O9-Dy1-O19	72.92(15)	O10-Dy2-O22	72.44(12)
O16-Dy1-O17	50.28(14)	O29-Dy2-O28	50.09(13)
O16-Dy1-O14	111.32(12)	O23-Dy2-O29	69.56(14)
O16-Dy1-O20	120.02(13)	O23-Dy2-O28	75.63(15)
O16-Dy1-O13	66.84(14)	O26-Dy2-O29	112.16(13)

O16-Dy1-O19	117.09(14)	O26-Dy2-O23	120.66(12)
O17-Dy1-O14	118.24(13)	O26-Dy2-O28	67.26(14)
O20-Dy1-O17	76.51(15)	O25-Dy2-O29	117.25(13)
O20-Dy1-O14	67.67(15)	O25-Dy2-O23	75.16(14)
O20-Dy1-O13	72.76(16)	O25-Dy2-O26	50.54(13)
O20-Dy1-O19	50.80(15)	O25-Dy2-O28	72.06(15)
O13-Dy1-O17	72.19(15)	O22-Dy2-O29	116.59(13)
O13-Dy1-O14	50.27(13)	O22-Dy2-O23	50.75(14)
O19-Dy1-O17	70.62(16)	O22-Dy2-O26	114.95(13)
O19-Dy1-O14	114.35(14)	O22-Dy2-O28	119.75(13)
O19-Dy1-O13	117.41(15)	O22-Dy2-O25	69.69(14)

Table 4.4. Selected bond lengths (Å) and bond angle (deg) parameters of compound **4.2**

Ho1-O3	2.220(6)	Ho2-O4	2.240(5)
Ho1-O5	2.232(5)	Ho2-O2	2.243(5)
Ho1-O16	2.440(6)	Ho2-O6	2.274(6)
Ho1-O1	2.229(6)	Ho2-O28	2.503(6)
Ho1-O17	2.533(6)	Ho2-O26	2.493(6)
Ho1-O13	2.490(7)	Ho2-O29	2.526(6)
Ho1-O19	2.504(6)	Ho2-O22	2.484(6)
Ho1-O20	2.519(6)	Ho2-O25	2.501(6)
Ho1-O14	2.502(6)	Ho2-O23	2.513(6)
O3-Ho1-O5	83.87(19)	O4-Ho2-O2	85.98(18)
O3-Ho1-O16	155.05(18)	O4-Ho2-O6	86.2(2)
O3-Ho1-O1	85.6(2)	O4-Ho2-O28	77.83(19)
O3-Ho1-O17	149.8(3)	O4-Ho2-O26	73.1(2)
O3-Ho1-O13	85.3(2)	O4-Ho2-O29	86.0(2)
O3-Ho1-O19	125.5(2)	O4-Ho2-O22	148.4(2)
O3-Ho1-O20	75.0(2)	O4-Ho2-O25	124.7(2)
O3-Ho1-O14	78.8(2)	O4-Ho2-O23	154.15(19)
O5-Ho1-O16	74.5(2)	O2-Ho2-O6	87.43(19)
O5-Ho1-O17	124.2(3)	O2-Ho2-O28	156.27(19)
O5-Ho1-O13	144.3(2)	O2-Ho2-O26	79.5(2)
O5-Ho1-O19	87.8(2)	O2-Ho2-O29	147.2(2)
O5-Ho1-O20	77.75(19)	O2-Ho2-O22	123.1(2)
O5-Ho1-O14	155.4(2)	O2-Ho2-O25	85.5(2)
O16-Ho1-O17	49.7(2)	O2-Ho2-O23	72.74(19)
O16-Ho1-O13	119.5(2)	O6-Ho2-O28	74.4(2)
O16-Ho1-O19	66.8(2)	O6-Ho2-O26	156.10(18)
O16-Ho1-O20	111.4(2)	O6-Ho2-O29	123.6(2)
O16-Ho1-O14	117.1(2)	O6-Ho2-O22	83.4(2)
O1-Ho1-O5	87.35(19)	O6-Ho2-O25	147.6(2)
O1-Ho1-O16	81.2(2)	O6-Ho2-O23	78.5(2)
O1-Ho1-O17	85.0(2)	O28-Ho2-O29	49.4(2)
O1-Ho1-O13	125.6(2)	O28-Ho2-O23	117.0(2)
O1-Ho1-O19	147.7(3)	O26-Ho2-O28	111.5(2)
O1-Ho1-O20	156.6(2)	O26-Ho2-O29	67.8(2)

O1-Ho1-O14	74.0(3)	O26-Ho2-O25	51.6(2)
O13-Ho1-O17	77.1(3)	O26-Ho2-O23	115.7(2)
O13-Ho1-O19	71.3(3)	O22-Ho2-O28	70.6(2)
O13-Ho1-O20	66.6(2)	O22-Ho2-O26	120.5(2)
O13-Ho1-O14	51.6(2)	O22-Ho2-O29	75.3(2)
O19-Ho1-O17	71.7(2)	O22-Ho2-O25	74.2(2)
O19-Ho1-O20	50.6(2)	O22-Ho2-O23	50.4(2)
O20-Ho1-O17	118.4(2)	O25-Ho2-O28	118.0(2)
O14-Ho1-O17	71.0(3)	O25-Ho2-O29	73.3(2)
O14-Ho1-O19	116.5(2)	O25-Ho2-O23	69.1(2)
O14-Ho1-O20	113.9(2)	O23-Ho2-O29	119.9(2)

Table 4.5. Selected bond lengths (Å) and bond angle (deg) parameters of compound **4.3**

Nd1-O1	2.309(4)	Nd2-O6	2.316(5)
Nd1-O5	2.353(5)	Nd2-O2	2.325(5)
Nd1-O3	2.328(5)	Nd2-O13	2.542(6)
Nd1-O25	2.578(6)	Nd2-O20	2.549(5)
Nd1-O22	2.575(6)	Nd2-O14	2.576(6)
Nd1-O28	2.577(5)	Nd2-O4	2.303(5)
Nd1-O26	2.610(6)	Nd2-O19	2.591(5)
Nd1-O29	2.582(5)	Nd2-O16	2.604(7)
Nd1-O23	2.556(7)	Nd2-O17	2.549(7)
O1-Nd1-O5	86.85(17)	O6-Nd2-O2	82.92(17)
O1-Nd1-O3	87.06(17)	O6-Nd2-O13	153.27(17)
O1-Nd1-O25	73.43(17)	O6-Nd2-O20	75.96(18)
O1-Nd1-O22	82.46(18)	O6-Nd2-O14	151.1(2)
O1-Nd1-O28	150.4(2)	O6-Nd2-O19	125.6(2)
O1-Nd1-O26	122.27(19)	O6-Nd2-O16	80.7(2)
O1-Nd1-O29	157.50(17)	O6-Nd2-O17	87.0(2)
O1-Nd1-O23	79.7(2)	O2-Nd2-O13	72.80(18)
O5-Nd1-O25	79.18(19)	O2-Nd2-O20	79.99(19)
O5-Nd1-O22	150.7(2)	O2-Nd2-O14	123.0(2)
O5-Nd1-O28	122.0(2)	O2-Nd2-O19	89.12(19)
O5-Nd1-O26	84.48(18)	O2-Nd2-O16	155.6(2)
O5-Nd1-O29	72.75(18)	O2-Nd2-O17	148.4(2)
O5-Nd1-O23	155.27(19)	O13-Nd2-O20	109.69(18)
O3-Nd1-O5	86.40(19)	O13-Nd2-O14	50.3(2)
O3-Nd1-O25	156.19(17)	O13-Nd2-O19	66.2(2)
O3-Nd1-O22	120.0(2)	O13-Nd2-O16	118.1(2)
O3-Nd1-O28	88.33(18)	O13-Nd2-O17	119.6(2)
O3-Nd1-O26	148.6(2)	O20-Nd2-O14	117.85(19)
O3-Nd1-O29	82.4(2)	O20-Nd2-O19	49.7(2)
O3-Nd1-O23	72.4(2)	O20-Nd2-O16	113.0(3)
O25-Nd1-O26	48.87(19)	O20-Nd2-O17	68.5(2)
O25-Nd1-O29	110.7(2)	O14-Nd2-O19	72.0(2)
O22-Nd1-O25	71.6(2)	O14-Nd2-O16	70.6(3)
O22-Nd1-O28	74.7(2)	O4-Nd2-O6	83.4(2)

O22-Nd1-O26	78.4(2)	O4-Nd2-O2	88.43(19)
O22-Nd1-O29	120.01(18)	O4-Nd2-O13	84.9(2)
O28-Nd1-O25	115.37(19)	O4-Nd2-O20	157.4(2)
O28-Nd1-O26	71.5(2)	O4-Nd2-O14	84.7(2)
O28-Nd1-O29	49.32(19)	O4-Nd2-O19	150.3(3)
O29-Nd1-O26	66.2(2)	O4-Nd2-O16	71.9(3)
O23-Nd1-O25	116.0(2)	O4-Nd2-O17	120.1(3)
O23-Nd1-O22	47.7(2)	O19-Nd2-O16	115.1(2)
O23-Nd1-O28	71.0(2)	O17-Nd2-O14	76.4(2)
O23-Nd1-O26	120.25(19)	O17-Nd2-O19	72.7(2)
O23-Nd1-O29	115.4(2)	O17-Nd2-O16	48.2(3)

Table 4.6. Selected bond lengths (Å) and bond angle (deg) parameters of compound **4.4**

Y1-O3	2.222(4)	Y2-O4	2.226(3)
Y1-O1	2.231(4)	Y2-O23	2.496(4)
Y1-O15	2.509(4)	Y2-O2	2.245(4)
Y1-O21	2.453(5)	Y2-O6	2.235(4)
Y1-O14	2.495(4)	Y2-O27	2.468(4)
Y1-O5	2.244(4)	Y2-O29	2.487(4)
Y1-O17	2.471(4)	Y2-O30	2.506(4)
Y1-O18	2.493(5)	Y2-O26	2.481(4)
Y1-O20	2.505(4)	Y2-O24	2.499(4)
O3-Y1-O1	84.60(13)	O4-Y2-O23	74.88(13)
O3-Y1-O15	78.31(13)	O4-Y2-O2	86.85(13)
O3-Y1-O21	74.47(14)	O4-Y2-O6	87.33(14)
O3-Y1-O14	88.04(15)	O4-Y2-O27	83.34(13)
O3-Y1-O5	87.46(14)	O4-Y2-O29	147.73(16)
O3-Y1-O17	145.40(18)	O4-Y2-O30	156.66(13)
O3-Y1-O18	154.71(15)	O4-Y2-O26	78.12(14)
O3-Y1-O20	124.65(16)	O4-Y2-O24	125.28(16)
O1-Y1-O15	75.56(14)	O23-Y2-O30	111.72(14)
O1-Y1-O21	155.36(13)	O23-Y2-O24	50.55(15)
O1-Y1-O14	125.88(17)	O2-Y2-O23	78.50(14)
O1-Y1-O5	85.53(15)	O2-Y2-O27	147.94(18)
O1-Y1-O17	85.08(14)	O2-Y2-O29	123.83(15)
O1-Y1-O18	78.27(15)	O2-Y2-O30	73.23(14)
O1-Y1-O20	148.76(17)	O2-Y2-O26	154.17(14)
O21-Y1-O15	111.79(14)	O2-Y2-O24	86.20(14)
O21-Y1-O14	67.15(16)	O6-Y2-O23	157.05(13)
O21-Y1-O17	119.55(14)	O6-Y2-O2	86.29(14)
O21-Y1-O18	116.43(17)	O6-Y2-O27	123.47(17)
O21-Y1-O20	50.20(16)	O6-Y2-O29	85.23(14)
O14-Y1-O15	50.49(15)	O6-Y2-O30	79.53(15)
O14-Y1-O20	71.27(17)	O6-Y2-O26	72.28(15)
O5-Y1-O15	157.20(14)	O6-Y2-O24	145.98(17)
O5-Y1-O21	80.77(16)	O27-Y2-O23	69.48(17)
O5-Y1-O14	147.63(18)	O27-Y2-O29	74.90(16)

O5-Y1-O17	124.47(19)	O27-Y2-O30	120.00(14)
O5-Y1-O18	72.89(17)	O27-Y2-O26	51.22(16)
O5-Y1-O20	85.22(15)	O27-Y2-O24	75.02(16)
O17-Y1-O15	67.14(17)	O29-Y2-O23	117.52(14)
O17-Y1-O14	71.78(18)	O29-Y2-O30	50.62(15)
O17-Y1-O18	51.61(18)	O29-Y2-O24	71.78(17)
O17-Y1-O20	75.85(16)	O26-Y2-O23	116.71(15)
O18-Y1-O15	114.52(16)	O26-Y2-O29	69.70(16)
O18-Y1-O14	117.08(16)	O26-Y2-O30	115.27(15)
O18-Y1-O20	70.49(18)	O26-Y2-O24	119.62(14)
O20-Y1-O15	117.52(14)	O24-Y2-O30	66.54(16)

Table 4.7. Selected bond lengths (Å) and bond angle (deg) parameters of compound **4.5**

Nd1-O1[1]	2.603(4)	Nd1-O2	2.519(4)
Nd1-O1	2.603(4)	Nd2-O5[2]	2.219(5)
Nd1-O1[2]	2.603(4)	Nd2-O5[3]	2.219(5)
Nd1-O4[2]	2.339(4)	Nd2-O5[1]	2.219(5)
Nd1-O4[1]	2.339(4)	Nd2-O5[4]	2.219(5)
Nd1-O4	2.339(4)	Nd2-O5[5]	2.219(5)
Nd1-O2[1]	2.519(4)	Nd2-O5	2.219(5)
Nd1-O2[2]	2.519(4)		

[1]+Y-X,1-X,+Z; [2]1-Y,1+X-Y,+Z; [3]2/3-Y+X,1/3+X,1/3-Z; [4]-1/3+Y,1/3-X+Y,1/3-Z; [5]2/3-X,4/3-Y,1/3-Z

O1[1]-Nd1-O1[2]	113.55(8)	O2[2]-Nd1-O1	118.12(16)
O1[2]-Nd1-O1	113.55(8)	O2[2]-Nd1-O1[2]	49.21(14)
O1[1]-Nd1-O1	113.55(8)	O2[1]-Nd1-O1[2]	118.12(16)
O4-Nd1-O1[2]	75.68(14)	O2-Nd1-O1[2]	68.12(16)
O4[2]-Nd1-O1	158.07(15)	O2[2]-Nd1-O1[1]	68.12(16)
O4-Nd1-O1	77.63(14)	O2-Nd1-O1[1]	118.12(16)
O4-Nd1-O1[1]	158.07(15)	O2[1]-Nd1-O2	74.61(19)
O4[1]-Nd1-O1[1]	77.63(14)	O2[1]-Nd1-O2[2]	74.60(19)
O4[1]-Nd1-O1[2]	158.07(15)	O2[2]-Nd1-O2	74.61(19)
O4[1]-Nd1-O1	75.69(14)	O5[1]-Nd2-O5[3]	94.60(18)
O4[2]-Nd1-O1[2]	77.63(14)	O5[1]-Nd2-O5[4]	94.60(18)
O4[2]-Nd1-O1[1]	75.69(14)	O5-Nd2-O5[3]	180
O4[2]-Nd1-O4[1]	87.67(16)	O5[2]-Nd2-O5[3]	94.60(18)
O4[2]-Nd1-O4	87.67(16)	O5[1]-Nd2-O5	85.40(18)
O4[1]-Nd1-O4	87.67(16)	O5[2]-Nd2-O5[4]	180
O4[1]-Nd1-O2	124.82(16)	O5[3]-Nd2-O5[5]	85.40(18)
O4-Nd1-O2[2]	124.82(16)	O5-Nd2-O5[4]	94.60(18)
O4[2]-Nd1-O2[2]	83.63(17)	O5[3]-Nd2-O5[4]	85.40(18)
O4[1]-Nd1-O2[1]	83.63(17)	O5[1]-Nd2-O5[5]	180
O4[2]-Nd1-O2	145.75(16)	O5[4]-Nd2-O5[5]	85.40(18)
O4[1]-Nd1-O2[2]	145.75(16)	O5-Nd2-O5[5]	94.60(18)
O4[2]-Nd1-O2[1]	124.82(16)	O5[2]-Nd2-O5	85.40(18)
O4-Nd1-O2[1]	145.75(16)	O5[1]-Nd2-O5[2]	85.40(18)
O4-Nd1-O2	83.63(17)	O5[2]-Nd2-O5[5]	94.60(18)
O2[1]-Nd1-O1[1]	49.20(14)	O5[1]-Nd2-O5[3]	94.60(18)
O2-Nd1-O1	49.20(14)	O5[1]-Nd2-O5[4]	94.60(18)
O2[1]-Nd1-O1	68.13(16)		

Table 4.8. Selected bond lengths (Å) and bond angle (deg) parameters of compound **4.6**

Pr1-O1[1]	2.358(5)	Pr1-O6	2.589(6)
Pr1-O1[2]	2.358(5)	Pr1-O5[1]	2.534(6)
Pr1-O1	2.358(5)	Pr1-O5	2.534(6)
Pr1-O6[2]	2.589(6)	Pr1-O5[2]	2.534(6)
Pr1-O6[1]	2.589(6)	Pr2-O2	2.290(5)

[1]+Y-X,1-X,+Z; [2]1-Y,1+X-Y,+Z

O1[1]-Pr1-O1[2]	88.6(2)	O5[2]-Pr1-O6[2]	47.3(2)
O1[1]-Pr1-O1	88.6(2)	O5-Pr1-O6	47.3(2)
O1[2]-Pr1-O1	88.6(2)	O5-Pr1-O6[1]	118.0(2)
O1[2]-Pr1-O6[1]	75.8(2)	O5[1]-Pr1-O6[1]	47.3(2)
O1[1]-Pr1-O6[2]	159.6(2)	O5[1]-Pr1-O6	68.6(2)
O1[2]-Pr1-O6[2]	77.99(18)	O5[2]-Pr1-O6	118.0(2)
O1[1]-Pr1-O6	75.8(2)	O5[1]-Pr1-O6[2]	118.0(2)
O1[1]-Pr1-O6[1]	77.99(18)	O2[3]-Pr2-O2[2]	180.00(19)
O1-Pr1-O6	77.99(18)	O2-Pr2-O2[2]	84.6(2)
O1-Pr1-O6[2]	75.8(2)	O2[3]-Pr2-O2[1]	95.4(2)
O1-Pr1-O61	159.6(2)	O2[4]-Pr2-O2[2]	95.4(2)
O1[2]-Pr1-O6	159.6(2)	O2[4]-Pr2-O2[5]	84.6(2)
O1[1]-Pr1-O5	123.1(2)	O2[3]-Pr2-O2[4]	84.6(2)
O1[1]-Pr1-O5[1]	82.3(2)	O2[1]-Pr2-O2	84.6(2)
O1[1]-Pr1-O5[2]	146.5(2)	O2[5]-Pr2-O2	95.4(2)
O1[2]-Pr1-O5[2]	82.3(2)	O2[1]-Pr2-O2[2]	84.6(2)
O1-Pr1-O5[1]	146.5(2)	O2[1]-Pr2-O2[4]	95.4(2)
O1[2]-Pr1-O5[1]	123.1(2)	O2[4]-Pr2-O2	180
O1-Pr1-O5[2]	123.1(2)	O2[3]-Pr2-O2[5]	84.6(2)
O1[2]-Pr1-O5	146.5(2)	O2[5]-Pr2-O2[2]	95.4(2)
O1-Pr1-O5	82.3(2)	O2[1]-Pr2-O2[5]	180
O6[1]-Pr1-O6[2]	112.84(12)	O2[3]-Pr2-O2	95.4(2)
O6-Pr1-O6[2]	112.84(12)	O5[1]-Pr1-O5	76.1(3)
O6-Pr1-O6[1]	112.84(12)	O5-Pr1-O5[2]	76.1(3)
O5[2]-Pr1-O6[1]	68.6(2)	O5[1]-Pr1-O5[2]	76.1(3)
O5-Pr1-O6[2]	68.6(2)		

[1]+Y-X,1-X,+Z; [2]1-Y,1+X-Y,+Z; [3]2/3-X,4/3-Y,4/3-Z; [4]2/3-Y+X,1/3+X,4/3-Z; [5]-1/3+Y,1/3-X+Y,4/3-Z

Table 4.9. Selected bond lengths (Å) and bond angle (deg) parameters of compound **4.7**

Dy1-O5[1]	2.424(11)	Dy1-O6	2.512(11)
Dy1-O5	2.424(11)	Dy2-O2[3]	2.214(12)
Dy1-O5[2]	2.424(11)	Dy2-O2[1]	2.214(12)
Dy1-O1[1]	2.289(9)	Dy2-O2[4]	2.214(12)
Dy1-O1	2.289(9)	Dy2-O2[5]	2.214(12)
Dy1-O1[2]	2.289(9)	Dy2-O2	2.214(12)
Dy1-O6[1]	2.512(11)	Dy2-O2[2]	2.214(12)
Dy1-O6[2]	2.512(11)		

[1]1-Y,+X-Y,+Z; [2]1+Y-X,1-X,+Z; [3]1/3-Y+X,-1/3+X,2/3-Z; [4]1/3+Y,2/3-X+Y,2/3-Z; [5]4/3-X,2/3-Y,2/3-Z

O5[1]-Dy1-O5[2]	77.2(5)	O1[1]-Dy1-O6[2]	76.0(4)
O5[1]-Dy1-O5	77.2(5)	O1-Dy1-O6[2]	156.2(4)
O5[2]-Dy1-O5	77.2(5)	O1-Dy1-O6[1]	76.0(4)
O5[2]-Dy1-O6[1]	120.5(5)	O1[2]-Dy1-O6	76.0(4)
O5[1]-Dy1-O6	120.5(5)	O1-Dy1-O6	77.4(4)
O5[2]-Dy1-O6	49.3(4)	O1[1]-Dy1-O6	156.2(4)

O5[1]-Dy1-O6[2]	49.3(4)	O1[1]-Dy1-O6[1]	77.4(4)
O5[1]-Dy1-O6[1]	68.4(4)	O6[2]-Dy1-O6[1]	114.1(2)
O5-Dy1-O62	120.5(5)	O6[1]-Dy1-O6	114.1(2)
O5-Dy1-O6	68.4(4)	O6[2]-Dy1-O6	114.1(2)
O5-Dy1-O6[1]	49.3(4)	O2[1]-Dy2-O2[2]	84.5(4)
O5[2]-Dy1-O6[2]	68.4(4)	O2[3]-Dy2-O2[1]	95.5(4)
O1[1]-Dy1-O5[2]	144.2(5)	O2[4]-Dy2-O2[3]	84.5(4)
O1[2]-Dy1-O5	144.2(5)	O2[4]-Dy2-O2	95.5(4)
O1[1]-Dy1-O5	126.7(4)	O2[5]-Dy2-O2[2]	95.5(4)
O1-Dy1-O5[1]	144.2(5)	O2[5]-Dy2-O2[3]	84.5(4)
O1[1]-Dy1-O5[1]	82.7(5)	O2[4]-Dy2-O2[1]	180
O1[2]-Dy1-O5[1]	126.7(4)	O2[3]-Dy2-O2[2]	180
O1-Dy1-O5	82.7(5)	O2[4]-Dy2-O2[2]	95.5(4)
O1-Dy1-O5[2]	126.7(4)	O2[5]-Dy2-O2	180
O1[2]-Dy1-O5[2]	82.7(5)	O2-Dy2-O22	84.5(4)
O1-Dy1-O1[2]	86.1(5)	O2[4]-Dy2-O2[5]	84.5(4)
O1[1]-Dy1-O1[2]	86.1(5)	O2[3]-Dy2-O2	95.5(4)
O1[1]-Dy1-O1	86.1(5)	O2[1]-Dy2-O2	84.5(4)
O1[2]-Dy1-O6[1]	156.2(4)	O2[5]-Dy2-O2[1]	95.5(4)
O1[2]-Dy1-O6[2]	77.4(4)		

[1]1-Y,+X-Y,+Z; [2]1+Y-X,1-X,+Z; [3]1/3-Y+X,-1/3+X,2/3-Z; [4]1/3+Y,2/3-X+Y,2/3-Z; [5]4/3-X,2/3-Y,2/3-Z

Table 4.10. Selected bond lengths (Å) and bond angle (deg) parameters of compound **4.8**

Nd1-O2[1]	2.219(5)	La2-O1	2.368(5)
Nd1-O2[2]	2.219(5)	La2-O5[2]	2.623(6)
Nd1-O2	2.219(5)	La2-O5	2.623(6)
Nd1-O2[3]	2.219(5)	La2-O5[3]	2.623(6)
Nd1-O2[4]	2.219(5)	La2-O6[3]	2.552(6)
Nd1-O2[5]	2.219(5)	La2-O6	2.552(6)
La2-O1[2]	2.368(5)	La2-O6[2]	2.552(6)
La2-O1[3]	2.368(5)		

[1]-1/3+Y,-2/3-X+Y,1/3-Z; [2]-1-Y,+X-Y,+Z; [3]-1+Y-X,-1-X,+Z; [4]-4/3-X,-2/3-Y,1/3-Z; [5]-1/3-Y+X,1/3+X,1/3-Z

O2[1]-Nd1-O2[2]	85.2(2)	O1[5]-La2-O5[5]	158.7(2)
O2[3]-Nd1-O2[4]	94.8(2)	O1[4]-La2-O6	125.0(2)
O2[1]-Nd1-O2[4]	94.8(2)	O1[5]-La2-O6[5]	145.5(2)
O2-Nd1-O2[4]	85.2(2)	O1[5]-La2-O6	83.1(2)
O2[2]-Nd1-O2[5]	94.8(2)	O1-La2-O6[5]	125.0(2)
O2[3]-Nd1-O2[5]	94.8(2)	O1[5]-La2-O6[4]	125.0(2)
O2[1]-Nd1-O2[3]	85.2(2)	O1[4]-La2-O6[5]	83.1(2)
O2[1]-Nd1-O2	94.8(2)	O1[4]-La2-O6[4]	145.5(2)
O2[2]-Nd1-O2[3]	85.2(2)	O1-La2-O6[4]	83.1(2)
O2[1]-Nd1-O2[5]	180	O1-La2-O6	145.5(2)
O2-Nd1-O2[3]	180	O5[4]-La2-O5	112.83(11)
O2[2]-Nd1-O2	94.8(2)	O5[5]-La2-O5	112.83(11)
O2-Nd1-O2[5]	85.2(2)	O5[4]-La2-O5[5]	112.83(11)
O2[2]-Nd1-O2[4]	180	O6[5]-La2-O5	67.5(2)
O2[4]-Nd1-O2[5]	85.2(2)	O6[5]-La2-O5[5]	48.3(2)
O1-La2-O1[5]	87.3(2)	O6[4]-La2-O5[4]	48.3(2)
O1-La2-O1[4]	87.3(2)	O6[4]-La2-O5	118.0(2)
O1[5]-La2-O1[4]	87.3(2)	O6[5]-La2-O5[4]	118.0(2)
O1-La2-O5[4]	78.10(18)	O(6)-La(2)-O5[5]	118.0(2)
O1[4]-La2-O5[5]	78.10(18)	O6-La2-O5[4]	67.5(2)
O1[5]-La2-O5[4]	76.67(19)	O6-La2-O5	48.3(2)

O1[5]-La2-O5	78.10(18)	O6[4]-La2-O5[5]	67.5(2)
O1-La2-O5[5]	76.67(19)	O6[4]-La2-O6[5]	75.7(3)
O1[4]-La2-O5[4]	158.7(2)	O6[5]-La2-O6	75.7(3)
O1[4]-La2-O5	76.67(19)	O6[4]-La2-O6	75.7(3)
O1-La2-O5	158.7(2)		

[1]-1/3+Y,-2/3-X+Y,1/3-Z; [2]-1/3-Y+X,1/3+X,1/3-Z; [3]-4/3-X,-2/3-Y,1/3-Z; [4]-1+Y-X,-1-X,+Z; [5]-1-Y,+X-Y,+Z

Table 4.11. Shape calculation of compound **4.1**

S.No.	Geometry			Cshm value for Dy1	Cshm value for Dy2
1	EP-9	D9h	Enneagon	33.912	33.278
2	OPY-9	C8v	Octagonal pyramid	24.030	24.341
3	HBPY-9	D7h	Heptagonal bipyramid	18.490	18.539
4	JTC-9	C3v	Johnson triangular cupola J3	12.943	12.838
5	JCCU-9	C4v	Capped cube J8	10.459	10.476
6	CCU-9	C4v	Spherical-relaxed capped cube	9.289	9.270
7	JCSAPR-9	C4v	Capped square antiprism J10	3.474	3.577
8	CSAPR-9	C4v	Spherical capped square antiprism	2.516	2.663
9	JTCTPR-9	D3h	Tricapped trigonal prism J51	3.148	3.080
10	**TCTPR-9**	**D3h**	**Spherical tricapped trigonal prism**	**2.390**	**2.448**
11	JTDIC-9	C3v	Tridiminished icosahedron J63	11.498	11.658
12	HH-9	C2v	Hula-hoop	12.552	12.562
13	MFF-9	Cs	Muffin	2.605	2.647

Table 4.12. Shape calculation of compound **4.2**

S.No.	Geometry			Cshm value for Ho1	Cshm value for Ho2
1	EP-9	D9h	Enneagon	34.282	34.282
2	OPY-9	C8v	Octagonal pyramid	24.080	24.080
3	HBPY-9	D7h	Heptagonal bipyramid	18.743	18.743
4	JTC-9	C3v	Johnson triangular cupola J3	13.160	13.160
5	JCCU-9	C4v	Capped cube J8	10.339	10.339
6	CCU-9	C4v	Spherical-relaxed capped cube	9.191	9.191
7	JCSAPR-9	C4v	Capped square antiprism J10	3.460	3.460
8	CSAPR-9	C4v	Spherical capped square antiprism	2.461	2.461
9	JTCTPR-9	D3h	Tricapped trigonal prism J51	3.166	3.166
10	**TCTPR-9**	**D3h**	**Spherical tricapped trigonal prism**	**2.310**	**2.310**
11	JTDIC-9	C3v	Tridiminished icosahedron J63	11.563	11.563
12	HH-9	C2v	Hula-hoop	12.553	12.553
13	MFF-9	Cs	Muffin	2.510	2.510

Table 4.13. Shape calculation of compound **4.3**

S.No.	Geometry			Cshm value for Nd1	Cshm value for Nd2
1	EP-9	D9h	Enneagon	32.679	34.062
2	OPY-9	C8v	Octagonal pyramid	24.274	24.563
3	HBPY-9	D7h	Heptagonal bipyramid	18.039	18.405
4	JTC-9	C3v	Johnson triangular cupola J3	12.589	12.781
5	JCCU-9	C4v	Capped cube J8	10.275	10.548
6	CCU-9	C4v	Spherical-relaxed capped cube	8.969	9.153
7	JCSAPR-9	C4v	Capped square antiprism J10	4.154	3.748
8	CSAPR-9	C4v	Spherical capped square antiprism	3.188	2.881
9	JTCTPR-9	D3h	Tricapped trigonal prism J51	3.651	3.718
10	**TCTPR-9**	**D3h**	**Spherical tricapped trigonal prism**	**2.993**	**2.786**
11	JTDIC-9	C3v	Tridiminished icosahedron J63	11.351	10.710
12	HH-9	C2v	Hula-hoop	12.386	11.806
13	MFF-9	Cs	Muffin	3.172	2.791

Table 4.14. Shape calculation of compound **4.4**

S.No.	Geometry			Cshm value for Y1	Cshm value for Y2
1	EP-9	D9h	Enneagon	34.256	33.325
2	OPY-9	C8v	Octagonal pyramid	24.084	24.106
3	HBPY-9	D7h	Heptagonal bipyramid	18.713	18.432
4	JTC-9	C3v	Johnson triangular cupola J3	13.312	12.980
5	JCCU-9	C4v	Capped cube J8	10.413	10.434
6	CCU-9	C4v	Spherical-relaxed capped cube	9.243	9.267
7	JCSAPR-9	C4v	Capped square antiprism J10	3.421	3.441
8	CSAPR-9	C4v	Spherical capped square antiprism	2.464	2.552
9	JTCTPR-9	D3h	Tricapped trigonal prism J51	3.112	2.973
10	**TCTPR-9**	**D3h**	**Spherical tricapped trigonal prism**	**2.283**	**2.394**
11	JTDIC-9	C3v	Tridiminished icosahedron J63	11.575	11.790
12	HH-9	C2v	Hula-hoop	12.704	12.614
13	MFF-9	Cs	Muffin	2.535	2.596

Table 4.15. Shape calculation of compound **4.5**

S.No.	Geometry			Cshm value for Nd1
1	EP-9	D9h	Enneagon	33.007
2	OPY-9	C8v	Octagonal pyramid	24.358
3	HBPY-9	D7h	Heptagonal bipyramid	19.048
4	JTC-9	C3v	Johnson triangular cupola J3	12.881
5	JCCU-9	C4v	Capped cube J8	10.884
6	CCU-9	C4v	Spherical-relaxed capped cube	9.783
7	JCSAPR-9	C4v	Capped square antiprism J10	3.917
8	CSAPR-9	C4v	Spherical capped square antiprism	3.028
9	JTCTPR-9	D3h	Tricapped trigonal prism J51	3.042
10	**TCTPR-9**	**D3h**	**Spherical tricapped trigonal prism**	**2.715**
11	JTDIC-9	C3v	Tridiminished icosahedron J63	12.815

12	HH-9	C2v	Hula-hoop	13.187
13	MFF-9	Cs	Muffin	2.985

Table 4.16. Shape calculation of compound **4.5**

S.No.	Geometry			Cshm value for Nd2
1	HP-6	1 D6h	Hexagon	31.742
2	PPY-6	2 C5v	Pentagonal pyramid	29.639
3	**OC-6**	**3 Oh**	**Octahedron**	**0.308**
4	TPR-6	4 D3h	Trigonal prism	15.403
5	JPPY-6	5 C5v	Johnson pentagonal pyramid J2	32.971

Table 4.17. Shape calculation of compound **4.6**

S.No.	Geometry			Cshm value for Pr1
1	EP-9	D9h	Enneagon	32.097
2	OPY-9	C8v	Octagonal pyramid	24.138
3	HBPY-9	D7h	Heptagonal bipyramid	18.691
4	JTC-9	C3v	Johnson triangular cupola J3	12.591
5	JCCU-9	C4v	Capped cube J8	11.018
6	CCU-9	C4v	Spherical-relaxed capped cube	9.837
7	JCSAPR-9	C4v	Capped square antiprism J10	4.474
8	CSAPR-9	C4v	Spherical capped square antiprism	3.514
9	JTCTPR-9	D3h	Tricapped trigonal prism J51	3.573
10	**TCTPR-9**	**D3h**	**Spherical tricapped trigonal prism**	**3.296**
11	JTDIC-9	C3v	Tridiminished icosahedron J63	13.036
12	HH-9	C2v	Hula-hoop	12.992
13	MFF-9	Cs	Muffin	3.372

Table 4.18. Shape calculation of compound **4.6**

S.No.	Geometry			Cshm value for Pr2
1	HP-6	1 D6h	Hexagon	31.497
2	PPY-6	2 C5v	Pentagonal pyramid	29.543
3	**OC-6**	**3 Oh**	**Octahedron**	**0.425**
4	TPR-6	4 D3h	Trigonal prism	15.222
5	JPPY-6	5 C5v	Johnson pentagonal pyramid J2	32.827

Table 4.19. Shape calculation of compound **4.7**

S.No.	Geometry			Cshm value for Dy2
1	HP-6	1 D6h	Hexagon	31.468

2	PPY-6	2 C5v	Pentagonal pyramid	29.533
3	**OC-6**	**3 Oh**	**Octahedron**	**0.440**
4	TPR-6	4 D3h	Trigonal prism	15.200
5	JPPY-6	5 C5v	Johnson pentagonal pyramid J2	32.811

Table 4.20. Shape calculation of compound **4.7**

S.No.	Geometry			Cshm value for Dy1
1	EP-9	D9h	Enneagon	33.178
2	OPY-9	C8v	Octagonal pyramid	23.968
3	HBPY-9	D7h	Heptagonal bipyramid	19.429
4	JTC-9	C3v	Johnson triangular cupola J3	12.714
5	JCCU-9	C4v	Capped cube J8	11.175
6	CCU-9	C4v	Spherical-relaxed capped cube	10.078
7	JCSAPR-9	C4v	Capped square antiprism J10	3.924
8	CSAPR-9	C4v	Spherical capped square antiprism	3.019
9	JTCTPR-9	D3h	Tricapped trigonal prism J51	3.012
10	**TCTPR-9**	**D3h**	**Spherical tricapped trigonal prism**	**2.749**
11	JTDIC-9	C3v	Tridiminished icosahedron J63	13.334
12	HH-9	C2v	Hula-hoop	13.146
13	MFF-9	Cs	Muffin	2.996

Table 4.21. Shape calculation of compound **4.8**

S.No.	Geometry			Cshm value for La
1	EP-9	D9h	Enneagon	33.015
2	OPY-9	C8v	Octagonal pyramid	24.188
3	HBPY-9	D7h	Heptagonal bipyramid	19.159
4	JTC-9	C3v	Johnson triangular cupola J3	12.624
5	JCCU-9	C4v	Capped cube J8	11.126
6	CCU-9	C4v	Spherical-relaxed capped cube	9.980
7	JCSAPR-9	C4v	Capped square antiprism J10	4.195
8	CSAPR-9	C4v	Spherical capped square antiprism	3.261
9	JTCTPR-9	D3h	Tricapped trigonal prism J51	3.336
10	**TCTPR-9**	**D3h**	**Spherical tricapped trigonal prism**	**2.977**
11	JTDIC-9	C3v	Tridiminished icosahedron J63	13.131
12	HH-9	C2v	Hula-hoop	13.128
13	MFF-9	Cs	Muffin	3.139

Table 4.22. Shape calculation of compound **4.8**

S.No.	Geometry			Cshm value for Nd
1	HP-6	1 D6h	Hexagon	31.684
2	PPY-6	2 C5v	Pentagonal pyramid	29.616
3	**OC-6**	**3 Oh**	**Octahedron**	**0.333**

4	TPR-6	4 D3h	Trigonal prism	15.360
5	JPPY-6	5 C5v	Johnson pentagonal pyramid J2	32.936

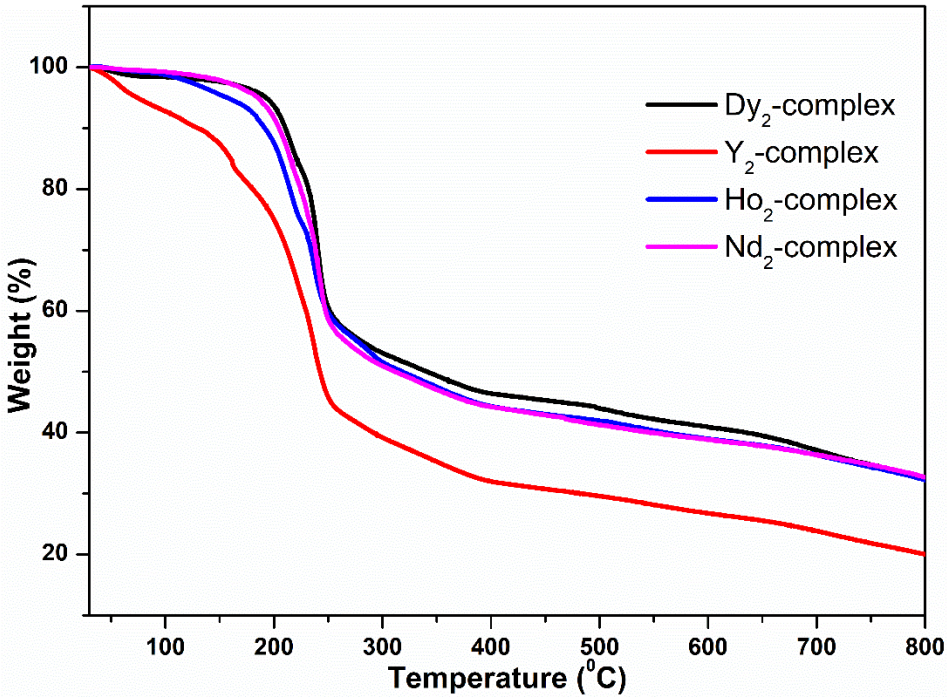

Figure 4.13. TGA of compound **4.1-4.4.**

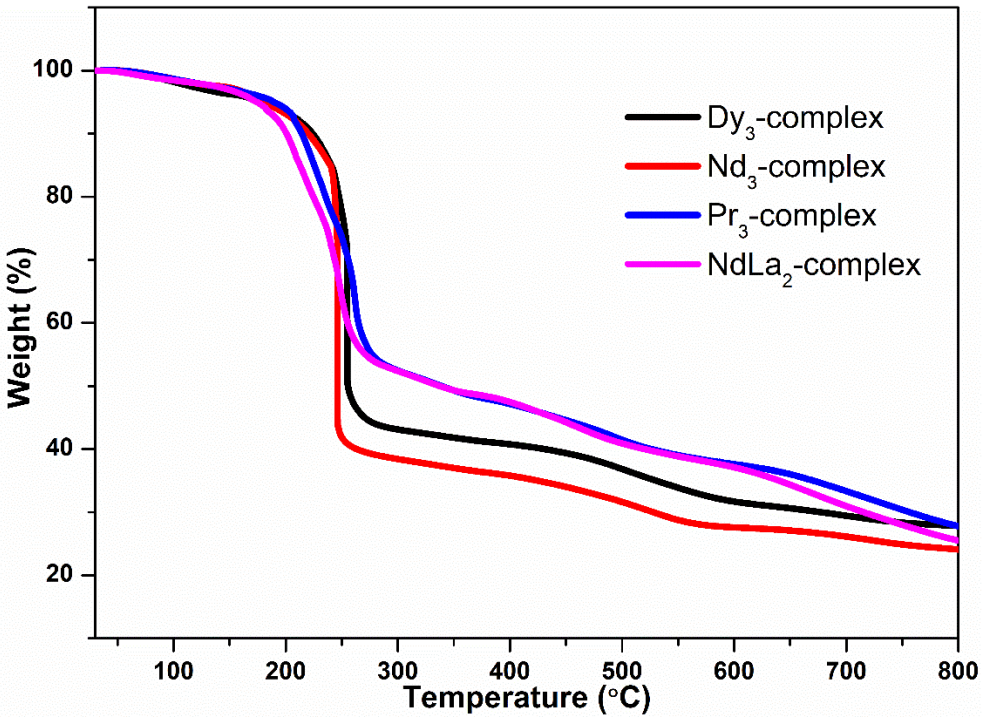

Figure 4.14. TGA of compound **4.5-4.8.**

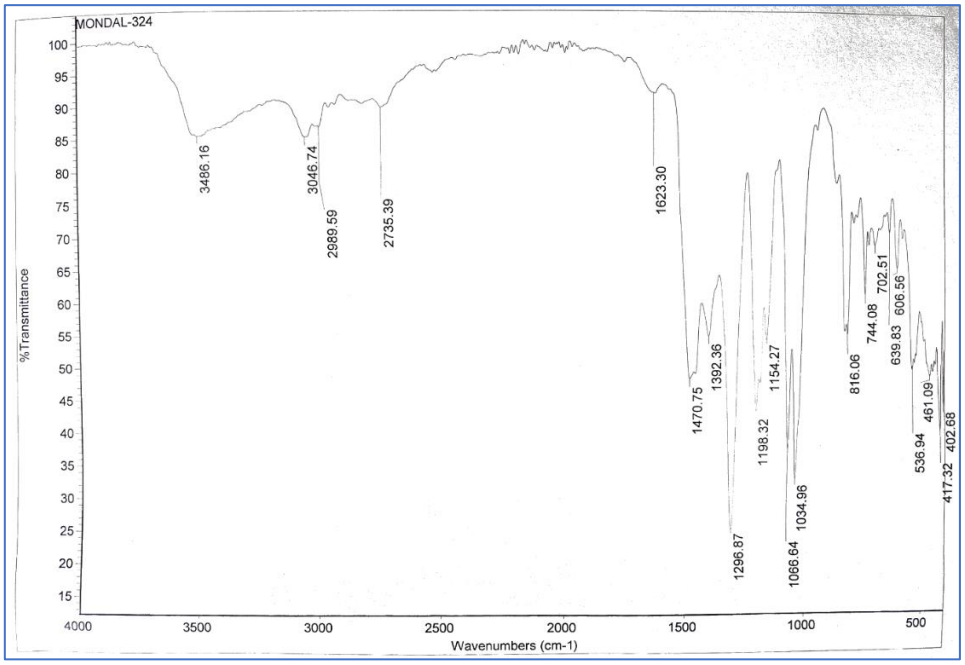

Figure 4.15. IR spectra of compound **4.1**

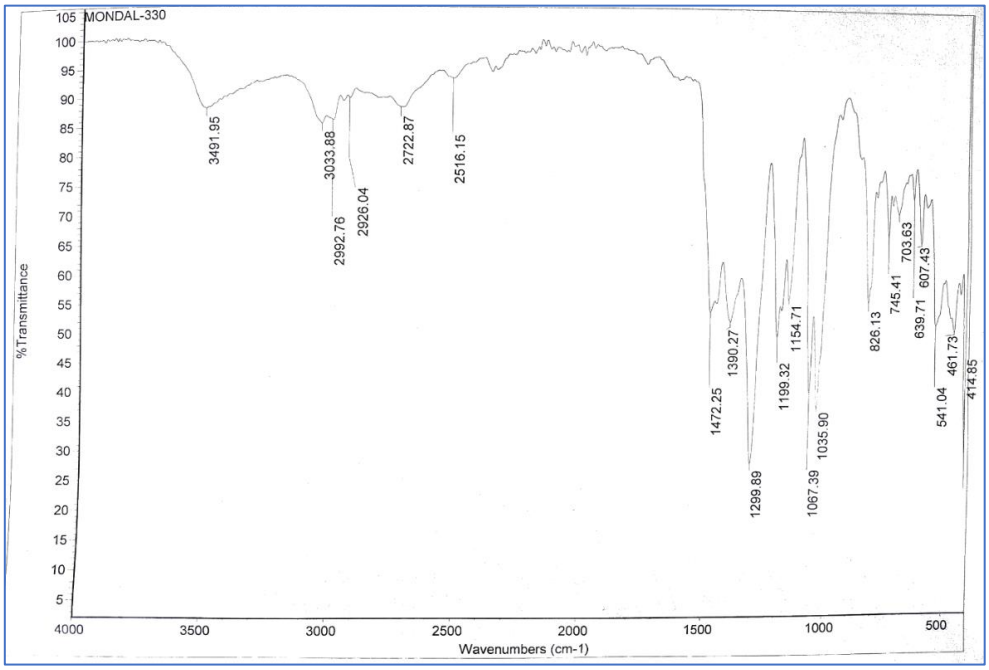

Figure 4.16. IR spectra of compound **4.2**

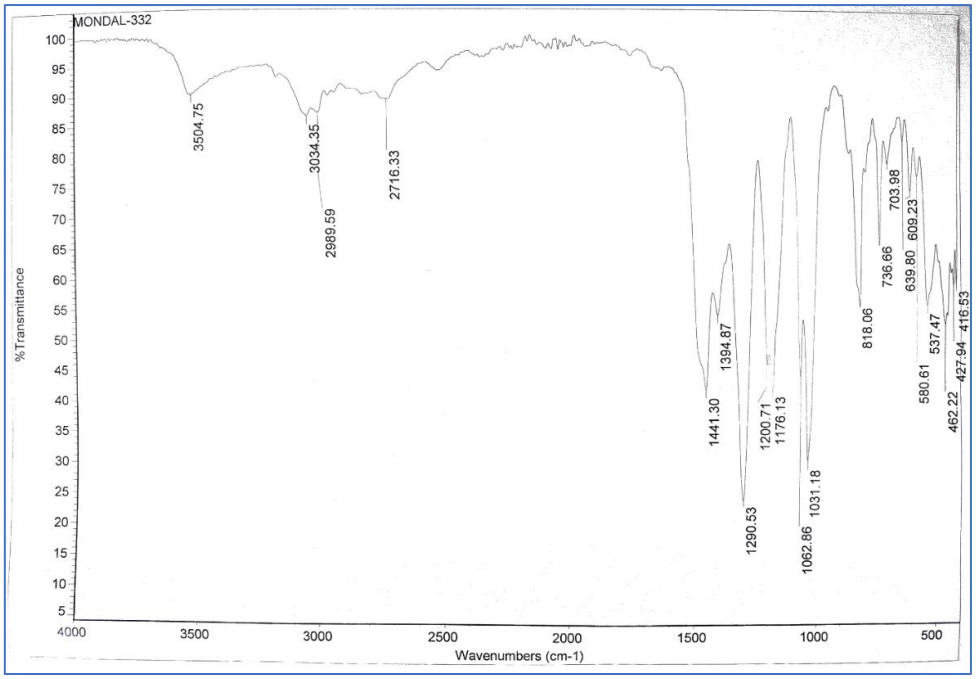

Figure 4.17. IR spectra of compound **4.3**

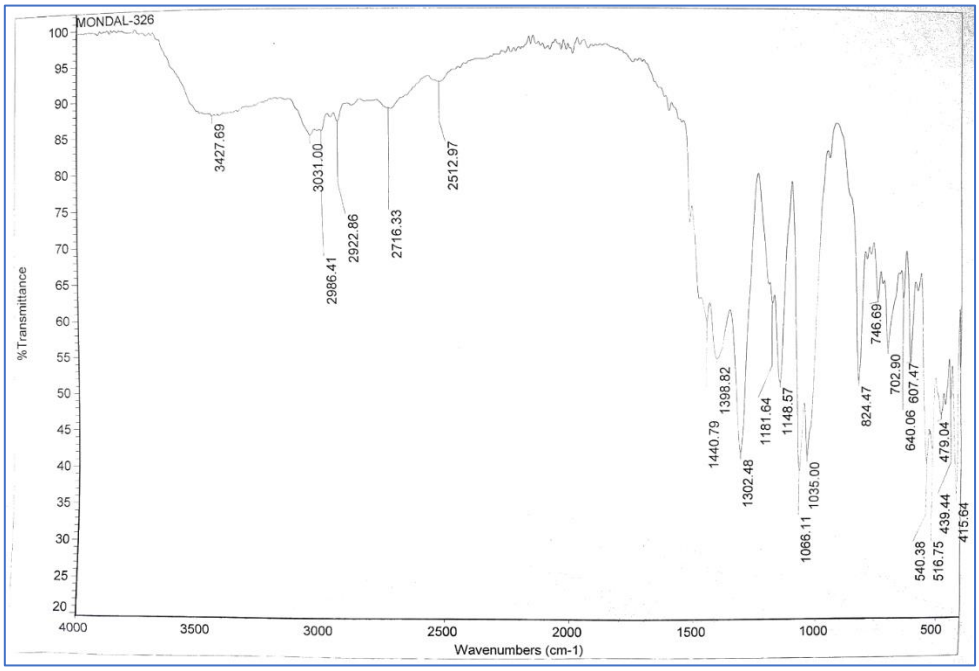

Figure 4.18. IR spectra of compound **4.4**

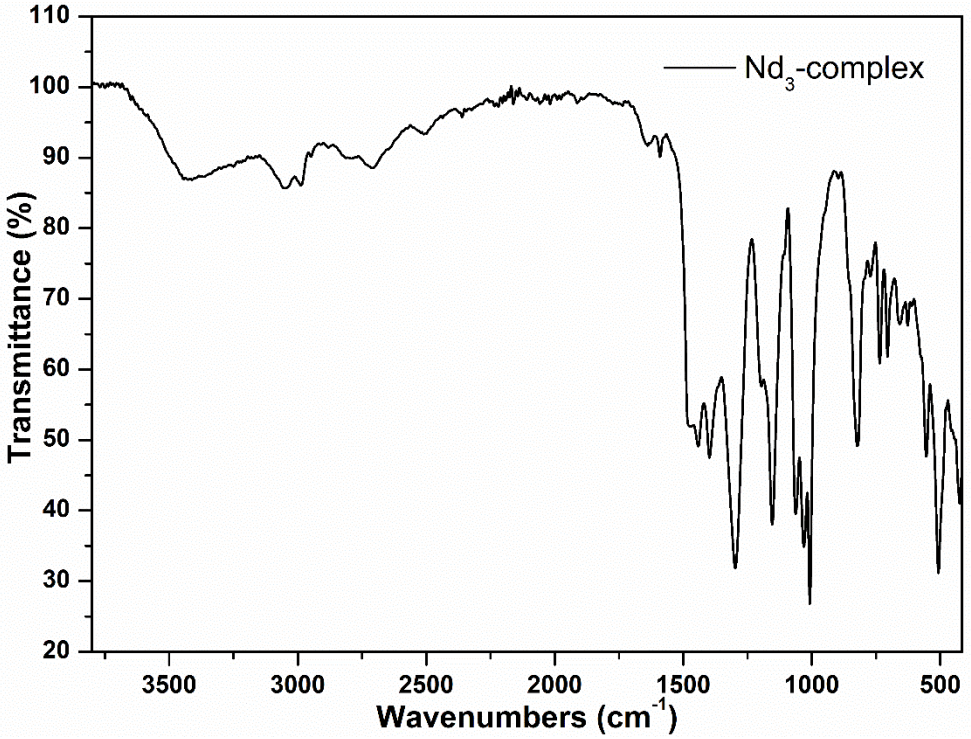

Figure 4.19. IR spectra of compound **4.5**

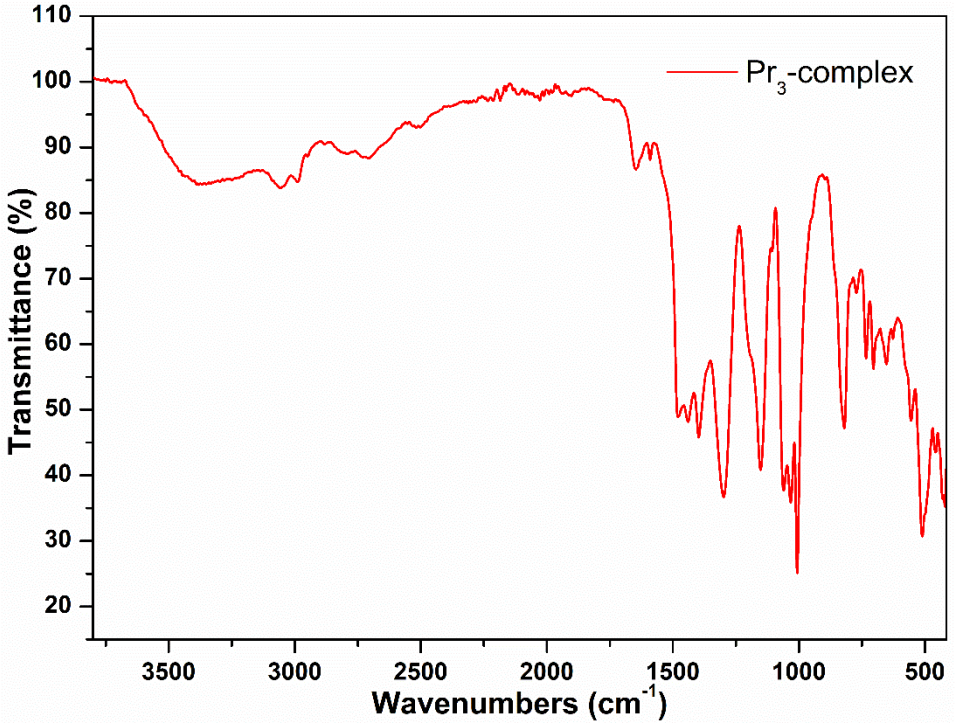

Figure 4.20. IR spectra of compound **4.6**

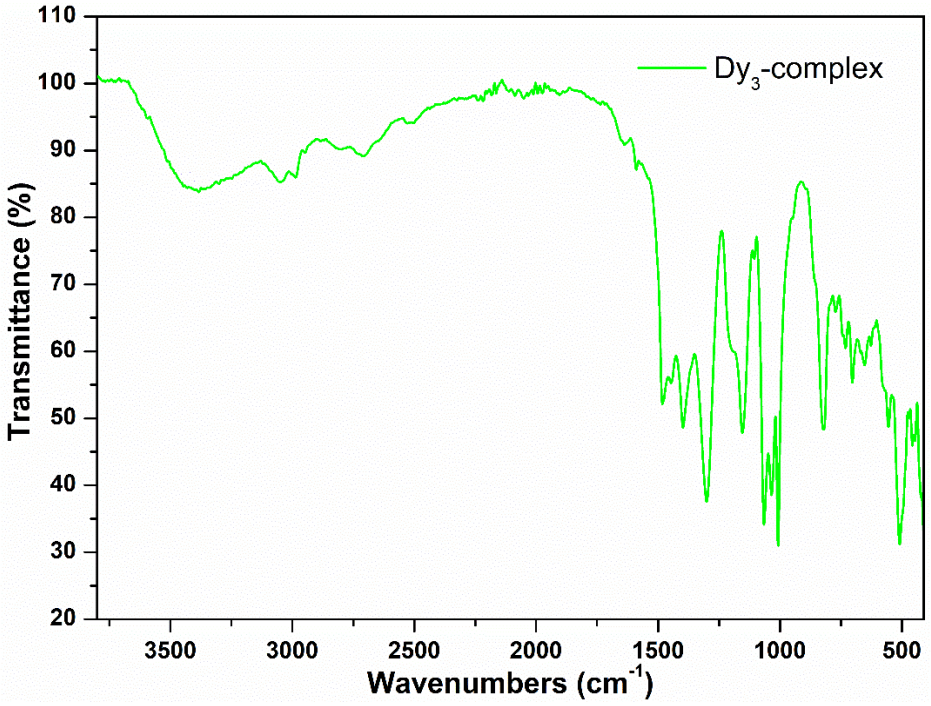

Figure 4.21. IR spectra of compound **4.7**

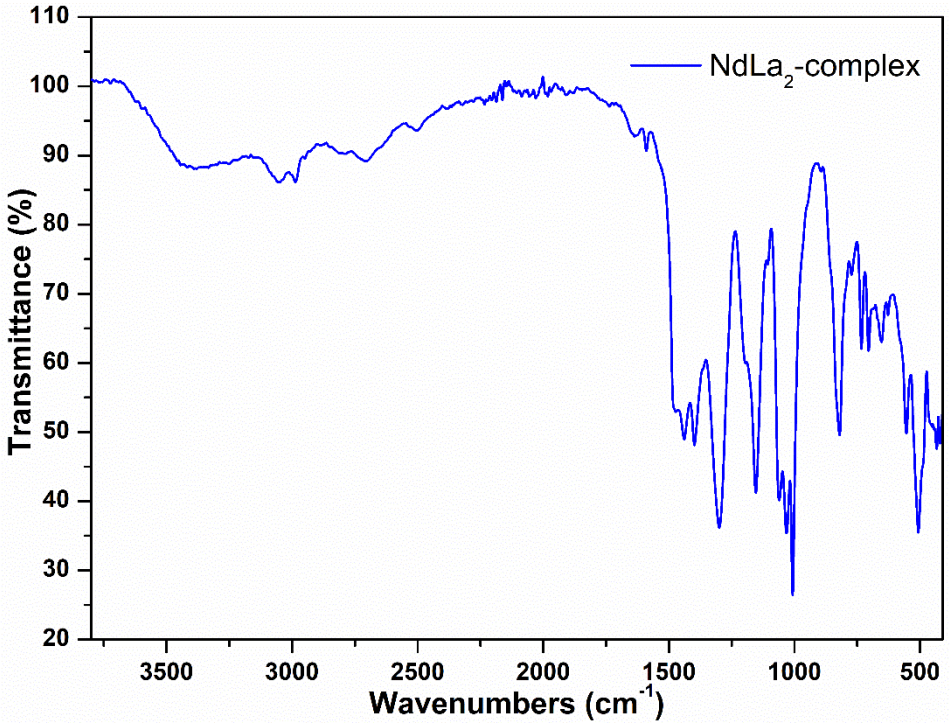

Figure 4.22. IR spectra of compound **4.8**

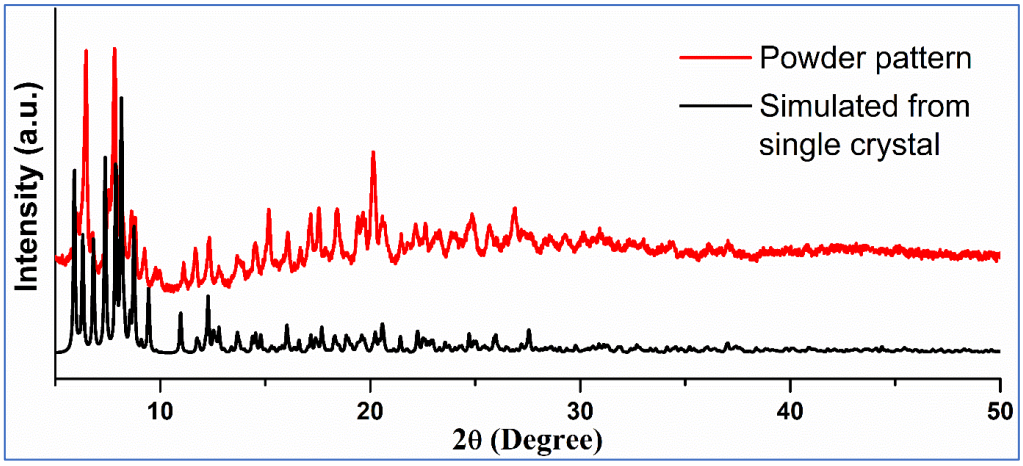

Figure 4.23. Powder X-ray diffraction pattern of a bulk sample of **4.1** compared to the simulated powder pattern extracted from single crystal diffraction data.

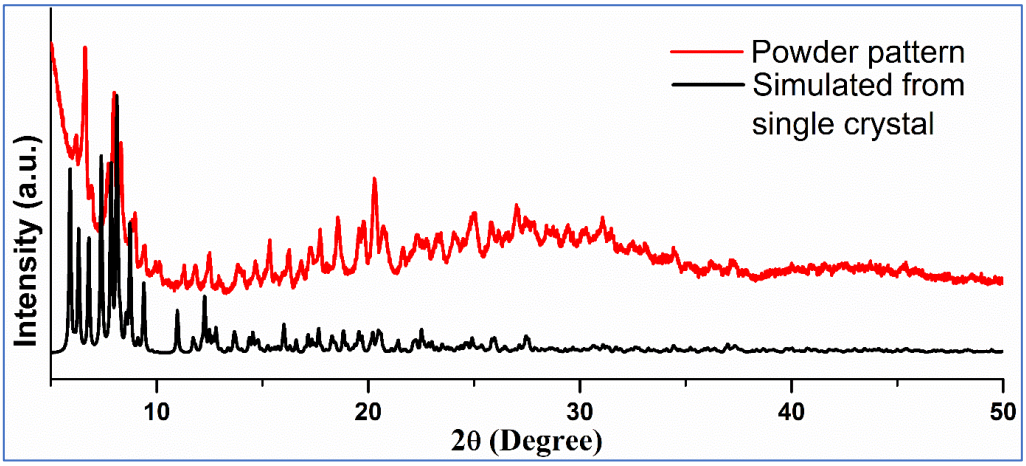

Figure 4.24. Powder X-ray diffraction pattern of a bulk sample of **4.2** compared to the simulated powder pattern extracted from single crystal diffraction data.

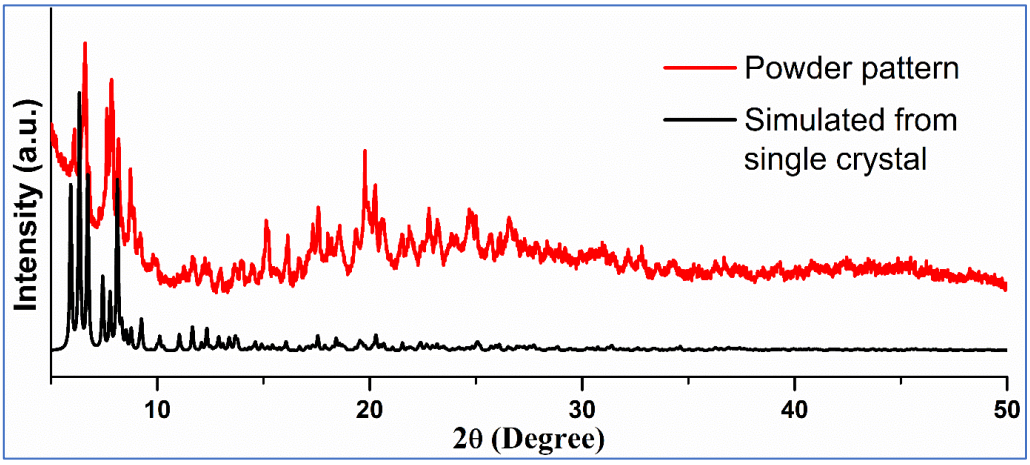

Figure 4.25. Powder X-ray diffraction pattern of a bulk sample of **4.3** compared to the simulated powder pattern extracted from single crystal diffraction data.

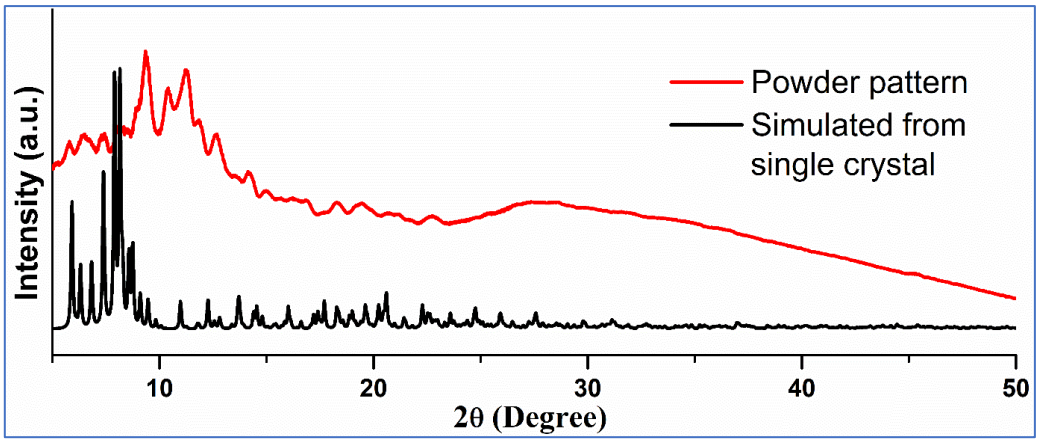

Figure 4.26. Powder X-ray diffraction pattern of a bulk sample of **4.4** compared to the simulated powder pattern extracted from single crystal diffraction data.

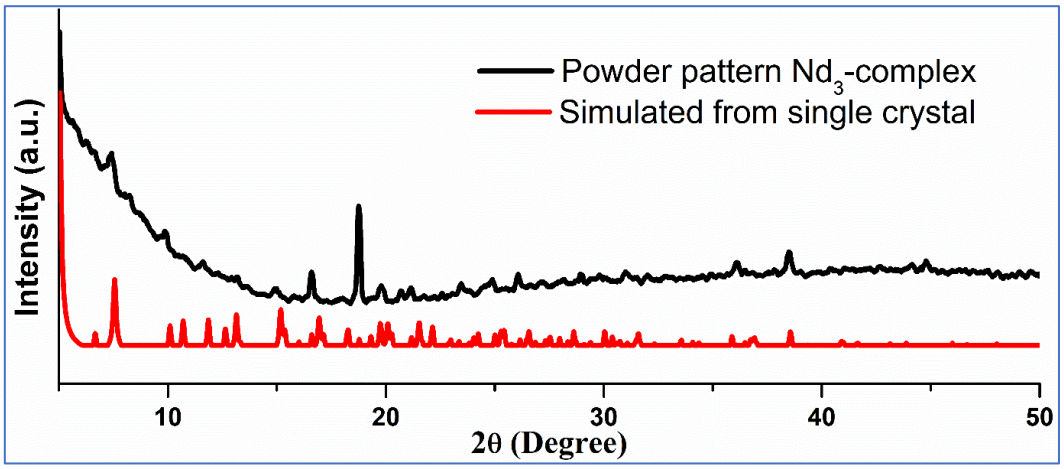

Figure 4.27. Powder X-ray diffraction pattern of a bulk sample of **4.5** compared to the simulated powder pattern extracted from single crystal diffraction data.

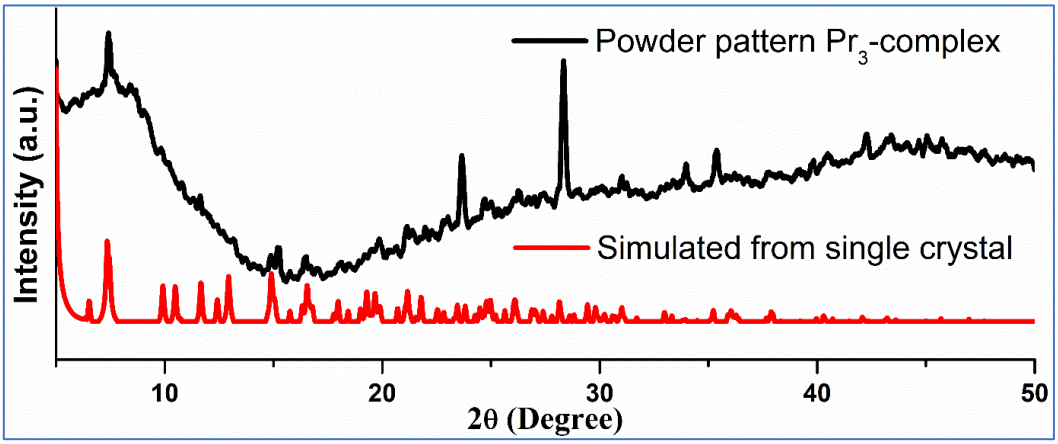

Figure 4.28. Powder X-ray diffraction pattern of a bulk sample of **4.6** compared to the simulated powder pattern extracted from single crystal diffraction data.

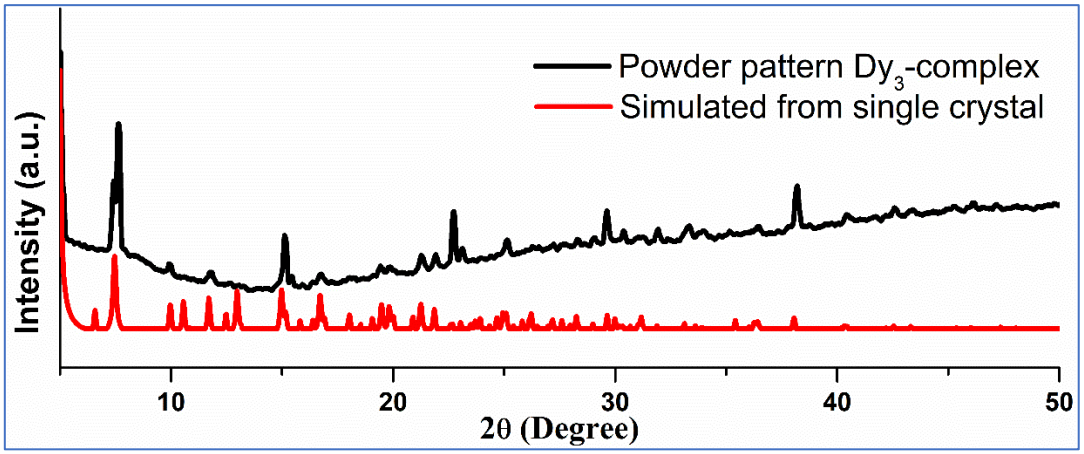

Figure 4.29. Powder X-ray diffraction pattern of a bulk sample of **4.7** compared to the simulated powder pattern extracted from single crystal diffraction data.

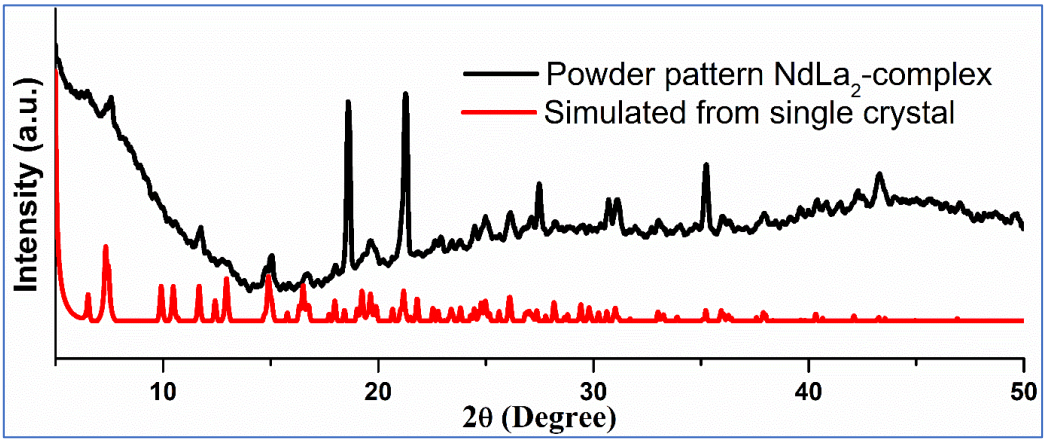

Figure 4.30. Powder X-ray diffraction pattern of a bulk sample of **4.8** compared to the simulated powder pattern extracted from single crystal diffraction data.

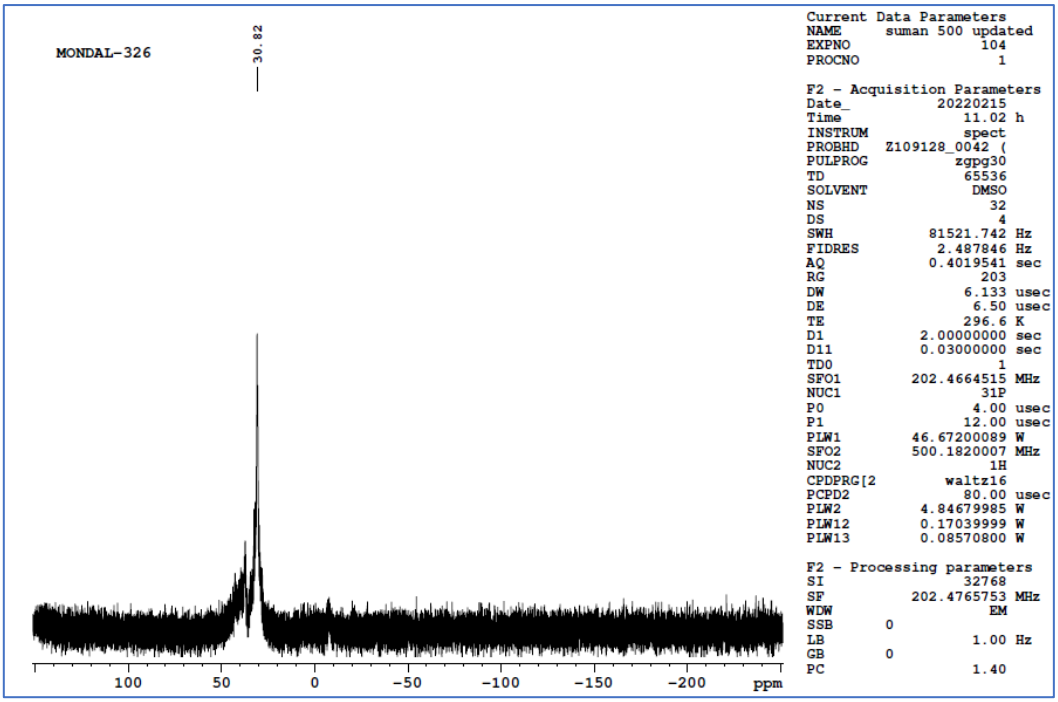

Figure 4.31. $^{31}P\{H\}$ NMR of compound **4.4**

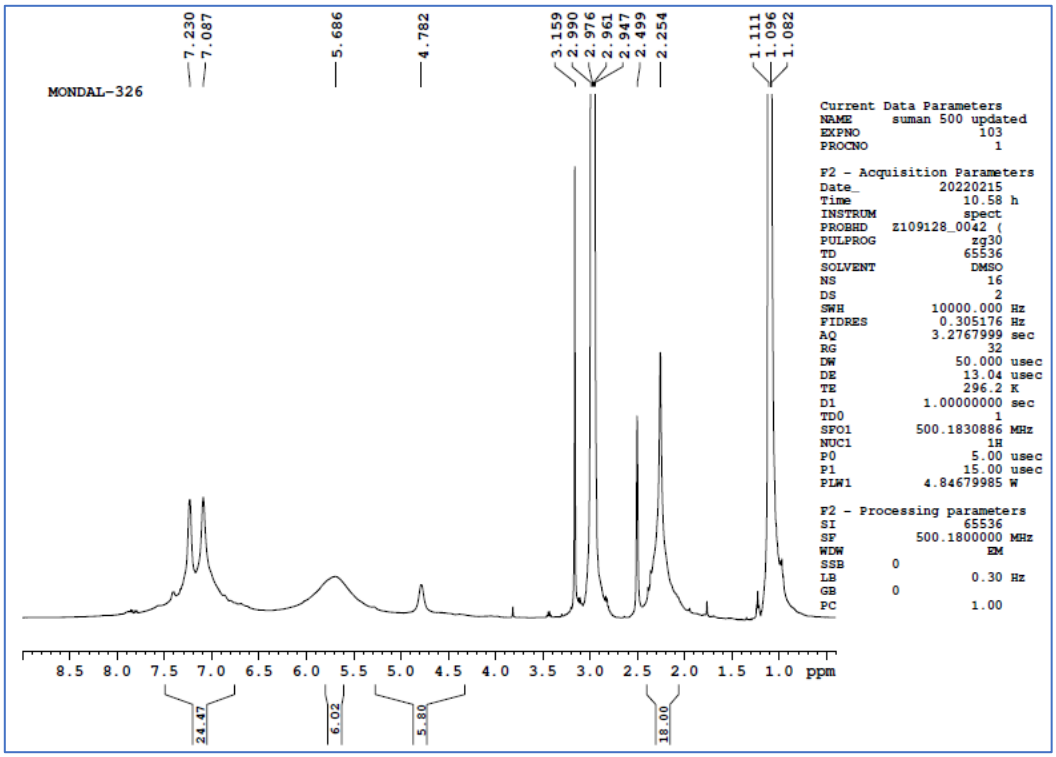

Figure 4.32. ^{1}H NMR of compound **4.4**

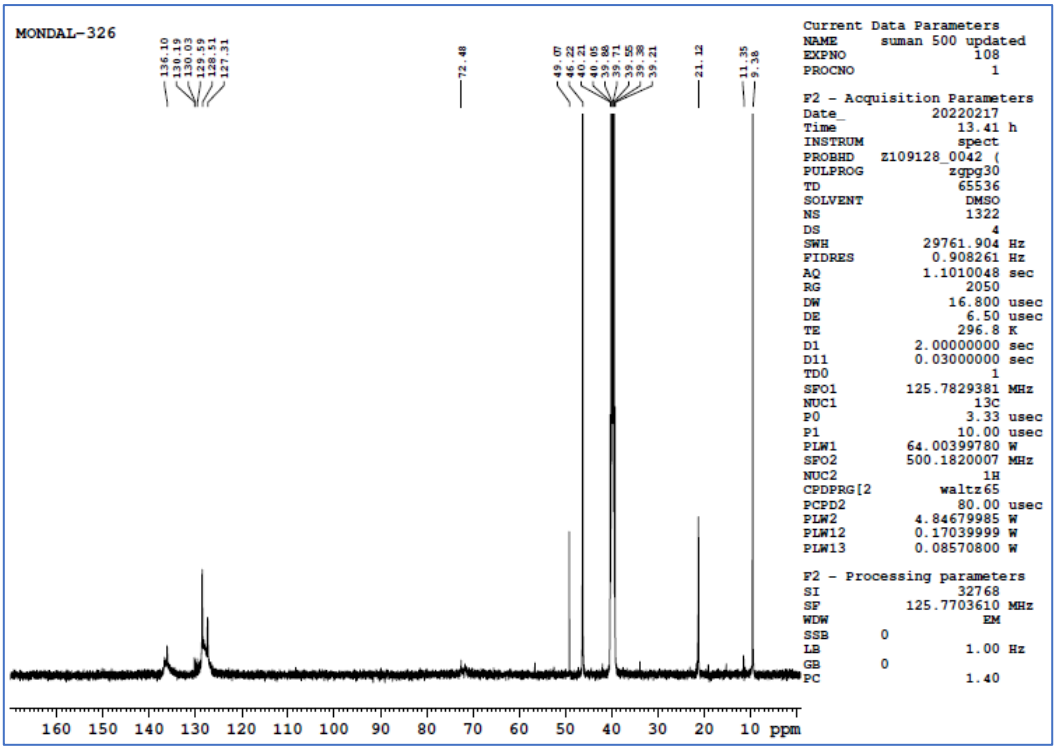

Figure 4.33. ^{13}C NMR of compound **4.4**

Element	Weight%	Atomic%
C K	45.12	58.11
N K	4.20	4.64
O K	35.79	34.60
P K	0.91	0.45
Br L	7.79	1.51
La L	4.12	0.46
Nd L	2.07	0.22
Totals	100.00	

(a)

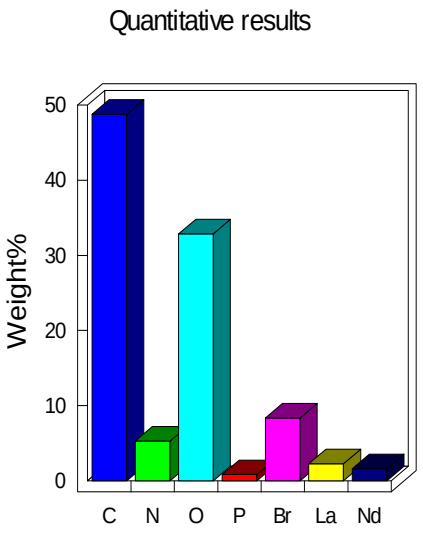

(b)

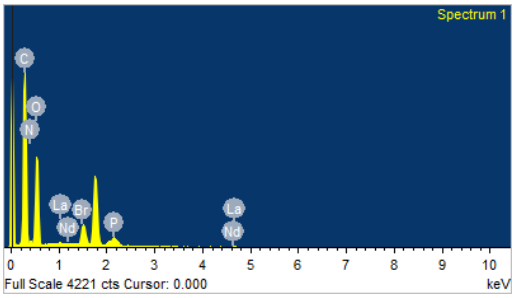

(c)

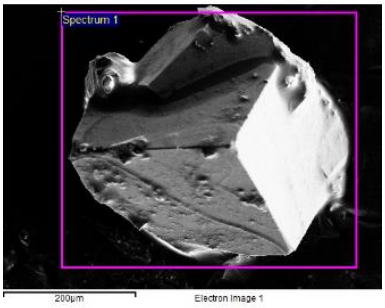

(d)

Figure 4.34. (a), (b), (c) EADX and **(d)** SEM image of compound **4.7**

4.6 References:

[1] R. Sessoli, D. Gatteschi, A. Caneschi and M.A. Novak, *Nature*, 1993, **365,** 141-143.

[2] N. Ishikawa, M. Sugita, and W. Wernsdorfer, *Angewandte Chemie International Edition*, 2005, **44,** 2931-2935.

[3] (a) J.M. Frost, K.L. Harriman and M. Murugesu, *Chemical science*, 2016, **7,** 2470-2491.

(b) M. Mannini, F. Pineider, P. Sainctavit, C. Danieli, E. Otero, C. Sciancalepore, A.M. Talarico, M.A. Arrio, A. Cornia, D. Gatteschi and R. Sessoli, *Nature materials*, 2009, **8,** 194-197.

(c) S. Thiele, F. Balestro, R. Ballou, S. Klyatskaya, M. Ruben and W. Wernsdorfer, *Science*, 2014, **344,** 1135-1138.

(d) L. Bogani and W. Wernsdorfer, *Nanoscience and technology: a collection of reviews from nature journals*, 2010, 194-201.

(e) M. Affronte, F. Troiani, A. Ghirri, A. Candini, M. Evangelisti, V. Corradini, S. Carretta, P. Santini, G. Amoretti, F. Tuna and G. Timco, *Journal of Physics. D, Applied Physics*, 2007, **40**.

(f) W. Wernsdorfer, *Nature materials*, 2007, **6,** 174-176.

(g) C.A. Timco, S. Carretta, F. Troiani, R.J. Pritchard, A. Muryn, E.J. McInnes, A. Ghirri and A. Candini, P. G. Santini, M. Amoretti, Affronte and R.E. Winpenny, *Nat. Nanotech*, 2009,**4,** 173-178.

(h) H. Tian, R. Liu, X. Wang, P. Yang, Z. Li, L. Li and D. Liao, *European Journal of Inorganic Chemistry*,2009, 4498-4502.

(i) R. Liu, C. Zhang, L. Li, D. Liao and J.P. Sutter, *Dalton Transactions*, 2012, **41,** 12139-12144.

(j) G.Q. Bian, T. Kuroda-Sowa, H. Konaka, M. Hatano, M. Maekawa, M. Munakata, H. Miyasaka and M. Yamashita, *Inorganic chemistry*, 2004, **43,** 4790-4792.

(k) Y. Bi, X.T. Wang, W. Liao, X. Wang, R. Deng, H. Zhang and S. Gao, *Inorganic chemistry*, 2009, **48,** 11743-11747.

(l) R. Liu, C. Zhang, L. Li, D. Liao and J.P. Sutter, *Dalton Transactions*, 2012, **41,** 12139-12144.

(m) I.J. Hewitt, J. Tang, N.T. Madhu, C.E. Anson, Y. Lan, J. Luzon, M. Etienne, R. Sessoli and A.K. Powell, *Angewandte Chemie International Edition*, 2010, **49,** 6352-6356.

(n) S. Xue, X.H. Chen, L. Zhao, Y.N. Guo and J. Tang, *Inorganic chemistry*, 2012, **51,** 13264-13270.

(o) S. Xue, L. Zhao, Y.N. Guo, R. Deng, Y. Guo and J. Tang, *Dalton Transactions*, 2011, **40,** 8347-8352.

(p) K.H. Zangana, E.M. Pineda and R.E. Winpenny, *Dalton Transactions*, 2015, **44,** 12522-12525.

[4] (a) J.D. Rinehart and J.R. Long, *Chemical Science*, 2011, **2,** 2078-2085.

(b) L. Sorace, C. Benelli and D. Gatteschi, *Chemical Society Reviews*, 2011, **40,** 3092-3104.

(c) Y.N. Guo, G.F. Xu, Y. Guo and J. Tang, *Dalton Transactions*, 2011, **40,** 9953-9963.

(d) R. Sessoli and A.K. Powell, *Coordination Chemistry Reviews*, 2009, **253,** 2328-2341.

(e) B. Wang, S. Jiang, X. Wang and S. Gao, *Science in China Series B: Chemistry*, 2009, **52,** 1739-1758.

(f) F. Habib and M. Murugesu, *Chemical Society Reviews*, 2013, **42,** 3278-3288.

[5] (a) J.D. Rinehart and J.R. Long, *Chemical Science*, 2011, **2,** 2078-2085.

(b) A. Dey, P. Kalita and V. Chandrasekhar, *ACS omega*, 2018, **3,** 9462-9475.

(c) J. Mayans, L. Tesi, M. Briganti, M.E. Boulon, M. Font-Bardia, A. Escuer and L. Sorace, *Inorganic Chemistry*, 2021, **60,** 8692-8703.

(d) W. Wegner, J.J. Zakrzewski, M. Zychowicz and S. Chorazy, *Scientific reports*, 2021, **11,** 1-13.

(e) M. Nakano and H. Oshio, *Chemical Society Reviews*, 2011, **40,** 3239-3248.

[6] N. Ishikawa, M. Sugita, T. Ishikawa, S.Y. Koshihara and Y. Kaizu, *Journal of the American Chemical Society*, 2003, **125,** 8694-8695.

[7] J.D. Rinehart and J.R. Long, *Chemical Science*, 2011, **2,** 2078-2085.

[8] (a) D.N. Woodruff, R.E. Winpenny and R.A. Layfield, *Chemical reviews*, 2013, **113,** 5110-5148.

(b) S.M. Neville, G.J. Halder, K.W. Chapman, M.B. Duriska, B. Moubaraki, K.S. Murray and C.J. Kepert, *Journal of the American Chemical Society*, 2009, **131,** 12106-12108.

(c) L. Ungur, S.K. Langley, T.N. Hooper, B. Moubaraki, E.K. Brechin, K.S. Murray and L.F. Chibotaru, *Journal of the American Chemical Society*, 2012, **134,** 18554-18557.

(d) J.J. Le Roy, L. Ungur, I. Korobkov, L.F. Chibotaru and M. Murugesu, *Journal of the American Chemical Society*, 2014, **136,** 8003-8010.

(e) N.F. Chilton, D. Collison, E.J.L. McInnes, R.E.P. Winpenny and A. Soncini, *Nat. Commun.*, 2013.

(f) V., Chandrasekhar, P. Bag and E. Colacio, *Inorganic chemistry*, 2013, **52,** 4562-4570.

(g) V. Chandrasekhar, A. Dey, S. Das, M. Rouzières and R. Clérac, *Inorganic chemistry*, 2013, **52,** 2588-2598.

(h) J. Goura, J.P. Walsh, F. Tuna and V. Chandrasekhar, *Inorganic chemistry*, 2014, **53,** 3385-3391.

(i) J. Goura, V. Mereacre, G., Novitchi, A.K. Powell and V. Chandrasekhar, *European Journal of Inorganic Chemistry*, 2015, **1**, 156-165.

(j) A. Baniodeh, V. Mereacre, N. Magnani, Y. Lan, J.A. Wolny, V. Schünemann, C.E. Anson and A.K. Powell, *Chemical Communications*, 2013, **49,** 9666-9668.

(k) A. Baniodeh, N. Magnani, S. Bräse, C.E. Anson and A.K. Powell, *Dalton Transactions*, 2015, **44,** 6343-6347.

[9] (a) V. Chandrasekhar and P. Sasikumar, *Dalton Transactions*, 2008, **45,** 6475-6480.

(b) Y.Z. Zheng, M. Evangelisti and R.E. Winpenny, *Angewandte Chemie*, 2011, **123,** 3776-3779.

(c) C.Q. Jiao, J.C. Zhang, Y. Zhao, Z.G. Sun, Y.Y. Zhu, L.L. Dai, S.P. Shi and W. Zhou, *Dalton Transactions*, 2014, **43,** 1542-1549.

(d) S.K. Gupta, S.K. Langley, K. Sharma, K.S. Murray and R. Murugavel, *Inorganic chemistry*, 2017, **56,** 3946-3960.

(d) S.K. Gupta, G.A. Bhat and R. Murugavel, *Inorganic chemistry*, 2017, **56,** 9071-9083.

[10] (a) A. Mendiratta, C.C. Cummins, F.A. Cotton, S.A. Ibragimov, C.A. Murillo and D. Villagrán, *Inorganic chemistry*, 2006, **45,** 4328-4330.

(b) F.A. Cotton, E.A. Hillard, C.A. Murillo and X. Wang, *Inorganic chemistry*, 2003, **42,** 6063-6070.

(c) F.A. Cotton, L.M. Daniels, C.A. Murillo and P. Schooler, *Journal of the Chemical Society, Dalton Transactions*, 2000, **13,** 2007-2012.

(d) A. Elangovan, M. Umadevi and V. Muthuraj, *Journal of Molecular Structure*, 2019, **1176,** 591-604.

(e) E. Reisner, J. Telser and S.J. Lippard, *Inorganic chemistry*, 2007, **46,** 10754-10770.

(f) S. Friedle, J.J. Kodanko, K.L. Fornace and S.J. Lippard, *Journal of molecular structure*, 2008, **890,** 317-327.

(g) G.M. Chiarella, F.A. Cotton, C.A. Murillo, K. Ventura, D. Villagrán and X. Wang, *Journal of the American Chemical Society*, 2014, **136,** 9580-9589.

(h) F.A. Cotton, N.S. Dalal, P. Huang, C.A. Murillo, A.C. Stowe and X. Wang, *Inorganic chemistry*, 2003, **42,** 670-672.

(i) K. Pang, J.S. Figueroa, I.A. Tonks, W. Sattler and G. *Inorganica chimica acta*, **362,** 4609-4615.

(j) T. Hamaguchi, R. Shimazaki and I. Ando, *Journal of Molecular Structure*, 2018, **1173,** 345-348.

(k) M. Cortijo, P. Delgado-Martinez, R. Gonzalez-Prieto, S. Herrero, R. Jimenez-Aparicio, J. J.L. Perles and M.R. Torres, *Inorganica Chimica Acta*, 2015, **424,** 176-185.

(l) C. Bronner, S.A. Baudron and M.W. Hosseini, *Inorganic chemistry*, 2010, **49,** 8659-8661.

(m) S.J. Jenniefer and P.T. Muthiah, *Chemistry Central Journal*, 2013, **7,** 1-15.

(n) M. Perec, R. Baggio, R.P. Sartoris, R.C. Santana, O. Peña and R. Calvo, *Inorganic chemistry*, 2010, **49,** 695-703.

(o) D.L. Reger, A. Debreczeni and M.D. Smith, *Inorganic chemistry*, 2011, **50,** 11754-11764.

(p) J. Li, Y. Peng, H. Liang, Y. Yu, B. Xin, G. Li, Z. Shi and S. Feng, *European Journal of Inorganic Chemistry*, 2011, **2011,** 2712-2719.

(q) F.A. Cotton, Z. Li, C.A. Murillo, P.V. Poplaukhin and J.H. Reibenspies, *Journal of Cluster Science*, 2008, **19,** 89-97.

[11] (a) Y. Li, F.K. Zheng, X. Liu, W.Q. Zou, G.C. Guo, C.Z. Lu and J.S. Huang, *Inorganic chemistry*, 2006, **45,** 6308-6316.

(b) J. She, C. Gao, K. Cui, C. Hou, W. Zhao, W. Wei and B. Peng, *Structural Chemistry*, 2008, **19,** 905-910.

(c) A. Thirumurugan and S. Natarajan, *Dalton Transactions*, 2004, **18,** 2923-2928.

(d) A.F. Kateshali, S.G. Dogaheh, J. Soleimannejad and A.J. Blake, *Coordination Chemistry Reviews*, 2020, **419,** 213392.

(e) F.N. Shi, L. Cunha-Silva, T. Trindade, F.A.A. Paz and J., Rocha, *Crystal Growth and Design*, 2009, **9,** 2098-2109.

(f) X. Zhao, X.Y. Yu, T.L. Chen, Y.H. Luo, J.J. Yang and H. Zhang, *Inorganic Chemistry Communications*, 2012, **20,** 247-251.

(g) F. Li, X. Zhao and R. Cao, *Inorganic Chemistry Communications*, 2012, **21,** 118-121.

(h) R. Sen, D.K. Hazra, S. Koner, M. Helliwell, M. Mukherjee and A. Bhattacharjee, *Polyhedron*, 2010, **29,** 3183-3191.

(i) G. Guangsheng, L. Yangchun, J. Zhang and G.U.O. Hongyou, *Journal of rare earths*, 2008, **26,** 633-637.

[12] (a) M. U. Anwar, S. S. Tandon, L. N. Dawe, F. Habib, M. Murugesu and L. K. Thompson, *Inorg. Chem.*, 2012, **51**, 1028–1034.

(b) G. B. Deacon, C. M. Forsyth, P. C. Junk and A. Urbatsch, *Eur. J. Inorg. Chem.*, 2010, **2010,** 2787–2797.

(c) J. B. Peng, Y. P. Ren, X. J. Kong, L. S. Long, R. Bin Huang and L. S. Zheng, *CrystEngComm*, 2011, **13**, 2084–2090.

(d) V. Velasco, L. A. Barrios, M. Schütze, O. Roubeau, F. Luis, S. J. Teat, D. Aguilà and G. Aromí, *Chem. - A Eur. J.*, 2019, **25**, 15228–15232.

(d) A. Sarkar, C. J. Gómez-García, S. Benmansour and H. P. Nayek, *Chempluschem*, 2019, **84**, 974–980.

(e) L. Lee, D. J. Berg and G. W. Bushnell, *Inorg. Chem.*, 1994, **33**, 5302–5308.

(f) I. J. Hewitt, Y. Lan, C. E. Anson, J. Luzon, R. Sessoli and A. K. Powell, *Chem. Commun.*, 2009, **3**, 6765–6767.

(g) W. H. Su, Y. H. Guo, Y. Z. Yu and Y. X. Wang, *Inorg. Chem. Commun.*, 2020, **120**, 108161.

(h) C. Sen Liu, M. Du, E. C. Sañudo, J. Echeverria, M. Hu, Q. Zhang, L. M. Zhou and S. M. Fang, *Dalt. Trans.*, 2011, **40**, 9366–9369.

(i) T. P. Latendresse, N. S. Bhuvanesh and M. Nippe, *J. Am. Chem. Soc.*, 2017, **139**, 14877–14880.

[13] (a) B. Kaboudin and H. Haghighat, *J. Org. Chem.*, 2006, **71,** 6604–6606.

(b) B. Kaboudin and N. As-Habei, *Tetrahedron Lett.*, 2004, **45,** 9099–9101.

[14] O. V. Dolomanov, L. J. Bourhis, R. J. Gildea, J. A. K. Howard, H. Puschmann, *J. Appl. Crystallogr.*, 2009, **42 ,** 339–341.

[15] G. M. Sheldrick, *Acta Crystallogr. Sect. A Found. Crystallogr.*, 2015, **71,** 3–8.

[16] (a) G. M. Sheldrick, *Acta Crystallogr. Sect. C Struct. Chem.*, 2015, **71,** 3–8.

(b) L. J. Bourhis, O. V. Dolomanov, R. J. Gildea, J. A. K. Howard, H. Puschmann, *Acta Crystallogr. Sect. A Found. Crystallogr.*, 2015, **71,** 59–75.

A new type of square grid [2×2] lanthanide Ln(III)$_4$ complexes self-assembled with chiral racemic (R, R / S, S)bis-[α-hydroxy(*p*-bromophenyl)methyl]phosphinic acid ligand.

CHAPTER

5

A series of isostructural tetranuclear [2 × 2] square-grid like Ln (III) clusters have been synthesized in reaction with chiral phosphinic acid ligand [Bis-[α-hydroxy(p-bromophenyl)methyl]phosphinic acid] {(R_2PO_2H)[R= CH(OH)PhBr]} represented as [$Ln_4(\mu_2\text{-}\eta^1\text{:}\eta^1\text{-}PO_2R_2)_8(\eta^2\text{-}CO_2Bu^t)_4$] where Ln= Er (**5.1**), Dy (**5.2**), Tb (**5.3**) and characterized by SCXRD. Synthesis, structural interpretation are discussed in this chapter.

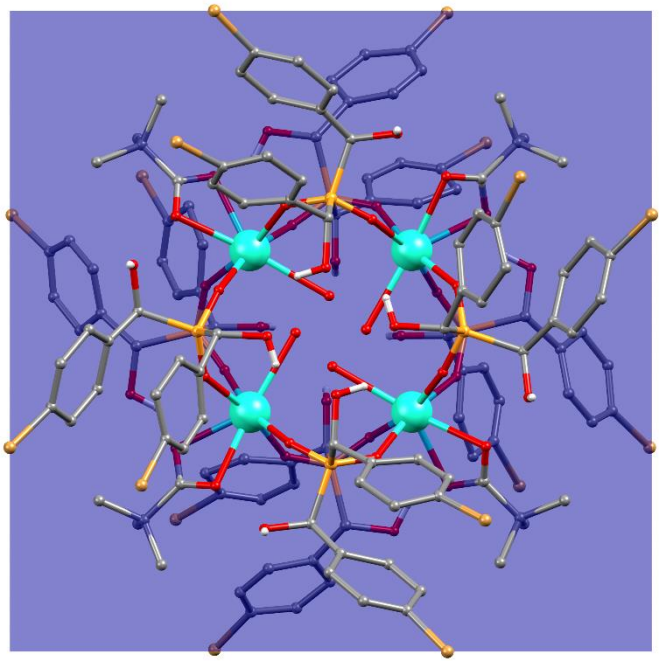

5.1 Introduction:

Polynuclear lanthanide clusters have great attention since the past decades due to their applications in various fields of luminescence,[1,2] catalysis,[3] magnetic refrigeration,[4–8] and molecule magnets[9] such as single ion magnets (SIMs), single chain magnets (SCMs), single molecular magnets (SMMs). Among them, molecular magnetism has been investigated a lot since the discovery of the famous Mn_{12}-SMM behavior.[10] Lanthanide ions inherent in large single-ion anisotropy and magnetic bistability are the key to good SMMs. U_{eff} (anisotropic energy barrier) and T_B (blocking temperature) are the two terms associated with SMM behavior. Larger U_{eff} and higher T_B is the characteristic of a decent SMM. Dy, Tb, and Er are the most promising candidates for SMM for their large spin-orbit coupling and large magnetic moment.[9] Very recently two Dy complexes have been reported as having high blocking temperature (20 K)[11] and effective energy barrier(1025 K)[12]. Dy SMMs are the most useful among the lanthanides due to their strong uniaxial magnetic anisotropy($g_z >> g_{x,y}$). Di-nuclear[13], trinuclear[14], tetranuclear(butterfly, square, cubane, rhombus shape, chain-like, linear, Y-shape, sea-saw, zig-zag irregular shape)[15–47,47–51], and higher nuclear[52–54] lanthanide clusters are reported in literatures.

Among them, Dy_4-cluster has observed interesting SMM behavior by Chandrasekhar et al.[55] Tetranuclear [2×2] square-grid topology reported the highest U_{eff} (143 cm^{-1}) by Tong et al.[56] Self-assembled polymetallic square-grid [n × n] (n= 2-5) (M_4 to M_{25}) complexes are quite common for transition metals such as Mn, Fe, Co, Ni, Cu, Zn using poly n-topic hydrazone related ligands.[57–59] The first genuine heteroleptic self-assembled [2 × 2] grid is reported by Murugesu et al.[60] This grid arrangement of Dy shows the high U_{eff} (270 K) (τ_0= 4.0 x 10^{-10} s) by a peak maxima shifted towards the high-temperature regime, implies that the reduction of QTM (quantum tunneling of magnetization). Several square grids [2 × 2] were synthesized in the literature[23,56,60–78] utilizing thiolate, thiacalix[4]arene, triazole ligand, Schiff-base ligand, and hydrazide, hydrazone-based Schiff-base ligands.

Along with SMM, the tetranuclear Dy_4 cluster's square grid structures often show an aesthetic feature called single molecule toroics (SMT).[79,80] This is triggered by the vortex arrangement of magnetic dipoles,[81–83] $T = \sum_{j=1}^{N} r_i \times s_i$ (N ≥ 2 spins per unit cell)(where T= toroidal magnetic moment, r= displacement of the magnetic-ions from the centre-position, s = spins of the magnetic ions). [Dy_3] triangle, reported[14] by Powell's group in 2006, first demonstrated the fascinating property of SMM even though it has a non-magnetic ground state. This opens a new class of magnetic materials.[82,83] Tong et al. in 2012 first reported tetranuclear toroidal

moment SMT for planar Dy_4 cluster.[84] This area of research is now a growing field and the property of SMT is now not only limited to the planar [Dy_3] triangle[14,54,85–92] but also several wheel shape topologies viz. [Dy_4] planar,[84] [Dy_4] square,[61,66,68] [Dy_6] wheel,[93–98] coupled [Dy_3][91] containing SMT have been reported. Even [Dy_4]-cubic[99] and [Dy_4] tetrahedral[99] topology recently opens the area more extensively from planar (2D) to non-planar (3D) SMTs.

Herein we have synthesized a series of isostructural lanthanide complexes(**5.1-5.3**) of [2 × 2] grid topology using Bis-[α-hydroxy(p-bromophenyl)methyl]phosphinic acid and pivalic acid as co-ligand. From the literature reviews, it is presumed that probably this is the first example of a square grid [2 × 2] complex of phosphinic acid ligand.

5.2 Experimental Section:

5.2.1 General Information:

All the general chemicals were purchased commercially and used without further purification. Bis-[α-hydroxy(p-bromophenyl)methyl]phosphinic acid was prepared by the reported procedure.[100,101] Hydrated lanthanide chloride salts were synthesized from their corresponding oxides by neutralizing with concentrated HCl, followed by evaporation to dryness.

The synthetic procedure followed for synthesizing these complexes is detailed below.

5.2.2 Synthesis:

To a 60 ml methanolic solution of Bis-[α-hydroxy(p-bromophenyl)methyl]phosphinic acid (R_2PO_2H) [R= CH(OH)PhBr], $LnCl_3.6H_2O$ was added and stirred for a few minutes (2-3 min). Then dropwise tetramethylammonium hydroxide was added and stirring was continued. After 30 minutes a 2 ml methanolic solution of pivalic acid with Me_4NOH was added to it. The reaction mixture was stirred at room temperature for 5 h. The solvent was evaporated with rotor vapor. A white color solid was formed, it was washed with diethyl ether twice and crystallized in acetonitrile to get X-ray-quality single crystals.

Compound 5.1: R_2PO_2H (0.100 g, 0.229 mmol), $ErCl_3.6H_2O$ (0.043 g, 0.114 mmol), pivalic acid (0.023 g, 0.229 mmol), Me_4NOH (in 25% MeOH) (0.035 ml + 0.011 ml, 0.458 mmol). Yield: 0.92 g, 70.76% (Based on $ErCl_3.6H_2O$). IR (cm^{-1}): 3352.37 (br), 2962.16(m), 2872.02(w), 1645.27(w), 1534.57(s), 1484.33(s), 1435.83(w), 1403.47(s), 1362.17(m), 1171.52(s), 1069.73(s), 1008.60(s), 948.74(s), 906.91(m), 863.42(m), 821.87(s), 703.87(w), 605.00(w), 557.40(m).

Compound 5.2: R_2PO_2H (0.100 g, 0.229 mmol), $DyCl_3.6H_2O$ (0.042 g, 0.114 mmol), pivalic acid (0.023 g, 0.229 mmol), Me_4NOH (in 25% MeOH) (0.035 ml + 0.011 ml, 0.458 mmol).

Yield: 0.085 g, 66.40% (Based on $DyCl_3.6H_2O$). IR (cm^{-1}): 3344.72(br), 2970.18(m), 2872.02(w), 1645.54(w), 1575.64(w), 1524.34(s), 1484.89(s), 1436.30(m), 1401.19(m), 1364.32(w), 1192.49(m), 1169.89(s), 1103.55(w), 1069.20(s), 1008.88(s), 947.75(m), 907.36(m), 863.97(m), 821.57(s), 776.38(w), 730.28(m), 704.21(w), 648.11(w), 607.37(w), 555.58(m).

Compound 5.3: R_2PO_2H (0.100 g, 0.229 mmol), $TbCl_3.6H_2O$ (0.042 g, 0.114 mmol), pivalic acid (0.023 g, 0.229 mmol), Me_4NOH (in 25% MeOH) (0.035 ml + 0.011 ml, 0.458 mmol). Yield: 0.089 g, 68.99% (Based on $TbCl_3.6H_2O$). IR(cm^{-1}): 3359.15(br), 2961.85(m), 2868.84(w), 1646.07(w), 1530.96(s), 1484.22(s), 1439.01(w), 1401.73(s), 1369.11(w), 1192.49(m), 1169.92(s), 1103.60(w), 1068.98(s), 1008.53(s), 948.28(s), 905.04(m), 862.64(m), 822.42(s), 774.93(w), 729.77(m), 703.69(m), 647.98(w), 605.09(w), 556.37(m).

5.2.3 Instrumentation:

Infrared spectra were recorded with a NICOLET iS5 FTIR Spectrometer. Elemental analysis was performed with a Flash EA Series 1112 CHNS analyzer. TGA was recorded with a PerkinElmer STA 8000 thermogravimetric analyzer under a nitrogen gas flow rate of 20 ml/min and a heating rate of 10°C/min. The SCXRD data for 5.1-5.3 were collected at 100K with a Bruker APEX-II CCD diffractometer system [λ (Mo Kα) = 0.71073Å] with a graphite monochromator using the φ-ω scan technique. The data were reduced using Bruker SAINT package. Absorption correction was performed using the SADABS program. The structures were solved by the direct methods and refined on F^2 by full-matrix least-squares using the program SHELXL-2018/3. The structure was solved with the **Olex2**[102], **ShelXT**[103] structure solution program using Intrinsic Phasing and refined with the **SHELXL**[104,105]- 2018/3 refinement package using Least Squares minimization. All non-hydrogen atoms were refined anisotropically and hydrogen atoms were fixed at calculated positions and refined as a horse riding model. EADP, RIGU, SIMU, DELU, SADI, and FLAT constrained/restrained commands were used to fix the disordered atoms. Graphics of the crystal structures have been done with Diamond(version 2.1e) and Mercury(version 3.10.3) software. The details of the data have been given in supporting information. For **1-3**, the Olex2 solvent mask (similar to PLATON/SQUEEZE) was used to mask out the electron density of disordered counterions. The details of the solvent masks used are given below-

For compound **5.1** a solvent mask was calculated and 396 electrons were found in a volume of 4546 $Å^3$ in 4 voids. This is consistent with the presence of 2[CH_3CN], 2[H_2O], 4[CH_3CN], 2[CH_3CN] per formula unit which accounts for 392.0 electrons.

For compound **5.2** a solvent mask was calculated and 270 electrons were found in a volume of 4264 $Å^3$ in 3 voids. This is consistent with the presence of 4[CH_3CN], 2[CH_3CN], 2[H_2O], 0.6[H_2O] per formula unit which accounts for 316.0 electrons.

For compound **5.3** a solvent mask was calculated and 488 electrons were found in a volume of 4218 $Å^3$ in 3 voids. This is consistent with the presence of 6[CH_3CN], 4[CH_3CN], 2[H_2O] per formula unit which accounts for 480.0 electrons.

5.3 Results and discussions:

The ligand was synthesized according to the literature procedure.[100,101] The complexes **5.1-5.3** were synthesized as summarized in **scheme1.** The hydrated lanthanide chloride salts were reacted in a methanolic solution of the ligand following the addition of the base tetramethylammonium hydroxide in a 1:2:2 ratio. A clear solution was stirred for 30 minutes at room temperature. To the clear solution, deprotonated pivalic acid with tetramethylammonium hydroxide (1:1) was added dropwise. After 5 hr clear reaction mixture was evaporated with rotor vapor and washed the white solid twice with diethyl ether and kept for crystallization in acetonitrile. Single crystal X-ray quality crystals were obtained after slow evaporation of the solution. Standard analytical and spectroscopic techniques were used to characterize the products.

The IR spectra of **5.1-5.3** show (**figure. 5.4, 5.12, 5.20**) the characteristic peaks of aromatic and aliphatic C-H stretching of the ligand around 2868-2970 cm^{-1}, O-H stretching band of ligand and coordinated water molecule shows in between 3344-3359 cm^{-1}, water bending 1645-1646 cm^{-1}, P-O stretching around 1008-1069 cm^{-1}, C-O stretching(for CH_2OH) 1169-1192 cm^{-1}, symmetric CO_2^- stretching shows 1364-1369 cm^{-1}, asymmetric CO_2^- stretching around 1524-1534 cm^{-1}, aromatic C-Br stretching 1103 cm^{-1}, C=C stretching shows 1435-1484 cm^{-1}, C-H out-of-plane bending at around 821-822 cm^{-1}.

TGA studies (**figure. 5.5, 5.13, 5.21**) reveal that major weight loss occurred for **5.1-5.3** at 289 °C, 287 °C, and 288 °C respectively. Crystallinity and phase purity of the bulk samples for **5.1-5.3** were represented by the PXRD data (**figure . 5.11, 5.19, 5.27**).

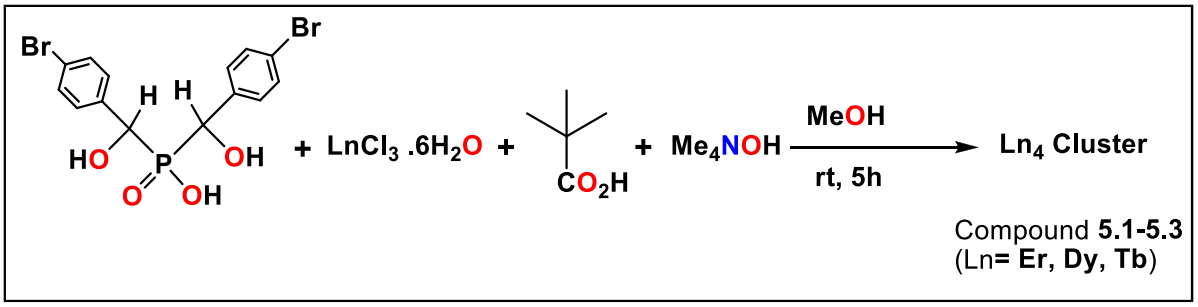

Scheme 1: Synthesis scheme of compounds **5.1-5.3**

Crystal Structure :

Complexes **5.1-5.3** were crystallized in the tetragonal crystal lattice system in the I4 space group with Z = 2. The asymmetric unit consists of one-fourth of the molecule. Two molecules are present in the unit cell structure and both of them are similar. The crystal structure of **5.2** was taken as a representative of the whole isostructural series **5.1-5.3.** The molecular structure of the compound was confirmed by SCXRD. A representative neutral crystal structure of **5.2** is formed self-assembled [2 × 2] square grid-like which is shown in (**figure 5.1(a)**). Each Dy-atom is hepta-coordinated, SHAPE analysis shows pentagonal bipyramidal ($\mathbf{D_{5h}}$) structure (**table 5.2**). The hepta-coordination is satisfied with four oxygen atoms from four phosphinic acid ligands (**HL**), two oxygen atoms from one bidentate η^2 pivalic acid, and one oxygen atom from one water molecule, therefore O_5 coordination environment around the Dy-atom. In the core structure (**figure 5.1(b)**) two neighboring dysprosium atoms are connected through two phosphinic acids with [2.11] mode according to Harris notation and each dysprosium atom is coordinately saturated with one pivalic acid in a [1.11] mode. In the crystal structure, four Dy-atoms are located on the four vertices of a parallelogram displaying a square grid [2 × 2] motif since all the neighboring intramolecular Dy…Dy distance is 4.672 Å and diagonally situated Dy…Dy distance is 6.607 Å. All the Dy-O bond distances fall in the range 2.221-2.640 Å and Dy-O_{H2O} bond distance is 2.640 Å. From the crystal packing diagram, the intermolecular distance between the two shortest Dy…Dy is ca. 12.048 Å. Selected bond distances (**table 5.1**) and bond angles for **5.1-5.3** are given in **table 5.4-5.6.** More closely screening the crystal structure reveals that all the phosphinic acid ligands arranged themselves in a specific conformation where the two phenyl rings of a particular ligand have π-π interaction (3.654-3.858 Å) (**figure 5.1(e)**) itself within the ligand(intra-ligand π-π interaction)(**figure 5.1(d)**).

Table1. Important bond distances(Å) for complexes **5.1-5.3** in this work.

Er….Er 4.653	Dy….Dy 4.672	Tb….Tb 4.709
Er….Er$^{(d)}$ 6.580	Dy….Dy$^{(d)}$ 6.607	Tb….Tb$^{(d)}$ 6.659
Er-O_{PA} 2.191-2.311	Dy-O_{PA} 2.221-2.284	Tb-O_{PA} 2.275-2.281
Er-O_{piv} 2.464-2.488	Dy-O_{piv} 2.464-2.474	Tb-O_{piv} 2.456-2.468
Er-OH_2 2.273	Dy-OH_2 2.640	Tb-OH_2 2.670
Er….Er$^{(ps)}$ 12.089	Dy….Dy$^{(ps)}$ 12.048	Tb….Tb$^{(ps)}$ 12.116

$^{(d)}$ diagonal, PA= Phosphinic acid, piv=Pivalic acid, $^{(ps)}$ Packing shortest.

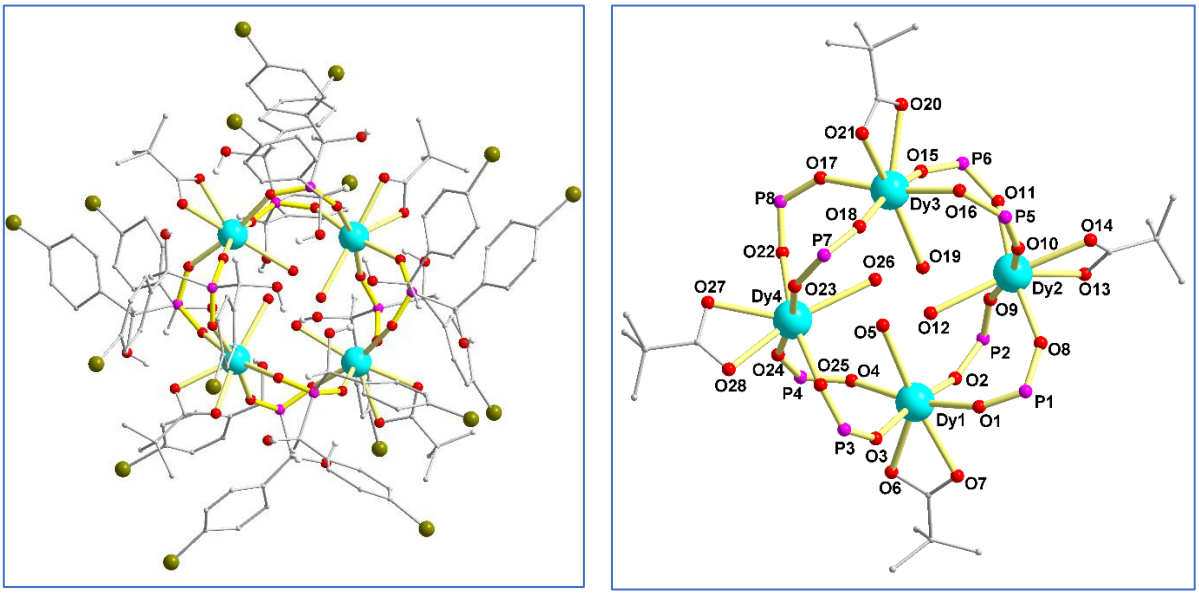

(a) **(b)**

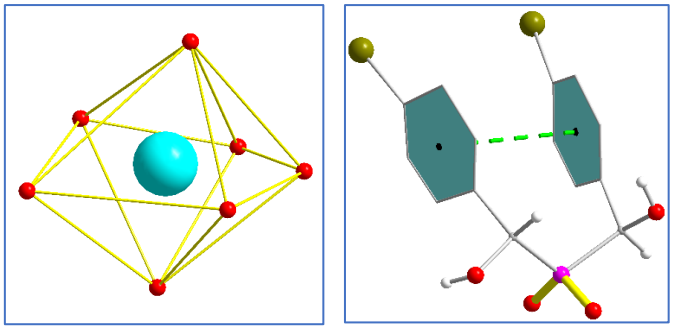

(c) **(d)**

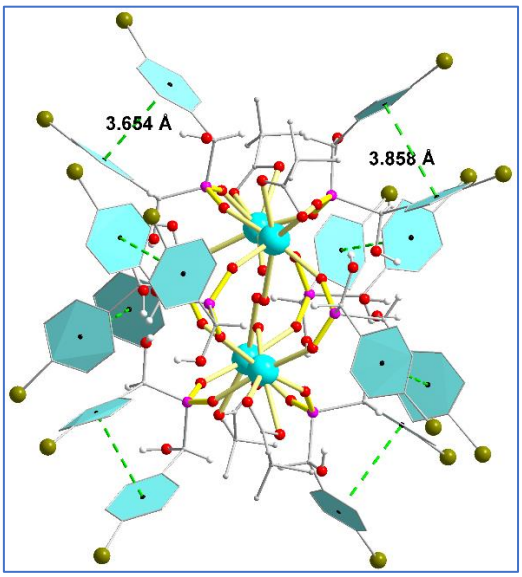

(e)

Figure 5.1. Ball and stick view **(a)** showing solid-state structure side view of **5.2**, **(b)** showing the core structure of **5.2, (c)** representation of coordination geometry of Dy(III) ions in **5.2, (d)** ligand conformation in the crystal structure, **(e)** intra-ligand π-π interaction of **5.2.**

Another important aspect of the crystal structure is that all four Dy-atoms are existing on the same molecular plane forming a [2 × 2] square grid-like structure (**figure. 5.2(a)**). A total eight number of phosphinic acid ligand molecules are present in the crystal structure. Four of them are present above and another four are below the Dy_4-molecular plane. Each ligand phosphinic acid has two hydroxy groups, among these groups one hydroxy group is directed towards the inside with interaction.(**figure 5.1(a)**) Four sets of these hydroxy groups formed a plane above the Dy_4-molecular plane while another four sets of hydroxy groups formed a plane below the Dy_4-molecular plane. The plane formed by four sets of water molecules attached to dysprosium atoms is ca. 3.937Å and 3.948Å distance from the above and below the plane of hydroxy groups of the ligands (**Figure 5.2(b)**).

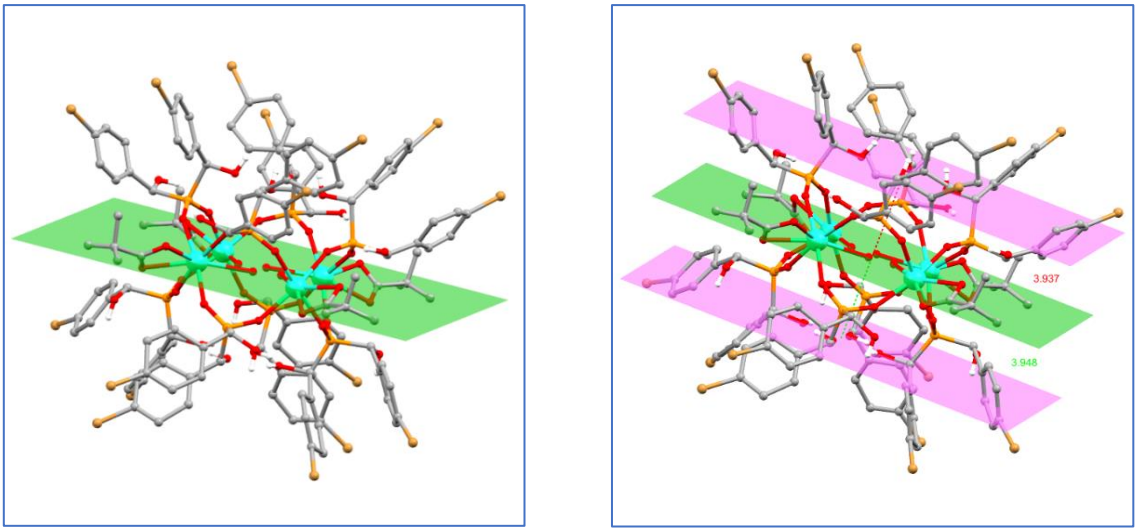

(a) **(b)**

Figure 5.2. Ball and stick view **(a)** showing the tetranuclear lanthanide Dy(III) ions are in the same plane. **(b)** showing the plane of four set H_2O molecules attached with Dy(III) ions and the plane of the four-set hydroxyl groups of the above ligands and four set hydroxyl groups of the below ligands.

In the crystal unit cell packing of **1,** empty-space/void is present (3978.47Å^3) which is calculated using the contact surface 1.2 Å probe radius and 0.7 grid spacing which is 21% of the unit cell in the packing diagram.(**figure 5.3(a)**) When the empty voids are calculated using solvent accessible surface it is 1495.66 Å^3 which is 7.9% of the unit cell volume.(**figure 5.3(b)**)

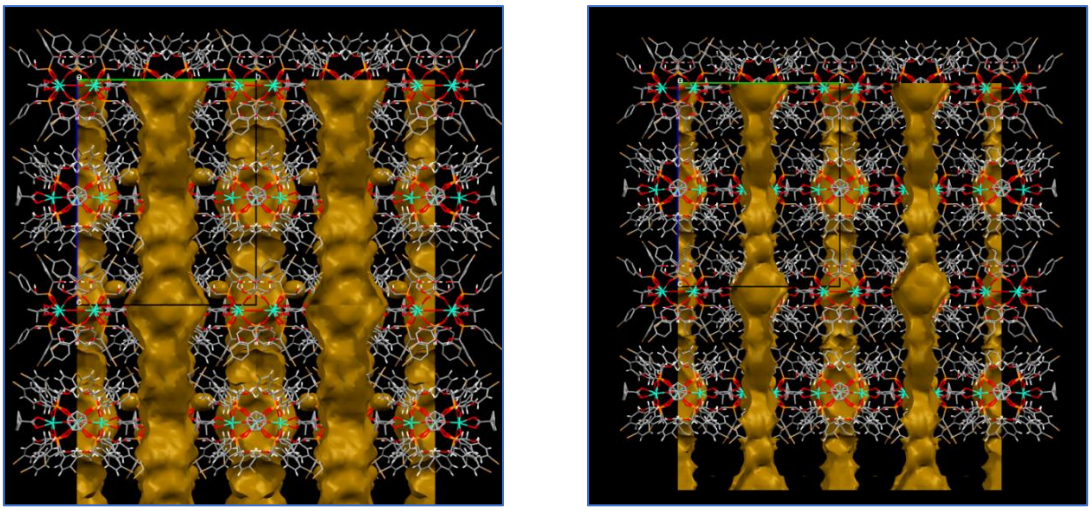

(a) **(b)**

Figure 5.3. Packing diagram view of void/empty space **(a)** using contact surface for **5.2**. **(b)** using the solvent accessible surface for **5.2**.

5.4 Conclusion:

We have successively synthesized and characterized tetranuclear self-assembled [2 × 2] grid-like topological structures where all the lanthanide metal atoms are present in the same plane. The neutral tetranuclear Ln_4-cluster is formed using chiral racemic bis-[α-hydroxy(p-bromophenyl)methyl]phosphinic acid. Probably it is the first example of a tetranuclear [2 × 2] square grid-like structure using such a chiral phosphinic acid ligand.

5.5 *Analytical and Spectroscopic Data*

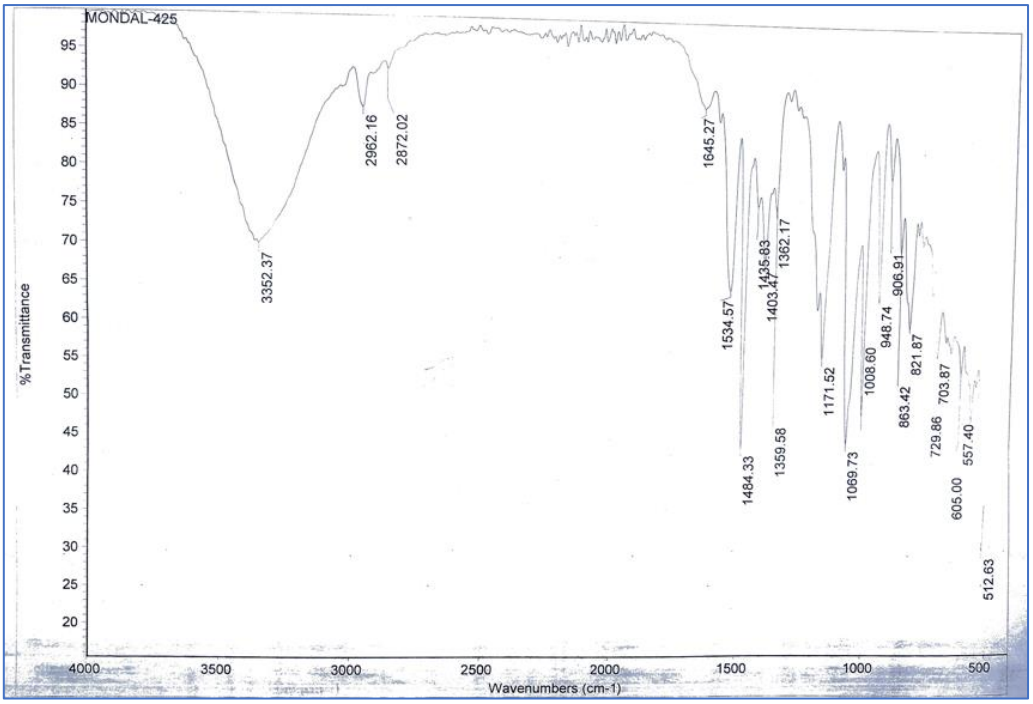

Figure 5.4. IR spectra of compound **5.1**

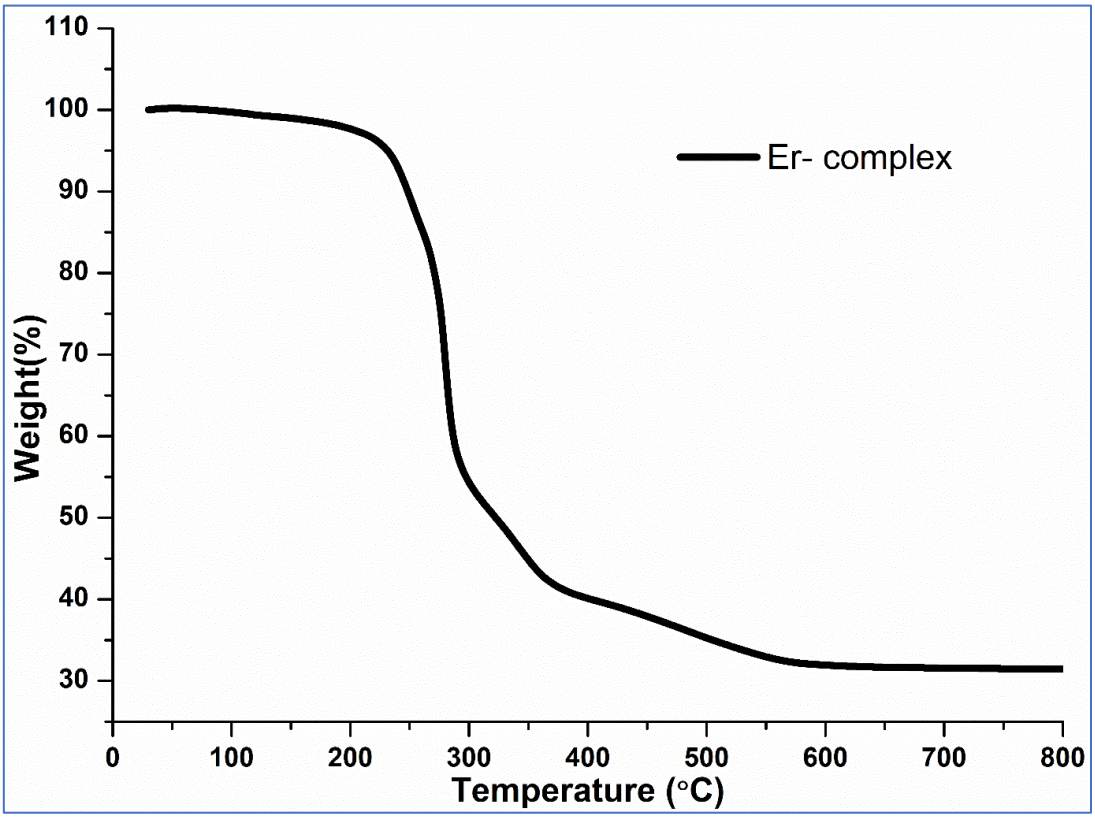

Figure 5.5. TGA of compound **5.1**

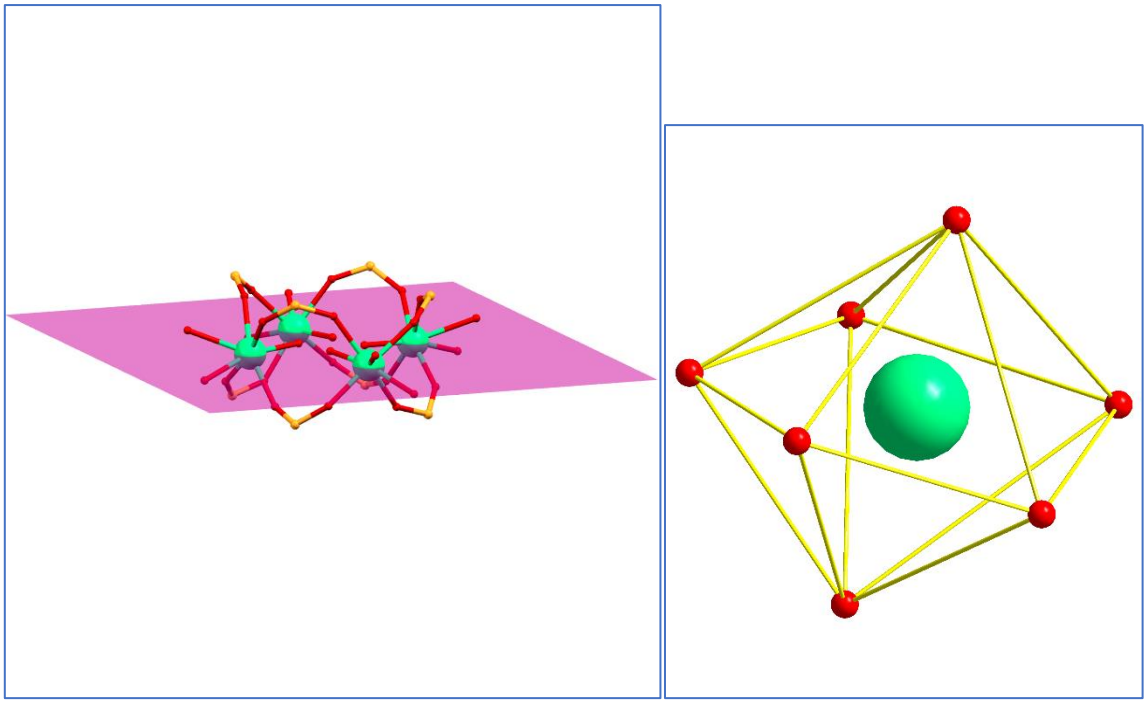

Figure 5.6. (a) A View of the square grid core of **5.1** where all the Er(III) ions are in the same plane **(b)** Ball and stick representation of coordination geometry of dysprosium atoms in **5.1**

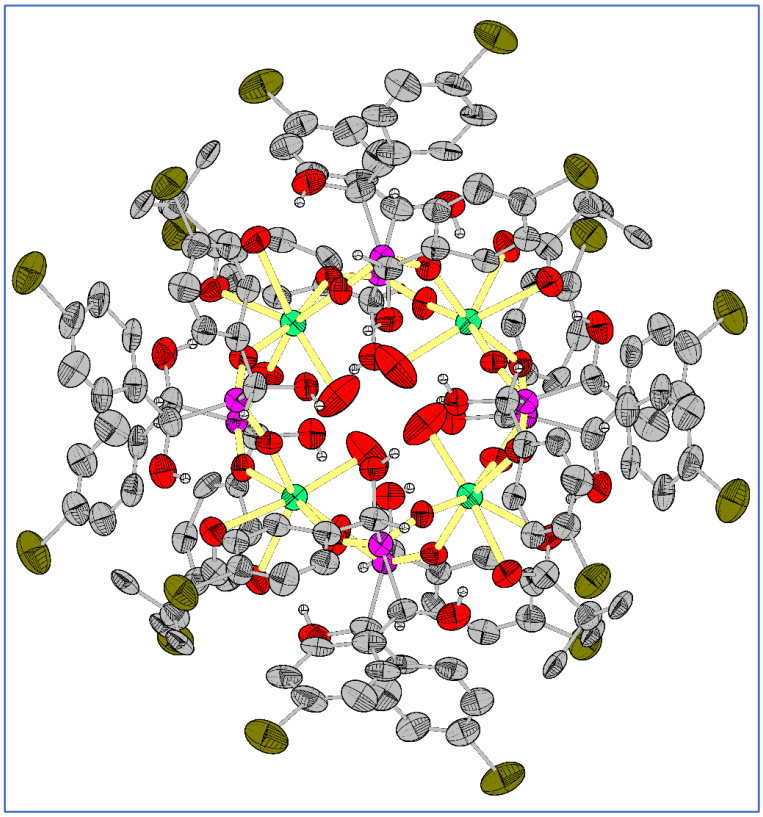

Figure 5.7. ORTEP view of **5.1** with thermal ellipsoids shown at 30%probability.

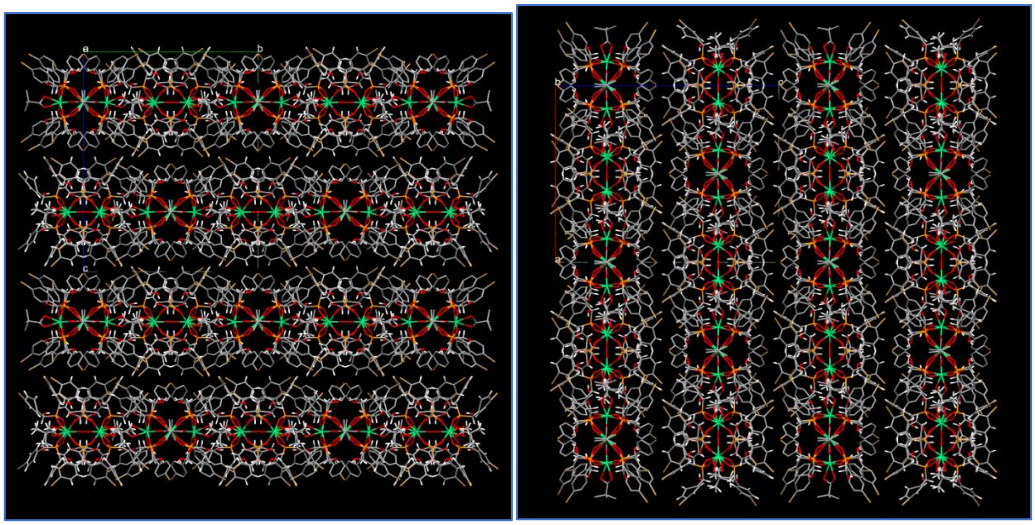

(a) (b)

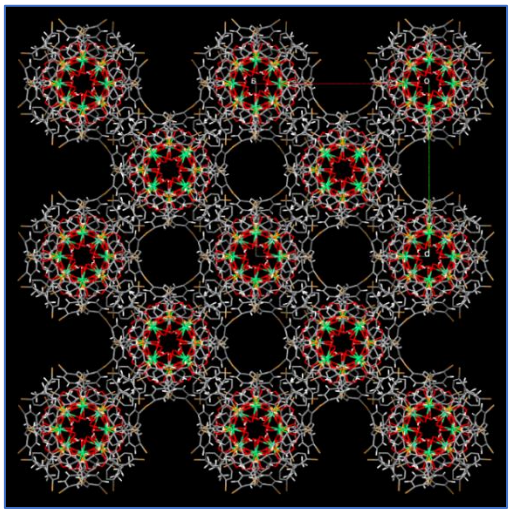

(c)

Figure 5.8. Packing diagram of **5.1** along **(a)** a-axis, **(b)** b-axis, **(c)** c-axis**.**

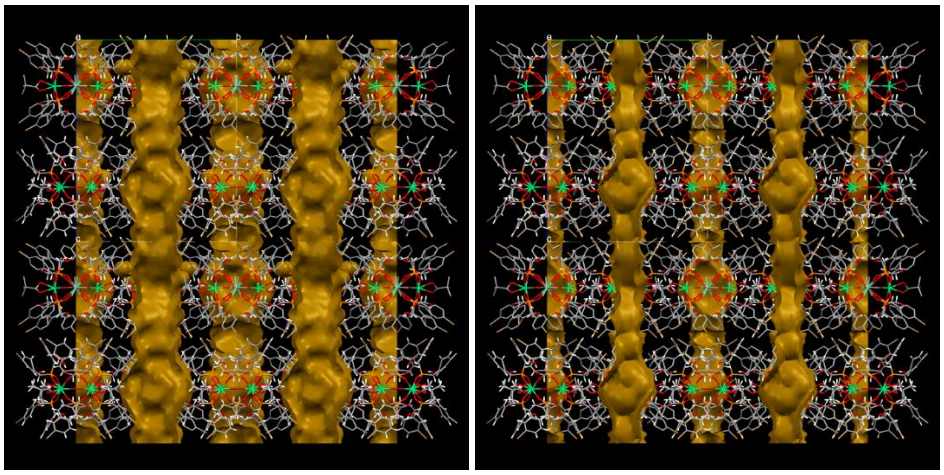

Figure 5.9. (a) Crystal packing diagram of **5.1** showing voids/empty spaces. (b) Crystal packing diagram of **5.1** showing solvent accessible surface.

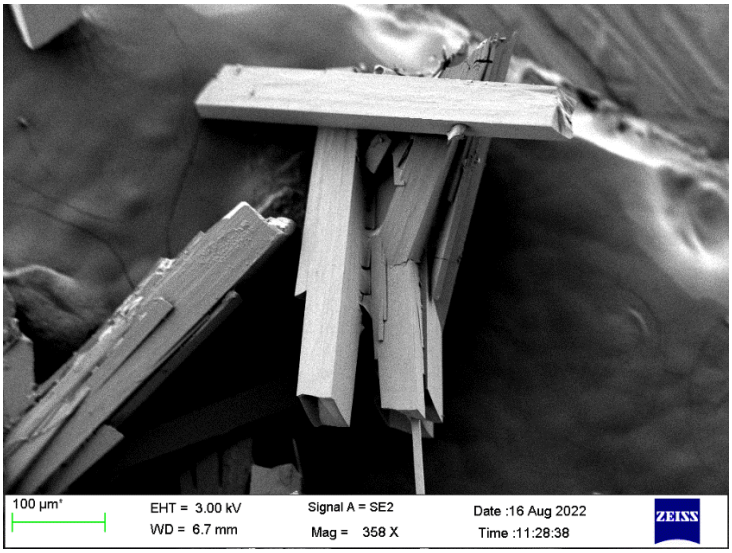

Figure 5.10. SEM image of **5.1**

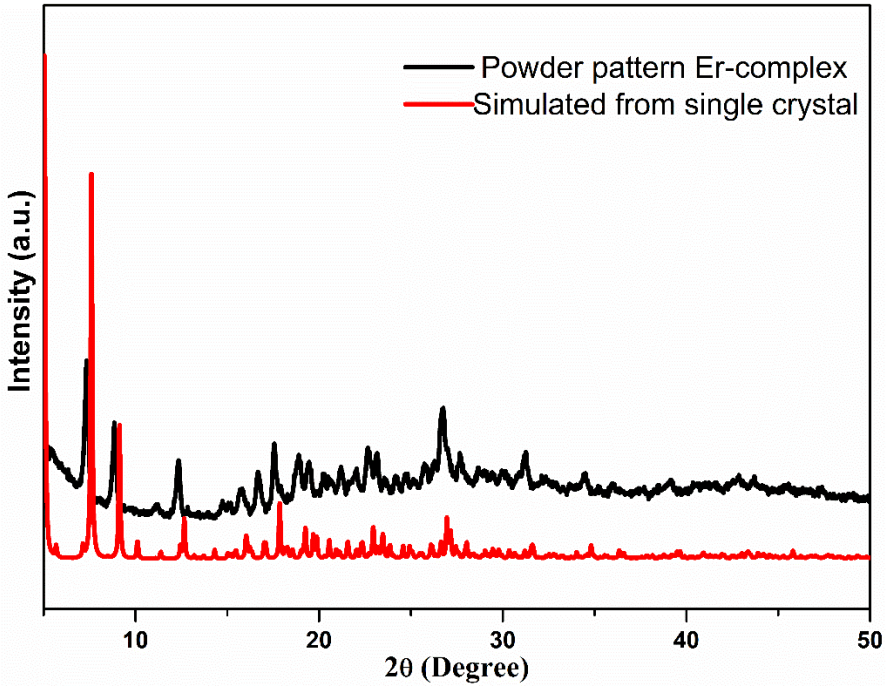

Figure 5.11. Powder X-ray diffraction pattern of a bulk sample of **5.1** compared to the simulated powder pattern extracted from single crystal diffraction data.

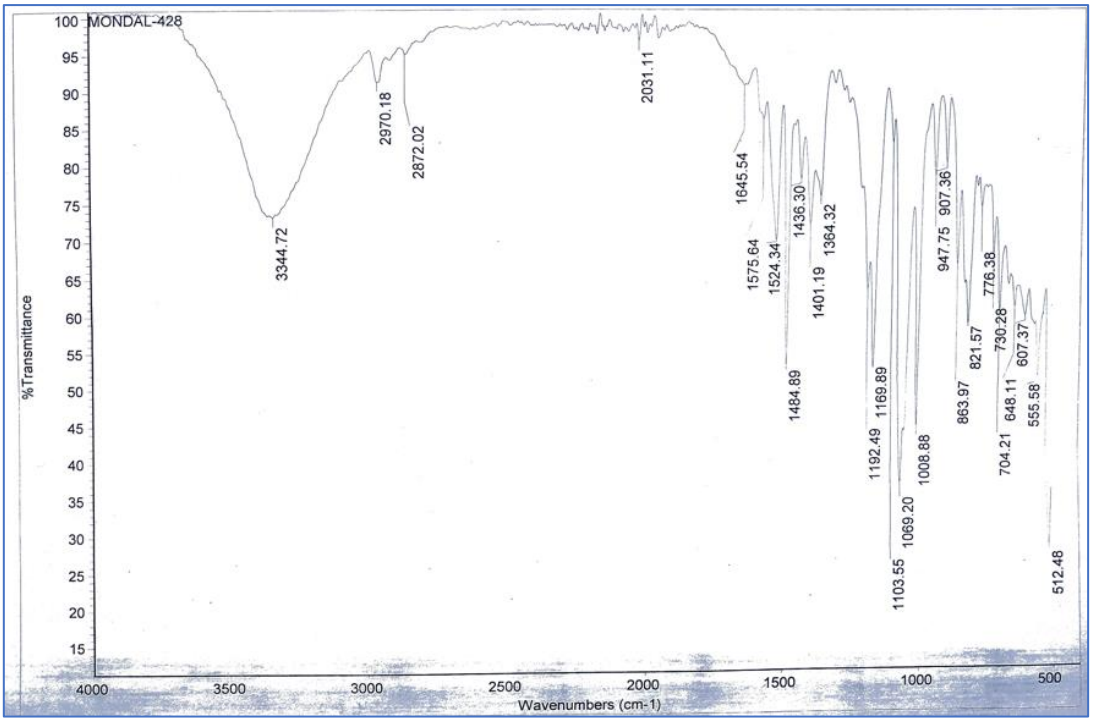

Figure 5.12. IR spectra of compound **5.2**

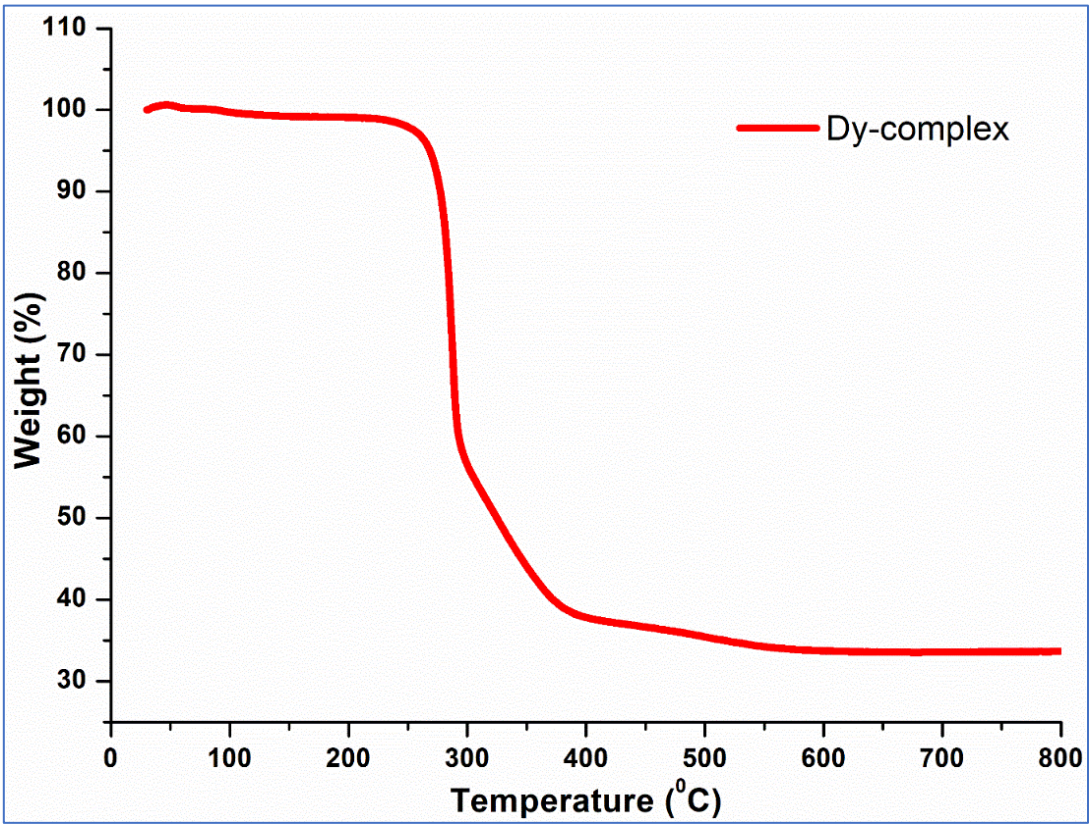

Figure 5.13. TGA of compound **5.2**

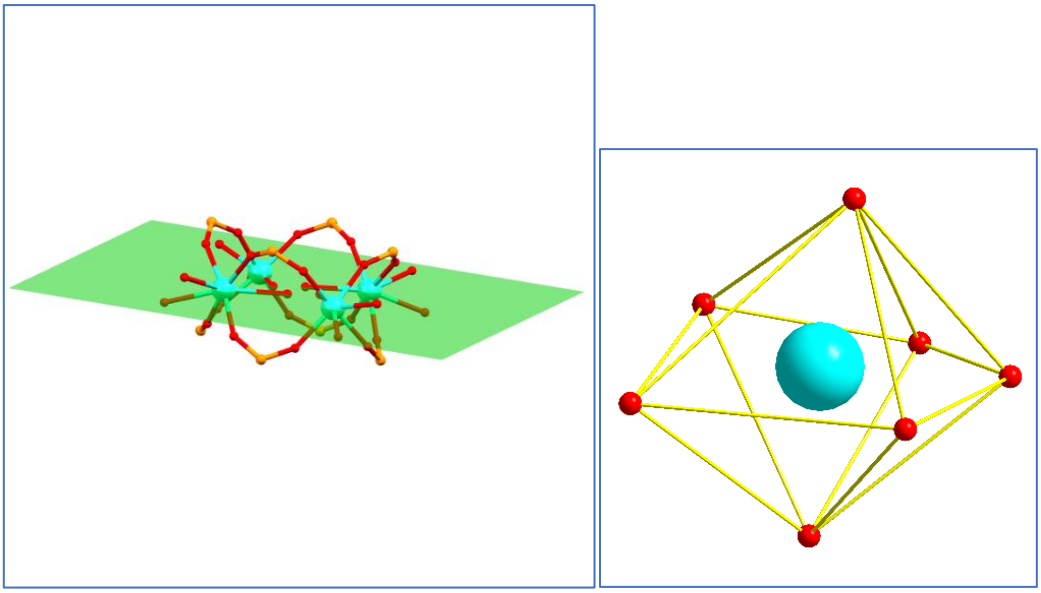

Figure 5.14. (a) A View of the square grid core of **5.2** where all the Dy(III) ions are in the same plane **(a)** Ball and stick representation of coordination geometry of dysprosium atoms in **5.2**

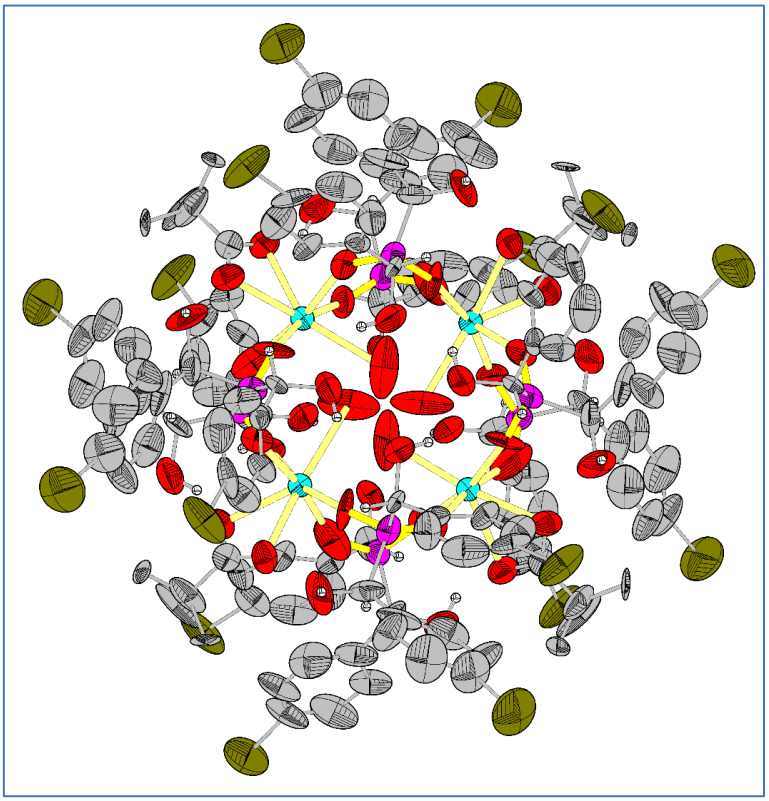

Figure 5.15. ORTEP view of **5.2** with thermal ellipsoids shown at 30%probability.

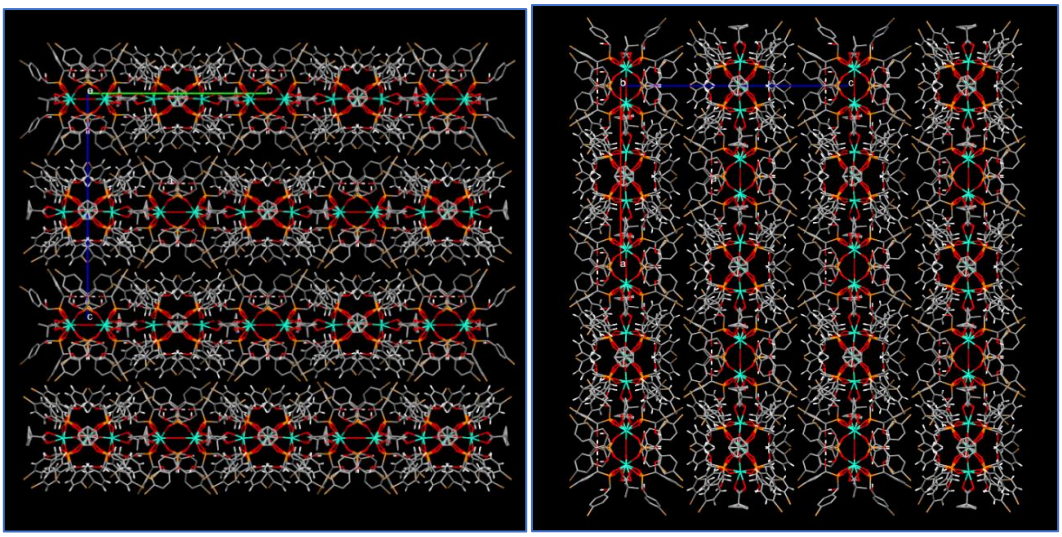

(a) (b)

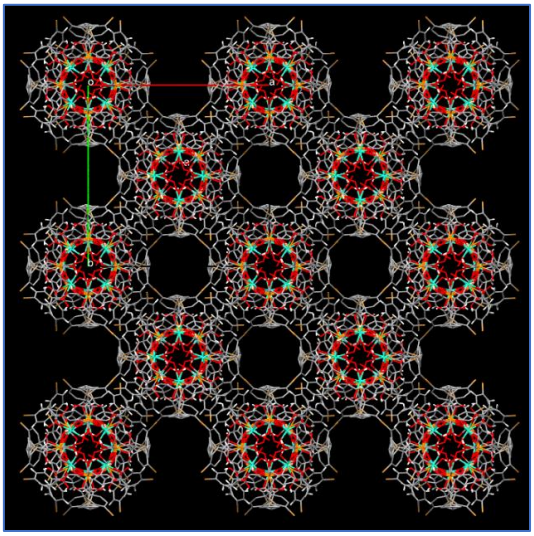

(c)

Figure 5.16. Packing diagram of **5.2.** along **(a)** a-axis, **(b)** b-axis, **(c)** c-axis**.**

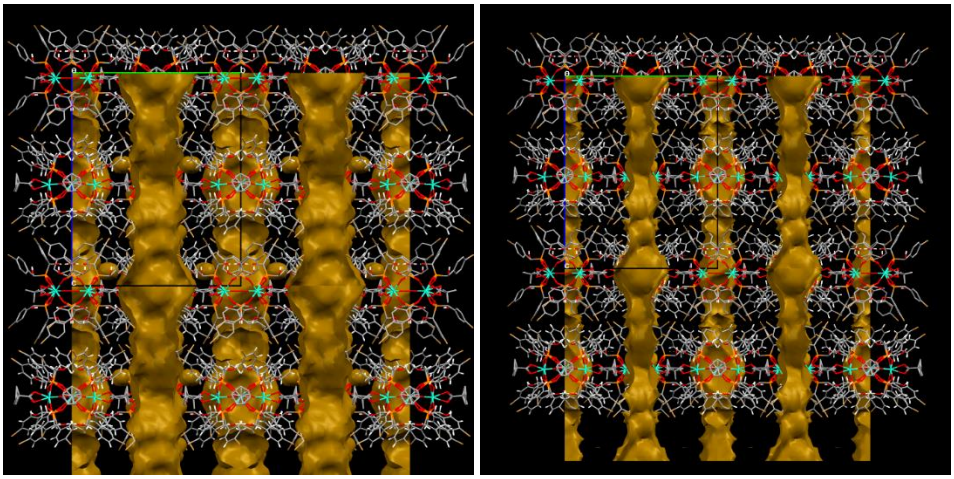

Figure 5.17. (a) Crystal packing diagram of **5.2** showing voids/empty spaces. (b) Crystal packing diagram of **5.2** showing solvent accessible surface.

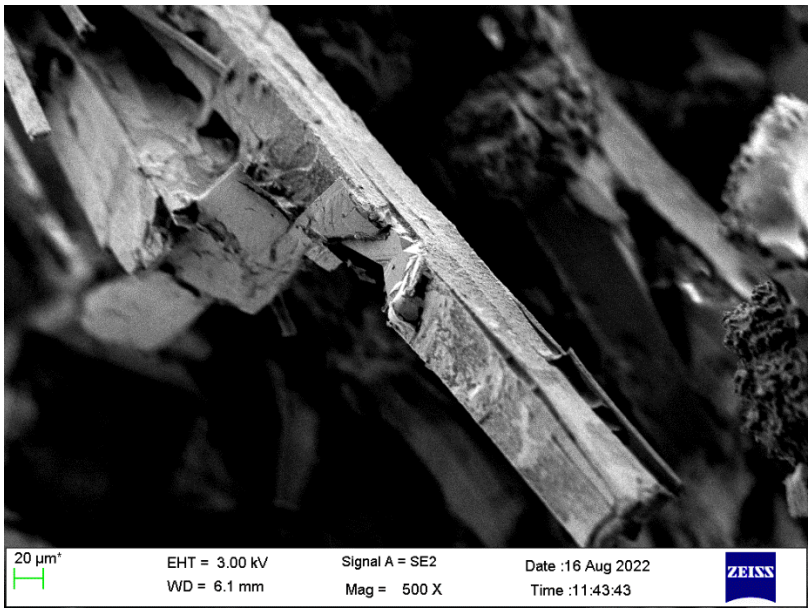

Figure 5.18. SEM image of **5.2**

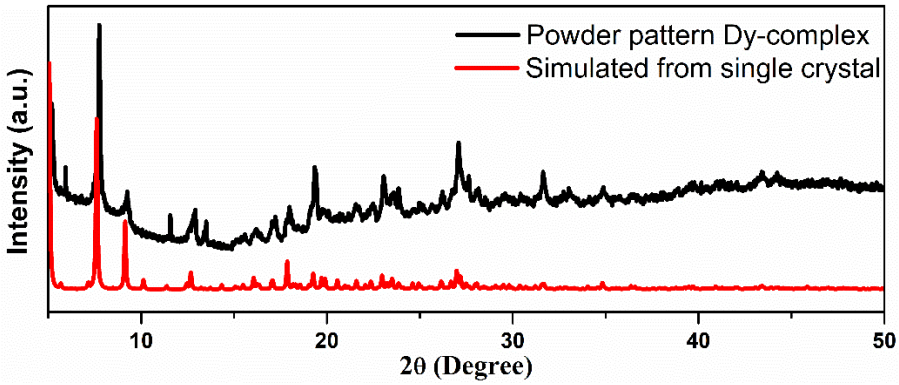

Figure 5.19. Powder X-ray diffraction pattern of a bulk sample of **5.2** compared to the simulated powder pattern extracted from single crystal diffraction data.

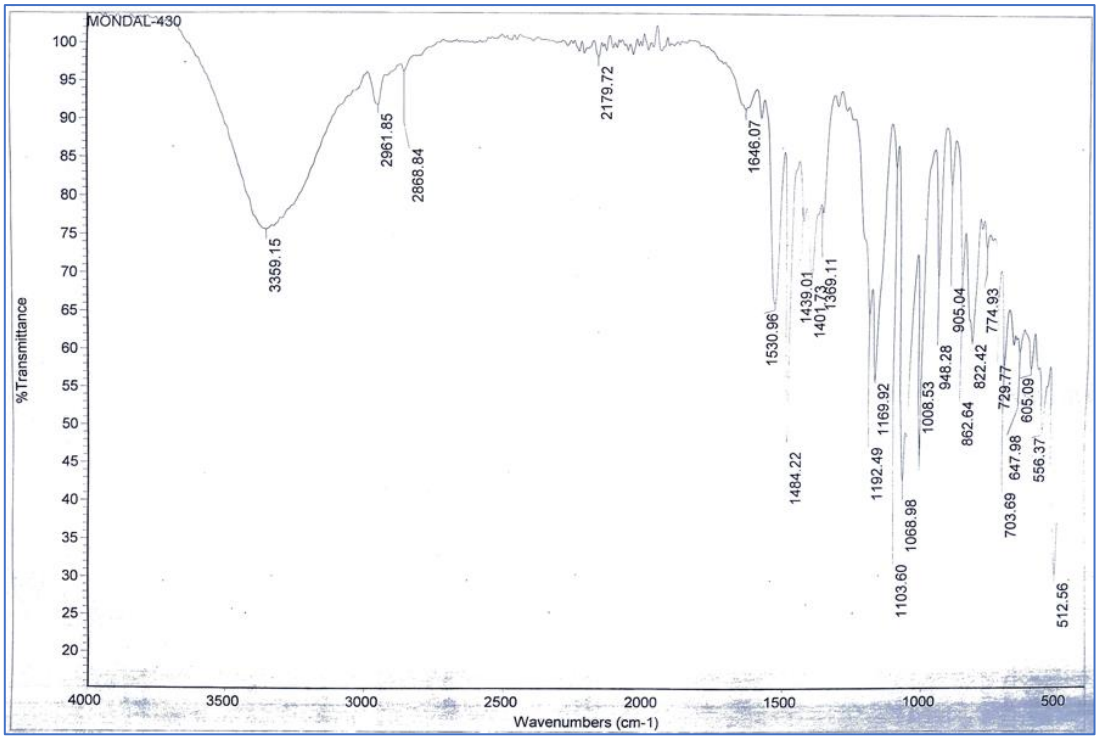

Figure 5.20. IR spectra of compound **5.3**

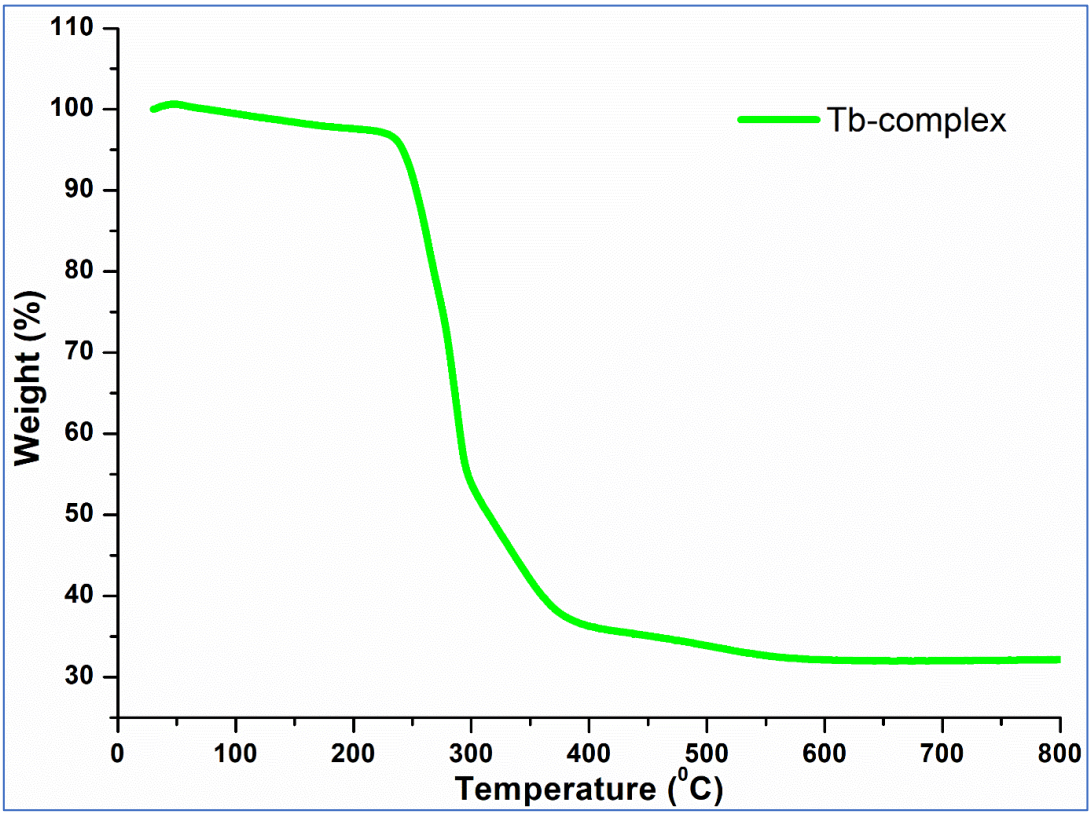

Figure 5.21. TGA of compound **5.3**

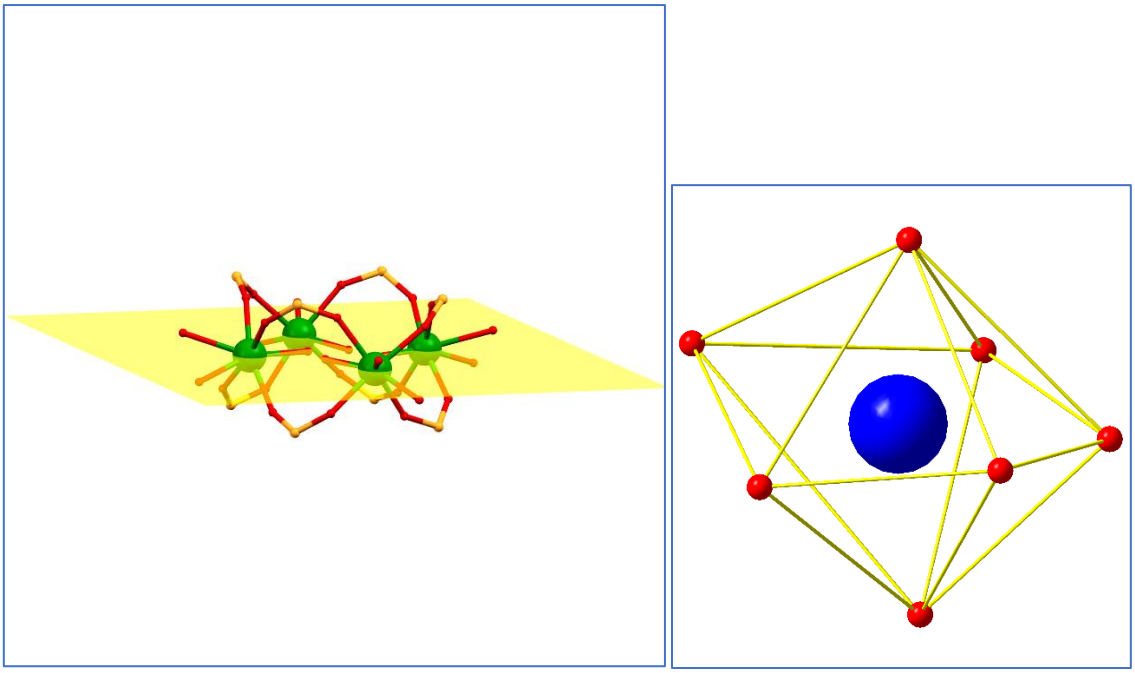

Figure 5.22. (a) A View of the square grid core of **5.3** where all the Tb(III) ions are in the same plane **(b)** Ball and stick representation of coordination geometry of dysprosium atoms in **5.3**

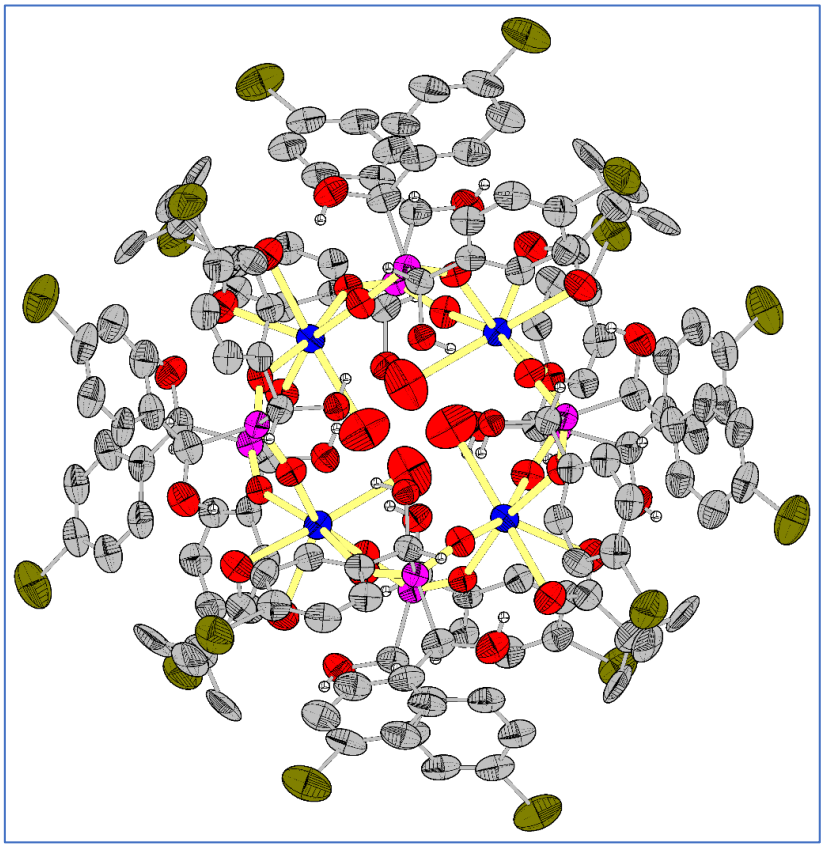

Figure 5.23. ORTEP view of **5.3** with thermal ellipsoids shown at 30%probability.

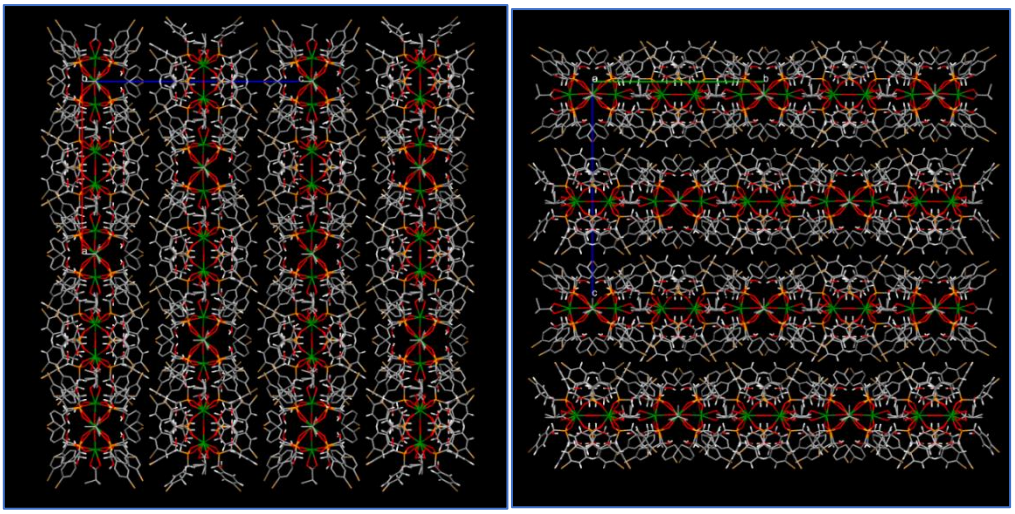

(a)…… **(b)**……

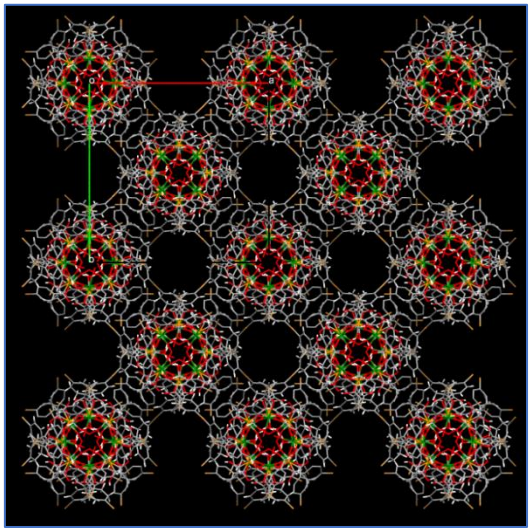

(c)

Figure 5.24. Packing diagram of **5.3.** along **(a)** a-axis, **(b)** b-axis, **(c)** c-axis**.**

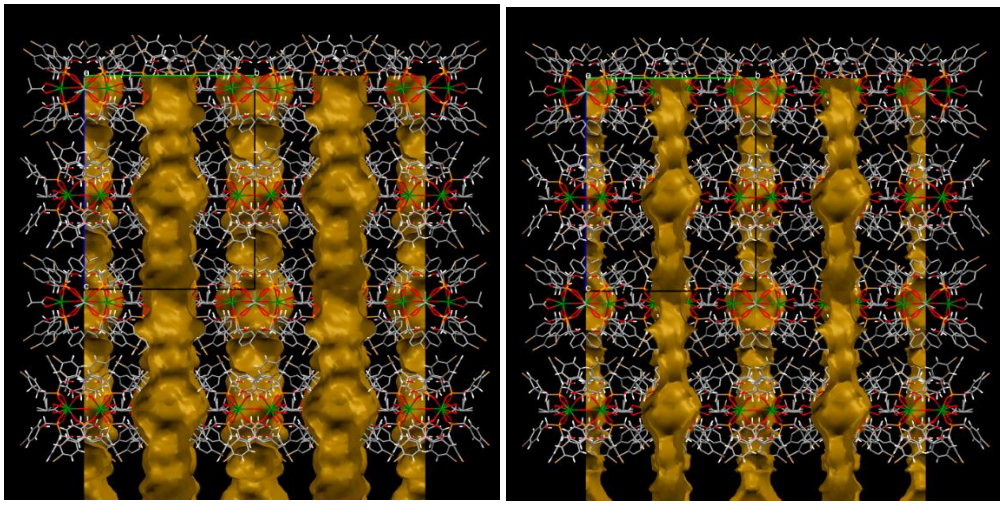

Figure 5.25. (a) Crystal packing diagram of **5.3** showing voids/empty spaces. (b) Crystal packing diagram of **5.3** showing solvent accessible surface.

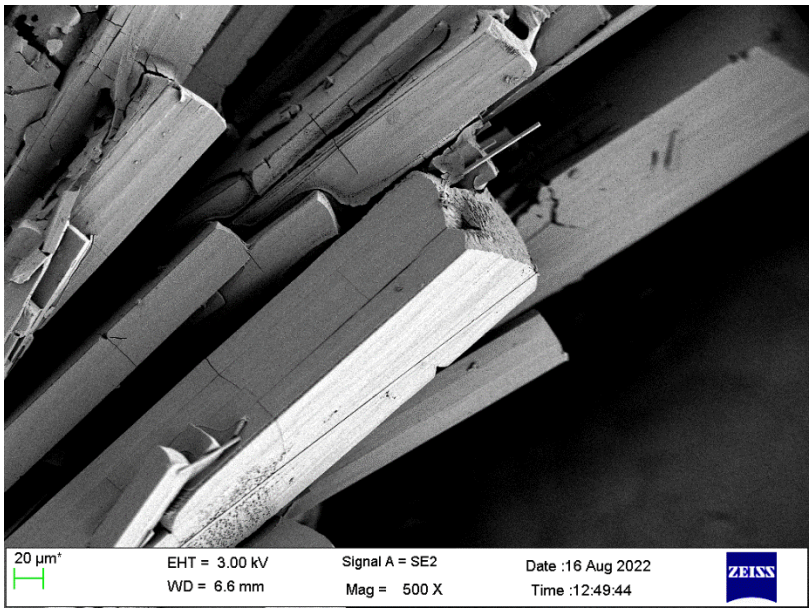

Figure 5.26. SEM image of **5.3.**

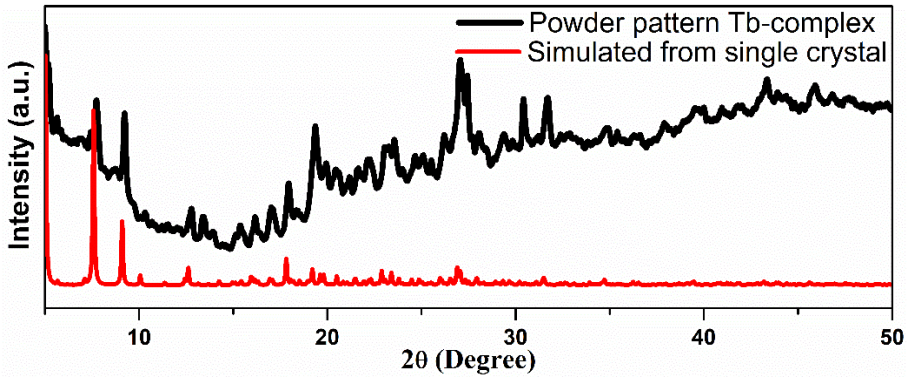

Figure 5.27. Powder X-ray diffraction pattern of a bulk sample of **5.3** compared to the simulated powder pattern extracted from single crystal diffraction data.

Table 5.2. Shape calculation of compound **5.1-5.3**

Sl. No.	Geometry	Cshm value for Er	Cshm value for Dy	Cshm value for Tb
1	HP-7 D_{7h} Heptagon	30.813	30.505	31.766
2	HPY-7 C_{6v} Hexagonal pyramid	22.593	22.163	22.893
3	PBPY-7 D_{5h} Pentagonal bipyramid	**1.451**	**2.653**	**2.458**
4	COC-7 C_{3v} Capped octahedron	7.009	7.333	6.605
5	CTPR-7 C_{2v} Capped trigonal prism	5.694	6.269	5.647
6	JPBPY-7 D_{5h} Johnson pentagonal bipyramid J13	4.215	5.406	5.139
7	JETPY-7 C_{3v} Johnson elongated triangular pyramid J7	22.831	21.738	21.459

Table 5.3. Crystallographic information of compound **5.1-5.3**.

	5.1	5.2	5.3
Empirical formula	$Br_{32}C_{268}Er_8H_{256}N_8O_{89.32}P_{16}$	$Br_{32}C_{270}Dy_8H_{215.2}N_6O_{90.6}P_{16}$	$Br_{32}C_{278}H_{226}N_{10}O_{90}P_{16}Tb_8$
Formula weight	9408.63	9345.91	9470.67
Temperature/K	100.0	100.0	100.0
Crystal system	tetragonal	tetragonal	tetragonal
Space group	I4	I4	I4
a/Å	24.729(2)	24.695(2)	24.841
b/Å	24.729(2)	24.695(2)	24.841
c/Å	31.087(4)	31.094(4)	31.117
α/°	90	90	90
β/°	90	90	90

γ/°	90	90	90
Volume/Å^3	19011(4)	18962(4)	19201.4
Z	2	2	2
ρ_{calc}g/cm^3	1.644	1.637	1.638
μ/mm^{-1}	5.244	5.063	4.919
F(000)	9077.0	8980.0	9128.0
Crystal size/mm^3	0.05 × 0.04 × 0.02	0.05 × 0.02 × 0.02	0.05 × 0.02 × 0.02
Radiation	MoKα (λ= 0.71073)	MoKα (λ= 0.71073)	MoKα (λ=0.71073)
2Θ range for data collection/°	2.104 to 55	2.106 to 52.878	2.098 to 52.684
Index ranges	-32 ≤ h ≤ 32, -32 ≤ k ≤ 31, -40 ≤ l ≤ 36	-30 ≤ h ≤ 30, -30 ≤ k ≤ 30, -38 ≤ l ≤ 38	-30 ≤ h ≤ 30, -30 ≤ k ≤ 30, -38 ≤ l ≤ 38
Reflections collected	215222	303295	214980
Independent reflections	21370 [R_{int} = 0.1190, R_{sigma} = 0.0764]	19470 [R_{int} = 0.1758, R_{sigma} = 0.1006]	19554 [R_{int} = 0.1439, R_{sigma} = 0.1086]
Data/restraints/parameters	21370/897/909	19470/99/918	19554/837/891
Goodness-of-fit on F^2	1.018	1.023	1.041
Final R indexes [I>=2σ (I)]	R_1 = 0.0880, wR_2 = 0.2458	R_1 = 0.0829, wR_2 = 0.1748	R_1 = 0.0859, wR_2 = 0.1891
Final R indexes [all data]	R_1 = 0.1511, wR_2 = 0.2967	R_1 = 0.1614, wR_2 = 0.2103	R_1 = 0.1814, wR_2 = 0.2326
Largest diff. peak/hole / e Å^{-3}	4.55/-1.08	1.17/-0.84	2.46/-1.26
Flack parameter	0.413(5)	0.191(9)	0.071(7)

Table 5.4. Selected bond lengths (Å) and bond angle (deg) parameters of compound **5.1**

Er1-O5	2.124(16)	Er1-O11	2.26(3)
Er1-O2^1	2.234(16)	Er2-O13	2.311(15)
Er1-O10	2.429(15)	Er2-O21	2.488(16)
Er1-O6^1	2.250(16)	Er2-O14^2	2.273(14)
Er1-O1	2.248(13)	Er2-O17	2.262(15)
Er1-O9	2.432(15)	Er2-O22	2.464(17)
Er1-O12	1.96(2)	Er2-O18^3	2.191(15)
Er1-O11^1	2.76(5)	Er2-O23	2.27(3)

^{1}+Y,-X,+Z; ^{2}+Y,1-X,+Z; ^{3}1-Y,+X,+Z

O5-Er1-O2^1	157.9(8)	O12-Er1-O6^1	90.3(8)
O5-Er1-O10	127.6(7)	O12-Er1-O1	98.1(8)
O5-Er1-O6^1	86.8(6)	O12-Er1-O9	160.6(11)
O5-Er1-O1	95.3(6)	O12-Er1-O11^1	19.7(14)
O5-Er1-O9	78.9(7)	O11-Er1-O10	161.6(18)
O5-Er1-O11	67.6(18)	O11-Er1-O9	138.8(16)

O5-Er1-O11[1]	94.6(13)	O11-Er1-O11[1]	46(2)
O2[1]-Er1-O10	74.4(7)	O13-Er2-O21	70.6(7)
O2[1]-Er1-O6[1]	94.2(6)	O13-Er2-O22	123.2(6)
O2[1]-Er1-O1	86.9(7)	O14[2]-Er2-O13	83.1(6)
O2[1]-Er1-O9	123.2(7)	O14[2]-Er2-O21	82.7(7)
O2[1]-Er1-O11	91.5(18)	O14[2]-Er2-O22	80.5(6)
O2[1]-Er1-O11[1]	64.4(14)	O14[2]-Er2-O23	105.0(10)
O10-Er1-O9	50.1(6)	O17-Er2-O13	160.9(6)
O10-Er1-O11[1]	131.4(10)	O17-Er2-O21	128.4(6)
O6[1]-Er1-O10	82.7(7)	O17-Er2-O14[2]	96.6(5)
O6[1]-Er1-O9	89.9(6)	O17-Er2-O22	75.2(6)
O6[1]-Er1-O11	110.7(17)	O17-Er2-O23	90.2(10)
O6[1]-Er1-O11[1]	76.0(13)	O22-Er2-O21	53.7(6)
O1-Er1-O10	89.6(6)	O18[3]-Er2-O13	95.0(6)
O1-Er1-O6[1]	171.5(6)	O18[3]-Er2-O21	84.9(7)
O1-Er1-O9	82.5(7)	O18[3]-Er2-O14[2]	167.4(6)
O1-Er1-O11[1]	111.9(13)	O18[3]-Er2-O17	89.3(6)
O1-Er1-O11	77.7(17)	O18[3]-Er2-O22	90.3(6)
O9-Er1-O11[1]	164.8(15)	O18[3]-Er2-O23	86.1(11)
O12-Er1-O5	81.8(12)	O23-Er2-O13	71.6(10)
O12-Er1-O2[1]	76.1(12)	O23-Er2-O21	140.1(11)
O12-Er1-O10	149.0(11)	O23-Er2-O22	165.0(9)

[1]+Y,-X,+Z; [2]+Y,1-X,+Z; [3]1-Y,+X,+Z; [4]-Y,+X,+Z

Table 5.5. Selected bond lengths (Å) and bond angle (deg) parameters of compound **5.2**

Dy2-O16	2.22(2)	Dy1-O2	2.277(16)
Dy2-O20	2.474(18)	Dy1-O6[3]	2.211(14)
Dy2-O13[1]	2.284(17)	Dy1-O10	2.458(19)
Dy2-O21	2.460(19)	Dy1-O5	2.262(15)
Dy2-O12	2.258(12)	Dy1-O1[3]	2.263(15)
Dy2-O17[2]	2.24(5)	Dy1-O9	2.442(19)
Dy2-O22[2]	2.72(3)	Dy1-O11[3]	2.77(7)
Dy2-O22	2.64(3)	Dy1-O11	2.56(7)

[1]1-Y,+X,+Z; [2]+Y,1-X,+Z; [3]+Y,2-X,+Z; [4]2-Y,+X,+Z

O16-Dy2-O20	75.0(8)	O2-Dy1-O10	85.8(6)
O16-Dy2-O13[1]	95.1(7)	O2-Dy1-O9	82.2(6)
O16-Dy2-O21	124.5(7)	O2-Dy1-O11[3]	112.1(8)
O16-Dy2-O12	166.5(7)	O2-Dy1-O11	88.2(11)
O16-Dy2-O17[2]	86.3(16)	O6[3]-Dy1-O2	167.0(6)
O16-Dy2-O22[2]	91.6(8)	O6[3] -Dy1-O10	81.8(6)
O16-Dy2-O22	72.1(7)	O6[3]-Dy1-O5	88.4(6)
O20-Dy2-O22	143.0(8)	O6[3]-Dy1-O1[3]	95.1(5)
O20-Dy2-O22[2]	164.5(7)	O6[3]-Dy1-O9	87.2(6)
O13[1]-Dy2-O20	82.9(7)	O6[3]-Dy1-O11[3]	80.3(9)
O13[1]-Dy2-O21	87.7(7)	O6[3]-Dy1-O11	104.7(11)
O13[1]-Dy2-O22	83.6(9)	O10-Dy1-O11[3]	141.7(9)
O13[1]-Dy2-O22[2]	106.2(7)	O10-Dy1-O11	166.6(7)
O21-Dy2-O20	50.4(6)	O5-Dy1-O2	95.2(6)
O21-Dy2-O22[2]	140.5(7)	O5-Dy1-O10	123.5(6)
O21-Dy2-O22	162.0(7)	O5-Dy1-O1[3]	162.6(6)
O12-Dy2-O20	118.5(7)	O5-Dy1-O9	71.1(6)
O12-Dy2-O13[1]	87.0(7)	O5-Dy1-O11	69.1(8)
O12-Dy2-O21	68.8(7)	O5-Dy1-O11[3]	89.7(7)
O12-Dy2-O22	94.9(7)	O1[3]-Dy1-O2	85.1(6)

O12-Dy2-O22[2]	75.1(7)	O1[3]-Dy1-O10	73.9(7)
O17[2]-Dy2-O20	88.5(10)	O1[3]-Dy1-O9	125.9(6)
O17[2]-Dy2-O13[1]	170.6(9)	O1[3]-Dy1-O11	93.6(9)
O17[2]-Dy2-O21	83.9(12)	O1[3]-Dy1-O11[3]	74.3(7)
O17[2]-Dy2-O12	93.9(15)	O9-Dy1-O10	52.9(7)
O17[2]-Dy2-O22	105.6(11)	O9-Dy1-O11[3]	157.4(7)
O17[2]-Dy2-O22[2]	83.0(10)	O9-Dy1-O11	137.9(10)
O22-Dy2-O22[2]	31.2(11)	O11-Dy1-O11[3]	32.7(12)

[1]1-Y,+X,+Z; [2]+Y,1-X,+Z; [3]+Y,2-X,+Z; [4]2-Y,+X,+Z

Table 5.6. Selected bond lengths (Å) and bond angle (deg) parameters of compound **5.3**

Tb1-O5	2.333(16)	Tb2-O15	2.280(14)
Tb1-O1	2.326(16)	Tb2-O20	2.274(17)
Tb1-O10	2.493(18)	Tb2-O22	2.277(15)
Tb1-O9	2.477(17)	Tb2-O19	2.455(18)
Tb1-O6[1]	2.252(18)	Tb2-O18	2.469(19)
Tb1-O2[2]	2.250(18)	Tb2-O12	2.271(16)
Tb1-O11	2.70(2)	Tb2-O21	2.64(4)
Tb1-O11[2]	2.69(3)	Tb2-O21[3]	2.68(4)

[1]1-Y,+X,+Z; [2]+Y,1-X,+Z; [3]1-Y,1+X,+Z; [4]-1+Y,1-X,+Z

O5-Tb1-O10	89.1(6)	O15-Tb2-O19	82.5(6)
O5-Tb1-O9	81.7(7)	O15-Tb2-O18	88.6(6)
O5-Tb1-O11	107.3(8)	O15-Tb2-O21	109.7(9)
O5-Tb1-O11[1]	84.0(8)	O15-Tb2-O21[3]	83.7(7)
O1-Tb1-O5	168.6(6)	O20-Tb2-O15	87.3(6)
O1-Tb1-O10	80.4(7)	O20-Tb2-O22	94.7(6)
O1-Tb1-O9	88.3(7)	O20-Tb2-O19	124.6(7)
O1-Tb1-O11[1]	107.3(8)	O20-Tb2-O18	73.5(7)
O1-Tb1-O11	83.8(8)	O20-Tb2-O21[3]	92.6(8)
O10-Tb1-O11[1]	163.7(8)	O20-Tb2-O21	72.2(8)
O10-Tb1-O11	140.8(7)	O22-Tb2-O15	168.7(6)
O9-Tb1-O10	51.9(6)	O22-Tb2-O19	87.2(6)
O9-Tb1-O11[1]	140.7(7)	O22-Tb2-O18	81.3(6)
O9-Tb1-O11	162.6(8)	O22-Tb2-O21[3]	107.3(7)
O6[2]-Tb1-O5	86.3(7)	O22-Tb2-O21	81.5(9)
O6[2]-Tb1-O1	94.8(6)	O19-Tb2-O18	52.0(6)
O6[2]-Tb1-O10	73.3(6)	O19-Tb2-O21[3]	139.4(8)
O6[2]-Tb1-O9	123.8(6)	O19-Tb2-O21	160.8(8)
O6[2]-Tb1-O11	72.5(8)	O18-Tb2-O21	140.0(9)
O6[2]-Tb1-O11[1]	91.4(7)	O18-Tb2-O21[3]	164.4(8)
O2[1]-Tb1-O5	95.1(7)	O12-Tb2-O15	94.5(6)
O2[1]-Tb1-O1	87.2(7)	O12-Tb2-O20	161.2(6)
O2[1]-Tb1-O10	123.7(6)	O12-Tb2-O22	87.1(6)
O2[1]-Tb1-O9	73.2(6)	O12-Tb2-O19	74.1(6)
O2[1]-Tb1-O6[2]	162.9(6)	O12-Tb2-O18	125.2(7)
O2[1]-Tb1-O11[1]	71.9(8)	O12-Tb2-O21	89.7(8)
O2[1]-Tb1-O11	90.9(8)	O12-Tb2-O21[3]	69.1(8)
O11[1]-Tb1-O11	31.4(10)	O21-Tb2-O21[3]	34.4(10)

[1]+Y,1-X,+Z; [2]1-Y,+X,+Z; [3]1-Y,1+X,+Z; [4]-1+Y,1-X,+Z

5.6 References:

1 Y. Shi, L. He, X. Wang, Z. Wu, N. Gao, H. Zhang, W. Wang and J. Cui, *J. Rare Earths*, 2020, **38**, 1231–1236.

2 J. Heine and K. Müller-Buschbaum, *Chem. Soc. Rev.*, 2013, **42**, 9232–9242.

3 Z. Wu, X. Lan, Y. Zhang, M. Li and G. Bai, *Dalt. Trans.*, 2019, **48**, 11063–11069.

4 C. Das, A. Upadhyay, K. U. Ansari, N. Ogiwara, T. Kitao, S. Horike and M. Shanmugam, *Inorg. Chem.*, 2018, **57**, 6584–6598.

5 S. J. Liu, C. Cao, C. C. Xie, T. F. Zheng, X. L. Tong, J. S. Liao, J. L. Chen, H. R. Wen, Z. Chang and X. H. Bu, *Dalt. Trans.*, 2016, **45**, 9209–9215.

6 S. J. Liu, S. De Han, J. P. Zhao, J. Xu and X. H. Bu, *Coord. Chem. Rev.*, 2019, **394**, 39–52.

7 T. F. Zheng, X. M. Tian, L. H. Wu, S. J. Liu, S. L. Yao, K. H. He, H. Huang, J. Liao, J. L. Chen and H. R. Wen, *New J. Chem.*, 2019, **43**, 18445–18450.

8 S. J. Liu, C. Cao, S. L. Yao, T. F. Zheng, Z. X. Wang, C. Liu, J. S. Liao, J. L. Chen, Y. W. Li and H. R. Wen, *Dalt. Trans.*, 2017, **46**, 64–70.

9 D. N. Woodru, R. E. P. Winpenny and R. A. Lay, *Chem. Rev.*, 2013, **113**, 5110–5148.

10 M. A. Novak, R. Sessoli, D. Gatteschi and A. Caneschi, *Nature*, 1993, **365**, 141–143.

11 Y. C. Chen, J. L. Liu, L. Ungur, J. Liu, Q. W. Li, L. F. Wang, Z. P. Ni, L. F. Chibotaru, X. M. Chen and M. L. Tong, *J. Am. Chem. Soc.*, 2016, **138**, 2829–2837.

12 J. Liu, Y. C. Chen, J. L. Liu, V. Vieru, L. Ungur, J. H. Jia, L. F. Chibotaru, Y. Lan, W. Wernsdorfer, S. Gao, X. M. Chen and M. L. Tong, *J. Am. Chem. Soc.*, 2016, **138**, 5441–5450.

13 J. Long, F. Habib, P. H. Lin, I. Korobkov, G. Enright, L. Ungur, W. Wernsdorfer, L. F. Chibotaru and M. Murugesu, *J. Am. Chem. Soc.*, 2011, **133**, 5319–5328.

14 and A. K. P. Jinkui Tang, Ian Hewitt, N. T. Madhu, Guillaume Chastanet, Wolfgang Wernsdorfer, Christopher E. Anson, Cristiano Benelli, Roberta Sessoli, *Angew. Chemie*, 2006, **118**, 1761–1765.

15 A. K. Jami, J. Ali, S. Mondal, J. Homs-Esquius, E. C. Sañudo and V. Baskar, *Polyhedron*, 2018, **151**, 90–99.

16 C. M. Liu and X. Hao, *ACS Omega*, 2022, **7**, 20229–20236.

17 H. L. Gao, S. X. Huang, X. P. Zhou, Z. Liu and J. Z. Cui, *Dalt. Trans.*, 2018, **47**, 3503–3511.

18 Y. X. Zhang, M. Li, B. Y. Liu, Z. L. Wu, H. Y. Wei and W. M. Wang, *RSC Adv.*, 2017, **7**, 55523–55535.

19 S. K. Langley, N. F. Chilton, I. A. Gass, B. Moubaraki and K. S. Murray, *Dalt. Trans.*, 2011, **40**, 12656–12659.

20 S. Biswas, S. Das, T. Gupta, S. K. Singh, M. Pissas, G. Rajaraman and V. Chandrasekhar, *Chem. - A Eur. J.*, 2016, **22**, 18532–18550.

21 H.-L. Gao, L. Jiang, S. Liu, H.-Y. Shen, W.-M. Wang and J.-Z. Cui, *Dalt. Trans.*, 2016, **45**, 253–264.

22 D. I. Alexandropoulos, L. Cunha-Silva, L. Pham, V. Bekiari, G. Christou and T. C. Stamatatos, *Inorg. Chem.*, 2014, **53**, 3220–3229.

23 M. Yadav, A. Mondal, V. Mereacre, S. K. Jana, A. K. Powell and P. W. Roesky, *Inorg. Chem.*, 2015, **54**, 7846–7856.

24 S. Y. Lin and J. Tang, *Polyhedron*, 2014, **83**, 185–196.

25 C. M. Liu, D. Q. Zhang and D. Ben Zhu, *Dalt. Trans.*, 2013, **42**, 14813–14818.

26 A. Rasamsetty, C. Das, E. C. Sañudo, M. Shanmugam and V. Baskar, *Dalt. Trans.*, 2018, **47**, 1726–1738.

27 M. Gebrezgiabher, S. Schlittenhardt, C. Rajnák, A. Sergawie, M. Ruben, M. Thomas and R. Boča, *Inorganics*, 2022, **10**, 1–11.

28 S. Y. Lin, L. Zhao, H. Ke, Y. N. Guo, J. Tang, Y. Guo and J. Dou, *Dalt. Trans.*, 2012, **41**, 3248–3252.

29 S. Das, A. Dey, S. Biswas, E. Colacio and V. Chandrasekhar, *Inorg. Chem.*, 2014, **53**, 3417–3426.

30 P. Kumar, J. Flores Gonzalez, P. P. Sahu, N. Ahmed, J. Acharya, V. Kumar, O. Cador, F. Pointillart, S. K. Singh and V. Chandrasekhar, *Inorg. Chem. Front.*, , DOI:10.1039/d2qi01260j.

31 A. K. Jami, V. Baskar and E. C. Sañudo, *Inorg. Chem.*, 2013, **52**, 2432–2438.

32 W. M. Wang, X. Y. Hu, Y. Yang, J. Q. Zhao, Y. X. Zhang, X. M. Kang and Z. L. Wu, *New J. Chem.*, 2020, **44**, 8494–8502.

33 W. Bin Sun, B. L. Han, P. H. Lin, H. F. Li, P. Chen, Y. M. Tian, M. Murugesu and P. F. Yan, *Dalt. Trans.*, 2013, **42**, 13397–13403.

34 Y. S. Xue, H. Qiao, X. Y. Zhao, S. Y. Liu, M. Xu, L. Bai and W. M. Wang, *Polyhedron*, 2018, **147**, 126–130.

35 V. Chandrasekhar, S. Hossain, S. Das, S. Biswas and J. Sutter, *Inorg. Chem.*, 2013, **52**, 6346–6353.

36 J. Goura, J. P. S. Walsh, F. Tuna and V. Chandrasekhar, *Inorg. Chem.*, 2014, **53**, 3385–3391.

37 H. Yu, J. X. Yang, J. Q. Han, P. F. Li, Y. L. Hou, W. M. Wang and M. Fang, *New J. Chem.*, 2019, **43**, 8067–8074.

38 P. Kumar, A. Swain, J. Acharya, Y. Li, V. Kumar, G. Rajaraman, E. Colacio and V. Chandrasekhar, *Inorg. Chem.*, 2022, **61**, 11600–11621.

39 S. Biswas, S. Das, S. Hossain, A. K. Bar, J. P. Sutter and V. Chandrasekhar, *Eur. J. Inorg. Chem.*, 2016, **2016**, 4683–4692.

40 P. Y. Chen, M. Z. Wu, T. Li, X. J. Shi, L. Tian and Z. Y. Liu, *Inorg. Chem.*, 2018, **57**, 12466–12470.

41 F. Luan, T. Liu, P. Yan, X. Zou, Y. Li and G. Li, *Inorg. Chem.*, 2015, **54**, 3485–3490.

42 Y. Wu, S. Morton, X. Kong, G. S. Nichol and Z. Zheng, *Dalt. Trans.*, 2011, **40**, 1041–1046.

43 B. H. Koo, K. S. Lim, D. W. Ryu, W. R. Lee, E. K. Koh and C. S. Hong, *Dalt. Trans.*, 2013, **42**, 7204–7209.

44 S. Xue, Y. N. Guo, L. Zhao, P. Zhang and J. Tang, *J. Chem. Soc. Dalt. Trans.*, 2014, **43**, 1564–1570.

45 V. Baskar and P. W. Roesky, *Zeitschrift fur Anorg. und Allg. Chemie*, 2005, **631**, 2782–2785.

46 X. Li, Y. Liu, X. W. Chi, G. Z. Zhu and F. Gao, *Zeitschrift fur Anorg. und Allg. Chemie*, 2020, **646**, 1292–1296.

47 C. Yang, Y. H. Wei, S. Xu, H. Y. Zhang, Y. Q. Yang, B. Zhang and M. Fang, *New J. Chem.*, 2021, **45**, 14103–14110.

48 D. Grebenyuk, M. Zobel, M. Polentarutti, L. Ungur, M. Kendin, K. Zakharov, P. Degtyarenko, A. Vasiliev and D. Tsymbarenko, *Inorg. Chem.*, 2021, **60**, 8049–8061.

49 Y. X. Zhang, Y. H. Zhang, B. Y. Liu, W. M. Wang, G. P. Tang, H. Y. Wei and Z. L. Wu, *New J. Chem.*, 2018, **42**, 18305–18311.

50 Z. H. Zhu, H. F. Wang, S. Yu, H. H. Zou, H. L. Wang, B. Yin and F. P. Liang, *Inorg. Chem.*, 2020, **59**, 11640–11650.

51 Y. Shi, Y. X. Zhang, M. Li, Y. H. Zhang, B. Y. Liu, G. P. Tang, Z. Q. Zhang, K. X. Liu, Z. L. Wu and W. M. Wang, *Polyhedron*, 2019, **157**, 292–296.

52 H. Tian, Y. N. Guo, L. Zhao, J. Tang and Z. Liu, *Inorg. Chem.*, 2011, **50**, 8688–8690.

53 R. Sessoli and A. K. Powell, *Coord. Chem. Rev.*, 2009, **253**, 2328–2341.

54 I. J. Hewitt, J. Tang, N. T. Madhu, C. E. Anson, Y. Lan, J. Luzon, M. Etienne, R. Sessoli and A. K. Powell, *Angew. Chemie - Int. Ed.*, 2010, **49**, 6352–6356.

55 V. Chandrasekhar, S. Hossain, S. Das, S. Biswas and J. P. Sutter, *Inorg. Chem.*, 2013, **52**, 6346–6353.

56 P. H. Guo, J. Liu, Z. H. Wu, H. Yan, Y. C. Chen, J. H. Jia and M. L. Tong, *Inorg. Chem.*, 2015, **54**, 8087–8092.

57 L. N. Dawe, K. V. Shuvaev and L. K. Thompson, *Chem. Soc. Rev.*, 2009, **38**, 2334–2359.

58 V. A. Milway, S. M. T. Abedin, V. Niel, T. L. Kelly, L. N. Dawe, S. K. Dey, D. W. Thompson, D. O. Miller, M. S. Alam, P. Müller and L. K. Thompson, *J. Chem. Soc. Dalt. Trans.*, 2006, 2835–2851.

59 L. N. Dawe, K. V. Shuvaev and L. K. Thompson, *Inorg. Chem.*, 2009, **48**, 3323–3341.

60 M. U. Anwar, L. K. Thompson, L. N. Dawe, F. Habib and M. Murugesu, *Chem. Commun.*, 2012, **48**, 4576–4578.

61 J. Wu, S. Y. Lin, S. Shen, X. L. Li, L. Zhao, L. Zhang and J. Tang, *Dalt. Trans.*, 2017,

46, 1577–1584.

62 Y. Bi, X. T. Wang, W. Liao, X. Wang, R. Deng, H. Zhang and S. Gao, *Inorg. Chem.*, 2009, **48**, 11743–11747.

63 S. Biswas, J. Goura, S. Das, C. V. Topping, J. Brambleby, P. A. Goddard and V. Chandrasekhar, *Inorg. Chem.*, 2016, **55**, 8422–8436.

64 W. M. Wang, X. Z. Li, L. Zhang, J. L. Chen, J. H. Wang, Z. L. Wu and J. Z. Cui, *New J. Chem.*, 2019, **43**, 7419–7426.

65 S. Xue, L. Zhao, Y. N. Guo and J. Tang, *Dalt. Trans.*, 2012, **41**, 351–353.

66 A. Gusev, R. Herchel, I. Nemec, V. Shul'gin, I. L. Eremenko, K. Lyssenko, W. Linert and Z. Trávníček, *Inorg. Chem.*, 2016, **55**, 12470–12476.

67 S. Xue, L. Zhao, Y. N. Guo, X. H. Chen and J. Tang, *Chem. Commun.*, 2012, **48**, 7031–7033.

68 [b] Chinmoy Das,[a] Shefali Vaidya,[a] TulikaGupta,[a] Jamie M. Frost,[c] Mattia Righi,[b] Euan K. Brechin,[c] MarcoAffronte, [a] and Gopalan Rajaraman and M. Shanmugam*[a, *Chem. - A Eur. J.*, 2015, **21**, 15639–15650.

69 C. Sourav Biswas,[a] Sourav Das,[a] Jan van Leusen,[b] Paul Kögerler,*[b] and Vadapalli Chandrasekhar*[a and Keywords:, *Eur. J. Inorg. Chem.*, 2014, 4159–4167.

70 E. C. C. Baly, *Inorg. Chem. Front.*, 2022, **9**, 36–72.

71 E. Sourav Biswas,[a] Sourav Das,[b] Sakiat Hossain,[a] Arun Kumar Bar,[c, d] Jean-Pascal Sutter,*[c, d] and Vadapalli Chandrasekhar*[a, *Eur. J. Inorg. Chem.*, 2016, 4683–4692.

72 Q. Yang, L. Ungur, W. Wernsdorfer and J. Tang, *Inorg. Chem. Front.*, 2022, **9**, 784–791.

73 N. M. Randell, M. U. Anwar, M. W. Drover, L. N. Dawe and L. K. Thompson, *Inorg. Chem.*, 2013, **52**, 6731–6742.

74 D. N. Woodruff, F. Tuna, M. Bodensteiner, R. E. P. Winpenny and R. A. Layfield, *Organometallics*, 2013, **32**, 1224–1229.

75 C. Xu, Z. Wu, C. Fan, L. Yan, W. Wang and B. Ji, *J. Rare Earths*, 2021, **39**, 1082–1088.

76 S. Q. Wu, Q. W. Xie, G. Y. An, X. Chen, C. M. Liu, A. L. Cui and H. Z. Kou, *Dalt. Trans.*, 2013, **42**, 4369–4372.

77 T. Ashebr, X.-L. Li, C. Zhao, Q. Yang and J. Tang, *CrystEngComm*, 2022, 6688–6695.

78 W. Huang, F. X. Shen, S. Q. Wu, L. Liu, D. Wu, Z. Zheng, J. Xu, M. Zhang, X. C. Huang, J. Jiang, F. Pan, Y. Li, K. Zhu and O. Sato, *Inorg. Chem.*, 2016, **55**, 5476–5484.

79 V. M. Dubovik and V. V. Tugushev, *Phys. Rep.*, 1990, **187**, 145–202.

80 B. B. Van Aken, J. P. Rivera, H. Schmid and M. Fiebig, *Nature*, 2007, **449**, 702–705.

81 M. Fiebig, *J. Phys. D. Appl. Phys.*, , DOI:10.1088/0022-3727/38/8/R01.

82 X. L. Li and J. Tang, *Dalt. Trans.*, 2019, **48**, 15358–15370.

83 L. Ungur, S. Y. Lin, J. Tang and L. F. Chibotaru, *Chem. Soc. Rev.*, 2014, **43**, 6894–6905.

84 P. H. Guo, J. L. Liu, Z. M. Zhang, L. Ungur, L. F. Chibotaru, J. D. Leng, F. S. Guo and M. L. Tong, *Inorg. Chem.*, 2012, **51**, 1233–1235.

85 M. Gysler, F. El Hallak, L. Ungur, R. Marx, M. Hakl, P. Neugebauer, Y. Rechkemmer, Y. Lan, I. Sheikin, M. Orlita, C. E. Anson, A. K. Powell, R. Sessoli, L. F. Chibotaru and J. Van Slageren, *Chem. Sci.*, 2016, **7**, 4347–4354.

86 J. Luzon, K. Bernot, I. J. Hewitt, C. E. Anson, A. K. Powell and R. Sessoli, *Phys. Rev. Lett.*, 2008, **100**, 1–4.

87 G. Novitchi, G. Pilet, L. Ungur, V. V. Moshchalkov, W. Wernsdorfer, L. F. Chibotaru, D. Luneau and A. K. Powell, *Chem. Sci.*, 2012, **3**, 1169–1176.

88 L. Zhong, W. Bin Chen, Z. J. Ouyang, M. Yang, Y. Q. Zhang, S. Gao, M. Schulze, W. Wernsdorfer and W. Dong, *Chem. Commun.*, 2020, **56**, 2590–2593.

89 S. Xue, X. H. Chen, L. Zhao, Y. N. Guo and J. Tang, *Inorg. Chem.*, 2012, **51**, 13264–13270.

90 Y. X. Wang, W. Shi, H. Li, Y. Song, L. Fang, Y. Lan, A. K. Powell, W. Wernsdorfer, L. Ungur, L. F. Chibotaru, M. Shen and P. Cheng, *Chem. Sci.*, 2012, **3**, 3366–3370.

91 X. L. Li, J. Wu, J. Tang, B. Le Guennic, W. Shi and P. Cheng, *Chem. Commun.*, 2016, **52**, 9570–9573.

92 S. Y. Lin, W. Wernsdorfer, L. Ungur, A. K. Powell, Y. N. Guo, J. Tang, L. Zhao, L. F. Chibotaru and H. J. Zhang, *Angew. Chemie - Int. Ed.*, 2012, **51**, 12767–12771.

93 A. Baniodeh, N. Magnani, S. Bräse, C. E. Anson and A. K. Powell, *Dalt. Trans.*, 2015, **44**, 6343–6347.

94 J. Wu, O. Cador, X. L. Li, L. Zhao, B. Le Guennic and J. Tang, *Inorg. Chem.*, 2017, **56**, 11211–11219.

95 L. Ungur, S. K. Langley, T. N. Hooper, B. Moubaraki, E. K. Brechin, K. S. Murray and L. F. Chibotaru, *J. Am. Chem. Soc.*, 2012, **134**, 18554–18557.

96 S. K. Langley, B. Moubaraki, C. M. Forsyth, I. A. Gass and K. S. Murray, *Dalt. Trans.*, 2010, **39**, 1705–1708.

97 J. Wu, X. L. Li, M. Guo, L. Zhao, Y. Q. Zhang and J. Tang, *Chem. Commun.*, 2018, **54**, 1065–1068.

98 J. Wu, L. Zhao, L. Zhang, X. L. Li, M. Guo, A. K. Powell and J. Tang, *Angew. Chemie - Int. Ed.*, 2016, **55**, 15574–15578.

99

100 B. Kaboudin and N. As-Habei, *Tetrahedron Lett.*, 2004, **45**, 9099–9101.

101 B. Kaboudin and H. Haghighat, *J. Org. Chem.*, 2006, **71**, 6604–6606.

102 O. V. Dolomanov, L. J. Bourhis, R. J. Gildea, J. A. K. Howard and H. Puschmann, *J.*

Appl. Crystallogr., 2009, **42**, 339–341.

103 G. M. Sheldrick, *Acta Crystallogr. Sect. A Found. Crystallogr.*, 2015, **71**, 3–8.

104 G. M. Sheldrick, *Acta Crystallogr. Sect. C Struct. Chem.*, 2015, **71**, 3–8.

105 L. J. Bourhis, O. V. Dolomanov, R. J. Gildea, J. A. K. Howard and H. Puschmann, *Acta Crystallogr. Sect. A Found. Crystallogr.*, 2015, **71**, 59–75.

A few crystal structures

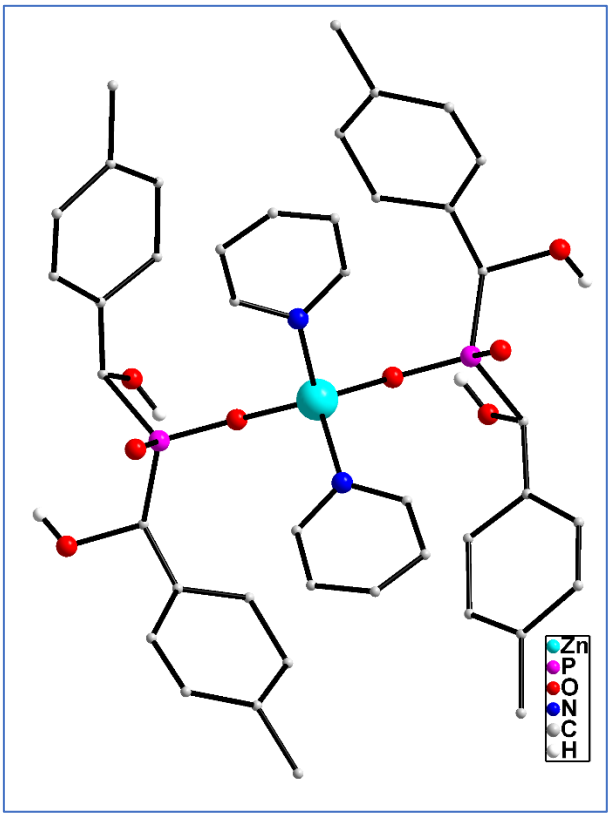

Figure 6.1. Ball and stick view of zinc phosphinate molecular structure.

checkCIF/PLATON report

Structure factors have been supplied for datablock(s) vb8211-7-2019

THIS REPORT IS FOR GUIDANCE ONLY. IF USED AS PART OF A REVIEW PROCEDURE FOR PUBLICATION, IT SHOULD NOT REPLACE THE EXPERTISE OF AN EXPERIENCED CRYSTALLOGRAPHIC REFEREE.

No syntax errors found. CIF dictionary Interpreting this report

Datablock: vb8211-7-2019

Bond precision: C-C = 0.0254 A Wavelength=0.71073

Cell: a=18.6380(5) b=8.4379(4) c=25.8086(11)
alpha=90 beta=90 gamma=90
Temperature: 100 K

	Calculated	Reported
Volume	4058.8(3)	4058.8(3)
Space group	C m c m	C m c m
Hall group	-C 2c 2	-C 2c 2
Moiety formula	C58 H58 N2 O8 P2 Zn, O	0.5(C116 H116 N4 O16 P4 Zn2), O
Sum formula	C58 H58 N2 O9 P2 Zn	C58 H58 N2 O9 P2 Zn
Mr	1054.39	1054.37
Dx,g cm-3	1.725	1.725
Z	4	4
Mu (mm-1)	0.760	0.760
F000	2208.0	2208.0
F000'	2210.84	
h,k,lmax	23,10,32	22,10,32
Nref	2308	2228
Tmin,Tmax	0.808,0.840	0.832,1.000
Tmin'	0.808	

Correction method= # Reported T Limits: Tmin=0.832 Tmax=1.000
AbsCorr = MULTI-SCAN

Data completeness= 0.965 Theta(max)= 26.904

R(reflections)= 0.1521(1634) wR2(reflections)= 0.4328(2228)

S = 1.685 Npar= 195

Datablock vb8211-7-2019 - ellipsoid plot

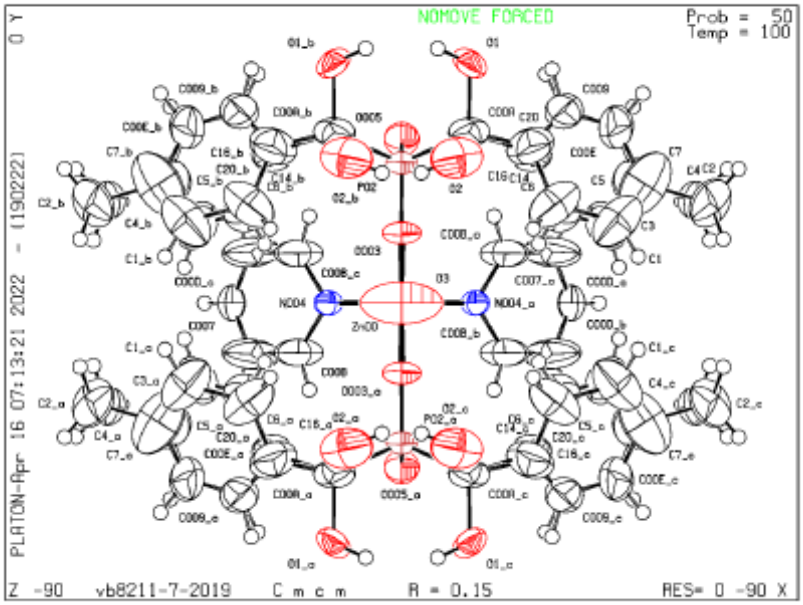

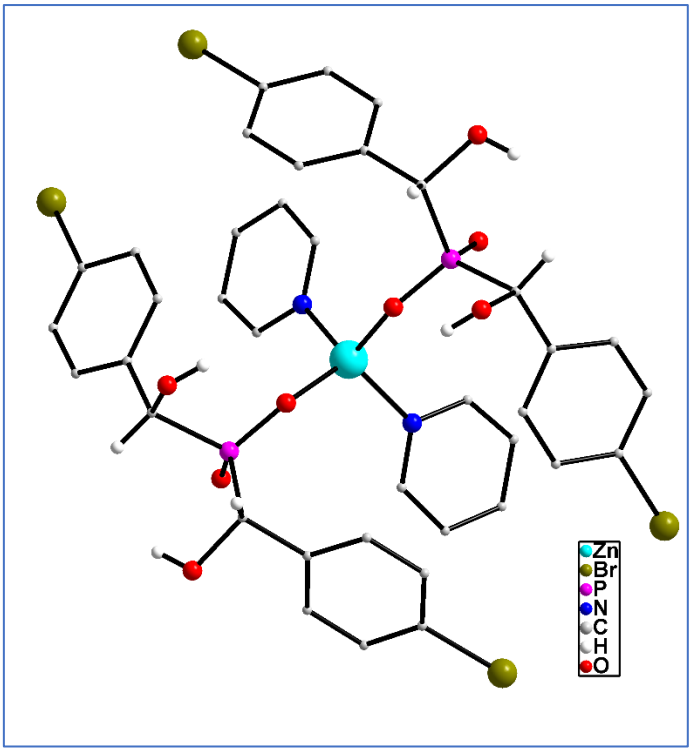

Figure 6.2. Ball and stick view of zinc phosphinate molecular structure.

checkCIF/PLATON report

Structure factors have been supplied for datablock(s) vb97

THIS REPORT IS FOR GUIDANCE ONLY. IF USED AS PART OF A REVIEW PROCEDURE FOR PUBLICATION, IT SHOULD NOT REPLACE THE EXPERTISE OF AN EXPERIENCED CRYSTALLOGRAPHIC REFEREE.

No syntax errors found. CIF dictionary Interpreting this report

Datablock: vb97

Bond precision: C-C = 0.0145 A Wavelength=0.71073

Cell: a=18.5509(8) b=26.9299(8) c=8.2742(3)
alpha=90 beta=90 gamma=90
Temperature: 100 K

	Calculated	Reported
Volume	4133.6(3)	4133.6(3)
Space group	C c c 2	C c c 2
Hall group	C 2 -2c	C 2 -2c
Moiety formula	C38 H34 Br4 N2 O8 P2 Zn, O	C38 H34 Br4 N2 O8 P2 Zn, O
Sum formula	C38 H34 Br4 N2 O9 P2 Zn	C38 H34 Br4 N2 O9 P2 Zn
Mr	1109.60	1109.62
Dx,g cm-3	1.783	1.783
Z	4	4
Mu (mm-1)	4.594	4.594
F000	2192.0	2192.0
F000'	2190.37	
h,k,lmax	23,34,10	23,34,10
Nref	4520[2426]	3489
Tmin,Tmax	0.896,0.955	0.379,1.000
Tmin'	0.871	

Correction method= # Reported T Limits: Tmin=0.379 Tmax=1.000
AbsCorr = MULTI-SCAN

Data completeness= 1.44/0.77 Theta(max)= 26.985

R(reflections)= 0.0544(2475) wR2(reflections)= 0.1161(3489)

S = 1.029 Npar= 276

Datablock vb97 - ellipsoid plot

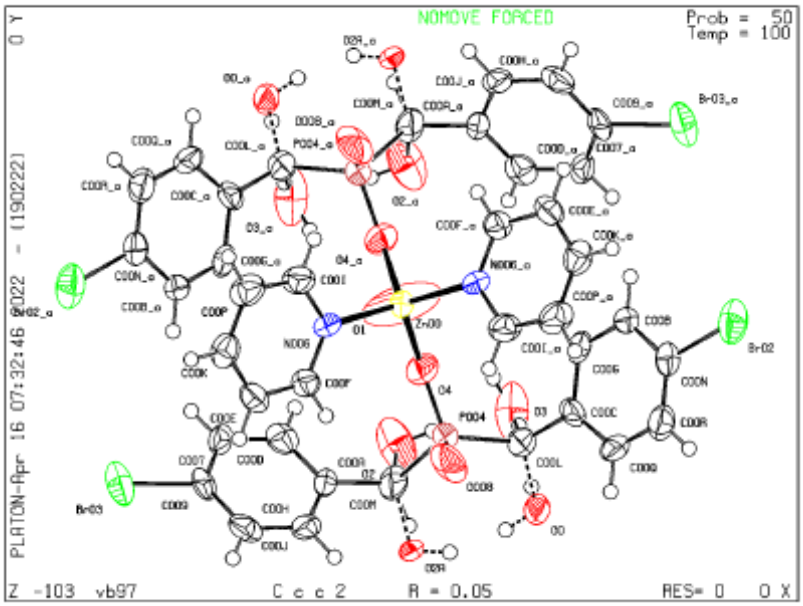

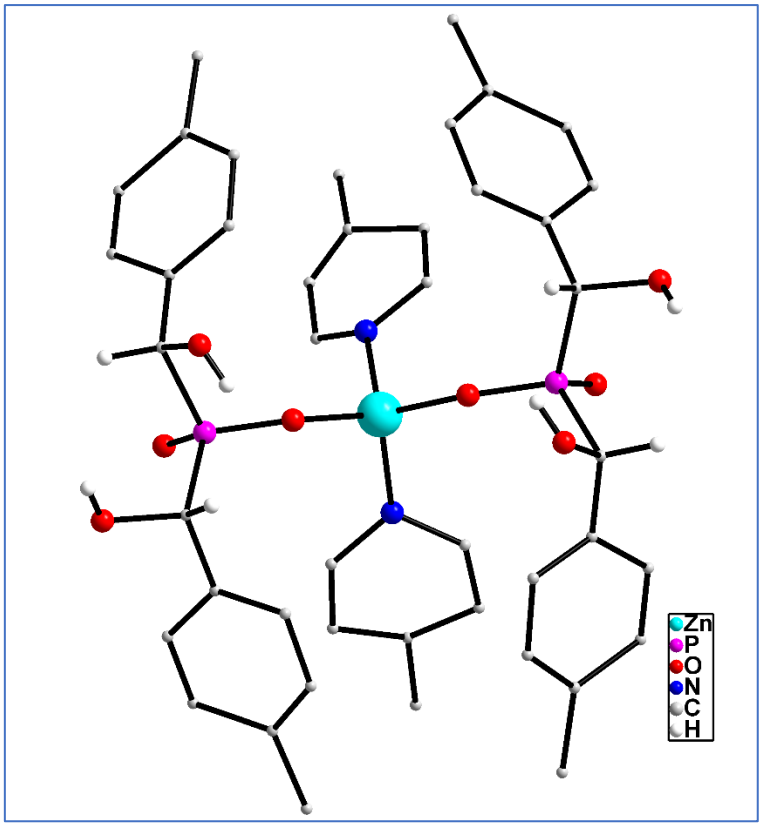

Figure 6.3. Ball and stick view of zinc phosphinate molecular structure.

checkCIF/PLATON report

Structure factors have been supplied for datablock(s) aaaaaaaaaa

THIS REPORT IS FOR GUIDANCE ONLY. IF USED AS PART OF A REVIEW PROCEDURE FOR PUBLICATION, IT SHOULD NOT REPLACE THE EXPERTISE OF AN EXPERIENCED CRYSTALLOGRAPHIC REFEREE.

No syntax errors found. CIF dictionary Interpreting this report

Datablock: aaaaaaaaaa

Bond precision: C-C = 0.0090 A Wavelength=0.71073

Cell: a=17.807(2) b=9.4594(9) c=27.140(3)
alpha=90 beta=90 gamma=90

Temperature: 299 K

	Calculated	Reported
Volume	4571.6(8)	4571.6(8)
Space group	C m c m	C m c m
Hall group	-C 2c 2	-C 2c 2
Moiety formula	C44 H47.20 N2 O8 P2 Zn, O	C44 H47.2 N2 O8 P2 Zn, O
Sum formula	C44 H47.20 N2 O9 P2 Zn	C44 H47.20 N2 O9 P2 Zn
Mr	875.37	875.34
Dx,g cm-3	1.272	1.272
Z	4	4
Mu (mm-1)	0.660	0.660
F000	1828.8	1829.0
F000'	1831.50	
h,k,lmax	22,11,34	22,11,34
Nref	2483	2477
Tmin,Tmax	0.969,0.980	0.642,0.745
Tmin'	0.961	

Correction method= # Reported T Limits: Tmin=0.642 Tmax=0.745
AbsCorr = MULTI-SCAN

Data completeness= 0.998 Theta(max)= 26.438

R(reflections)= 0.0556(1807) wR2(reflections)= 0.1540(2477)

S = 1.085 Npar= 211

Datablock aaaaaaaaaa - ellipsoid plot

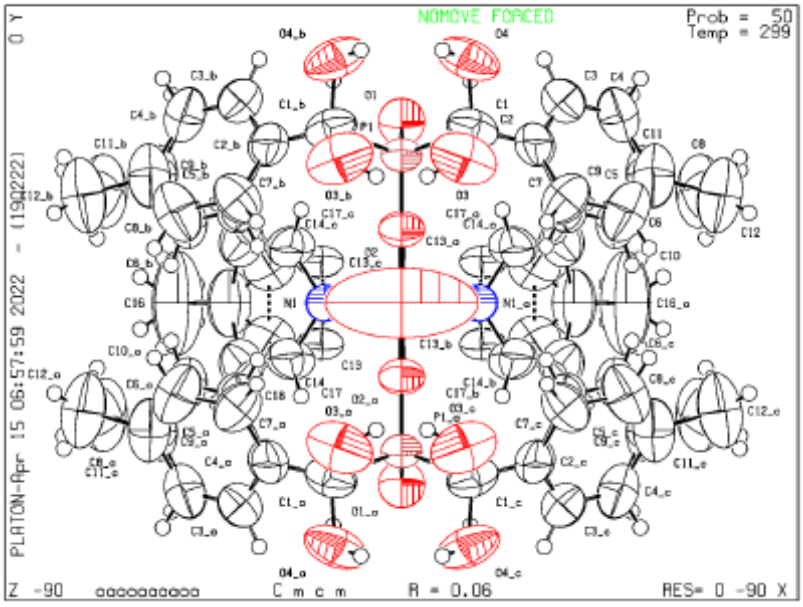

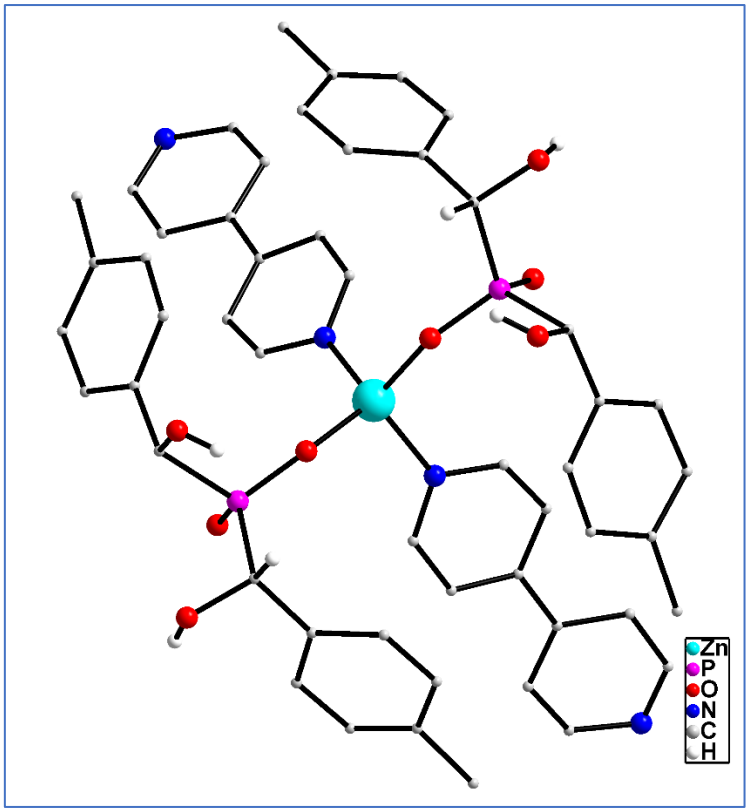

Figure 6.4. Ball and stick view of zinc phosphinate molecular structure.

checkCIF/PLATON report

Structure factors have been supplied for datablock(s) vb168

THIS REPORT IS FOR GUIDANCE ONLY. IF USED AS PART OF A REVIEW PROCEDURE FOR PUBLICATION, IT SHOULD NOT REPLACE THE EXPERTISE OF AN EXPERIENCED CRYSTALLOGRAPHIC REFEREE.

No syntax errors found. CIF dictionary Interpreting this report

Datablock: vb168

Bond precision: C-C = 0.0231 A Wavelength=0.71073

Cell: a=17.6268(8) b=9.7270(5) c=30.8467(18)
alpha=90 beta=101.854(5) gamma=90
Temperature: 295 K

	Calculated	Reported
Volume	5176.1(5)	5176.1(5)
Space group	C 2/c	C 1 2/c 1
Hall group	-C 2yc	-C 2yc
Moiety formula	C52 H50 N4 O8 P2 Zn	C52 H50 N4 O8 P2 Zn
Sum formula	C52 H50 N4 O8 P2 Zn	C52 H52 N4 O8 P2 Zn
Mr	986.29	988.28
Dx,g cm-3	1.266	1.268
Z	4	4
Mu (mm-1)	0.591	0.591
F000	2056.0	2064.0
F000'	2058.74	
h,k,lmax	22,12,39	22,12,39
Nref	5630	5385
Tmin,Tmax	0.838,0.868	0.802,1.000
Tmin'	0.838	

Correction method= # Reported T Limits: Tmin=0.802 Tmax=1.000
AbsCorr = MULTI-SCAN

Data completeness= 0.956 Theta(max)= 26.967

R(reflections)= 0.1830(2952) wR2(reflections)= 0.4641(5385)

S = 1.526 Npar= 313

Datablock vb168 - ellipsoid plot

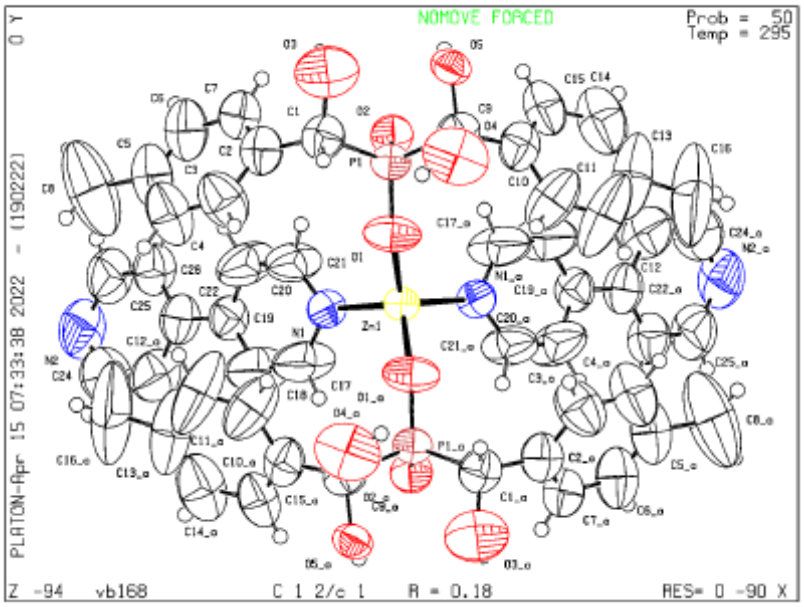

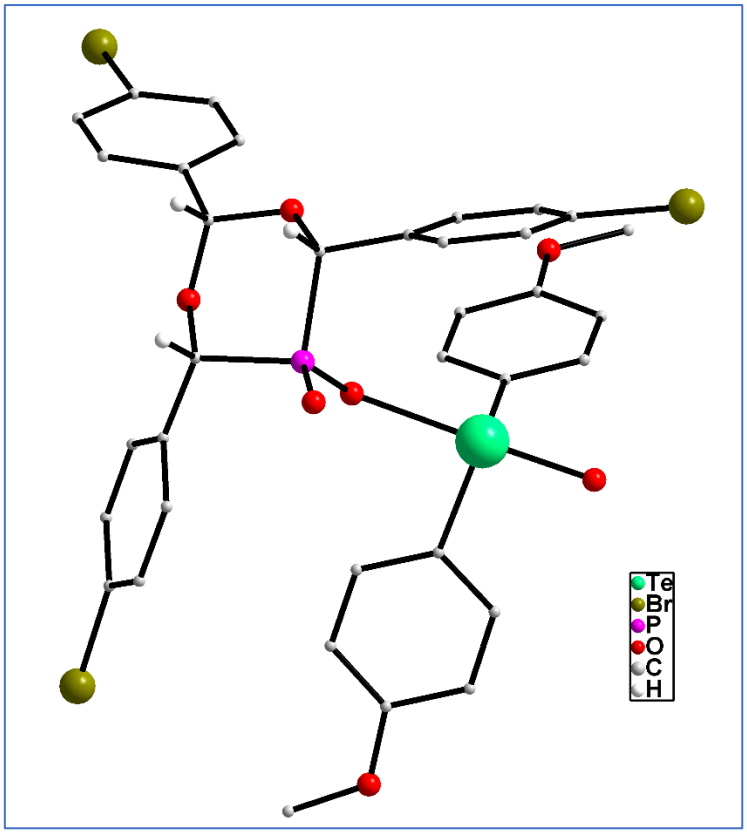

Figure 6.5. Ball and stick view of tellurium phosphinate molecular structure.

checkCIF/PLATON report

Structure factors have been supplied for datablock(s) vb103

THIS REPORT IS FOR GUIDANCE ONLY. IF USED AS PART OF A REVIEW PROCEDURE FOR PUBLICATION, IT SHOULD NOT REPLACE THE EXPERTISE OF AN EXPERIENCED CRYSTALLOGRAPHIC REFEREE.

No syntax errors found. CIF dictionary Interpreting this report

Datablock: vb103

Bond precision: C-C = 0.0141 A Wavelength=0.71073

Cell: a=8.8626(5) b=13.1694(8) c=29.8407(15)
alpha=90 beta=92.748(5) gamma=90
Temperature: 102 K

	Calculated	Reported
Volume	3478.9(3)	3478.9(3)
Space group	P 21/c	P 1 21/c 1
Hall group	-P 2ybc	-P 2ybc
Moiety formula	C35 H29 Br3 O7 P Te	C35 H29 Br3 O7 P Te
Sum formula	C35 H29 Br3 O7 P Te	C35 H29 Br3 O7 P Te
Mr	959.85	959.88
Dx,g cm-3	1.833	1.833
Z	4	4
Mu (mm-1)	4.394	4.394
F000	1868.0	1868.0
F000'	1863.71	
h,k,lmax	11,16,38	11,16,37
Nref	7586	7288
Tmin,Tmax	0.304,0.333	0.754,1.000
Tmin'	0.281	

Correction method= # Reported T Limits: Tmin=0.754 Tmax=1.000
AbsCorr = MULTI-SCAN

Data completeness= 0.961 Theta(max)= 26.972

R(reflections)= 0.0806(4771) wR2(reflections)= 0.1890(7288)

S = 1.102 Npar= 426

Datablock vb103 - ellipsoid plot

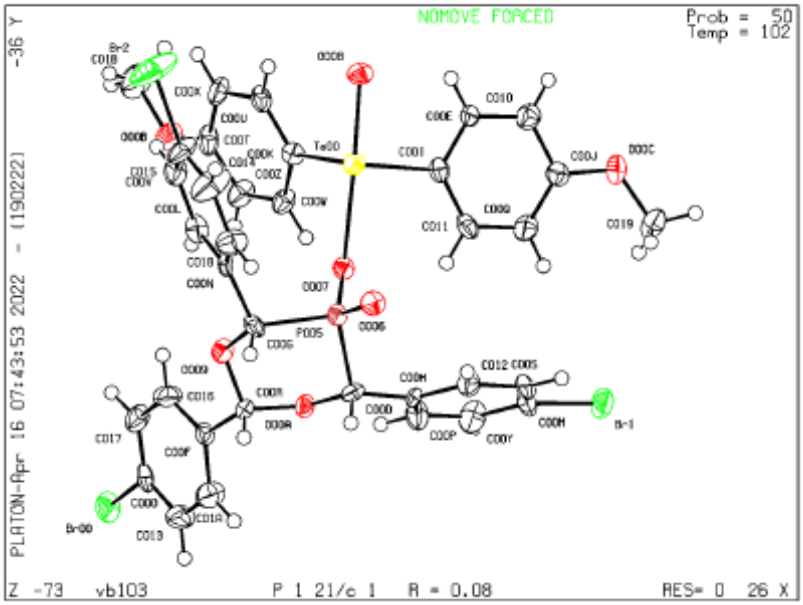

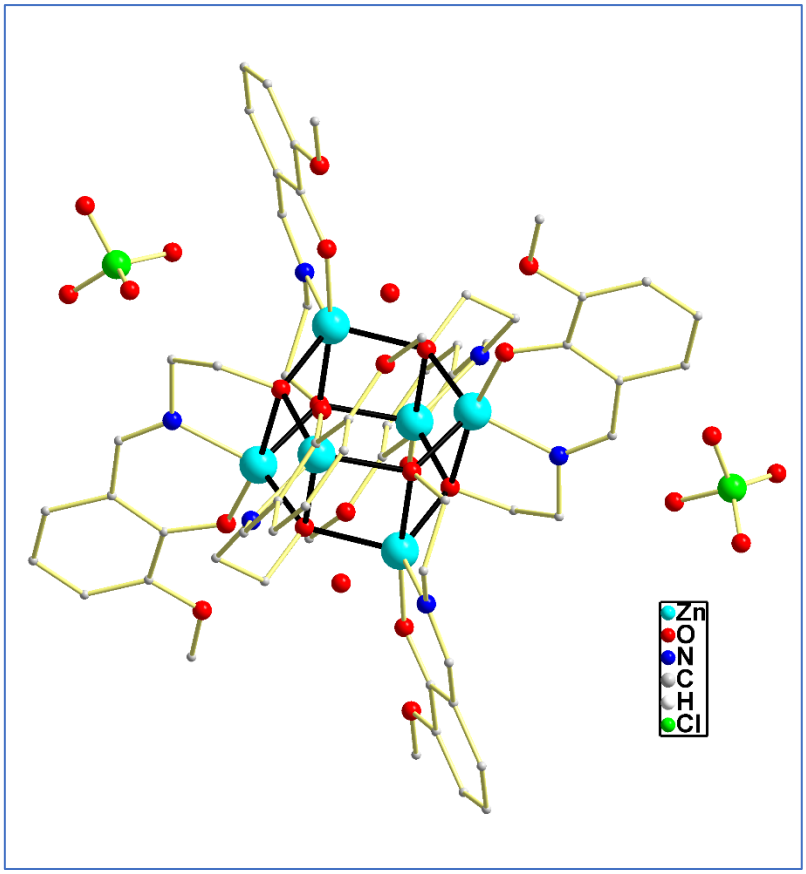

Figure 6.6. Ball and stick view of zinc Schiff-base molecular structure.

checkCIF/PLATON report

Structure factors have been supplied for datablock(s) vb600_0m_a

THIS REPORT IS FOR GUIDANCE ONLY. IF USED AS PART OF A REVIEW PROCEDURE FOR PUBLICATION, IT SHOULD NOT REPLACE THE EXPERTISE OF AN EXPERIENCED CRYSTALLOGRAPHIC REFEREE.

No syntax errors found. CIF dictionary Interpreting this report

Datablock: vb600_0m_a

Bond precision: C-C = 0.0060 A Wavelength=0.71073

Cell: a=14.458(4) b=17.322(4) c=17.354(4)
alpha=101.005(11) beta=102.455(11) gamma=109.370(11)
Temperature: 100 K

	Calculated	Reported
Volume	3837.8(17)	3837.9(17)
Space group	P -1	P -1
Hall group	-P 1	-P 1
Moiety formula	C60 H66 N6 O18 Zn6, 2(Cl O4), 2(H2 O) [+ solvent]	2(C30 H33 N3 O9 Zn3), 2(Cl O4), 2(H2 O), 1[C2H3N], 1[CH4O]
Sum formula	C60 H70 Cl2 N6 O28 Zn6 [+ solvent]	C63 H77 Cl2 N7 O29 Zn6
Mr	1786.46	1859.43
Dx,g cm-3	1.546	1.609
Z	2	2
Mu (mm-1)	1.995	1.999
F000	1820.0	1900.0
F000'	1824.78	
h,k,lmax	18,22,22	18,22,22
Nref	17887	17772
Tmin,Tmax	0.909,0.961	0.468,0.746
Tmin'	0.905	

Correction method= # Reported T Limits: Tmin=0.468 Tmax=0.746
AbsCorr = MULTI-SCAN

Data completeness= 0.994 Theta(max)= 27.646

Datablock vb600_0m_a - ellipsoid plot

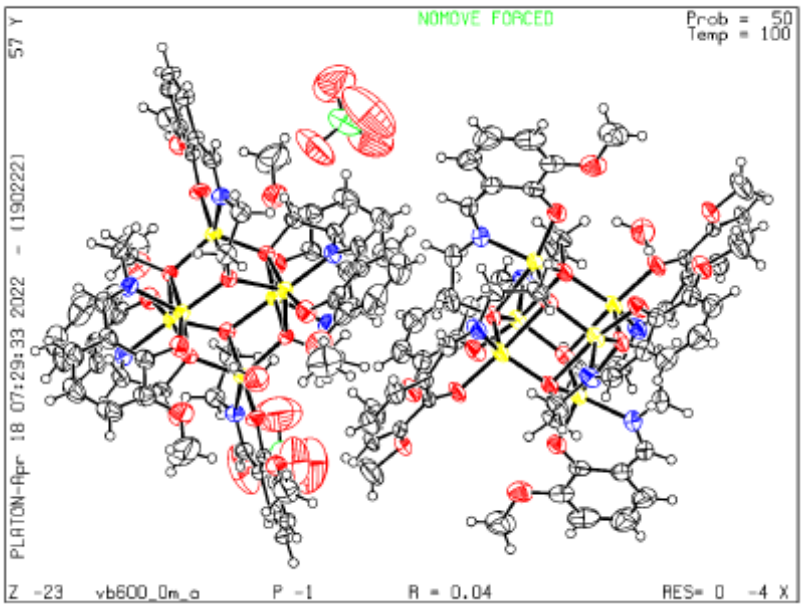

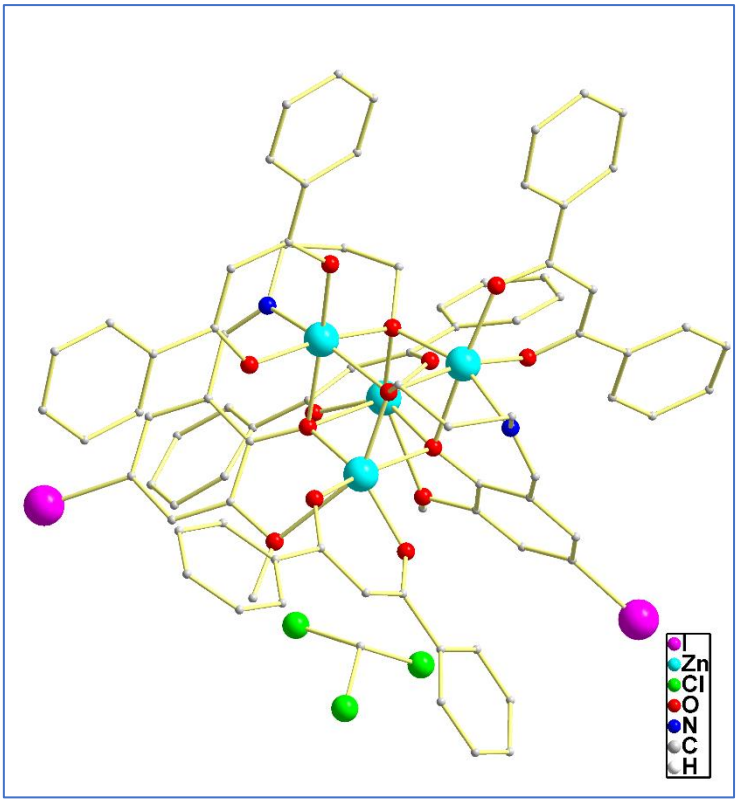

Figure 6.7. Ball and stick view of zinc Schiff-base molecular structure.

checkCIF/PLATON report

Structure factors have been supplied for datablock(s) vb107

THIS REPORT IS FOR GUIDANCE ONLY. IF USED AS PART OF A REVIEW PROCEDURE FOR PUBLICATION, IT SHOULD NOT REPLACE THE EXPERTISE OF AN EXPERIENCED CRYSTALLOGRAPHIC REFEREE.

No syntax errors found. CIF dictionary Interpreting this report

Datablock: vb107

Bond precision: C-C = 0.0048 A Wavelength=0.71073

Cell: a=19.1643(3) b=21.2394(3) c=19.2084(3)
alpha=90 beta=104.889(2) gamma=90

Temperature: 100 K

	Calculated	Reported
Volume	7556.1(2)	7556.0(2)
Space group	P 21/n	P 1 21/n 1
Hall group	-P 2yn	-P 2yn
Moiety formula	C82 H68 I2 N2 O14 Zn4, C H Cl3	C82 H68 I2 N2 O14 Zn4, C H Cl3
Sum formula	C83 H69 Cl3 I2 N2 O14 Zn4	C83 H69 Cl3 I2 N2 O14 Zn4
Mr	1940.12	1940.03
Dx,g cm-3	1.706	1.705
Z	4	4
Mu (mm-1)	2.246	2.246
F000	3880.0	3880.0
F000'	3883.90	
h,k,lmax	24,27,24	24,27,24
Nref	16512	15789
Tmin,Tmax	0.515,0.597	0.618,1.000
Tmin'	0.505	

Correction method= # Reported T Limits: Tmin=0.618 Tmax=1.000
AbsCorr = MULTI-SCAN

Data completeness= 0.956 Theta(max)= 27.008

R(reflections)= 0.0381(11351) wR2(reflections)= 0.0825(15789)

S = 1.060 Npar= 975

Datablock vb107 - ellipsoid plot

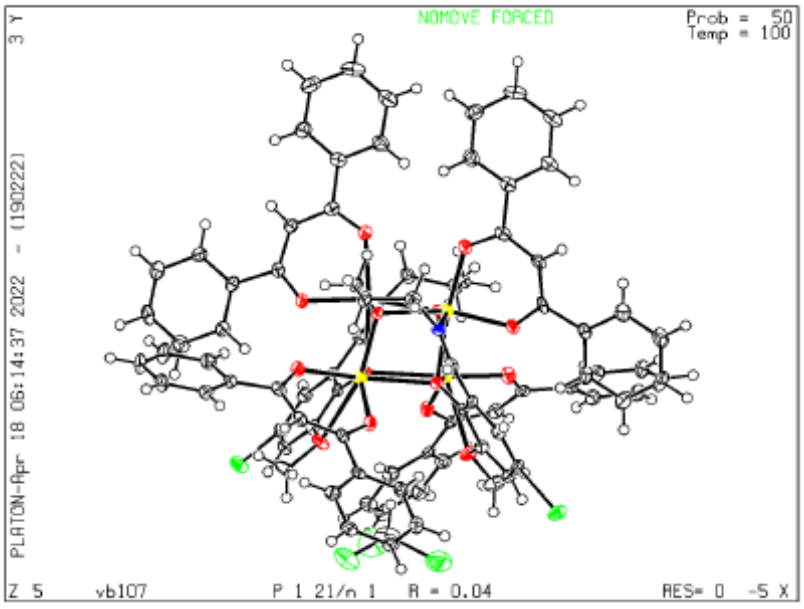

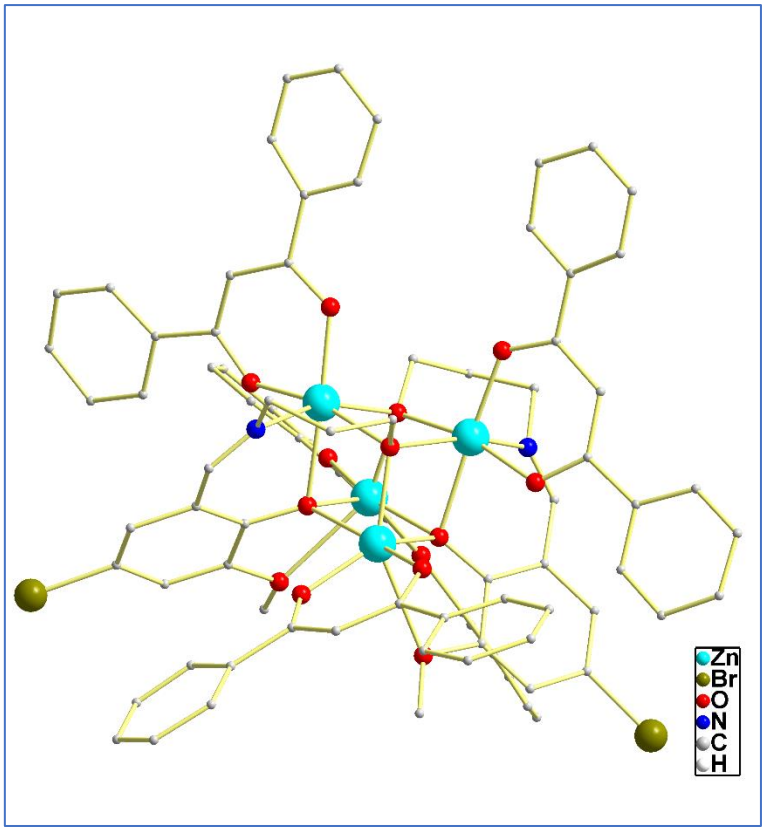

Figure 6.8. Ball and stick view of zinc Schiff-base molecular structure.

checkCIF/PLATON report

Structure factors have been supplied for datablock(s) vb109

THIS REPORT IS FOR GUIDANCE ONLY. IF USED AS PART OF A REVIEW PROCEDURE FOR PUBLICATION, IT SHOULD NOT REPLACE THE EXPERTISE OF AN EXPERIENCED CRYSTALLOGRAPHIC REFEREE.

No syntax errors found. CIF dictionary Interpreting this report

Datablock: vb109

```
Bond precision:   C-C = 0.0143 A          Wavelength=0.71073

Cell:             a=19.1503(3)     b=21.2975(4)        c=19.0539(3)
                  alpha=90         beta=104.782(2)     gamma=90
Temperature:      104 K
```

	Calculated	Reported
Volume	7514.0(2)	7514.0(2)
Space group	C 2/c	C 1 2/c 1
Hall group	-C 2yc	-C 2yc
Moiety formula	C82 H68 Br2 N2 O14 Zn4, O2, 2(H2 O), 2(C H3)	C82 H68 Br2 N2 O14 Zn4, 2(H2 O), C2 H6 O2
Sum formula	C84 H78 Br2 N2 O18 Zn4	C82 H68 Br2 N2 O20 Zn4
Mr	1824.84	1822.68
Dx,g cm-3	1.613	1.611
Z	4	4
Mu (mm-1)	2.400	2.402
F000	3720.0	3696.0
F000'	3723.74	
h,k,lmax	24,27,24	24,26,24
Nref	8186	7809
Tmin,Tmax	0.528,0.576	0.619,1.000
Tmin'	0.518	

```
Correction method= # Reported T Limits: Tmin=0.619 Tmax=1.000
AbsCorr = MULTI-SCAN

Data completeness= 0.954          Theta(max)= 26.970

R(reflections)= 0.0817( 5544)                    wR2(reflections)=
                                                 0.2265( 7809)
S = 1.037                 Npar= 501
```

Datablock vb109 - ellipsoid plot

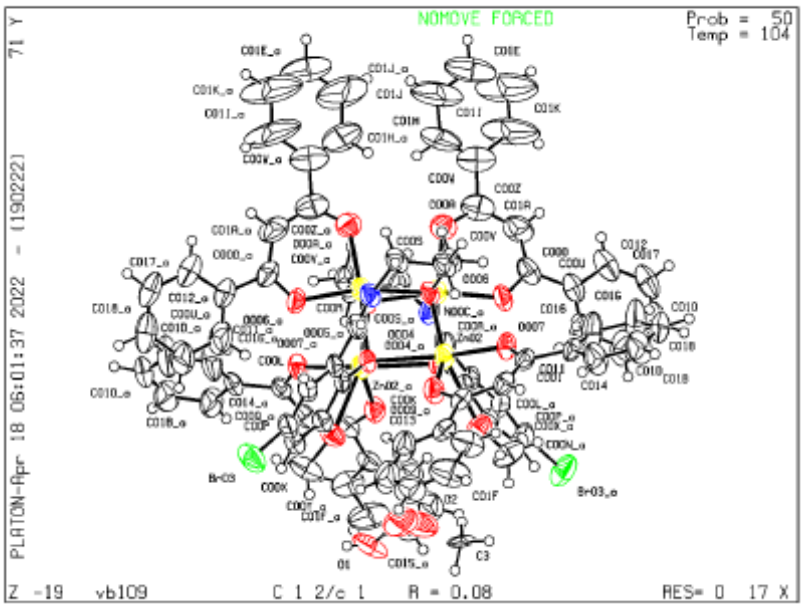

Future Scope of the thesis

In the thesis, we have worked mainly with two ligand systems- Schiff-base ligand and chiral phosphinic acid. In chapter 2 we have synthesized and characterized zinc Schiff-base complexes of mononuclear to polynuclear (compound **2.1-2.5**) using various chain lengths and substituents containing Schiff-bases in the presence and absence of co-ligands. 3d-metal Schiff base complexes are used in various catalytic/enzymatic applications such as catecholase or phenoxazinone activity. It can be also done with these zinc Schiff-base clusters. By replacing another 3d metal (Cu, Ni, Co, Mn, Fe, etc) salts using a similar strategy different complexes can also be synthesized. Manganese and cobalt complexes of such clusters can be used for potential applications in electrocatalysis.

In chapter 3, we synthesized cadmium phosphinates (compound **3.1-3.4**) of zero-dimension (0D), and coordination polymers (1D, 2D) by varying aza-donor co-ligands using phosphinic acid. This type of cadmium coordination polymer can act as a photocatalyst. Similarly can be tried with other 3d metal ions, which is the scope of this work.

Lanthanide phosphinates are mostly insoluble for their polymeric formation behavior. In chapter 4 and chapter 5 we have synthesized soluble lanthanide clusters using chiral phosphinic acid ligand Bis-(α-hydroxy)phosphinic acids. In chapter 4 dinuclear and trinuclear lanthanide-phosphinate clusters (compound **4.1-4.8**) are synthesized and characterized. These can be further used for catalytic application. Cerium analog of this can be used for electrochemistry applications.

In chapter 5, tetranuclear [2×2] square-grid lanthanide clusters (compound **5.1-5.3**) are synthesized and characterized. In the crystal structure, each lanthanide ion is coordinately saturated with one terminal carboxylic acid ligand and which is on the same plane. There has still scope for the development of this chemistry by changing these carboxylic acids with di-carboxylic acids (e.g. terephthalic acid) to the formation of a 2D or 3D framework. Cerium analog of these can be used for electrochemistry applications.

List of Publications

[1] Dy2 and Dy4 hydroxo clusters assembled using o-vanillin based Schiff bases as ligands and β-diketone co-ligands: Dy4 cluster exhibits slow magnetic relaxation

A. K. Jami, J. Ali, **S. Mondal**, J. Homs-Esquius, E. Carolina Sañudo, V. Baskar, *Polyhedron* 2018, **151**, 90–9991.

[2] In Situ Assembled Polynuclear Zinc Oxo Clusters Using Modified Schiff Bases as Ligands

S. Mondal, S. P. Behera, M. Alamgir, V. Baskar, *ACS Omega* 2022, **7**, 1090-1099.

[3] Lutetium oxo clusters utilizing mixed ligand System: Isolation of a rare Lu4 oxo cluster in a tetrahedral architecture

A. K. Jami, S. P. Behera, **S. Mondal**, *Inorganic Chemistry Communications* 2022, **143**, 109784.

[4] Aza-donor ligands-A key to synthesizing mononuclear to coordination polymers of cadmium phosphinates.

S. Mondal, C. Samuel, V. Baskar, *Journal of Molecular Structure* 2023, **1273**, 134274.

[5] Synthesis and characterization of paddlewheel dinuclear and trinuclear lanthanide phosphinate cluster.

S. Mondal, V. Baskar (Manuscript under preparation)

[6] A new type of square grid [2 × 2] lanthanide(III)4 complexes self-assembled with chiral racemic (R,R / S,S)bis-[α-hydroxy(*p*-bromo-phenyl)methyl]phosphine acid ligand.

S. Mondal, V. Baskar (Manuscript under preparation)

Poster and Oral Presentations

[1] Poster Presentation entitled " Synthesis and Characterization of Mono to Polynuclear Zinc Schiff-Base Clusters." 17th annual in-house symposium, **CHEMFEST-2020**, Held at the School of Chemistry, University of Hyderabad.

[2] Oral Presentation entitled "A One-Pot Synthesis of Zinc Schiff-Base Clusters." 18th annual in-house symposium, **CHEMFEST-2021**, Held at the School of Chemistry, University of Hyderabad.

[3] Poster Presentation entitled "Self-Assembly of Zinc-Oxo Clusters."
An international conference on "**MTIC (Modern Trends In Inorganic Chemistry)-XIX**", 2022, held at Banaras Hindu University.

Self-assembly of 3d and 4f metal ions using chiral/flexible ligands

by Suman Mondal

Submission date: 27-Dec-2022 11:14AM (UTC+0530)
Submission ID: 1986836686
File name: Suman_Thesis_16CHPH29.pdf (7.28M)
Word count: 26172
Character count: 134829

Self-assembly of 3d and 4f metal ions using chiral/flexible ligands

ORIGINALITY REPORT

32%	21%	32%	2%
SIMILARITY INDEX	INTERNET SOURCES	PUBLICATIONS	STUDENT PAPERS

PRIMARY SOURCES

1	www.ncbi.nlm.nih.gov Internet Source	11%
2	Suman Mondal, Calvin Samuel, Viswanathan Baskar. "Aza-donor ligands—A key to synthesizing mononuclear to coordination polymers of cadmium phosphinates", Journal of Molecular Structure, 2023 Publication	11%
3	Suman Mondal, Smruti Prangya Behera, Mohammed Alamgir, Viswanathan Baskar. "In Situ Assembled Polynuclear ZincOxo Clusters Using Modified Schiff Bases as Ligands", ACS Omega Internet Source	2%
4	Suman Mondal, Smruti Prangya Behera, Mohammed Alamgir, Viswanathan Baskar. "In Situ Assembled Polynuclear Zinc Oxo Clusters Using Modified Schiff Bases as Ligands", ACS Omega, 2021 Publication	2%

Suman Mondal
ACS Omega 2021

V. Baskar

V. BASKAR
Professor
School of Chemistry
University of Hyderabad
Hyderabad - 500 046.

5	Suman Mondal, Calvin Samuel, Viswanathan Baskar. "Aza-donor ligands- A key to synthesizing mononuclear to coordination polymers of cadmium phosphinates.", Journal of Molecular Structure, 2022 Publication	2%
6	www.researchgate.net Internet Source	1%
7	Joydeb Goura, Vadapalli Chandrasekhar. "Molecular Metal Phosphonates", Chemical Reviews, 2015 Publication	<1%
8	Gao, Qian, Yaru Qin, Yanmei Chen, Wei Liu, Haiyan Li, Bing Wu, Yahong Li, and Wu Li. "Cubane-type {M4O4} (M = CoII, ZnII, CuII) clusters: synthesis, crystal structures, and luminescent and magnetic properties", RSC Advances, 2015. Publication	<1%
9	Andoni Zabala-Lekuona, José Manuel Seco, Enrique Colacio. "Single-Molecule Magnets: From Mn12-ac to dysprosium metallocenes, a travel in time", Coordination Chemistry Reviews, 2021 Publication	<1%
10	pubs.rsc.org Internet Source	<1%

V. BASKAR
Professor
School of Chemistry
University of Hyderabad
Hyderabad - 500 046.